



TESIS DOCTORAL

**Técnicas de optimización avanzada para la mejora de la
eficiencia energética en redes 5G/6G ultradensas**

Jesús Galeano Brajones

PROGRAMA DE DOCTORADO EN TECNOLOGÍAS INFORMÁTICAS

Con la conformidad de los directores

Dr. Javier Carmona Murillo & Dr. Francisco Luna Valero

Esta tesis cuenta con la autorización del director y codirector de la misma y de la Comisión Académica del programa. Dichas autorizaciones constan en el Servicio de la Escuela Internacional de Doctorado de la Universidad de Extremadura

Mérida, 2024



PHD THESIS

**Advanced Optimization Techniques for Energy
Efficiency Improvement in Ultra-Dense 5G/6G
Networks**

Jesús Galeano Brajones

DOCTORAL PROGRAM IN INFORMATION TECHNOLOGIES

With the approval of the supervisors

Dr. Javier Carmona Murillo & Dr. Francisco Luna Valero

Mérida, 2024

“The measure of intelligence is the ability to change.”

Albert Einstein

PREFACE

This thesis, presented as a compendium of articles, is submitted in accordance with the requirements of the University of Extremadura (Spain) for the attainment of the International PhD degree in the Doctoral Program in Information Technologies. Dr. Javier Carmona Murillo and Dr. Francisco Luna Valero have supervised the research presented in this document. The research results have been developed mainly at the University of Extremadura.

AGRADECIMIENTOS

Al cerrar esta etapa tan significativa de mi vida, no puedo evitar sentirme profundamente agradecido por todas las personas que han hecho posible este viaje. Es un honor poder compartir este logro con quienes me han apoyado incondicionalmente.

Deseo comenzar expresando mi más profundo agradecimiento a mis directores, Javi y Paco. Su incansable paciencia, guía experta y constante estímulo han sido el faro que me ha guiado a través de este proceso. Su pasión y dedicación, junto a su cercanía, no solo han sido una fuente de inspiración sino también de motivación constante. Gracias por creer en mí.

También quiero extender un especial agradecimiento a Mihaela, cuyo apoyo incondicional y valiosos consejos han sido fundamentales buena parte de este tiempo. A Juanfra, le estoy igualmente agradecido por cada sabio consejo y por su guía esclarecedora. Mi gratitud se extiende al grupo de investigación GITACA y a todos sus miembros, quienes me han acogido y brindado un apoyo indispensable. Su colaboración ha sido esencial para la culminación de esta tesis.

Mi sincero agradecimiento se extiende también a la Universidad de Extremadura, y de manera muy especial al Centro Universitario de Mérida, cuyos pasillos me han visto dar mis primeros pasos académicos y, hoy, culminar mi doctorado. Agradezco profundamente a cada uno de los profesores que han contribuido a mi formación, no solo por su excepcional calidad docente sino también por su invaluable humanidad. De igual manera, mi gratitud hacia cada compañero que ha compartido este viaje conmigo, haciéndolo significativamente más enriquecedor y llevadero. Gracias por ser parte de este viaje.

Durante mi estancia en Dinamarca, muchas personas han dejado una huella imborrable en mi experiencia. Mi agradecimiento a Daniela de Nokia Aalborg, quien me ofreció orientación, y de manera especial a Carlos, Kun y los malagueños, cuya presencia fue esencial en cada paso del camino. Su compañerismo durante la estancia fue clave para hacer este periodo no solo más llevadero, sino también increíblemente enriquecedor.

Y para finalizar, pero no por ello menos importante, debo mi más sincero agradecimiento a mi familia. Especialmente a mis padres, Conchi y Jesús, mi hermana Laura, mi abuela Fide, mi tío Luis y mi pareja Laura. Su apoyo incondicional ha sido mi fortaleza, incluso en los momentos más difíciles. Sin su amor, paciencia y creencia en mí, no estaría donde estoy hoy. Gracias por influir en mi vida de maneras que solo una familia puede hacerlo, por hacerme ser la persona que soy. Vuestra presencia y apoyo constante son los regalos más valiosos que he recibido. Con profundo cariño y gratitud, os dedico este logro.

Jesús Galeano Brajones
Mérida, España, Marzo 2024

ABSTRACT

In the rapidly evolving landscape of wireless communication technologies, this thesis aims to enhance the energy efficiency of ultra-dense 5G/6G networks by developing advanced techniques in multi-objective evolutionary algorithms (MOEAs). In the middle of the global push towards digitalization, catalyzed by the deployment of 5G and the anticipation of 6G technologies, this research tackles the dual challenge of meeting the soaring demand for stringent network performance while minimizing environmental impact. Focused on the critical Cell Switch-Off (CSO) problem, this study addresses the complexities of network optimization, emphasizing the reduction of energy consumption without compromising network key performance indicators. Central to this thesis is the exploration of the landscape of the CSO problem, significantly influenced by the spatial heterogeneity of traffic. Through meticulous analysis, it was discovered that the severity of spatial traffic heterogeneity simplifies the optimization landscape and amplifies the effectiveness of algorithmic searches. A novel contribution of this research is the development of specialized search operators for metaheuristics, informed by an in-depth understanding of the problem landscape, thereby enhancing the ability of MOEAs to identify solutions closer to the optimal Pareto front. This work goes beyond canonical approaches by integrating problem-specific operators with MOEAs, thus extending the limit in network energy optimization. Empirical evidence underscores the superiority of these specialized operators in refining search strategies, leading to significant advances in energy efficiency. Furthermore, this thesis extends its insights to address other challenges within the 5G/6G domain, notably through a novel methodology for analyzing and classifying network flows using L-moments, which showcases the versatility and applicability of optimized techniques in broader network management contexts. In conclusion, the findings of this dissertation underscore the critical role of advanced optimization techniques in the multi-objective optimization domain for enhancing energy efficiency in 5G/6G networks. The strategic application of these methodologies not only contributes to the sustainable evolution of wireless networks but also sets a precedent for future research to optimize the emerging infrastructure of the digital era. By addressing the intricate balance between technological advancement and environmental stewardship, this work elaborates on the development of next-generation networks that are not only high-performing but also sustainable.

Keywords - next-generation networks, energy efficiency, multi-objective optimization, network management.

RESUMEN

En el panorama en constante evolución de las tecnologías de comunicación inalámbrica, esta tesis tiene como objetivo mejorar la eficiencia energética de las redes ultra-densas 5G/6G mediante la implementación de técnicas avanzadas en algoritmos evolutivos multiobjetivo (MOEAs, por sus siglas en inglés). En medio del impulso global hacia la digitalización, catalizado por el despliegue de las tecnologías 5G y la anticipación de las tecnologías 6G, esta investigación aborda el doble desafío de satisfacer la creciente demanda de un rendimiento de la red cada vez mayor, minimizando al mismo tiempo el impacto ambiental. Centrado en el problema crítico del apagado de celdas (CSO), este estudio aborda las complejidades de la optimización de redes, enfatizando la reducción del consumo de energía sin comprometer su rendimiento. Un aspecto fundamental en esta tesis es la exploración del *landscape* del problema CSO, significativamente influenciado por la heterogeneidad espacial del tráfico. A través de un análisis detallado, se ha descubierto que la diversidad en la heterogeneidad tráfico no solo simplifica el espacio de búsqueda (*landscape*) del problema de optimización, sino que también amplifica la eficacia de las búsquedas algorítmicas. Una contribución novedosa de esta tesis es el desarrollo de operadores de búsqueda especializados, informados por un conocimiento detallado del *landscape*, mejorando así la capacidad de los MOEAs para identificar soluciones más cercanas al frente óptimo de Pareto. Este trabajo va más allá de los enfoques tradicionales, integrando operadores específicos del problema en MOEAs, ampliando así los límites en la optimización del consumo energético de la red. La evidencia empírica subraya la superioridad de estos operadores especializados para refinar estrategias de búsqueda, conduciendo a avances significativos en eficiencia energética. Adicionalmente, esta tesis extiende su ámbito para abordar otros desafíos dentro del dominio 5G/6G a través de una metodología novedosa para analizar y clasificar flujos de red utilizando L-momentos, lo que demuestra la versatilidad y aplicabilidad de técnicas de optimización en contextos de gestión de redes más amplios. En conclusión, los resultados de esta tesis subrayan el papel crítico de las técnicas de optimización avanzadas en MOEAs para mejorar la eficiencia energética en las redes 5G/6G. La aplicación estratégica de estas metodologías no solo contribuye a la evolución sostenible de las redes inalámbricas sino que también establece un precedente para futuras investigaciones que tienen como objeto optimizar la creciente infraestructura tecnológica de la era digital. Al abordar el equilibrio siempre complejo entre el avance tecnológico y la gestión medioambiental, este trabajo aborda un aspecto fundamental para el desarrollo de redes de próxima generación que no solo son de alto rendimiento, sino también sostenibles.

Palabras clave - redes de próxima generación, eficiencia energética, optimización multiobjetivo, gestión de red.

CONTENTS

Agradecimientos	v
Abstract	vii
Resumen	ix
List of Abbreviations	xiii
1 Introduction	1
1.1 Background & Motivation	2
1.2 Objectives & Research Methodology	5
1.3 Thesis Results & Research Collaborations	6
2 Exploratory Landscape Analysis	11
2.1 Landscape-Enabled Algorithmic Design	12
2.2 3D-Map-Based CSO Optimization in 5G	48
3 Problem-Specific Operators	57
3.1 Addressing the CSO Problem with BPSO	58
3.2 Hybridization with Problem-Specific Operators	68
4 Extending Optimization to Other 5G Network Problems	87
4.1 Flow Analysis Using L-moments Theory	88
4.2 Optimization of the L-moments	96
4.2.1 Problem Modeling	96
4.2.2 Results	97
5 Conclusions and Future Work	101
5.1 Conclusions	102
5.2 Future Work	103
Bibliography	105
A ANTS22 Supplementary Material	109
A.1 UDN Modeling	110
A.2 Hypervolume	113
A.2.1 PSO Performance	113
A.2.2 Specific Operators in PSO	113
A.3 Average Comparison: Algorithm and Scenario	115
A.4 Average Comparison of All Algorithms	118

B	GENO Supplementary Material	119
B.1	Network Modeling	120
B.2	Approximations to the Pareto Front	124
B.3	HV Values	132
C	SWEVO Supplementary Material	135
C.1	HV Results	136
C.2	Attainment Surfaces	139
C.2.1	The Canonical and the Best Hybrid Versions	139
C.2.2	Canonical, Best Hybrid and Best SYN^{\uparrow}	143
C.3	Results of the Statistical Tests	147
C.3.1	Pairwise Comparison	147
C.3.2	Wilcoxon Test	162
C.3.3	Friedman Test	198
D	COMCOM Supplementary Material	235
D.1	Evaluation Metrics Results	236
E	Springer Rights	239

LIST OF ABBREVIATIONS

3GPP	3rd Generation Partnership Project
5G	5th Generation of Mobile Communications
6G	6th Generation of Mobile Communications
AF	Activity Factor
AI	Artificial Intelligence
ANOVA	ANalysis Of VAriance
BPSO	Binary Particle Swarm Optimization
BS	Base Station
BW	Bandwidth
CA	Carrier Aggregation
CC	Component Carrier
CIC	Canadian Institute for Cybersecurity
CSO	Cell Switch-Off
DDoS	Distributed Denial of Service
DL	Deep Learning
DL	Downlink
DPI	Deep Packet Inspection
DoS	Denial of Service
DrDoS	DDoS Reflection
EA	Evolutionary Algorithm
EAF	Empirical Attainment Function
EC	Energy Consumption
EC	Empty Cell operator
EE	Energy Efficiency
ELA	Exploratory Landscape Analysis
ETSI	European Telecommunications Standards Institute
FN	False Negatives
FP	False Positives
FTP	File Transfer Protocol
GRU	Gated Recurrent Unit
GSMA	Global System for Mobile Communications Association
HF	Higher Frequency operator
HTTP	Hypertext Transfer Protocol
HTTPS	Secure Hyper Text Transfer Protocol
HV	Hypervolume
IANA	Internet Assigned Numbers Authority
ICT	Information and Communication Technologies
IEEE	Institute of Electrical and Electronics Engineers
ISD	Inter-Site Distance

IoT	Internet of Things
KPI	Key Performance Indicator
LDAP	Lightweight Directory Access Protocol
LTE	Long Term Evolution
LmomRD	L-moment Ratio Diagram
MIMO	Multiple-Input Multiple-Output
ML	Machine Learning
mmWave	Millimeter-Wave Spectrum
MNO	Mobile Network Operator
MOCcell	Multi-Objective Cellular genetic algorithm
MOEA	Multi-Objective Evolutionary Algorithm
MOEA/D	MOEA based on Decomposition
MOP	Multi-Objective Problem
NES	Network Energy Saving
NGN	Next-Generation Network
NSGA-II	Non-Sorting Genetic Algorithm II
NTP	Network Time Protocol
PA	Power Amplifier
PC	Power Consumption
PF	Prioritize Femto operator
PLO	Pareto Local Optima
PPP	Poisson Point Process
PSC	Prioritize Small Cell operator
PSG	Power Saving Gain
PSO	Particle Swarm Optimization
QoS	Quality of Service
RAN	Radio Access Network
RBF	Radial Basis Function
RF	Radio Frequency
RPF	Reference Pareto Front
SA	Social Attractor
SBS	Small Base Station
SC	Single Cell operator
SDN	Software-Defined Networking
SINR	Signal-to-Interference-plus-Noise Ratio
SMOTE	Synthetic Minority Oversampling Technique
SMS-EMOA	S-Metric Selection MOEA
SNR	Signal-to-Noise Ratio
SSH	Secure Shell
SVM	Support Vector Machine
SparseEA	Sparse Evolutionary Algorithm
TCP	Transmission Control Protocol

TDD	Time Division Duplex
TFTP	Trivial File Transfer Protocol
TN	True Negatives
TP	True Positives
TR	Technical Report
UDN	Ultra-Dense Network
UDP	User Datagram Protocol
UE	User Equipment
UL	Uplink
UTP	User Throughput
kNN	k-Nearest Neighbors

1

INTRODUCTION

This chapter explores the background and motivation of the thesis, focusing on the evolution of 5G/6G networks, the urgent need for sustainability, and the exploration of advanced optimization techniques that remain unexplored in the existing literature. Detailed objectives are outlined to harness these domain information-based optimization strategies to boost energy efficiency in next-generation networks. Furthermore, it highlights tangible outcomes and collaborative milestones achieved, including published articles, communications at conferences, and a pivotal research stay, painting a comprehensive picture of the academic journey undertaken.

Contents

1.1	Background & Motivation	2
1.2	Objectives & Research Methodology	5
1.3	Thesis Results & Research Collaborations	6

1.1 Background & Motivation

The relentless evolution of wireless communication technologies has been a cornerstone of modern society shaping, enabling an interconnected world where digital interactions are seamless and ubiquitous [1,2]. This journey, which spans from the inception of the first generation to the advent of the fifth generation of mobile communications (5G) and the horizon of the sixth generation (6G), illustrates a continuous innovation trajectory aimed at meeting the ever-growing demands for improved connectivity [3,4]. Each leap forward has been motivated by the quest to support a broader range of use cases, from high-definition video streaming and virtual reality applications [5] to critical communications for autonomous vehicles and industrial automation [6], all demanding higher data rates, lower latency, and more reliable connections.

With an unprecedented technological revolution, the ever-increasing deployment of 5G [7] and the conceptualization of 6G networks are poised to redefine global communications [8]. As we navigate this new era, the emphasis shifts not only towards improving technological capabilities but also towards ensuring the environmental sustainability of these advanced networks [9]. The surge in global mobile data traffic, which now has volumes significantly higher than those seen in the previous decade, accentuates the critical need to mitigate the ecological footprint of this rapid expansion [10]. The rollout of 5G and its advanced iterations, which are expected to cover a considerable share of global subscriptions, is challenged by the dual objectives of delivering unparalleled performance and drastically reducing power consumption [11]. This effort aligns with the global initiative to reduce carbon emissions, which aims to alleviate the impacts of climate change. By 2027, 5G is projected to represent 49% of global subscriptions [12], promising data rates 13 times higher than current mobile connections by 2023, with speeds reaching 575 Mbps [13], sub-1 ms latencies, and support for more than a million devices per km². Achievement of such high performance to reduce 90% power consumption is crucial for the sustainability of this next-generation communication systems [14].

To meet the demanding design and performance requirements of next-generation networks, three main paradigms have been identified [15]: (i) using millimeter-wave spectrum (mmWave) to enable larger bandwidths, (ii) improving spectral efficiency through multi-antenna transmission (including massive and collaborative MIMO techniques), and (iii) increasing spatial reuse by densifying the network [16] both horizontally (in streets and hotspots) and vertically (within buildings such as apartments and offices) [17]. The expected use cases for 6G will require bandwidths that push the adoption of the mmWave spectrum [18], with wavelengths from 10 millimeters at 30 GHz to 1

millimeter at 300 GHz. A significant number of antennas are required at these frequencies to counteract propagation losses, considering the small dimensions of the antennas at such high frequencies [19]. Integrating massive MIMO with mmWave technology combines the benefits of extensive mmWave bandwidth and the gains from massive MIMO antenna arrays, thus allowing access to the 30-300 GHz bands and significantly enhancing spectral efficiency [20]. Moreover, this underscores the necessity for ultra-dense networks (UDNs), as transmitting at higher frequencies entails smaller coverage cells to overcome channel challenges such as blocking and path loss. Consequently, the main idea behind UDNs is to position access nodes as close to the end-users as possible, thereby enhancing connectivity and network performance. Figure 1.1 shows a heterogeneous UDN that showcases coverage cells: blue cells are generated by macro and micro BSs operating at sub-6GHz frequencies for broader coverage with primary backup roles, ensuring that no User Equipment (UE) remains unserved. In contrast, green cells represent small base stations (SBSs) that utilize mmWave spectrum frequencies, focused on delivering superior network performance despite facing significant propagation losses or blockages.

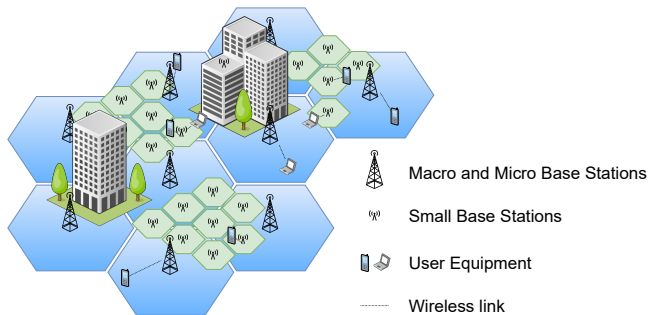


Figure 1.1: An example of a UDN.

In the context of these ambitious goals, the mobile network industry, a notable contributor to global CO₂ emissions [10] that represent approximately 0.4% of total emissions per year [21], is charged with innovating energy-efficient solutions. Highlighted as the segment with the highest energy consumption, the Radio Access Network (RAN) represents 56% of the total energy consumption of the network [22], highlighting the need for energy optimization at base stations, crucial for signal transmission and reception. Despite the improvement in the energy efficiency of 5G by 90% over LTE [23], releases 18 and 19 introduce adaptations to further energy savings during variable traffic loads. Consequently, recent standards and research initiatives aim to incorporate energy-saving measures into 5G and 6G, to significantly improve energy efficiency relative to traffic volume [24, 25].

Recent research initiatives have thoroughly investigated the advantages of

techniques aimed at saving energy within mobile networks. In particular, strategies such as micro-discontinuous transmission have been recognized for their potential to significantly reduce energy consumption [26–29]. This technique allows BSs to deactivate their power amplifiers for durations of at least one symbol, which is particularly beneficial under conditions of low user plane load, where predominantly control signals are transmitted. This method, alongside others discussed in various studies, underscores the critical balance between reducing energy use and maintaining essential network functionality. Furthermore, the literature reveals that optimizing the number of active antenna elements and their associated radio frequency (RF) components during periods of reduced traffic can prevent unnecessary energy expenditure [30–32]. However, the challenge arises in determining the optimal configuration that ensures energy savings without compromising the coverage and capacity of the network. It is a delicate balance to strike, as reducing the number of active RF components directly influences energy consumption, but can also inadvertently affect cell coverage and capacity.

In addition to individual cell energy management, comprehensive strategies have been explored for managing the energy consumption of serving cells as a whole. These include selective deactivation or transition of specific cells to sleep mode during times of low traffic demand, using advanced spatio-temporal traffic prediction models and sophisticated optimization techniques [33–36]. Such strategies aim to optimize network performance by adjusting the operational status of cells based on anticipated traffic patterns, thus achieving considerable energy savings. However, the implementation of these Cell Switch-Off (CSO) strategies in operational networks introduces complexities, primarily due to the intricate optimization challenges involved. Unique attributes of each cell, such as traffic load, coverage area, user quality of service (QoS) requirements, and power consumption, must be considered to design an effective CSO strategy. The inherent complexity of this optimization problem, classified as NP-complete [37], poses significant obstacles to finding optimal solutions in feasible computational times, highlighting ongoing challenges and the need for innovative approaches in the search for energy-efficient mobile networks.

The CSO problem has been extensively explored within the realms of mathematics, optimization, and artificial intelligence, including approaches such as clustering [38–40] and game theory [41]. Although exact techniques have been applied to this decision-making problem [42,43], the NP-complete computational complexity renders it impractical for larger scenarios. Consequently, heuristics [44–46] and metaheuristics [47, 48], both single [49, 50] and multi-objective [51, 52], have also been proposed to obtain acceptable solutions in reasonable computational times. However, these efforts have focused mainly on employing canonical versions of various metaheuristics without venturing

into more innovative or adapted versions specifically tailored for the CSO challenge.

In the field of multi-objective optimization using metaheuristics, numerous advanced techniques have emerged to enhance the efficiency and effectiveness of algorithmic search processes, such as tabu search [53], simulated annealing [54] and machine learning (ML) in metaheuristics [55]. This thesis focuses on two crucial techniques to understand the fundamentals of the CSO problem. First, exploratory landscape analysis (ELA) [56] is used to characterize and analyze the landscapes of optimization problems. Quantitatively assesses the search space without solving the optimization problem, providing insight into the topology of the landscape, such as the presence of multiple local optima and the structure of attraction basins. Second, the hybridization of metaheuristics [57] with problem-specific search operators informed by ELA insights. These operators aim to modify the landscape based on problem characteristics, facilitating more efficient exploration compared to generic operators. Therefore, hybridization improves solutions by adjusting decision variables based on expert knowledge about the problem.

1.2 Objectives & Research Methodology

In the context of the critical need for energy savings in 5G/6G networks and the untapped potential for advanced optimization not covered in existing literature, the main objective of this thesis is to explore and introduce advanced optimization techniques for enhancing energy efficiency within ultra-dense 5G/6G networks by utilizing multi-objective evolutionary algorithms. This overarching goal is further delineated into detailed objectives, each designed to tackle specific aspects of the energy optimization challenge. These objectives aim to methodically address the various dimensions and complexities involved in optimizing network energy efficiency, thus contributing to the development of more sustainable next-generation wireless communication systems. Through a structured approach, this thesis aims to explore advanced optimization techniques to push the limits of current technologies and propose solutions that improve existing practices in network energy management. In this regard, the specific objectives derived from the main one are as follows:

- O1. Study the impact of traffic spatial heterogeneity in the CSO problem landscape.** Understanding the problem landscape is crucial to proposing advanced optimization techniques. The landscape of a problem provides valuable information on how MOEAs should approach the search for better solutions. In this context, the analysis of the problem

landscape of CSO and its impact due to the deployments of SBSs and UEs is proposed as an objective of this thesis.

O2. Design problem-specific operators to improve metaheuristic searches. Building on the conclusions drawn from the analysis of the landscape of the previous objective, designing problem-specific operators that take advantage of this information is proposed as the second objective of this thesis. These operators will enable the use of the problem-specific knowledge acquired to enhance the search capabilities of the algorithms.

O3. Extending gained expertise to other problems in the field of 5G/6G networks. Extrapolating the experience gained from addressing the CSO problem to another challenge within the 5G/6G networks domain, specifically towards a proposed methodology for analyzing and classifying network flows.

To successfully achieve the proposed objectives, a methodology based on the state-of-the-art review of the CSO problem was adopted. This approach focused specifically on advanced optimization techniques in metaheuristics applied to energy savings in 5G/6G, while also considering other exact and heuristic methods. This review highlighted the limited research surrounding the use of advanced optimization techniques with multi-objective metaheuristics in addressing the problem.

1.3 Thesis Results & Research Collaborations

This section presents the outcomes of the research conducted in this thesis and the collaborations with other researchers throughout the doctoral stage. The research results and contributions of this thesis are encapsulated in the following publications, which collectively support the thesis as a compendium of publications:

- [J1] **J. Galeano-Brajones**, F. Luna-Valero, J. Carmona-Murillo, Antonio J. Nebro, Carlos A. Coello Coello, and J. F. Valenzuela-Valdés, “Landscape-Enabled Algorithmic Design for the Cell Switch-Off Problem in 5G Ultra-Dense Networks,” accepted in *Engineering Optimization*, 2024. Journal Impact Factor: 2.7 (Q2)

- [J2] **J. Galeano-Brajones**, F. Luna-Valero, J. Carmona-Murillo, P. H. Z. Cano, and J. F. Valenzuela-Valdés, “Designing problem-specific operators for solving the Cell Switch-Off problem in ultra-dense 5G networks with hybrid MOEAs,” *Swarm and Evolutionary Computation*, vol. 78, p. 101290, 2023. Journal Impact Factor: 10.0 (D1)

- [J3] **J. Galeano-Brajones**, M. I. Chidean, F. Luna, and J. Carmona-Murillo, “A novel approach for flow analysis in software-based networks using L-moments theory,” *Computer Communications*, vol. 201, pp. 116–122, 2023. Journal Impact Factor: 6.0 (Q1)

Furthermore, the research line followed in this thesis has led to a collaboration with the Wireless Communication Networks Section of the Department of Electronic Systems at Aalborg University (AAU) and Nokia Bell Labs through a three-month research stay in Aalborg, Denmark, in 2023. Nokia is keenly interested in providing energy-saving solutions for 5G/6G networks to achieve zero-emissions mobile networks. In this context, the research stay aimed to merge the interests of both parties by applying the academic knowledge from this thesis to a Nokia-proprietary 3D-map-based radio planner, which incorporates realistic propagation models designed by the company.

In addition to journal articles, several communications related to the thesis content have also been presented or submitted at various national and international conferences:

- [C1] **J. Galeano-Brajones**, J. J. Rico Palomo, M. I. Chidean, and J. Carmona-Murillo, “Detección de ataques de red mediante clasificación de flujos empleando L-momentos,” in *XV Jornadas de Ingeniería Telemática*, pp. 196–203, 2021.
- [C2] A. Quiñones-García, **J. Galeano-Brajones**, P. H. Zapata-Cano, F. Luna-Valero, J. Carmona-Murillo, and J. F. Valenzuela-Valdés, “El efecto de la multiconectividad en el problema del apagado selectivo de redes 5G ultradensas,” in *XIV Congreso Español De Metaheurísticas, Algoritmos Evolutivos y Bioinspirados*, pp. 446–451, 2021.
- [C3] J. J. Espinosa-Martínez, **J. Galeano-Brajones**, J. Carmona-Murillo, and F. Luna, “Binary Particle Swarm Optimization for Selective Cell Switch-Off in Ultra-Dense 5G Networks,” in *International Conference on Swarm Intelligence*, pp. 275–283, Springer, 2022.
- [C4] **J. Galeano-Brajones**, M. I. Chidean, F. Luna, and J. Carmona-Murillo, “Explorando los L-momentos de orden superior en el análisis y clasificación de flujos de red,” in *XVI Jornadas de Ingeniería Telemática*, pp. 43–46, 2023.
- [C5] **J. Galeano-Brajones**, Carlos Pupiales, Daniela Laselva, J. Carmona-Murillo, and Francisco Luna, “Applying Evolutionary Algorithms for Cell Switch-Off to Reduce Network Energy Consumption,” submitted to *IEEE 99th Vehicular Technology Conference (VTC2024-Spring)*, 2024.

Furthermore, in addition to the work carried out in this thesis, the need to meet the objectives of the research projects in which participation occurred has led to conducting research in another area related to cybersecurity in software-defined networks (SDN):

- [J4] **J. Galeano-Brajones**, J. Carmona-Murillo, J. F. Valenzuela-Valdés, and F. Luna-Valero, “Detection and mitigation of DoS and DDoS attacks in IoT-based stateful SDN: An experimental approach,” *Sensors*, vol. 20, no. 3, p. 816, 2020.
- [C6] **J. Galeano-Brajones**, D. Cortés-Polo, J. F. Valenzuela-Valdés, A. M. Mora, and J. Carmona-Murillo, “Detection and mitigation of DoS attacks in SDN. An experimental approach,” in *2019 Sixth International Conference on Internet of Things: Systems, Management and Security (IOTSMS)*, pp. 575–580, IEEE, 2019.

Finally, the doctoral stage has also been worthwhile in establishing connections with other researchers and collaborating on their research lines:

- [J5] J. J. Rico-Palomo, **J. Galeano-Brajones**, D. Cortes-Polo, J. F. Valenzuela-Valdes, and J. Carmona-Murillo, “Chained orchestrator algorithm for ran-slicing resource management: A contribution to ultra-reliable 6G communications,” *IEEE Access*, vol. 10, p. 113662, 2022.
- [J6] A. J. Nebro, **J. Galeano-Brajones**, F. Luna, and C. A. Coello Coello, “Is NSGA-II Ready for Large-Scale Multi-Objective Optimization?,” *Mathematical and Computational Applications*, vol. 27, no. 6, p. 103, 2022.
- [J7] M. Domínguez-Dorado, D. Cortés-Polo, J. Carmona-Murillo, F. J. Rodríguez-Pérez, and **J. Galeano-Brajones**, “Fast, lightweight, and efficient cybersecurity optimization for tactical–operational management,” *Applied Sciences*, vol. 13, no. 10, p. 6327, 2023.
- [J8] M. Domínguez-Dorado, J. Calle-Cancho, **J. Galeano-Brajones**, F.-J. Rodríguez-Pérez, and D. Cortés-Polo, “Detection and mitigation of security threats using virtualized network functions in software-defined networks,” *Applied Sciences*, vol. 14, no. 1, p. 374, 2023.
- [J9] M. Domínguez-Dorado, F. J. Rodríguez-Pérez, **J. Galeano-Brajones**, J. Calle-Cancho, and D. Cortés-Polo, “Fleco: A tool to boost the adoption of holistic cybersecurity management,” *Software Impacts*, p. 100614, 2024.

-
- [J10] J. Calle-Cancho, C. Cruz-Carrasco, D. Cortés-Polo, **J. Galeano-Brajones**, and J. Carmona-Murillo, “Enhancing programmability in next-generation networks: An innovative simulation approach,” *Electronics*, vol. 13, no. 3, p. 532, 2024.
- [J11] Diego Rossit, Francisco Luna Valero, **Jesús Galeano-Brajones**, Javier Carmona-Murillo, “Efficient linear and quadratic approximation models for the cell switch-off optimization problem in ultra-dense networks”, submitted to *International Journal of Industrial Engineering Computations*, 2024.
- [C7] I. García-Aguilar, **J. Galeano-Brajones**, F. Luna-Valero, J. Carmona-Murillo, and J. D. Fernández-Rodríguez, “Prediction of Optimal Locations for 5G Base Stations in Urban Environments using Neural Networks and Satellite Image Analysis”, submitted to *10th International Work-Conference on the Interplay Between Natural and Artificial Computation (IWINAC 2024)*, 2024.

2

EXPLORATORY LANDSCAPE ANALYSIS

This chapter contains two key articles that dive into the landscape of optimizing the CSO problem for energy efficiency in 5G/6G networks to meet objective O1. The first article tackles the CSO issue from a multi-objective optimization standpoint, particularly focusing on the impact of spatial demand heterogeneity in networks and proposing a local search operator to enhance metaheuristic efficiency. The second article addresses the landscape of the CSO problem using a constrained distributed multi-objective evolutionary algorithm alongside a 3D-maps-based radio planner simulator to optimize CSO decisions.

Contents

2.1	Landscape-Enabled Algorithmic Design	12
2.2	3D-Map-Based CSO Optimization in 5G	48

2.1 Landscape-Enabled Algorithmic Design

This paper examines how the heterogeneity of spatial network demands influences the multi-objective optimization landscape, proposing a novel landscape-enabled local search operator to navigate the CSO landscape effectively. This approach deepens our understanding of the complexity of the CSO problem and demonstrates the potential to significantly enhance the efficiency of metaheuristic algorithms in minimizing the power consumption of the network.

THIS IS THE PREPRINT VERSION OF THE PAPER:

J. Galeano-Brajonés, F. Luna-Valero, J. Carmona-Murillo, Antonio J. Nebro, Carlos A. Coello Coello, and J. F. Valenzuela-Valdés, “Landscape-Enabled Algorithmic Design for the Cell Switch-Off Problem in 5G Ultra-Dense Networks,” *Engineering Optimization*, 2024.

- Journal Impact Factor (JIF) in JCR 2022: 2.7
- Category: ENGINEERING, MULTIDISCIPLINARY. JIF Rank: 42/90 (Q2).
- Category: OPERATIONS RESEARCH & MANAGEMENT SCIENCE. JIF rank: 35/86 (Q2).

Supplementary material is available in the Appendix B.

Disclaimer:

This work has been accepted for publication in *Engineering Optimization*.

Copyright:

© 2024 The authors.

Landscape-Enabled Algorithmic Design for the Cell Switch-Off Problem in 5G Ultra-Dense Networks

Jesús Galeano-Brajones¹, Francisco Luna^{2, 3}, Javier Carmona-Murillo¹,
Antonio J. Nebro^{2, 3}, Carlos A. Coello Coello⁴, and Juan F.
Valenzuela-Valdés⁵

¹Dpto. de Ingeniería de Sistemas Informáticos y Telemáticos, Universidad de Extremadura, Centro Universitario de Mérida, Mérida, 06800, Spain, {*jjgaleanobra, jcarmur*}@unex.es

²Dpto. de Lenguajes y Ciencias de la Computación, Universidad de Málaga, E.T.S. de Ingeniería Informática, Málaga, 29071, Spain {*flv, antonio*}@lcc.uma.es

³ITIS Software, Universidad de Málaga, Edificio de Investigación Ada Byron, Málaga, 29071, Spain

⁴Evolutionary Computation Group, CINVESTAV-IPN, Ciudad de México 07360, Mexico, *ccoello@cs.cinvestav.mx*

⁵Dpto. de Teoría de la Señal, Telemática y Comunicaciones, CITIC, Universidad de Granada, Granada, 18014, Spain, *juanvalenzuela@ugr.es*

Abstract

The rapid evolution of mobile communications, notably the fifth generation (5G) and research-stage sixth (6G), highlights the need for numerous heterogeneous base stations to meet high demands. However, the deployment of many base stations entails a high energy cost, which contradicts the concept of green networks promoted by next-generation networks. The Cell Switch-Off (CSO) problem addresses this by aiming to reduce energy consumption in ultra-dense networks without compromising service quality. This article explores the CSO problem from a multi-objective optimization perspective, focusing on how spatial network demand heterogeneity affects the multi-objective landscape of the problem. In addition to the deep

landscape understanding, it introduces a local search operator designed to exploit these landscape characteristics, improving the multi-objective efficiency of metaheuristics. The results indicate that increasing heterogeneity simplifies the exploration of the problem space, with the operator achieving closer approximations to the Pareto front, particularly in minimizing network power consumption.

Keywords: exploratory landscape analysis, multi-objective optimization, metaheuristics, energy efficiency, 5G

List of Abbreviations

5G	5th Generation of Mobile Communications
6G	6th Generation of Mobile Communications
BW	Bandwidth
CSO	Cell Switch-Off
EAF	Empirical Attainment Function
ELA	Exploratory Landscape Analysis
HetNet	Heterogeneous wireless cellular network
HV	Hypervolume
ICT	Information and Communication Technologies
KPI	Key Performance Indicator
MIMO	Multiple-Input Multiple-Output
MOEA	Multi-Objective Evolutionary Algorithm
MOP	Multi-Objective Problem
NSGA-II	Non-Sorting Genetic Algorithm II
PC	Power Consumption
PLO	Pareto Local Optima
PPP	Poisson Point Process
QoS	Quality of Service
RPF	Reference Pareto Front
SA	Social Attractor
SINR	Signal-to-Interference-plus-Noise Ratio
SNR	Signal-to-Noise Ratio
SBS	Small Base Station
UE	User Equipment
UDN	Ultra-Dense Network

1 Introduction

Wireless communication technologies are under constant evolution motivated by use cases and application scenarios that require ever-increasing performance. From the first generation to the fifth (5G) [1], these technologies have operated at higher frequency bands, larger bandwidths, and higher data rates, providing users with enhanced quality of experience. Indeed, even before the first 5G networks were commercialized in 2019 and also coinciding with the 5G standardization [2], industry, academia, and standards organizations have begun to research the sixth generation (6G) of wireless communication systems [3, 4]. Among the key enabling technologies already established for 5G [5], the deployment of a large number of heterogeneous small base stations (SBSs) to increase the spatial reuse of the spectrum is key to improving the network capacity to meet the expected system performance [6]. These are known as ultra-dense networks (UDNs) [7, 8], and are still one of the key development trends for 6G [9, 3].

In this context, both environmental sustainability and operational expenditures are two major issues in Information and Communication Technologies (ICT) [10] in general, and in 5G/6G UDNs in particular [11, 12], as base stations account for 60% to 80% of the power consumption of the cellular network [13] and more than 1000 BS/km² are expected to be deployed [7, 6]. This is especially critical in periods of low or no traffic demands, when most of the SBSs are not serving any user. In these scenarios, either switching off or entering SBSs into sleep mode has been proposed as a useful strategy to enhance energy efficiency [14], which has even been included in the releases of standard bodies [15, 2]. The decision task of selecting which SBSs have to be deactivated has been approached in the literature from different perspectives such as clustering [16, 17], game theory [18] or, more recently, machine learning techniques [19, 20, 21]. This decision problem has also been formulated as a combinatorial optimization problem, named Cell Switch Off (CSO) [22], which is known to be NP-complete [23]. All different flavors of the CSO problem, in either their static [24] or dynamic [25] versions, must consider not only reducing the UDN energy consumption (trivially solved by deactivating all SBSs) but also any key performance indicator (KPI) of the user Quality of Service (QoS). The CSO problem has been addressed with exact [26, 27], heuristic [28, 29] and metaheuristic techniques [30], using a single [31, 32] *vs.* multi-objective [33] approaches. This work falls into the latter research domain, where compromise solutions

between energy consumption and network capacity are sought [34, 35, 36], but aims to deepen the characterization of the multi-objective landscape of the CSO problem to obtain a fundamental understanding of its difficulty and design improved search strategies. Given the nature of CSO, it can be considered as a large-scale sparse multi-objective combinatorial optimization problem [37] because many SBSs can be deactivated when traffic demand is low.

This work has its roots in the seminal work on multi-objective combinatorial landscape analysis by Liefvooghe *et al.* [38], extending the study from multi-objective NK-landscapes to the CSO problem. It aims at gaining insights into how two major problem descriptors, namely the spatial distribution of both the network infrastructure (i.e., SBSs) and the traffic demand (i.e., user equipments, UEs), impact the problem landscape and, hence, the difficulty for multi-objective metaheuristics to address it properly. To the best of our knowledge, this is the first time a study of the CSO problem has been undertaken. Other features considered to characterize the CSO landscape are a set of several black-box local measures that have been estimated from a sample of solutions [39] and computed over the smallest instances tackled in previous works, which have more than 1000 decision variables (the LL scenarios in [36]). As the work pursues realistic settings, global measures have been avoided because they require a full enumeration of the solution space, such as the proportion of Pareto optimal solutions [38], which is not computationally affordable in the context of this optimization problem.

Experiments were conducted over a set of 800 instances with different levels of network densification (i.e., the number of SBSs and UEs per km²) and different degrees of non-uniformity in the SBSs and UE locations throughout the wireless network (i.e., heterogeneity in spatial traffic demand) [40]. We have been able to provide empirical evidence indicating that, according to the exploratory landscape analysis, as long as SBSs and UEs get closer among them (higher non-uniform spatial distribution), the CSO problem becomes easier to solve. On the basis of these results, a novel local search operator that takes advantage of this severity in the heterogeneity of traffic demands has been devised. In order to show its effectiveness, we have generated a new set of instances in which the network is partitioned into several regions, each with different levels of traffic heterogeneity (see Figure 1). In summary, the main contributions of this work are as follows:

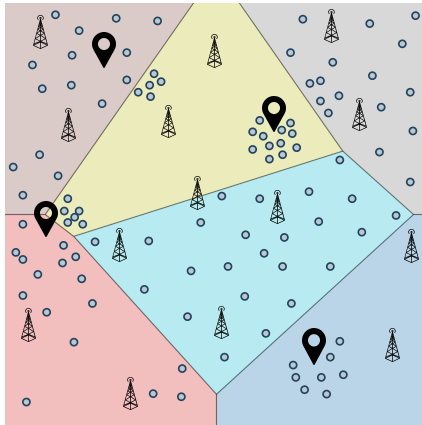


Figure 1: A wireless network with several regions, each one having a different level of non-uniformity in the spatial distribution of the traffic demands. The grey point \bullet represents users of the network, the icon \blacklozenge denotes social attractors, and the \blacktriangle denotes an SBS that includes sectors and cells.

- This is the very first time in which a multi-objective exploratory landscape analysis on a realistic problem like the CSO is carried out. This has required a huge amount of computational effort as realistic instances have been considered for the landscape sampling to capture the inherent problem characteristics.
- A novel landscape-aware local search operator has been engineered to capitalize on previous findings.
- Extensive experiments have been carried out to show empirical evidence of the effectiveness of the newly developed operator.

The rest of the paper is organized as follows. Section 2 outlines the background of this work, defining the CSO problem and the tools used for landscape characterization. Section 3 delves deeply into the analysis of the exploratory landscape analysis of the CSO problem. Then, Section 4 defines the landscape-aware local search operator proposed. Section 5 presents the findings on landscape explorability with respect to heterogeneity and the landscape-aware operator. Finally, Section 6 summarizes the conclusions reached and outlines some future research directions.

2 Background

2.1 The CSO Problem

This section provides the reader with the background related to this work. First, the CSO problem is described, beginning with the modeling of the ultra-dense 5G network, the strategy for user and base station deployment, and the formulation of the problem objectives. Then, the characterization of multi-objective landscapes is outlined.

2.1.1 Network Modeling

The foundation of network modeling is based on that used in previous research (see Section 3 of [36]). For this reason, we have decided to move the complete modeling to Appendix A of this article, limiting ourselves to describing the modifications made in this section.

Regarding the UE-cell association, two modifications have been made to the modeling. First, in previous work, the association was based on the highest SINR (Signal-to-Interference-plus-Noise Ratio) received by the UE. Since interferences are largely mitigated and can be disregarded due to intelligent frequency reuse [41, 42], this article opts instead for the use of the SNR (Signal-to-Noise Ratio). Therefore, the SNR in UE k is defined as follows:

$$SNR_k[dB] = P_{rx,j,k}[dBm] - P_n[dBm] \quad (1)$$

where $P_{rx,j,k}$ represents the signal power received by UE k from cell j , and P_n denotes the noise power (Equation A.5).

Second, the allocation mechanism adapted in this work is based on the theoretical maximum capacity that can be offered to the UE, assuming that the cell has no associated UEs and can dedicate its entire bandwidth to the UE. This mechanism encourages the association of UEs with smaller cells and higher working frequencies, which in turn provide greater capacity while inducing lower consumption.

2.1.2 Deployment Strategy

It is common to find scientific literature where Poisson Point Processes (PPP) are used for the deployment of BSs and/or UEs in mobile networks. This is because PPPs provide a simple mathematical model to represent the random

and spatial distribution in deployments. Additionally, they are useful because the locations of both BSs and UEs in the real world can be quite random and scattered. The PPP model can be extended or modified to accommodate additional network features, such as UEs clustering or spatial correlations, providing a good balance between accuracy and complexity.

In this sense, Mirahsan *et al.* [40] propose to overcome the limitations of PPPs through a heterogeneous spatial model that allows statistical adjustments. The model tweaks two statistical parameters related to the distribution of UEs: the coefficient of variation of a distance measure between UEs and the correlation coefficient between the locations of UEs and BSs. This model is suggested for heterogeneous wireless cellular networks (HetNets) to demonstrate the impact of heterogeneous and correlated traffic with BSs on network performance.

Based on this model, the deployment process used is described as follows.

1. *Deployment of BSs and UEs.* First, the deployment of BSs and UEs is carried out following a PPP.
2. *Deployment of social attractors (SAs).* Subsequently, SAs are deployed randomly in the scenario. These SAs represent real-world points of interest for UEs, such as central streets, shopping centers, etc.
3. *Adjustment of the location of SAs.* Each SA is moved towards its nearest BS in terms of received power, by a factor of $\alpha \in [0, 1]$. Therefore, the new location of the i -th SA is as follows:

$$SA_i^{new} = \alpha BS_{SA_i} + (1 - \alpha) SA_i^{old} \quad (2)$$

where SA_i^{new} is the new location of the SA, SA_i^{old} is the initial location, and BS_{SA_i} is the BS from which SA receives the highest power.

4. *Adjustment of the locations of the UEs.* With the SAs relocated, each UE is moved towards its nearest SA in terms of Euclidean distance, by a factor β . Consequently, the new location of i -th UE is:

$$UE_i^{new} = \beta SA_{UE_i} + (1 - \beta) UE_i^{old} \quad (3)$$

where UE_i^{new} is the new location of the UE, UE_i^{old} the initial location, and SA_{UE_i} is the closest SA. This approach of UEs moving towards

SAs can lead to some areas of the network becoming devoid of UEs. This implies that the distribution of UEs does not change; it simply contracts towards the SAs. To address this problem, the authors of [40] modify the value of β , shifting from a fixed value to modeling it as a random variable $\beta \sim \mathcal{N}(\mu_\beta, \sigma_\beta)$, where μ_β is the mean of β and σ_β is defined as $\sigma_\beta = (0.5 - |\mu_\beta - 0.5|)/3$ to minimize the probability that β falls outside $[0, 1]$. Thus, instead of moving all UEs towards the SAs by a fixed value, the amount of movement is varied according to a normal distribution, which aids in maintaining a more uniform distribution of UEs across the scenario and preventing areas without UEs.

Consequently, by modifying the factors α and β , the spatial distribution of the UEs can be altered in the scenario. This distribution alteration is visible in Figure 2. The figure illustrates the deployments for combinations of α and β that arise from all combinations of values $[0.0, 0.3, 0.6, 0.9]$. Moving to the right implies an increase in the value of β , while moving down indicates an increase in α . Furthermore, each combination of α and β entails limits on the maximum values of the two problem objectives, since a higher concentration of UEs near SBSs will concentrate allocations in a smaller number of cells, thereby resulting in lower consumption, since more cells can be switched off, and lower capacity as the bandwidth is shared among more UEs.

2.1.3 Problem Objectives

Let \mathcal{B} be the set of SBSs deployed by a PPP and \mathcal{C}_b the set of cells in SBS b , for every $b \in \mathcal{B}$. A CSO solution is represented as a bitstring s , where s_c^b indicates whether the cell c in SBS b is active or not. The first objective, minimizing Power Consumption (PC), is achieved as follows:

$$\min f_{PC}(s) = \sum_{b \in \mathcal{B}} P_b \sum_{c \in \mathcal{C}_b} s_c^b \quad (4)$$

where P_b represents the power consumption of SBS b (as detailed in Eq. A.8). It is important to note that P_b includes both the transmission power of each cell c within \mathcal{C}_b and the maintenance power.

Next, to calculate the total capacity of the system, the UEs initially associate themselves with the active cell, providing them with the highest theoretical capacity. Let \mathcal{U} be the set of UEs, also deployed by a PPP, \mathcal{C} the complete set of cells within \mathcal{B} , and $\mathcal{A}(s) \in (0, 1)^{|\mathcal{U}| \times |\mathcal{C}|}$ the matrix where

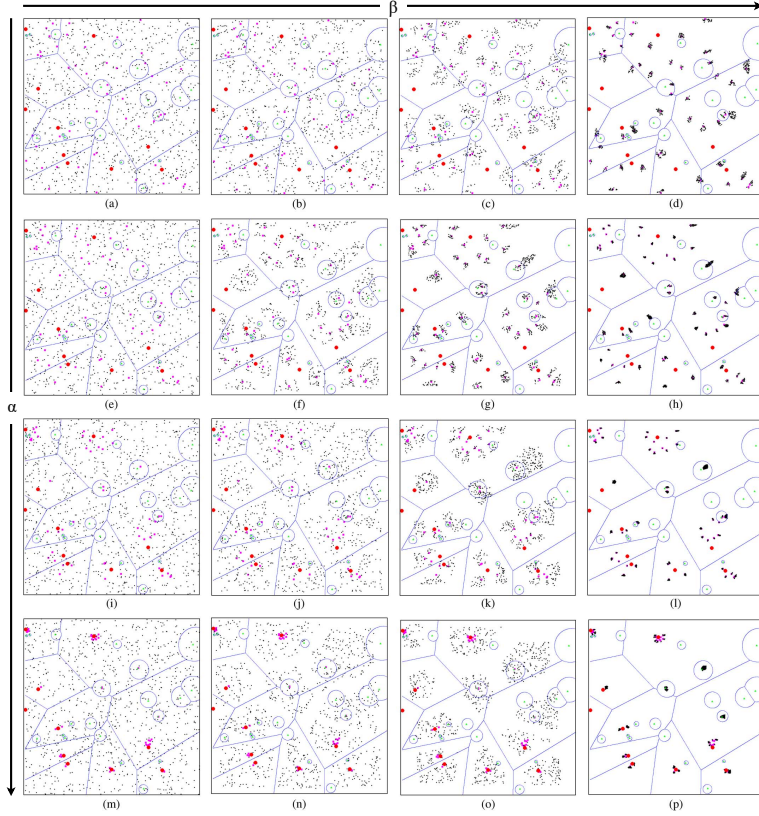


Figure 2: Deployments of UEs and SBSs for combinations of α and β resulting from combining the values 0.0, 0.3, 0.6, and 0.9 for each parameter. In the matrix, moving down the rows indicates an increase in α , while moving to the right in the columns implies an increase in β [40].

$a_{ij} = 1$ if $s_j = 1$ and cell j serves the UE i with the highest theoretical capacity, and $a_{ij} = 0$ otherwise. The second objective, which is to maximize the total capacity (Cap) provided to all UEs, is calculated as follows:

$$\max f_{Cap}(s) = \sum_{c \in \mathcal{C}} \min(C_c^{cumulative}(s), C_c^{max}) \quad (5)$$

$$C_c^{cumulative}(s) = \sum_{i=1}^{|\mathcal{U}|} \sum_{j=1}^{|\mathcal{C}|} s_j \cdot a_{ij} \cdot C_i^j \quad (6)$$

where $C_c^{cumulative}(s)$ is the cumulative capacity that cell $c \in C$ provides to the UEs in the scenario. C_c^{max} represents the maximum capacity that cell c can offer, calculated assuming an $SNR = 25$ dB. C_i^j denotes the capacity that cell j provides to UE i (as detailed in Eq. A.6). The term $\min(C_c^{cumulative}(s), C_c^{max})$ ensures that capacities that exceed the maximum capacity threshold set in cells are not added to the capacity objective. It is crucial to note that the two objectives of the problem conflict: turning off cells leads to reduced network consumption but also affects the capacity provided to UEs. This conflict occurs because the switching off of cells increases the UE-cell distance (leading to higher propagation losses) and decreases the available bandwidth for serving the UEs.

It is also crucial to note the assumption that there is always a macrocell on in the scenario to prevent UEs from losing service. This macro cell is not included in the calculations of the objectives of the problem because the goal is to optimize the ultra-dense heterogeneous network. This provision ensures that, despite efforts to conserve energy by switching off certain cells, the fundamental service provision of the network (its capacity to connect UEs) is preserved, aligning with the core objective of balancing energy efficiency with service quality in ultra-dense network environments.

2.2 Multi-Objective Landscape Characterization

This section briefly describes the multi-objective landscape features that are the basis of this work, which can be categorized into global and local features, as defined in [38], and how they are measured. On the one hand, global features require enumerating the entire search space to be computed. They include, for example, the proportion of Pareto optimal solutions, the distance among them, their connectedness, etc. Given the context of our problem, set within a realistic scenario where the smallest instance of interest contains over 1000 binary decision variables, these characteristics become impractical. On the other hand, local features are computed from the neighborhood of a sample of solutions and make the numerical effort affordable.

Before going into the details of the particular measures used, it is important to describe how sampling is performed. As defined in the previous section, a

solution to the CSO problem is a binary string, and for such a representation, we have used a neighborhood structure at a Hamming distance of 1. Therefore, sampling is a walk over such an induced landscape, defined as an ordered sequence of solutions (x_0, x_1, \dots, x_l) , such that x_t is neighbor of x_{t-1} [43]. Walks can be either random when neighbors are selected randomly at each step, or adaptive when an improved neighbor is required for the walk to continue. Random walks enable the computation of the first autocorrelation coefficient, which is a measure that characterizes the ruggedness of the landscape (the larger, the smoother) [43, 44]. This autocorrelation measure does not make sense in adaptive walks, as the solutions are better at each step. Finally, while the length of a random walk, l , is defined in advance, for adaptive walks, this measure is the number of steps until the walk gets trapped in a local optimum.

3 Landscape Analysis of the CSO Problem

This section outlines the landscape features and descriptors of the CSO problem used in this study, as well as the experimental setup that includes the preliminary studies and the correlations obtained.

3.1 Landscape Features

Before describing the experimental setup, it is crucial to thoroughly understand each of the landscape features used in this study and the descriptors of the CSO problem. Table 2 contains the nomenclature for each feature or descriptor, a brief description, and, where applicable, the reference to the work from which it was derived.

Regarding the problem descriptors, two proximity factors can be shown. As detailed in Section 2.1.2, the first is the proximity factor of each SA to the closest SBS, denoted as α , and the second is the proximity factor of each UE to its closest SA, denoted as β . These descriptors are fundamental for the subsequent discussion of the correlations and the design of the landscape-aware local search operator.

Following the problem descriptors in Table 2, we can show the local landscape features classified into three types: those related to the hypervolume indicator (HV) [45], Pareto dominance, and the solutions. The first two types are based on the work of Liefoghe *et al.* [38], while the last type is

predominantly a contribution of this study. It is important to note that, as detailed in Section 2.2, obtaining the correlation between the objectives and the autocorrelation coefficients is not useful for adaptive walks. HV is a Pareto-compliant quality indicator widely used in the multi-objective community because it is able to gather information about the convergence and diversity of non-dominated solutions among the approximations to the Pareto front in one scalar value. It is computed by summing up the volume in the objective space enclosed by a given set of the non-dominated solutions. The higher the HV, the better.

Regarding the HV, three features are identified: `hv_avg`, `hvd_avg`, and `nhv_avg`. The first feature provides information on the average HV of the solutions in the walk, the second gives the average HV difference between the solutions of the walk and those of each neighborhood, and the last indicates the average HV of each neighborhood. Moreover, from random walks, we can also obtain the first autocorrelation coefficients (named `r1`) for these three features (`hv_r1`, `hvd_r1`, and `nhv_r1`). As explained in Section 2.2, the first autocorrelation coefficient of features related to HV provides information on the ruggedness of the landscape. In particular, a strong correlation with `hv_r1` indicates that local improvements are easily achievable through neighborhood exploration. This information is crucial for the local improvement strategy proposed in this article for the CSO problem.

Furthermore, features related to the dominance among the solutions of the walk and their neighborhoods can be derived, in addition to those associated with HV. In this sense, we find the proportion of dominated neighbors (`#inf_avg`), dominating neighbors (`#sup_avg`), and incomparable neighbors (`#inc_avg`). We also obtain the first autocorrelation coefficients for these features to observe trends in dominance throughout the random walks.

Among the other features of the solution, some define proportions (starting with `#`) and are identified by the type of cell (micro, pico, or femto) and the type of support structure (SBS, sector, or cell). In this context, some features define the average proportion of active structures for microcells (`#micro_sbs_on_avg`, `#micro_sector_on_avg`, and `#micro_cell_on_avg`), picocells (`#pico_sbs_on_avg`, `#pico_sector_on_avg`, and `#pico_cell_on_avg`), and femtocells (`#femto_sbs_on_avg`, `#femto_sector_on_avg`, and `#femto_cell_on_avg`). An SBS and a sector are considered active if at least one of their cells is active. Furthermore, the average proportion of UEs allocated to each type of cell is defined as a descriptor (`#micro_ue_avg`, `#pico_ue_avg`, and `#femto_ue_avg`).

Furthermore, another defined descriptor is the average distance from each UE to the nearest cell of each type (`micro_dist_avg`, `pico_dist_avg`, and `femto_dist_avg`). The features related to the objectives of the problem are also defined: first, there is an estimation of the correlation between the objective values obtained from random walks (`f_cor`); second, we obtain the average values of the objectives from the walk (`obj1_avg` and `obj2_avg`) along with their correlation coefficients (`obj1_r1` and `obj2_r1`). Finally, from adaptive walks, we can obtain the walk length (`walk_length`) to know the number of steps needed to reach a Pareto local optima (PLO).

Problem descriptors		
α	Closeness factor of the SA to the nearest SBS	Eq. 2
β	Closeness factor of the UE to the nearest SA	Eq. 3
Local landscape features related to the HV indicator		
<code>hv_avg</code>	Average single solution's HV value	[38]
<code>hv_r1</code>	First autocorrelation coefficient of single solution's HV value (from random walks)	[46]
<code>hvd_avg</code>	Average single solution's HV difference value	[38]
<code>hvd_r1</code>	First autocorrelation coefficient of single solution's HV difference value (from random walks)	[46]
<code>nhv_avg</code>	Average neighborhood's HV value	[38]
<code>nhv_r1</code>	First autocorrelation coefficient of neighborhood's HV value (from random walks)	[38]
Local landscape features related to the Pareto dominance		
<code>#inf_avg</code>	Average proportion of neighbors dominated by the current solution	[38]
<code>#inf_r1</code>	First autocorrelation coefficient of the proportion of neighbors dominated by the current solution (from random walks)	[38]
<code>#sup_avg</code>	Average proportion of neighbors dominating the current solution	[38]
<code>#sup_r1</code>	First autocorrelation coefficient of the proportion of neighbors dominating the current solution (from random walks)	[38]
<code>#inc_avg</code>	Average proportion of neighbors incomparable to the current solution	[38]
<code>#inc_r1</code>	First autocorrelation coefficient of the proportion of neighbors incomparable to the current solution (from random walks)	[38]
Features of the solutions		
<code>#micro_sbs_on_avg</code>	Average proportion of active micro-SBS	
<code>#micro_sector_on_avg</code>	Average proportion of active micro-sectors	
<code>#micro_cell_on_avg</code>	Average proportion of active microcells	
<code>#pico_sbs_on_avg</code>	Average proportion of active micro-SBS	
<code>#pico_sector_on_avg</code>	Average proportion of active micro-sectors	
<code>#pico_cell_on_avg</code>	Average proportion of active microcells	
<code>#femto_sbs_on_avg</code>	Average proportion of active micro-SBS	
<code>#femto_sector_on_avg</code>	Average proportion of active micro-sectors	
<code>#femto_cell_on_avg</code>	Average proportion of active microcells	
<code>#micro_ue_avg</code>	Average proportion of UEs allocated with microcells	
<code>#pico_ue_avg</code>	Average proportion of UEs allocated with picocells	
<code>#femto_ue_avg</code>	Average proportion of UEs allocated with femtocells	
<code>micro_dist_avg</code>	Average distance from the nearest microcell to the UEs	
<code>pico_dist_avg</code>	Average distance from the nearest picocell to the UEs	
<code>femto_dist_avg</code>	Average distance from the nearest femtocell to the UEs	
<code>f_cor</code>	Estimated correlation between the objective values (from random walks)	[38]
<code>obj1_avg</code>	Average single solution's value of the first objective	Eq. 4
<code>obj1_r1</code>	First autocorrelation coefficient of the single solution's value of the first objective (from random walks)	
<code>obj2_avg</code>	Average single solution's value of the second objective	Eq. 5
<code>obj2_r1</code>	First autocorrelation coefficient of the single solution's value of the second objective (from random walks)	
<code>walk_length</code>	Average length of adaptive walks	[47]

Table 2: Problem descriptors, multi-objective landscape features, and characteristics of the solutions considered in this article.

3.2 Experimental Setup

3.2.1 Preliminary Studies

Given that the CSO problem is a real-world telecommunication challenge, the computational costs (both memory and computational time) are considerable. For this reason, before performing the walks, collecting landscape features and problem descriptors, and calculating correlations, we conducted preliminary studies to improve efficiency without losing landscape information on the problem.

As described in Appendix A, we define 9 types of scenarios with different densities of SBSs and UEs for the problem. Additionally, we used 50 different random seeds to generate 50 similar instances of the scenario, each consistent in terms of the densities of SBSs and UEs. Consequently, we dealt with a total of 450 instances. Therefore, before beginning the exploratory landscape analysis, we performed consistency tests of the features across the different density scenarios. This approach allowed us to focus on working with the 50 seeds of the lower-density scenario (that is, the one requiring the smaller computational resources) so that the conclusions drawn could be extrapolated to the rest of the 9 scenarios. Following this preliminary study, we concluded that there were no significant differences in the correlations found across the nine scenarios. Hence, we decided to focus on the lower-density scenario for exploratory landscape analysis in this work.

Then, another study was conducted to determine the maximum length of the random walks. To be consistent with previous works where we used 100000 evaluations as the stopping condition of the algorithms, we decided to set the walk size to the same number. However, we faced a significant time challenge: exploring the entire neighborhood at each step of the walk. As mentioned above, our analysis focused on the lower-density instance, meaning fewer decision variables. However, considering the landscape analysis required to evaluate the entire neighborhood at each step of the walk, we would need to perform roughly about 120 million evaluations per walk, which is unfeasible for a real-world problem. Consequently, we decided to evaluate if, instead of exploring the entire neighborhood, we could explore just a portion of it, which resulted in that we can limit our exploration to 5% of the neighborhood without losing information in the correlations while achieving a significant gain in computational time. The selection of which neighbors are explored is carried out through a random sampling of the complete neighborhood.

3.2.2 Correlations

In the analysis of landscape characteristics in multi-objective problems, understanding the interdependencies between different variables is crucial. For this purpose, the Kendall rank correlation coefficient [48], τ , a robust and nonparametric statistical measure, is used to quantify the association between two variables. The coefficient τ is calculated based on the number of concordant and discordant pairs in the dataset. A data pair is considered concordant if the observations in both variables maintain the same order; that is, if one observation is greater than another in one variable, it is also greater in the other. Conversely, a pair is deemed discordant when the order of observations in the two variables is opposite. The coefficient τ is calculated using the formula $\tau = \frac{N_c - N_d}{\sqrt{(N_0 - N_1)(N_0 - N_2)}}$, where N_c and N_d represent the number of concordant and discordant pairs, respectively. Here, $N_0 = \frac{n(n-1)}{2}$ is the total number of possible pairs in the dataset, with n being the number of observations. The terms $N_1 = \sum t_i(t_i - 1)/2$ and $N_2 = \sum u_i(u_i - 1)/2$ adjust the calculation of the ties within each of the variables, where t_i and u_i are the numbers of ties at the i^{th} observation of each variable, respectively. A value of τ close to 1 indicates a strong positive correlation, while a value close to -1 implies a strong negative correlation. A value around 0 implies no correlation. This coefficient is particularly useful in our study as it does not assume a linear relationship between the variables and is resilient to the presence of outliers.

To visually display the correlations between different features and descriptors, we have generated correlation boards for samples from adaptive walks and random walks, which are interpreted similarly to a correlation matrix. Blue circles indicate a positive correlation, while red circles indicate a negative correlation. The intensity of the color and the size of the circle are proportional to the strength of the correlation. Additionally, to provide an alternative visualization of the relationship between features, we have generated dendrograms using Ward’s hierarchical agglomerative clustering method [49]. This method allows us to separate clusters of features based on their dissimilarity, offering another layer of information about the landscapes and the justification of the correlations visualized in the boards.

Taking into account the wide range of features to be analyzed, this article focuses on three distinct subgroups: dominance, HV, and solution features, with a special emphasis on the problem descriptors α and β . Additionally,

the analysis of data collected through adaptive walks and random walks is conducted separately. This approach provides a comprehensive understanding of their respective behaviors within the solution space of the problem. Therefore, the correlations obtained through adaptive walks are represented on the correlation board in Figure 3, and in the dendrogram in Figure 4. Meanwhile, those obtained by random walks are shown in Figure 5, and the corresponding dendrogram in Figure 6.

Dominance-related features for adaptive walks From Figures 3 and 4, there is one main finding that can be drawn about the landscape and complexity of the problem, taking into account these features and the problem descriptors α and β . There is a strong correlation with `walk_length`, which suggests that, as long as SBSs and UEs are closer to each other (a higher level of clustering and, equivalently, a higher level of spatial heterogeneity in traffic demand), the landscape becomes easier to explore. Indeed, the number of steps of the adaptive walk increases, i.e., it is easier to find an improving solution. The positive correlation with `obj1_avg`, `obj2_avg`, `hv_avg` and `nhv_avg` corroborates this fact: the higher the values of α and β , the better the objectives of the problem, and thus the better the HV of the solutions and the neighborhood. A more clear trend can be seen in Table 3, where the data collected over the different β values is aggregated for different landscape features. It can be seen that the proportion of non-dominated solutions (`#inc_avg`) decreases with β , whereas the proportion of worse/dominated (`#inf_avg`) and better/dominating `#sup_avg` solutions increases. That is, on the one hand, the landscape is more informative (fewer non-dominated solutions, thus reducing the existence of plateaus), and, on the other hand, the probability of moving to an improving neighbor increases. Further experimentation conducted in Section 5 will support this fact.

β	<code>hv_avg</code>	<code>#inc_avg</code>	<code>#inf_avg</code>	<code>#sup_avg</code>
0.0	0.5735	0.2010	0.5951	0.2017
0.3	0.5667	0.1864	0.6063	0.2051
0.6	0.5642	0.1460	0.6373	0.2147
0.9	0.6137	0.0718	0.6936	0.2328

Table 3: Dominance-related landscape features aggregated over different values of β .

HV-related features for adaptive walks Apart from the correlations with `hv_avg` and `nhv_avg` discussed earlier, the negative correlation of α and β with `hvd_avg` suggests that a higher level of clustering implies greater variability in the HV of solutions compared to their neighborhoods. This indicates that as the spatial heterogeneity of traffic demands increases, the differences in HV between a solution and its surrounding solutions become less pronounced, reflecting a more uniform landscape. Therefore, higher values for α and β result in landscapes that are easier to explore.

Solution-related features for adaptive walks The spatial heterogeneity generated by α and β also has effects on the features of the solution traversed by the adaptive walk. Specifically, greater heterogeneity tends to produce solutions with a higher proportion of UEs associated with femtocells (positive correlation with `#femto_ue_avg`) and lower with microcells (negative correlation with `#micro_ue_avg`). Given that `hv_avg` and `nhv_avg` correlate positively with `#femto_ue_avg`, it can be observed that the associations of solutions that improve the objectives of the problem and the HV are primarily made with femtocells. This hypothesis is reinforced by the positive correlation of `#sup_avg` and slightly negative correlation of `#inf_avg` with `#femto_cell_on`, indicating that cell activation favors neighborhoods with a higher proportion of non-dominated solutions. Furthermore, the negative correlation of `#femto_ue_avg` with `hvd_avg` suggests that the difference in HV is smaller with a higher proportion of such associations. From this, it can be inferred that the ruggedness of the landscape is smoother in areas of high HV.

Dominance-related features for random walks Regarding the dominance features from random walks, a clear conclusion can be drawn with α and β : greater clustering results in neighborhoods with higher proportions of both dominated (strong positive correlation with `#inf_avg`) and non-dominated (strong positive correlation with `#sup_avg`) solutions compared to incomparable ones. This reinforces the hypothesis that a higher concentration of UEs towards SBSs makes the landscape easier to explore.

HV-related features for random walks The strong positive correlations of the problem descriptors with `hv_avg` and `nhv_avg` indicate that the solutions tend to be of higher quality in random samplings, corroborating the hypothesis

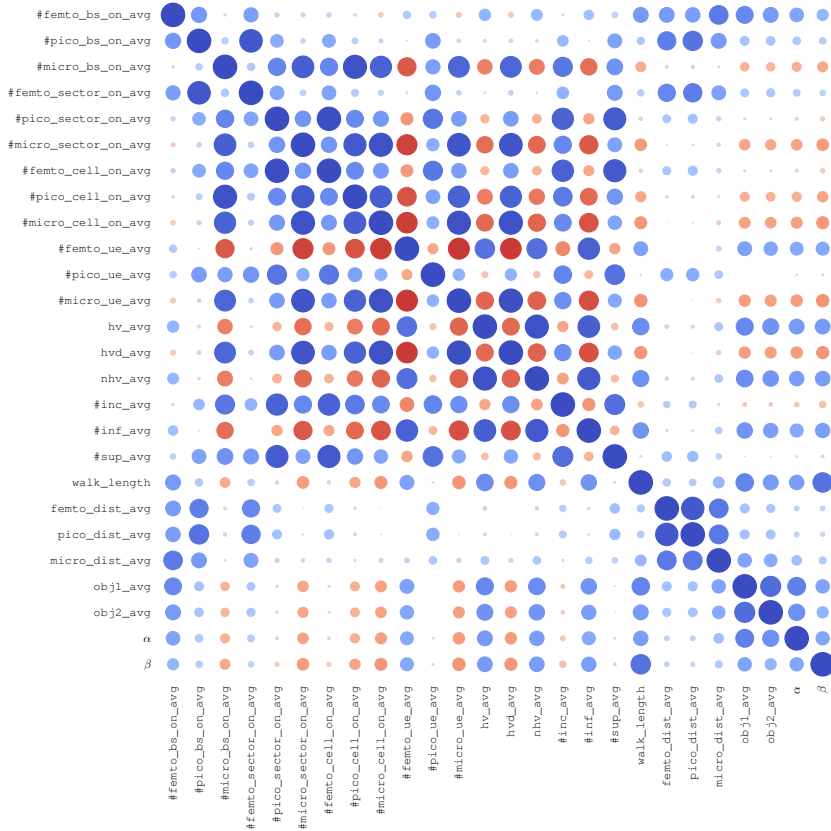


Figure 3: Correlation board for the features obtained through adaptive walks. Blue color indicates a positive correlation, while red color implies a negative correlation. Moreover, the intensity of the color and the size of the circle are proportional to the strength of the correlation.

that the landscape becomes easier to explore.

Solution-related features for random walks The correlations between the characteristics that define the proportion of active microcells and, to a lesser extent, picocells, with `#inc_avg` indicate that the highest proportion

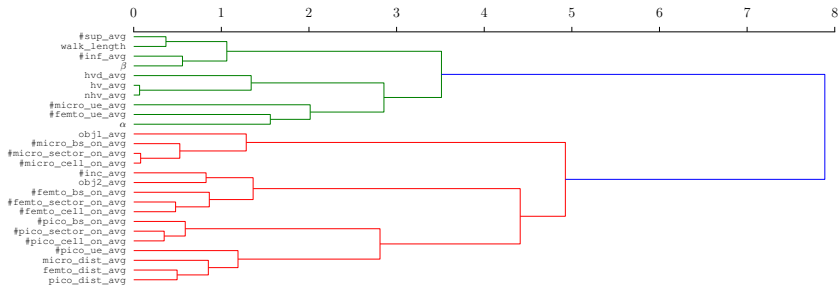


Figure 4: Ward’s dissimilarity measure among the features obtained through adaptive walks.

of incomparable solutions is found when many microcells are active and, therefore, when there is a higher `hvd_avg`. This suggests that the ruggedness of the landscape is greater, making it more difficult to explore. Additionally, `#inf_avg` and `#sup_avg` have a very positive correlation with cells operating at higher frequencies, particularly femtocells. Therefore, having a higher proportion of active femtocells, and to a lesser extent picocells, results in a higher proportion of both dominated and non-dominated solutions and a landscape easier to explore due to the more uniformity of the landscape, that is, less ruggedness. Consequently, it can be concluded that femtocells are key in guiding the search toward more promising areas of the landscape, while microcells present greater challenges. Regarding `hv_r1`, a negative correlation is observed with `#micro_cell_on_avg`, indicating that activating microcells leads to greater variability in HV throughout the walk. Furthermore, the strong positive correlation with `#femto_ue_avg` and negative with `#micro_ue_avg` suggest that favoring the use of femtocells tends to result in solutions with more similar HV values during the walk.

Finally, combining each analysis, two key conclusions can be drawn: a greater spatial heterogeneity in traffic demands results in a landscape that is easier to explore, and femtocells are of great importance for improving problem objectives and HV values. A previous paper [36] already elaborated on the line of this latter conclusion, in which the working hypothesis was that activation of femtocells can improve the search process. This was demonstrated by devising problem-specific operators. Meanwhile, the first conclusion is further developed in this article through the design of a local search operator that

leverages the information obtained with spatial traffic heterogeneity.

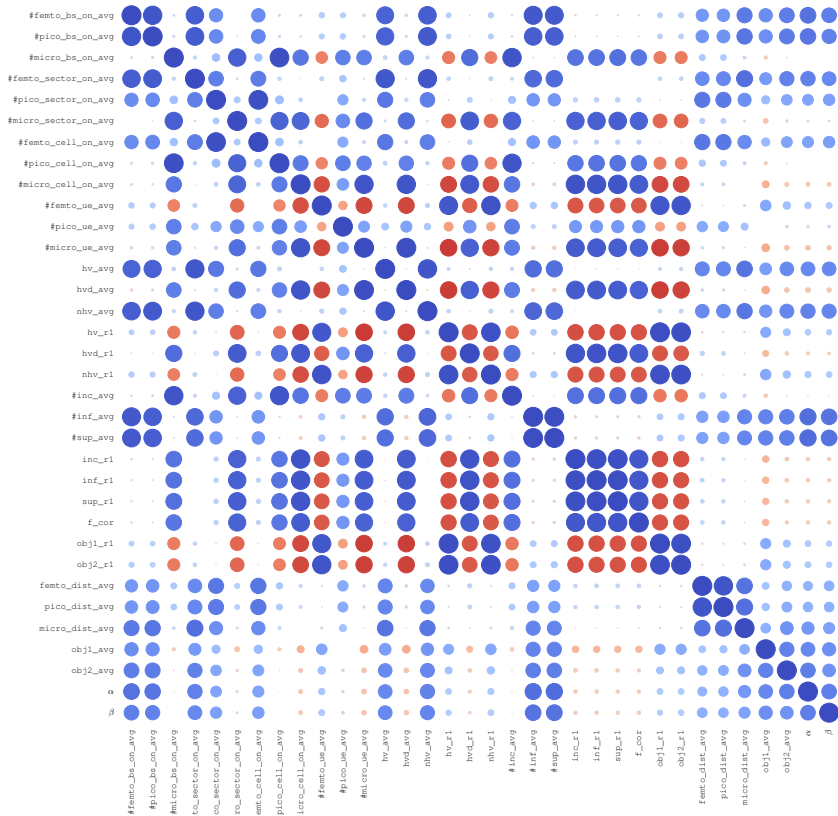


Figure 5: Correlation board for the features obtained through random walks.

4 Landscape-Aware Local Search

This section is devoted to describing a design of a local search operator that capitalizes on the knowledge acquired about the landscape characteristics detailed in the previous section. One of the key insights from the landscape

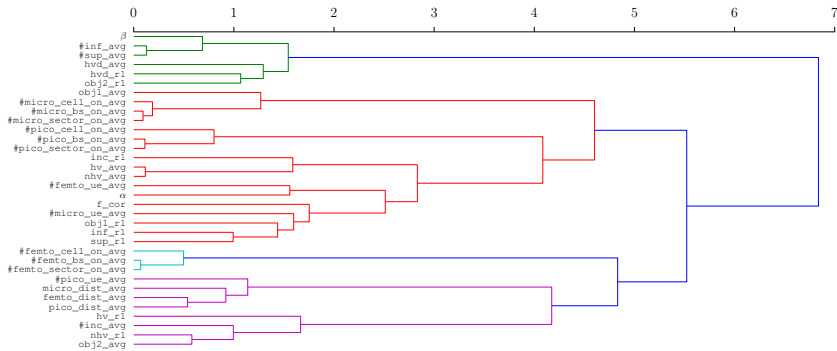


Figure 6: Ward’s dissimilarity measure among the features obtained through random walks.

analysis of the CSO problem is that greater spatial traffic heterogeneity makes local exploration of the search space easier. This is due to the proximity of UEs to SBSs, which makes higher-frequency cells (femtocells and, to a lesser extent, picocells) crucial for the optimization process. These types of cells have a low energy consumption and a high capacity, thus meeting the demands in small, highly-density areas. On the contrary, their size (i.e., the area they can serve) is small, thus UEs have to be close enough to establish a high-quality wireless link.

Algorithm 1 outlines the designed local search operator, which is based on performing a tailored adaptive walk (see Section 2.2) starting from a given solution chosen with a given rate, and that ends in a Pareto local optimum. The strategy of the operator is similar to that of a multi-objective hill climber. Still, the key aspect of the operator is the utilization of landscape information in the determination of how the neighborhood of each solution is explored. In the standard case, the neighborhood just consists of all solutions at a Hamming distance of 1 from the solution that is explored randomly (one randomly chosen neighbor at each time, moving only towards an improving one). The newly devised strategy uses the landscape information so that the neighborhood is biased according to the value of the proximity factor β . This is achieved by the way the neighborhood is explored, so that those cells located in areas where the spatial heterogeneity of the traffic demands is low (i.e., those in which β is known to be low and thus with more difficult

landscape) are visited first, to identify the improvement neighbors in that area. Specifically, a Hamming neighbor would become part of the neighborhood with a probability of $1 - \beta$ (as detailed in lines 4-5 of Algorithm 2).

Algorithm 1 Landscape-aware local search operator

```

1: procedure LOCALSEARCHOPERATOR(solution, rate)
2:   if RANDOM() < rate then
3:     current ← COPY(solution)
4:     last ← COPY(solution)
5:     EVALUATE(current)
6:     plo ← false
7:     while ¬plo do
8:       current ← GETDOMINANTNEIGHBOR(current)
9:       if current is null then
10:        plo ← true
11:       else
12:        last ← COPY(current)
13:       end if
14:     end while
15:   end if
16:   return last
17: end procedure

```

5 Results

This section presents a brief experimentation to validate the effectiveness of the local search operator that incorporates landscape information. First, the methodology is outlined, and then, two experiments are conducted to, on the one hand, validate the hypothesis that increased spatial heterogeneity of traffic makes an easier landscape to explore and, on the other hand, to undertake a preliminary comparison between the newly devised aware operator and a standard multi-objective hill climber to show that our proposal can effectively profit from the landscape information.

Algorithm 2 Get a dominant solution of the landscape-aware Hamming neighborhood

```

1: procedure GETDOMINANTNEIGHBOR(current)
2:   neighborhood  $\leftarrow$  []
3:   for i  $\leftarrow$  0 to GETNUMBEROFCELLS(solution) do
4:     probability  $\leftarrow$  1 - GETBETA(solution.GetCell(i))
5:     if random  $\leq$  probability then
6:       neighbor  $\leftarrow$  COPY(solution)
7:       neighbor.FlipBit(i)
8:       neighborhood  $\leftarrow$  neighborhood + [neighbor]
9:     end if
10:  end for
11:  neighborhoodSize  $\leftarrow$  SIZEOF(neighborhood)
12:  permutation  $\leftarrow$  GETINTEGERPERMUTATION(neighborhoodSize)
13:  for each i in permutation do
14:    neighbor  $\leftarrow$  neighborhood.GetNeighbor(i)
15:    EVALUATE(neighbor)
16:    if DOMINATES(neighbor, current) then
17:      return neighbor
18:    end if
19:  end for
20:  return null
21: end procedure

```

5.1 Experimental Methodology

NSGA-II [50] has been used as the base multi-objective solver in all the experiments. It has been configured to use a binary string representation with binary tournament selection, two-point crossover with a probability of 0.9, and bit flip mutation with a probability of $1/L$, where L is the total number of cells in the scenario. Furthermore, 100,000 evaluations have been used as the stopping condition. This metaheuristic configuration is inherited from [36].

NSGA-II has been hybridized by applying the local search operator right after the application of the crossover and mutation operators. The local search then starts from a given solution and continues until it converges to a Pareto local optimum, and at this point, it is inserted back into the

population. The evaluations of the objective functions consumed during the search are also counted towards reaching the stopping condition for a fair comparison, which means that, if the local search is applied with higher probabilities, the number of NSGA-II iterations is reduced, thus limiting the evolutionary process. Regarding the probability of application of the operator, the experiments were conducted with values of 0.001, 0.010, and 0.100.

5.2 Analysis of the Spatial Heterogeneity Impact on Landscape Explorability

For this exploratory analysis, the hybrid NSGA-II has been tested in 7200 different instances of the CSO problem, which is the result of performing an execution for each of the 50 different random seeds across the 9 density scenarios described in Appendix A and the 16 different heterogeneity factors devised in Figure 2 of Section 2.1.2. Considering the application of the three rates of the operator and the runs of the canonical metaheuristic, that is, without the local search operator, a total of 28,000 runs have been carried out.

In Figure 7, the difference in the HV values between the runs with the application of the multi-objective hill climber and the canonical metaheuristic is displayed (the raw HV values can be found in Appendix C). For this, the HV values have been averaged across all scenarios and seeds, in addition to the values of α , as β is the factor that shows more significant differences, as discussed in Section 3. This experiment aims to show that the HV difference tends to decrease with a higher value of β and, as a consequence, the exploration of the search space of the canonical NSGA-II with any intensification mechanism such as the multi-objective hill climber is able to reach much closer approximations to the Pareto fronts than those computed by the hybrid version of the algorithm. It can be concluded that the landscape can be easily explored when β is higher, that is, when traffic demands (UEs) are more clustered around the SBSs (cells).

The fact that the difference slightly increases for medium heterogeneity values, especially for the application ratio of 0.010, may be because an increase in β for a higher α does not strictly indicate lower heterogeneity in some cases. In Figure 2 of Section 3.2, it is observed that in deployment (k), with a higher α , there is greater heterogeneity than in (g), although the factor is lower. This issue could be responsible for the values observed for medium

heterogeneity.

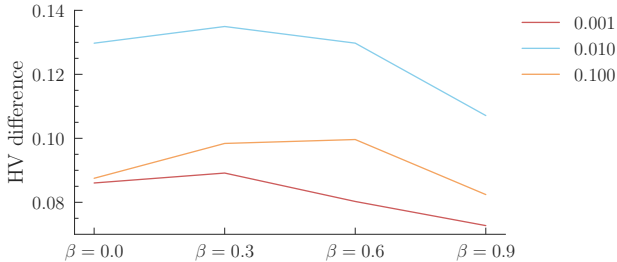


Figure 7: Average differences between the various application rates and the metaheuristic without local search.

To visually illustrate these differences, Figure 8 includes the attainment surfaces [51] for the HH scenario, the one with the highest density of UEs and SBSs. The empirical attainment function (EAF) [51] facilitates a graphical examination of the approximated Pareto fronts. Specifically, the EAF visually represents the expected performance and its variability of the Pareto fronts approximated by the multi-objective algorithm across several iterations. To put it simply, within the context of multi-objective optimization, the 50%-attainment surface serves a role similar to the median in single-objective optimization scenarios. The rest of the scenarios can be consulted in Appendix B. Therefore, in Figure 8 it can be observed that as the values of α and β increase, the difference between the Pareto front approximations with and without the application of the search operator decreases to the point of being very similar fronts. This corroborates that greater heterogeneity eases the search, and the metaheuristic does not require local search operators to achieve similar results. On the contrary, lower heterogeneity creates a landscape more amenable to the local search operator, particularly for improving the power energy consumption objective of the network.

5.3 Comparative Analysis of Local Search Operators Performance

To verify the effectiveness of the landscape-aware operator and validate the findings drawn from the feature correlations in Section 3.2, the hybrid NSGA-II

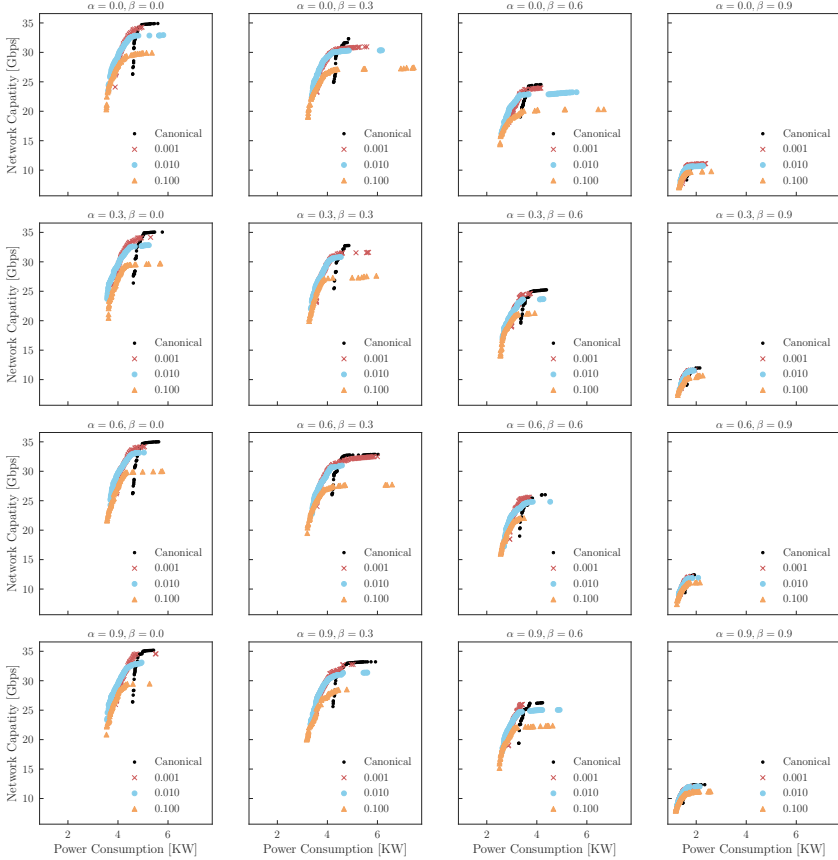


Figure 8: Approximations to the Pareto front for the different rates of application of the multi-objective hill climber in the HH scenario.

has been tested against 450 different instances. The spatial heterogeneity of traffic is divided into quadrants, with three of them exhibiting high heterogeneity ($\alpha = \beta = 0.9$), and one with low heterogeneity ($\alpha = \beta = 0.0$). Consequently, the landscape-aware operator will focus on improving the three quadrants with lower heterogeneity, which are inherently more challenging to explore, rather than concentrating efforts on the more navigable area of the

landscape, i.e., the network area with higher heterogeneity. In contrast, the multi-objective hill climber does not differentiate between areas, performing searches regardless of heterogeneity (i.e., the neighbors to be explored are chosen in a randomly uniform manner).

Figure 9 displays the HV gain achieved by the landscape-aware operator compared to the multi-objective hill climber for three different application rates: 0.001, 0.01, and 0.1. The application rate of 0.1 consistently provides the highest gain across all nine density scenarios. The 0.001 rate shows improvements in the majority of scenarios, seven out of nine, but these are quite marginal. The 0.01 rate achieves the least gains, outperforming the operator in only three of the nine scenarios. Nevertheless, for all rates, there is a discernible trend in scenarios of higher density, and it is more advantageous to apply the landscape-aware operator.

The results lead to the finding that landscape information, particularly regarding the spatial heterogeneity of network traffic, enables the enhancement of the outcomes of the metaheuristic. Conducting local searches targeted at more complex areas of the landscape allows the metaheuristic to achieve better approximations to the Pareto front, using the same stopping condition.

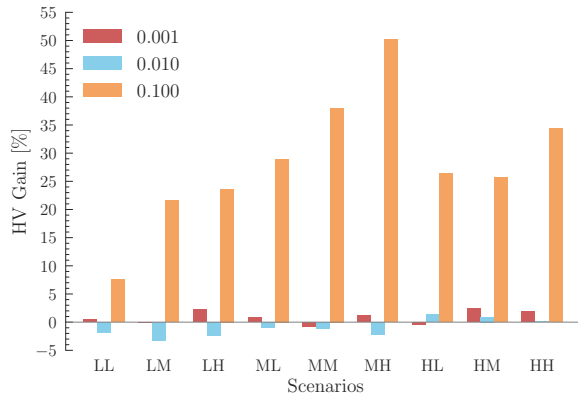


Figure 9: HV gain achieved by the landscape-aware operator compared to the multi-objective hill climber for three different application rates.

6 Conclusions and Future Work

After an in-depth analysis of the landscape of the CSO problem and examination of correlations between various features, this study has shown that an increase in the spatial heterogeneity of network traffic significantly smoothens the landscape, thus facilitating its exploration. To leverage this understanding, a novel search operator has been developed specifically to enhance multi-objective metaheuristics. This operator is designed to navigate the complexities of the landscape effectively, focusing on areas of the network characterized by lower heterogeneity. These regions, typically more challenging due to their uniformity, present unique opportunities for optimization that had previously been untapped. By strategically exploiting the information gleaned from the landscape analysis, the operator guides the search process towards more promising regions of the solution space. The empirical evidence presented confirms the efficacy of the operator, showcasing its ability to achieve better approximations to the Pareto front compared to traditional methods.

For future work, several directions are proposed that continue with the analysis of the problem landscape. First, an analysis of other problem descriptors, such as the association between UEs and cells, will be carried out. Second, we aim to continue the study of proposals for landscape-aware operators and genetic operators capable of operating with the information obtained from the landscape. Third, a study will be conducted on the problem-specific operators proposed in previous works to examine how the shape of the landscape, influenced by heterogeneity, affects the effectiveness of the operators. Fourth, due to the sparse nature of the CSO problem, where optimal solutions often involve a minimal number of active cells, there is a compelling interest in further investigating the landscape for sparse solutions.

Data Availability Statement

The authors confirm that the data supporting the findings of this study are available within the article and its supplementary materials.

Disclosure Statement

No potential competing interest was reported by the authors.

Acknowledgements

This work has been partially funded by the Spanish Ministry of Science and Innovation via grant PID2020-112545RB-C54, and by the European Union NextGenerationEU/PRTR under grants TED2021-131699B-I00 and TED2021-129938B-I00 (MCIN/AEI/10.13039/501100011033, FEDER). The authors also thank the Supercomputing and Bioinformatics Center of the Universidad de Málaga, for providing its services and the Picasso supercomputer facilities to perform the experiments (<http://www.scbi.uma.es/>).

References

- [1] M. Agiwal, A. Roy, and N. Saxena, “Next Generation 5G Wireless Networks: A Comprehensive Survey,” *IEEE Communications Surveys & Tutorials*, vol. 18, no. 3, pp. 1617–1655, 2016.
- [2] W. Chen, X. Lin, J. Lee, A. Toskala, S. Sun, C. F. Chiasserini, and L. Liu, “5G-Advanced Toward 6G: Past, Present, and Future,” *IEEE Journal on Selected Areas in Communications*, vol. 41, no. 6, pp. 1592–1619, 2023.
- [3] F. Salahdine, T. Han, and N. Zhang, “5G, 6G, and Beyond: Recent advances and future challenges,” *Annals of Telecommunications*, 2023.
- [4] H. Tataria, M. Shafi, A. F. Molisch, M. Dohler, H. Sjoland, and F. Tufvesson, “6G Wireless Systems: Vision, Requirements, Challenges, Insights, and Opportunities,” *Proceedings of the IEEE*, vol. 109, pp. 1166–1199, jul 2021.
- [5] J. G. Andrews, S. Buzzi, W. Choi, S. V. Hanly, A. Lozano, A. C. K. Soong, and J. C. Zhang, “What Will 5G Be?,” *IEEE Journal on Selected Areas in Communications*, vol. 32, pp. 1065–1082, jun 2014.
- [6] D. Lopez-Perez, M. Ding, H. Claussen, and A. H. Jafari, “Towards 1 Gbps/UE in Cellular Systems: Understanding Ultra-Dense Small Cell Deployments,” *IEEE Communications Surveys & Tutorials*, vol. 17, no. 4, pp. 2078–2101, 2015.

- [7] V. Stoyanov, V. Poulkov, Z. Valkova-Jarvis, G. Iliev, and P. Koleva, “Ultra-Dense Networks: Taxonomy and Key Performance Indicators,” *Symmetry*, vol. 15, no. 1, 2023.
- [8] A. Gotsis, S. Stefanatos, and A. Alexiou, “UltraDense Networks: The New Wireless Frontier for Enabling 5G Access,” *IEEE Vehicular Technology Magazine*, vol. 11, pp. 71–78, jun 2016.
- [9] C. X. Wang, X. You, X. Gao, X. Zhu, Z. Li, C. Zhang, H. Wang, Y. Huang, Y. Chen, H. Haas, J. S. Thompson, E. G. Larsson, M. D. Renzo, W. Tong, P. Zhu, X. Shen, H. Vincent Poor, and L. Hanzo, “On the Road to 6G: Visions, Requirements, Key Technologies, and Testbeds,” *IEEE Communications Surveys and Tutorials*, vol. 25, no. 2, pp. 905–974, 2023.
- [10] C. Freitag, M. Berners-Lee, K. Widdicks, B. Knowles, G. S. Blair, and A. Friday, “The real climate and transformative impact of ICT: A critique of estimates, trends, and regulations,” *Patterns*, vol. 2, p. 100340, sep 2021.
- [11] F. Salahdine, J. Opadere, Q. Liu, T. Han, N. Zhang, and S. Wu, “A survey on sleep mode techniques for ultra-dense networks in 5G and beyond,” *Computer Networks*, vol. 201, no. December 2020, 2021.
- [12] A. Mughees, M. Tahir, M. A. Sheikh, and A. Ahad, “Energy-Efficient Ultra-Dense 5G Networks: Recent Advances, Taxonomy and Future Research Directions,” *IEEE Access*, vol. 9, pp. 147692–147716, 2021.
- [13] M. Yao, M. M. Sohel, X. Ma, V. Marojevic, and J. H. Reed, “Sustainable green networking: exploiting degrees of freedom towards energy-efficient 5G systems,” *Wireless Networks*, vol. 25, pp. 951–960, apr 2019.
- [14] P. Kaur, R. Garg, and V. Kukreja, “Energy-efficiency schemes for base stations in 5G heterogeneous networks: a systematic literature review,” *Telecommunication Systems*, vol. 84, no. 1, pp. 115–151, 2023.
- [15] 3GPP, “Small Cell Enhancements for E-UTRA and E-UTRAN—Physical Layer Aspects,” tech. rep., 3rd Generation Partnership Project (3GPP), 2014.

- [16] J. Natarajan and B. Rebekka, “An energy efficient dynamic small cell on/off switching with enhanced k-means clustering algorithm for 5G HetNets,” *International Journal of Communication Networks and Distributed Systems*, vol. 29, no. 2, p. 209 – 237, 2023.
- [17] A. I. Abubakar, M. S. Mollel, M. Ozturk, S. Hussain, and M. A. Imran, “A lightweight cell switching and traffic offloading scheme for energy optimization in ultra-dense heterogeneous networks,” *Physical Communication*, vol. 52, p. 101643, 2022.
- [18] B. T. Tinh, L. D. Nguyen, H. H. Kha, and T. Q. Duong, “Practical Optimization and Game Theory for 6G Ultra-Dense Networks: Overview and Research Challenges,” *IEEE Access*, vol. 10, pp. 13311–13328, 2022.
- [19] K. Tan, D. Bremner, J. Le Kernec, Y. Sambo, L. Zhang, and M. A. Imran, “Graph neural network-based cell switching for energy optimization in ultra-dense heterogeneous networks,” *Scientific Reports*, vol. 12, no. 1, pp. 1–18, 2022.
- [20] M. Ozturk, A. I. Abubakar, J. P. B. Nadas, R. N. B. Rais, S. Hussain, and M. A. Imran, “Energy Optimization in Ultra-Dense Radio Access Networks via Traffic-Aware Cell Switching,” *IEEE Transactions on Green Communications and Networking*, vol. 5, no. 2, pp. 832–845, 2021.
- [21] J. Natarajan and B. Rebekka, “Machine Learning Based Small Cell ON/OFF for Energy Efficiency in 5G Heterogeneous Networks,” *Wireless Personal Communications*, vol. 130, no. 4, pp. 2367–2383, 2023.
- [22] M. Feng, S. Mao, and T. Jiang, “Base Station ON-OFF Switching in 5G Wireless Networks: Approaches and Challenges,” *IEEE Wireless Communications*, vol. 24, no. 4, pp. 46–54, 2017.
- [23] D. Gonzalez G., J. Hamalainen, H. Yanikomeroglu, M. Garcia-Lozano, and G. Senarath, “A Novel Multiobjective Cell Switch-Off Framework for Cellular Networks,” *IEEE Access*, vol. 4, pp. 7883–7898, 2016.
- [24] T. Beitelmal, S. S. Szyszkowicz, G. David González, and H. Yanikomeroglu, “Sector and site switch-off regular patterns for energy saving in cellular networks,” *IEEE Transactions on Wireless Communications*, vol. 17, no. 5, pp. 2932–2945, 2018.

- [25] F. Luna, P. H. Zapata-Cano, J. C. Gonzalez-Macias, and J. F. Valenzuela-Valdés, “Approaching the cell switch-off problem in 5G ultra-dense networks with dynamic multi-objective optimization,” *Future Generation Computer Systems*, vol. 110, pp. 876–891, 2020.
- [26] M. Dolfi, C. Cavdar, S. Morosi, P. Piunti, J. Zander, and E. Del Re, “On the trade-off between energy saving and number of switchings in green cellular networks,” *Transactions on Emerging Telecommunications Technologies*, vol. 28, no. 11, p. e3193, 2017.
- [27] F. Ahmed, M. Naem, W. Ejaz, M. Iqbal, A. Anpalagan, and M. Haneef, “Energy cooperation with sleep mechanism in renewable energy assisted cellular hetnets,” *Wireless Personal Communications*, vol. 116, no. 1, pp. 105–124, 2021.
- [28] G. Femenias, N. Lassoued, and F. Riera-Palou, “Access point switch ON/OFF strategies for green cell-free massive MIMO networking,” *IEEE Access*, vol. 8, pp. 21788–21803, 2020.
- [29] Y. Yang, Z. Liu, H. Zhu, X. Guan, and K. Y. Chan, “Energy minimization by dynamic base station switching in heterogeneous cellular network,” *Wireless Networks*, vol. 29, no. 2, pp. 669–684, 2023.
- [30] H. Fourati, R. Maaloul, L. Fourati, and M. Jmaiel, “An Efficient Energy-Saving Scheme Using Genetic Algorithm for 5G Heterogeneous Networks,” *IEEE Systems Journal*, vol. 17, no. 1, pp. 589–600, 2023.
- [31] A. Salem, S. El-Rabaie, and M. Shokair, “Energy efficient ultra-dense networks (UDNs) based on joint optimisation evolutionary algorithm,” *IET Communications*, vol. 13, no. 1, pp. 99–107, 2019.
- [32] K. Venkateswararao and P. Swain, “Binary-PSO-based energy-efficient small cell deployment in 5G ultra-dense network,” *The Journal of Supercomputing*, pp. 1–22, 2021.
- [33] D. G. González, J. Hämäläinen, H. Yanikomeroglu, M. García-Lozano, and G. Senarath, “A novel multiobjective cell switch-off framework for cellular networks,” *IEEE Access*, vol. 4, pp. 7883–7898, 2016.
- [34] F. Luna, R. Luque-Baena, J. Martínez, J. Valenzuela-Valdés, and P. Padilla, “Addressing the 5G Cell Switch-off Problem with a

- Multi-objective Cellular Genetic Algorithm,” in *IEEE 5G World Forum, 5GWF 2018 - Conference Proceedings*, pp. 422–426, 2018.
- [35] J. J. Espinosa-Martínez, J. Galeano-Brajones, J. Carmona-Murillo, and F. Luna, “Binary Particle Swarm Optimization for Selective Cell Switch-Off in Ultra-Dense 5G Networks,” in *Lecture Notes in Computer Science (including subseries Lecture Notes in Artificial Intelligence and Lecture Notes in Bioinformatics)*, vol. 13491 LNCS, pp. 275–283, Springer International Publishing, 2022.
- [36] J. Galeano-Brajones, F. Luna-Valero, J. Carmona-Murillo, P. H. Zapata Cano, and J. F. Valenzuela-Valdés, “Designing problem-specific operators for solving the Cell Switch-Off problem in ultra-dense 5G networks with hybrid MOEAs,” *Swarm and Evolutionary Computation*, vol. 78, no. March, p. 101290, 2023.
- [37] Y. Tian, X. Zhang, C. Wang, and Y. Jin, “An Evolutionary Algorithm for Large-Scale Sparse Multiobjective Optimization Problems,” *IEEE Transactions on Evolutionary Computation*, vol. 24, no. 2, pp. 380–393, 2020.
- [38] A. Liefooghe, F. Daolio, S. Verel, B. Derbel, H. Aguirre, and K. Tanaka, “Landscape-Aware Performance Prediction for Evolutionary Multiobjective Optimization,” *IEEE Transactions on Evolutionary Computation*, vol. 24, pp. 1063–1077, dec 2020.
- [39] R. Cosson, B. Derbel, A. Liefooghe, S. Verel, H. Aguirre, Q. Zhang, and K. Tanaka, “Cost-vs-accuracy of sampling in multi-objective combinatorial exploratory landscape analysis,” in *Proceedings of the Genetic and Evolutionary Computation Conference*, vol. 1, (New York, NY, USA), pp. 493–501, ACM, jul 2022.
- [40] M. Mirahsan, R. Schoenen, and H. Yanikomeroğlu, “HetHetNets: Heterogeneous Traffic Distribution in Heterogeneous Wireless Cellular Networks,” *IEEE Journal on Selected Areas in Communications*, vol. 33, no. 10, pp. 2252–2265, 2015.
- [41] M. A. Mohan and K. Giridhar, “Interference-Aware Accurate Signal Recovery in Sub-1 GHz UHF Band Reuse-1 Cellular OFDMA Downlinks,”

- IEEE Open Journal of the Communications Society*, vol. 3, pp. 2087–2105, 2022.
- [42] N. Al-Falahy and O. Y. Alani, “Network capacity optimisation in millimetre wave band using fractional frequency reuse,” *IEEE Access*, vol. 6, pp. 10924–10932, 2017.
- [43] E. Weinberger, “Correlated and uncorrelated fitness landscapes and how to tell the difference,” *Biological Cybernetics*, vol. 63, pp. 325–336, sep 1990.
- [44] I. Moser, M. Gheorghita, and A. Aleti, “Identifying Features of Fitness Landscapes and Relating Them to Problem Difficulty,” *Evolutionary Computation*, vol. 25, no. 3, pp. 407–437, 2017.
- [45] E. Zitzler and L. Thiele, “Multiobjective evolutionary algorithms: a comparative case study and the strength Pareto approach,” *IEEE Transactions on Evolutionary Computation*, vol. 3, no. 4, pp. 257–271, 1999.
- [46] A. Liefoghe, S. Verel, H. Aguirre, and K. Tanaka, “What makes an instance difficult for black-box 0–1 evolutionary multiobjective optimizers?,” in *International Conference on Artificial Evolution (Evolution Artificielle)*, pp. 3–15, Springer, 2013.
- [47] S. Verel, A. Liefoghe, L. Jourdan, and C. Dhaenens, “On the structure of multiobjective combinatorial search space: MNK-landscapes with correlated objectives,” *European Journal of Operational Research*, vol. 227, no. 2, pp. 331–342, 2013.
- [48] M. Hollander, D. A. Wolfe, and E. Chicken, *Nonparametric statistical methods*. John Wiley & Sons, 2013.
- [49] F. Murtagh and P. Legendre, “Ward’s hierarchical agglomerative clustering method: which algorithms implement Ward’s criterion?,” *Journal of classification*, vol. 31, pp. 274–295, 2014.
- [50] K. Deb, A. Pratap, S. Agarwal, and T. Meyarivan, “A Fast and Elitist Multiobjective Genetic Algorithm: NSGA-II,” *IEEE Transactions on Evolutionary Computation*, vol. 6, no. 2, pp. 182–197, 2002.

- [51] J. Knowles, “A summary-attainment-surface plotting method for visualizing the performance of stochastic multiobjective optimizers,” in *5th International Conference on Intelligent Systems Design and Applications (ISDA '05)*, pp. 552–557, IEEE, 2005.
- [52] B. Vucetic and J. Yuan, *Performance Limits of Multiple-Input Multiple-Output Wireless Communication Systems*, ch. 1, pp. 1–47. John Wiley & Sons, Ltd, 2005.
- [53] N. Piovesan, A. Fernandez Gambin, M. Miozzo, M. Rossi, and P. Dini, “Energy sustainable paradigms and methods for future mobile networks: A survey,” *Computer Communications*, vol. 119, no. December 2017, pp. 101–117, 2018.
- [54] J. Son, S. Kim, and B. Shim, “Energy Efficient Ultra-Dense Network Using Long Short-Term Memory,” in *2020 IEEE Wireless Communications and Networking Conference (WCNC)*, pp. 1–6, 2020.

2.2 3D-Map-Based CSO Optimization in 5G

In this paper, the landscape of the CSO problem is tackled for a more realistic network modeling using a Nokia-proprietary 3D-maps-based radio planner simulator. Focusing on a dense urban macro-scenario deployed in Aalborg, Denmark, and employing the base station power model outlined in the 3GPP TR 38.864 (Release 18), the problem is approached through a constrained distributed asynchronous version of the NSGA-II algorithm. The findings indicate a consistent reduction in RAN energy consumption while maintaining a minimum throughput threshold for all UEs and minimizing the impact of the switch-off on cell capacity.

THIS IS THE PREPRINT VERSION OF THE PAPER:

J. Galeano-Brajones, Carlos Pupiales, Daniela Laselva, J. Carmona-Murillo, and Francisco Luna, "Applying Evolutionary Algorithms for Cell Switch-Off to Reduce Network Energy Consumption," in *IEEE 99th Vehicular Technology Conference (VTC2024-Spring)*, 2024.

Disclaimer:

This work has been submitted to the IEEE 99th Vehicular Technology Conference (VTC2024-Spring).

Copyright:

© 2024 The authors.

Applying Evolutionary Algorithms for Cell Switch-Off to Reduce Network Energy Consumption

Jesús Galeano-Brajones¹, Carlos Pupiales², Daniela Laselva³, Javier Carmona-Murillo¹, Francisco Luna⁴
Dept. of Computing and Telematics System Engineering, Universidad de Extremadura, Spain¹

Aalborg University, Denmark²

Nokia Standards, Denmark³

Universidad de Málaga, Spain⁴

jgaleanobra@unex.es, chpy@es.aau.dk, daniela.laselva@nokia.com, jcarmur@unex.es, flv@lcc.uma.es

Abstract—The rising concerns about climate change motivate the industry and academia to actively work on techniques and strategies that help reduce energy consumption in mobile networks. One avenue under exploration involves methods for intelligently and temporarily deactivating serving cells during low-traffic periods. However, cell switch-off (CSO) decisions need to be taken carefully because they may severely impact the service quality. In this paper, we delve into optimizing the CSO decisions using an optimization framework that uses a constrained distributed multi-objective evolutionary algorithm along with a 3D-maps-based radio planner simulator. Firstly, the distributed version of the evolutionary algorithm aims to find near-optimal solutions within practical computational time. The solutions should satisfy a trade-off between reducing network energy consumption and maximizing cell throughput while ensuring a minimum throughput for all the active users in the network. Secondly, the radio planner simulator evaluates the objectives and constraints of the candidate solutions obtained by the evolutionary algorithm. Our findings indicate that using an aggressive but optimized CSO strategy reduces network power consumption by up to 80% during low traffic periods compared to an all-cells-on scenario.

Index Terms— energy efficiency, 5G, cell switch-off, power consumption, 6G

I. INTRODUCTION

Nowadays, the negative impact of global warming on our daily lives represents a huge concern worldwide. Hence, governments have agreed to reduce carbon emissions to avoid the global average temperature increasing more than 1.5°C [1]. The carbon footprint of the mobile networks industry represents approximately 0.4% of the total global CO₂ emissions per year [2], being the radio access network (RAN) the most significant contributor to these emissions with approximately 73% of the total energy consumed in a mobile network [3]. In the RAN, the cooling system and the RF equipment, e.g., power amplifier (PA), are the critical contributors with 40% and 50%, respectively [4].

In light of this, the 3GPP specifications have made significant contributions in recent years to reducing energy consumption (EC) at the base station (BS). Although 5G improves energy efficiency (EE) per unit of traffic by

90% compared to LTE [5], time-, frequency-, power-, and spatial-based adaptations for network energy saving (NES) are being introduced in Release 18 and 19 to enable further energy savings during low-to-medium traffic load. To maintain this efficiency trend, it is expected that the already standardized and future NES techniques can help 6G to achieve 20 to 40 times the 5G's EE [3, 6]. More specifically, the diverse NES techniques allow mobile network operators (MNO) to reduce EC by temporarily deactivating BS hardware components, particularly RF equipment, at different granularity. For instance, from symbol-level deactivation of PA or antenna elements, or adaptations of transmission power, to longer deactivation at the cell level or carrier level.

The potential benefits of these NES techniques have been studied in the literature. For instance, authors in [7–10] state that micro-discontinuous transmission allows the BS to deactivate the PA during at least a symbol duration, which depending on the traffic load, can provide significant NES gain, especially when the user plane load is low and mostly control signals need to be transmitted. Moreover, in [11–13], authors indicate that having all the antenna elements and their associated RF components active during low traffic conditions could be inefficient since BS keeps transmitting at full power even though that would not be needed during such conditions. Although the EC scales down with the number of inactive RF components, deactivating them can also lead to cell coverage and capacity issues. Hence, finding the optimal number of antennas and transmit power per RF component to satisfy coverage and capacity targets for active users with maximal EE is not trivial.

Different strategies to switch off serving cells and the corresponding impact on the network performance have been studied in [14–17]. The authors conclude that switching off some active cells significantly reduces network energy consumption. One of the strategies considers switching off the small cells located at the edge of the macro coverage and extending the coverage of the other small cells to maintain the service to active users. Likewise, a second approach considers putting into a sleeping mode the active cells with low

traffic demand. Their traffic is addressed either by a nearby user equipment (UE) in a device-to-device fashion, or by a neighbor's active cell. The strategies mentioned above use a combination of spatial-temporal traffic prediction models and complex optimization techniques to determine the location of the cells to deactivate, when to put them into sleeping mode, and when to wake them up.

As mentioned above, switching off certain serving cells seems to be very effective in reducing network energy consumption. Nevertheless, when limiting the number of active cells, it may be challenging to satisfy the quality of service (QoS) targets defined for the end-users. Implementing an effective CSO strategy in live networks is challenging because it implies solving a complex optimization problem, which requires from each cell in the network, for both uplink (UL) and downlink (DL), information such as traffic load, coverage provisioning, user QoS, and BS power consumption. Thus, exploring the complex space of solutions to find the optimal set(s) of cells to switch off is unfeasible since the problem has been proven to be NP-complete [18]. Therefore, there is no algorithm capable of finding optimal solutions to the problem in polynomial computational times.

In light of this, multi-objective evolutionary algorithms emerge as a powerful tool for tackling this real-world problem. By harnessing concepts such as genetic encoding, population generation, and the application of genetic operators, evolutionary algorithms can explore a vast space of potential solutions in reasonable computing time; thus, they enable the discovery of near-optimal solutions in complex and multidimensional contexts. Therefore, their effectiveness in handling multiple constraints and dynamic environments and their potential to uncover non-intuitive solutions make them suitable for tackling the CSO decision problem [19].

In this paper, we show how the constrained distributed multi-objective evolutionary algorithms can help MNOs to identify the serving cells that can be switched off to reduce network power consumption while simultaneously maximizing cell throughput and ensuring a minimum user throughput (UTP) in both DL and UL. To evaluate the impact of the CSO decisions on the UTP and network power consumption, we use a CSO optimization framework that uses the aforementioned evolutionary algorithms and a 3D-maps-based radio planner simulator. The performance evaluations are conducted using a realistic 5G dense urban deployment under different network loads. Therefore, this work novelty lies in developing a powerful, versatile, and scalable framework that integrates optimization algorithms and a radio planning simulator to solve a complex optimization problem with conflicting objectives within a reasonable timeframe.

The rest of this paper is structured as follows: Section II presents the BS power model and the CSO problem formulation. Section III details the scenario and the simulation setup used in our study. The numerical results are presented in Section IV and the conclusions are presented in Section V.

II. SYSTEM OVERVIEW

This section first introduces the 3GPP 5G BS power model. Then it presents the formulation of the CSO decision problem and finalizes with a description of the multi-objective evolutionary algorithm.

A. Base Station Power Model

To support various network architectures, the 3GPP has developed a generic BS power model [20], which indicates the relative power values, operational states, and reference configurations for a 5G BS. The BS can operate in either an active or sleep power state. In the former, the BS works in DL transmission or UL reception. On the other hand, in the latter, the BS operates in a power-saving mode, in which no data transmission or reception is possible. Depending on which hardware components are active and the time required to go from a sleeping mode to a fully functional state, the BS can be in a micro, light, or deep sleep state.

The configuration reference and power values defined for a one-sector BS, i.e., a single cell, are indicated in Tables I and II, respectively. It is worth mentioning that the power values are expressed relative to the deep sleep state and derived at the slot level.

For a BS in an active state, the power consumption (PC) in DL and UL is computed as the sum of dynamic (PC_{dyn}) and static (PC_{static}) components as

$$PC = PC_{dyn} + PC_{static} \quad (1)$$

The dynamic part refers to the power that can scale depending on the occupied bandwidth, the number of active RF components, the transmit power, and the number of component carriers (CCs). On the contrary, the static part refers to the power consumed to maintain the basic operation of the BS. The dynamic part for downlink (PC_{dyn}^{DL}) and uplink (PC_{dyn}^{UL}) are computed as

$$PC_{dyn}^{DL} = Sa * \left(PC_{dyn,ante}^{DL} + Sf * Sp * \frac{PC_{dyn,joint}}{\eta(Sf, Sp)} \right), \quad (2)$$

$$PC_{dyn}^{UL} = Sa * PC_{dyn,ante}^{UL}, \quad (3)$$

where Sa , Sp , Sf represent the ratio, concerning the reference configuration, of active RF components, transmit power, and occupied bandwidth, respectively. $PC_{dyn,ante}^{DL}$ and $PC_{dyn,ante}^{UL}$ are the dynamic part of the power that depends on the number of active RF components for DL and UL, respectively.

TABLE I
REFERENCE CONFIGURATION FOR BS [20]

	Set 1 FR1
Duplex	TDD
System bandwidth	100 MHz
Subcarrier spacing	30 KHz
Number of Tx in DL	64
Total Tx power in DL	55 dBm
Number of Rx in UL	64
Transmission and reception points (TRPs)	1

TABLE II
BS POWER CONSUMPTION FOR DIFFERENT CONFIGURATIONS [20]

Power state	BS Category 2		
	Set 1	Set 2	Set 3
Deep sleep (P1))	1		
Light sleep (P2)	2.1		
Micro sleep (P3)	5.5	5	3
Active DL (P4)	32	26	17.6
Active UL (P5)	6.5	5.8	4.2

$\frac{PC_{dyn,joint}}{\eta(Sf,Sp)}$ is the power part related to the PA, with $\eta(Sf,Sp)$ being the PA efficiency factor. Additionally, for evaluation purposes, the 3GPP suggested in [20] to assume $\eta(Sf,Sp) = 1$ and to use the following values

$$PC_{dyn,ante}^{DL} = 0.4 * (P4 - P3) \quad (4)$$

$$PC_{dyn,ante}^{UL} = P5 - P3 \quad (5)$$

$$PC_{dyn,joint} = 0.6 * (P4 - P3) \quad (6)$$

It is worth mentioning that power consumption in active state for DL and UL are separately modeled. Likewise, when carrier aggregation (CA) is used, the power consumption is computed as the sum of the power consumed by each CC; however, for intra-band CA, the power consumption is scaled by 0.7 for each additional CC. Lastly, the total power consumed in the network is computed as the sum of the power consumed by every cell in the network. For a further detailed description of the 3GPP BS power model, please refer to [20].

B. CSO Decision Optimization Problem

We consider a RAN comprising a set B of BSs deployed in the geographical area under investigation, and C_b represents the set of cells controlled by a BS $b \in B$. Each BS b is configured with a fixed number of frequency resources, which are divided into the active users following a proportional fair scheduling. We adopt the full buffer traffic model to characterize the traffic transmitted/received by an active user. Hence, users have an unlimited amount of data to transmit or an unlimited buffer size to receive data. A solution to the CSO decision problem is a binary string s of size $|B| \times |C_b|$, where s_c^b denotes whether the cell c in BS b is activated (1) or not (0). The first objective of the CSO decision optimization problem is to minimize the power consumption of the RAN deployment

$$\min f_{PC}(s) = \sum_b^B \sum_c^{C_b} PC_c \cdot s_c^b \quad (7)$$

where PC_c represents the power consumption of cell c in BS b (as detailed in Eq. 1), and s_c^b is 1 if cell c is active.

Let U represent the set of UEs deployed across the evaluation area. To calculate the total throughput of the RAN, each UE is assigned to the active cell offering the highest Signal-to-Interference-plus-Noise Ratio (SINR) (refer to Section III-A). Define $\mathcal{A}(s) \in \{0,1\}^{|U| \times |C|}$ as the matrix where $a_{ij} = 1$ if $s_j = 1$ and the cell j serves UE i , and $a_{ij} = 0$ otherwise. Additionally, the second objective of the

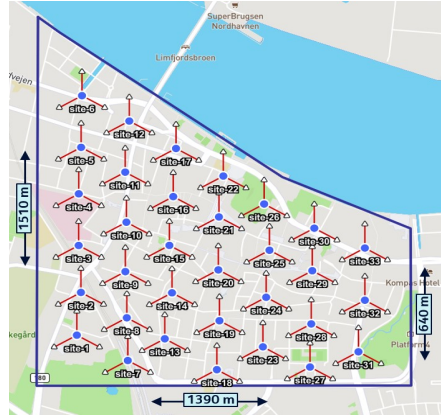


Fig. 1. Location of BSs across the area under investigation

CSO decision optimization problem is to maximize the total cell capacity, which includes both DL and UL throughput, in the RAN. The capacity for each is calculated as

$$\max f_{TP}(s) = \sum_{i=1}^{|U|} \sum_{j=1}^{|C|} s_j \cdot a_{ij} \cdot C_i^j \quad (8)$$

where s_j indicates if the cell j is active or inactive, and C_i^j represents the capacity provided by cell j to UE i (as detailed in Section III-B). The aggregation of DL and UL in the same objective may cause the search for solutions to be influenced primarily by the DL values since they are typically higher than UL. Nevertheless, the results in Section IV have demonstrated that UL values are not marginalized in the optimization process.

Furthermore, the problem is constrained by two UTP requirements, one for DL and another for UL. Let UTP_{DL}^u denote the UTP for the UE u in the DL, UTP_{UL}^u for the UL, UTP_{DL}^{req} the minimum UTP requirement in DL, and UTP_{UL}^{req} the minimum UTP requirement in UL. The constraints that ensure the minimum UTP in both DL and UL for all users in the network are defined as follows

$$UTP_{DL}^u \geq UTP_{DL}^{req}, \forall u \in U \quad (9)$$

$$UTP_{UL}^u \geq UTP_{UL}^{req}, \forall u \in U \quad (10)$$

It is important to note that objectives (7) and (8) conflict. However, a candidate solution to the CSO decision problem is considered feasible only if it simultaneously satisfies constraints (9) and (10). As a result, all UEs in the network must meet the minimum throughput requirements in both DL and UL.

III. SIMULATION SETUP AND METHODOLOGY

A. Scenario Description

This study was conducted utilizing a 5G network implemented in a dense urban macro scenario setting at

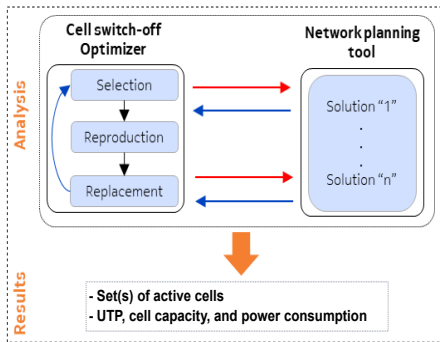


Fig. 2. CSO optimization framework workflow

the heart of Aalborg, Denmark. This location encompasses a mix of residential buildings, commercial establishments, and green spaces, providing a comprehensive environment for the study. Three-sector BSs have been uniformly distributed using an inter-site distance (ISD) of 200 m across an area of approximately 1.4 km², which has been also divided into pixels of 10 x 10 m resolution. The geographical area under investigation and the location of the three-sector BSs are depicted in Fig. 1. Moreover, each BS sector is configured to operate in a time division duplex (TDD) mode at 3.5 GHz, 100 MHz of bandwidth per carrier, and three CCs for DL and one CC for UL.

Moreover, we make the assumption that 2700¹ static UEs are randomly distributed across the evaluation area. We employ a snapshot-based methodology to facilitate the assessment of network performance under different numbers of concurrently connected users seeking a minimum of 9 Mbps for downlink and 4 Mbps for uplink. These network traffic conditions are modeled through an activity factor (AF) [21], which represents the mobile broadband traffic demand in the network at different times of the day. We use different AF values to characterize low, medium, and high traffic demands, i.e., 5%, 15%, and 25%, respectively.

Additionally, we use a 3D-maps-based network planning tool that incorporates a built-in simplified ray-tracing and radio propagation modeling to accurately and realistically predict the capacity and coverage in the network. This tool facilitates precise and realistic predictions by considering factors such as shadowing induced by buildings, terrain variations, and wooded areas. To enhance accuracy, the simulator incorporates up-to-date information corresponding to topography data, building location, and building heights extracted from the investigated area. Likewise, the simulator integrates the 3GPP BS power model, enabling the computation of the power consumption in the RAN deployment.

Furthermore, the active users are randomly distributed

¹ Assuming that the area of evaluation has 40% of the inhabitants of the urban area of Aalborg city, 40% of 5G subscription penetration, and 23% of operator market penetration

throughout the assessed area. Following path loss prediction and interference analysis, they are associated with the active cell that offers the highest SINR. Consequently, the achievable user throughput is calculated based on the user location in the cell and the resource blocks allocated by the packet scheduler that ensure the UE can attain a minimum of 9 Mbps in the downlink and 4 Mbps in the uplink. The maximum theoretical user throughput is obtained using Shannon's channel capacity equation. Lastly, we assume that the deactivated BSs operate in a deep sleep mode, see Section II-A.

B. Experimental Methodology

The CSO optimization framework used in our study consists of two components. The first component, known as the CSO optimizer, utilizes a distributed version of Non-dominated Sorting Genetic Algorithm II (NSGA-II) [24], a multi-objective evolutionary optimization algorithm. This algorithm is instrumental in identifying the decision variables, specifically the set(s) of active cells that meet the UTP target. The second component uses a network planning tool to estimate the UTP, cell capacity, and power consumption for each feasible solution set the CSO optimizer generates. The outcomes from the planning tool, encompassing UTP, cell capacity, and power consumption, serve as both objectives and constraint values for the CSO optimizer in subsequent optimization steps. This iterative process is visually represented in Fig. 2.

Considering the stochastic nature of the evolutionary algorithms, we conduct multiple experiments to ensure statistical confidence in our results. Specifically, we ran five experiments for each traffic load analyzed in our study. For the final solution, we use the median solution from each subset of experiments, based on the hypervolume indicator [25]. Further implementation, configuration, and tuning details of

TABLE III
SIMULATION PARAMETERS [22]

Parameter Description	Value
Network topology	Dense Urban with single macro layer (Hex. Grid); 33 * 3 = 99 cells, ISD = 200 m
Carrier frequency	3.5 GHz (n78 band)
Bandwidth	100 MHz
Carrier aggregation	Intra-band, 3 CCs in DL and 1 CC in UL per cell
Tx power	44 dBm per transmitter
BS noise figure	5 dB
BS antenna configuration	4Tx4Rx; 18.3 dB gain; sectorial; 25m height 0°, 120°, 240° azimuth; 2° downtilt
Frame structure	TDD semi-static with 3/7 UL/DL slot ratio
Modulation	256 QAM (1.5 dB power backoff)
MIMO scheme	single-user MIMO, 4 layers in DL and UL
BS power model	Set 1, Cat. 2
UE power class	23 dBm
UE antenna configuration	4Tx4Rx, 0 dB gain, 1.5m height
UE noise figure	4 dB
UL power control	Fractional power control $\alpha = 1$ Power spectral density target = -100 dBm
UE deployment	80% indoor and 20% outdoor (on average)
Building penetration loss	27 dB [23]
Avg. building height	15 m
Activity factor	5%, 15%, 25%

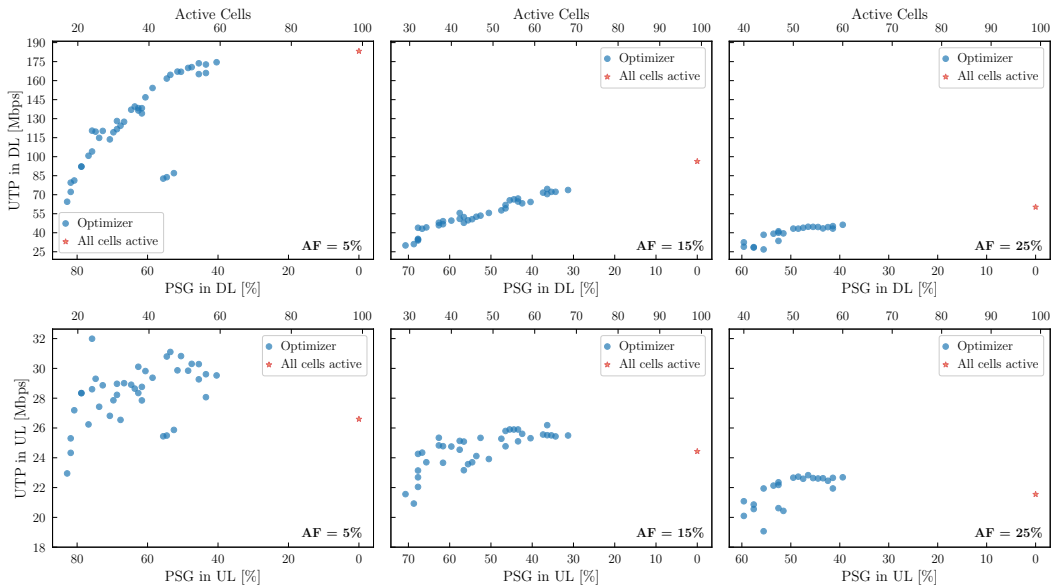


Fig. 3. Average UTP in DL (first row) and UL (second row), number of active cells and PSG for different traffic load conditions (the first column is for $AF = 5\%$, the second for $AF = 15\%$, and the third for $AF = 25\%$).

the multi-objective evolutionary optimization algorithm can be found in [19, 24].

Furthermore, the network planning tool utilizes a Monte Carlo process with 1000 iterations. In each iteration, the positions of active users across the evaluation area and the number of active users per cell change. This dynamic approach enhances the tool's precision in estimating the capacity and coverage in the deployed network. Consequently, our CSO decision optimization framework uses the average outcomes for cell capacity and UTP obtained after the 1000 iterations, alongside network power consumption, as the objectives and constraint values for the optimization process.

Finally, the multi-objective evolutionary algorithm is set to terminate after a maximum of 5000 evaluations of the objective functions. This stopping condition is complemented by a population size of 40 individuals, fostering the evolutionary development of candidate solutions. Furthermore, we use the following genetic operators: binary tournament selection, two-point crossover with a probability of 0.9, and bit-flip mutation with a probability of $1/L$, where L represents the total number of cells in the scenario. This configuration, along with other pertinent simulation parameters, is detailed in Table III.

IV. SIMULATION RESULTS

This section presents the results of the average UTP and power-saving gain (PSG) achieved with our CSO optimization framework. The PSG indicates the percentage reduction in power consumption achieved by a feasible solution compared to a reference scenario where all cells are active. The

feasible solutions, i.e., the set(s) of active cells that solve the optimization problem, as discussed in Section II-B, are depicted in Fig. 3 by blue dots. Likewise, a red star represents the results achieved for the reference scenario. It is important to note that the network performance for each feasible solution is independently analyzed for DL transmission and UL reception. In the reference scenario, characterized by a uniform hexagonal grid deployment, all 33 three-sector BSs are actively transmitting or receiving data to meet the UTP targets for all active users within the evaluation area, without any coverage gaps. Consequently, the results depicted in Fig. 3 reveal that the average UTP achieved under low (5% AF), medium (15% AF), and high (25% AF) traffic demands is approximately 180, 90, and 60 Mbps for downlink, and 27, 25, and 21 Mbps for uplink, respectively. For the sake of comparison and visualization in the next graph, the PSG for the reference scenario is set at 0%.

As illustrated in Fig. 3 for the DL scenario, it is evident that certain feasible solutions achieve lower average UTP values under low, medium, and high traffic demands compared to the reference scenario. However, the noteworthy aspect is the significantly reduced power consumption required to attain these UTP values across all traffic demands. For instance, the implementation of a conservative CSO scheme, utilizing 60%-70% of the total deployed cells, results in a PSG ranging from 30% to 40% across all assessed scenarios. Similarly, the adoption of a more aggressive CSO strategy can lead to a substantial decrease in power consumption by 60-80%, depending on the traffic load.

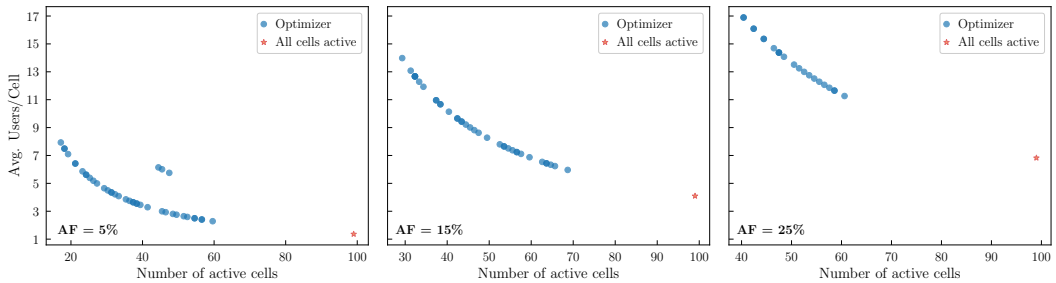


Fig. 4. Average number of users per cell in both DL and UL for different traffic load conditions (the first column is for $AF = 5\%$, the second for $AF = 15\%$, and the third for $AF = 25\%$).

Moreover, the distribution of active users and active cells throughout the evaluation area plays a key role in determining the achievable throughput. When cells are switched off, the number of active users per cell changes, as illustrated in Fig. 4, influencing the received power levels at each UE and the interference created in the cell. Therefore, the obtained throughput is influenced not only by the number of active cells but also by their specific spatial distribution. Consequently, two feasible solutions with an identical number of active cells may result in different throughput and PSG levels. Additionally, given the capacity to deploy up to three CCs in the downlink and one CC in the uplink within each BS sector, deactivating cells results in more substantial degradation of throughput in the DL compared to the UL. This disparity is particularly conspicuous in scenarios characterized by a 5% AF.

Additionally, due to the nature of evolutionary algorithms, the CSO optimizer starts the search for near-optimal solutions from a set of random possible solutions instead of starting from the scenario with all cells active, i.e., the reference scenario. This strategic approach enhances the diversity within the evolving solution set throughout the optimization process. Consequently, the CSO optimizer achieves 40% PSG for both low and high-traffic load, along with 30% PSG for medium-traffic load. Moreover, as depicted in Fig. 3, the maximum PSG experiences a reduction as the traffic load intensifies. In our specific scenario, this reduction ranges from 80% to 60% for both low and high traffic loads, respectively. This observed behavior is expected since a lower AF generally facilitates the algorithm in discovering feasible solutions with greater ease. This capability allows the algorithm to switch off cells more effectively while adhering to the constraints imposed by the problem.

Furthermore, the CSO optimizer finds a varying number of feasible solutions: 22 for 25% AF, 38 for 15%, and it reaches the maximum of 40 feasible solutions for 5%. This variation indicates that the complexity and the richness of the feasible solution space increase as the AF decreases. Considering a larger population size could potentially lead to the discovery of a greater number of near-optimal solutions.

However, this would require increasing the stopping condition, i.e., the maximum number of objective function evaluations. Such an adjustment would ensure the continuous evolution of the solution set throughout the evolutionary cycle, but it would also result in a larger computational time. The trade-off between the number of explored solutions and computational resources, i.e., time and processing power, are crucial aspects in the optimization process, particularly for problems with high-dimensional and complex search spaces like the one treated in this study.

The findings presented in Figs. 3 and 4 reveal the substantial variations in both UTP and PSG concerning the number of active cells and traffic demand. For instance, in our study, only three cells remain consistently active and two consistently inactive across all feasible solutions and traffic loads. This indicates that the optimal network deployment configuration would vary depending on the trade-off between power reduction and throughput degradation that the MNO wants to achieve, thus, reinforcing the non-trivial nature of decisions related to cell activation or deactivation.

V. CONCLUSIONS

In this work, we present an optimization framework for controlling cell switch-off decisions to help MNOs identify set(s) of serving cells that can be switched off to reduce energy consumption in the network under different traffic loads. The optimization framework takes advantage of constrained distributed multi-objective evolutionary algorithms to simultaneously guarantee, among conflicting objectives, a minimum user throughput in DL and UL, maximize the cell throughput, and reduce the total power consumption of the network. By adjusting the number of active cells based on traffic demands, the framework provides a solution to optimize network operations, meeting the user demands while also addressing environmental and economic concerns related to power consumption in telecommunications networks.

The simulations conducted within a realistic 5G network scenario, using a 3D-maps-based network planning tool that incorporates up-to-date topographic and building information of Aalborg city, revealed significant potential for reducing power consumption in the network. The results showed that

activating only 60-70% of the total deployed cells makes it possible to reduce the network power consumption by 30-40%, depending on the traffic load. Similarly, if the activation is limited to just 20-40% of the total cells, the reduction in power consumption can scale up to 60-80%.

Even though the average user throughput achieved with the feasible solutions is lower than those in the reference scenario, it is important to note that active users consistently attain more than 9 Mbps in the downlink and 4 Mbps in the uplink. The lowest average throughput values for low, medium, and high traffic demands are 65, 27, and 25 Mbps, respectively, for downlink, and 23, 21, and 17 Mbps, for uplink. These results confirm that achieving an optimal trade-off between system performance and energy savings demands complex switching-off decisions.

Lastly, while it may not be feasible for MNOs to adopt a real-time approach due to the complexity of the optimization problem and dynamic traffic variations in real-world deployments, they can still make more precise decisions about cell location and deactivation duration. In fact, by utilizing more granular traffic predictions in space and time and leveraging computing infrastructure, MNOs have the potential to significantly enhance network power consumption, even though the approach may not be real-time.

ACKNOWLEDGMENT

This work has been partially funded by the European Union's NextGenerationEU/PRTR under the project TED2021-131699B-I00 (MCIN/AEI/10.13039/501100011033, FEDER), and by the Spanish Ministry of Science and Innovation with the project PID2020-112545RB-C54.

REFERENCES

- [1] UNFCCC, "Paris agreement: Report of the conference of the parties to the united nations framework convention on climate change," 2015.
- [2] GSMA, "Mobile net zero state of the industry on climate action 2021," 2021.
- [3] H. Viswanathan *et al.*, "White paper: Energy efficiency in next-generation mobile networks," 2022. [Online]. Available: <https://www.bell-labs.com/institute/white-papers/energy-efficiency-in-next-generation-mobile-networks>
- [4] J. Erfanian *et al.*, "Green future networks - network energy efficiency," 2021.
- [5] GSMA, "Mobile net zero state of the industry on climate action 2023," 2023.
- [6] HEXA-X-II, "Deliverable d1.1 environmental, social, and economic drivers and goals for 6G," 2023.
- [7] P. Lahdekorpi *et al.*, "Energy efficiency of 5g mobile networks with base station sleep modes," 2017 *IEEE Conference on Standards for Communications and Networking, CSCN 2017*, pp. 163–168, 2017.
- [8] T. Islam, D. Lee, and S. S. Lim, "Enabling network power savings in 5G-advanced and beyond," *IEEE Journal on Selected Areas in Communications*, 2023.
- [9] P. Frenger and R. Tano, "More capacity and less power: How 5G NR can reduce network energy consumption." *IEEE VTC2019*, 2019.
- [10] F. E. Salem *et al.*, "Optimal policies of advanced sleep modes for energy-efficient 5G networks," 2019.
- [11] P. Frenger and K. W. Helmersson, "Massive mimo muting using dual-polarized and array-size invariant beamforming," vol. 2021-April, 2021.
- [12] K. N. V. Prasad, E. Hossain, and V. K. Bhargava, "Energy efficiency in massive mimo-based 5g networks: Opportunities and challenges," *IEEE Wireless Communications*, vol. 24, pp. 86–94, 2017.
- [13] E. Björnson *et al.*, "Optimal design of energy-efficient multi-user mimo systems: Is massive mimo the answer?" *IEEE Transactions on Wireless Communications*, vol. 14, pp. 3059–3075, 2015.
- [14] R. Tao *et al.*, "An energy saving small cell sleeping mechanism with cell range expansion in heterogeneous networks," *IEEE Transactions on Wireless Communications*, vol. 18, pp. 2451–2463, 2019.
- [15] G. Jang *et al.*, "Base station switching and sleep mode optimization with lstm-based user prediction," *IEEE Access*, vol. 8, pp. 711–723, 2020.
- [16] C. Peng *et al.*, "Greenbsn: Enabling energy-proportional cellular base station networks," *IEEE Transactions on Mobile Computing*, vol. 13, pp. 2537–2551, 2014.
- [17] W. Teng *et al.*, "Joint optimization of base station activation and user association in ultra dense networks under traffic uncertainty," *IEEE Transactions on Communications*, vol. 69, pp. 6079–6092, 2021.
- [18] D. Gonzalez G. *et al.*, "A Novel Multiobjective Cell Switch-Off Framework for Cellular Networks," *IEEE Access*, vol. 4, pp. 7883–7898, 2016.
- [19] J. Galeano-Brajones *et al.*, "Designing problem-specific operators for solving the cell switch-off problem in ultra-dense 5g networks with hybrid moeas," *Swarm and Evolutionary Computation*, vol. 78, 2023.
- [20] 3GPP, "TR 38.864 - v1.0.0; Study on network energy savings for NR," 2022.
- [21] GSMA, "Estimating the mid-band spectrum needs in the 2025-2030 time frame," 2021.
- [22] 3GPP, "TR 38.802 - v2.0.0; Study on new radio (NR) access technology; physical layer aspects," 2017.
- [23] 3GPP, "TR 38.901 - v16.1.0; Study on channel model for frequencies from 0.5 to 100 GHz," 2020.
- [24] K. Deb *et al.*, "A Fast and Elitist Multiobjective Genetic Algorithm: NSGA-II," *IEEE transactions on evolutionary computation*, vol. 6, no. 2, pp. 182–197, 2002.
- [25] E. Zitzler and L. Thiele, "Multiobjective evolutionary algorithms: a comparative case study and the strength pareto approach," *IEEE transactions on Evolutionary Computation*, vol. 3, no. 4, pp. 257–271, 1999.

3

PROBLEM-SPECIFIC OPERATORS

This chapter presents two articles that address the challenge of optimizing energy consumption in 5G and future mobile networks through the design of domain information-based problem-specific operators, thus fulfilling objective O2. The first article examines the efficacy of Binary Particle Swarm Optimization in navigating the multi-objective optimization landscape, integrating energy efficiency and user service capacity. The paper highlights significant enhancements in hybridizing the BPSO with specific operators. The second article ventures into the multi-objective problem introducing hybrid multi-objective evolutionary algorithms that leverage domain-specific knowledge through novel operators. This approach underscores the value of hybridization in surpassing canonical algorithmic performances through comprehensive experimentation and analysis.

Contents

3.1	Addressing the CSO Problem with BPSO	58
3.2	Hybridization with Problem-Specific Operators	68

3.1 Addressing the CSO Problem with BPSO

This article explores the utilization of binary particle swarm optimization (BPSO) to address the challenge of energy consumption in the next generations of mobile networks, emphasizing the need for sustainable solutions amid network densification. The paper introduces a multi-objective optimization approach that balances energy efficiency with user service capacity, employing a V-shaped function for binary codification. The study assesses the performance of BPSO in comparison to MOCcell and NSGA-II and examines the benefits of hybridizing BPSO with specific operators, highlighting significant improvements in algorithmic search efficiency.

THIS IS THE PUBLISHED VERSION OF THE PAPER:

J. J. Espinosa-Martínez, J. Galeano-Brajones, J. Carmona-Murillo, and F. Luna, “Binary Particle Swarm Optimization for Selective Cell Switch-Off in Ultra-Dense 5G Networks,” in *International Conference on Swarm Intelligence*, pp. 275–283, Springer, 2022.

Supplementary material is available in the Appendix A.

Disclaimer:

This work has been presented at the International Conference on Swarm Intelligence 2022 (ANTS 2022).




DOI: 10.1007/978-3-031-20176-9_23

Copyright:

© 2022 Springer Nature Switzerland AG. Springer grants the rights to use the article in this thesis under the terms and conditions set out in the Appendix E.



Binary Particle Swarm Optimization for Selective Cell Switch-Off in Ultra-Dense 5G Networks

Juan Jesús Espinosa-Martínez¹, Jesús Galeano-Brajones¹ ,
Javier Carmona-Murillo¹ , and Francisco Luna² 

¹ Department of Computing and Telematics System Engineering, Centro Universitario de Mérida, Universidad de Extremadura, Mérida, Spain
jespinosv@alumnos.unex.es, {jgaleanobra,jcarmur}@unex.es

² School of Computer Science and Engineering, Universidad de Málaga, Málaga, Spain
flv@lcc.uma.es

Abstract. The massive deployment of small base stations is one of the main pillars for the new generations of mobile networks to meet the expected growing in data traffic demands. This densification entails high energy consumption that needs to be minimized to ensure system sustainability in a context of reduced environmental impact. To address this issue, optimization algorithms that will rely on metaheuristics can be used due to the complexity and the large instance size of the problem. Therefore, it is a multi-objective optimization problem in which not only the energy efficiency criteria is taken into account, but also the service provided to the users in terms of capacity is considered. In this context, the aim of this work is to evaluate the performance of Binary Particle Swarm Optimization (BPSO) in solving this multi-objective problem, using a V-shaped function to deal with binary codification. The performance of our proposed solution is compared with the results obtained by MOCeII and NSGA-II in our previous works. In addition, the performance of the hybridization with specific operators proposed in one of our previous works is tested. The research showed that the hybridization brought very significant benefits to the algorithm's searches.

1 Introduction

The deployment of the fifth generation (5G) of cellular networks is expected to address the increasing demand for services with strict requirements for low latency and high reliability (e.g., autonomous driving), high bandwidth (e.g., Virtual Reality/Augmented Reality) and resilience to support scenarios with an extremely high density of devices connected. In this scenario, the massive

Supplementary Information The online version contains supplementary material available at https://doi.org/10.1007/978-3-031-20176-9_23.

deployment of many Small Base Stations (SBSs) per km^2 , known as Ultra Dense Networks (UDNs) [4], is becoming one of the mainstays of 5G networks due to the reuse of the electromagnetic spectrum and the increase in the network capacity that it provides. However, this densification implies a rise in the network power consumption, which is accentuated in periods of low demand in which some SBSs are switched on without serving any user.

Thus, in order to address this issue, the standardized strategy known as Cell Switch-Off (CSO) was proposed [1]. This strategy consists of selective switching off/on of SBSs to minimize the energy consumption of the network, but simultaneously trying to maximize the Quality of Service for the existing demand. This is a multi-objective combinatorial optimization problem that has been demonstrated as NP-complete [5] and whose resolution has been proposed in the literature with the use of multi-objective metaheuristics [7, 14]. Moreover, the UDNs are heterogeneous because they contain SBSs with different transmission power, cell size and working frequency due to different radio technologies.

In our previous work [8], we have proposed the hybridization of two well-known multi-objective metaheuristics, MOCell [11] and NSGA-II [3], with two specific operators that aim to improve the performance of these algorithms in the CSO problem. The research showed that the hybridization brought very significant benefits to the algorithm's search. The work presented in this paper builds on our previous work by evaluating the performance of Binary Particle Swarm Optimization (BPSO), using a V-shaped function to deal with binary codification. Furthermore, this work compares the BPSO performance with MOCell and NSGA-II, and hybridizes it with both of the proposed specific operators. The results show that BPSO intensifies the search in the objective of minimizing consumption better than the rest of the metaheuristics, and that the hybridization improves the BPSO search, but not significantly. In the literature, we can find proposals where PSO is used to optimize the CSO problem [2, 12, 13], but none of them compare its performance with other metaheuristics or hybridize it with specific operators.

The remainder of the paper is structured as follows. In Sect. 2, the optimization problem addressed has been formulated. The mechanism to adapt the PSO algorithm to the binary codification is described in Sect. 3. Section 4 details the experimental methodology and the detailed analysis of the results obtained. Finally, the last section includes the main conclusions reached, as well as the lines of future work that remain open.

2 The CSO Problem

Due to the limited length of this document, the modelling of the UDNs is available as supplementary material. For this reason, references to equations in this section refer to that material¹.

¹ <https://doi.org/10.6084/m9.figshare.19682955.v2>

Let \mathcal{B} be the set of the SBSs randomly deployed. A solution to the CSO problem is a binary string $s \in \{0, 1\}^{|\mathcal{B}|}$, where s_i indicates whether SBS i is activated or not. The first objective to be minimized is therefore computed as:

$$\min f_{Power}(s) = \sum_{i=1}^{|\mathcal{B}|} s_i \cdot P_i \quad (1)$$

where P_i is the power consumption of SBS i (Eq. sup. 7). Note that P_i includes both the transmission power on every cell contained in i and the maintenance power of the SBS.

Let \mathcal{U} be the set of the UEs also deployed as described in the supplementary material and \mathcal{C} the whole set of Cells contained in \mathcal{B} . Subsequently, in order to compute total capacity of the system, UEs are first assigned to the active Cell that provides it with the highest SINR. Let $\mathcal{A}(s) \in \{0, 1\}^{|\mathcal{U}| \times |\mathcal{C}|}$ be the matrix where $a_{ij} = 1$ if $s_j = 1$ and the Cell j serves UE i with the highest SINR, and $a_{ij} = 0$ otherwise. Then, the second objective to be maximized, which is the total capacity provided to all the UEs, is calculated as:

$$\max f_{Cap}(s) = \sum_{i=1}^{|\mathcal{U}|} \sum_{j=1}^{|\mathcal{C}|} s_j \cdot a_{ij} \cdot BW_i^j \quad (2)$$

where BW_i^j is the shared bandwidth of Cell j provided to UE i (Eq. sup. 6). We would like to remark that these two problem objectives are clearly conflicting one each other, since switching off base stations leads to a reduction of the power consumption of the network, but it also damages the capacity received by the user, as the UE-Cell distance increases (rising the propagation losses) at the same time as the available bandwidth to serve users is reduced.

3 Binary PSO

3.1 BPSO Modelling

The swarm consist of n particles, each one defined by a d -dimensional vector that represents all the SBSs present in the scenario, some being active and the rest switched off. Therefore, each position in the particle's position vector, x_{id}^k , represents one single SBS, that can be turned on (1) or turned off (0). Thus, for each particle i in a specific iteration k , the position vector is defined as $X_i^k = (x_{i1}^k, x_{i2}^k, \dots, x_{id}^k)$, and the velocity vector is $V_i^k = (v_{i1}^k, v_{i2}^k, \dots, v_{id}^k)$, where $i \in [1, 2, \dots, n]$, $d \in [1, 2, \dots, L]$, being L the number of SBSs, $x_{ij} \in \{0, 1\}$ and $V_{min} \leq v_{ij}^k \leq V_{max}$. The fitness value of each particle is F_i and the algorithm stores the best value for each particle, known as local best (P_{best}), and the best value of the whole swarm, known as global best (G_{best}).

3.2 Initialization and Update

The first step is to set up the parameters of the BPSO. This must be done carefully since these parameters will heavily influence the behaviour of BPSO. For this project, the parameters were selected according to the literature recommendations [9]: the swarm size is 100 particles; the inertia weights are $\omega_{max} = 0.9$ and $\omega_{min} = 0.4$; the acceleration coefficients are $c_1 = c_2 = 2.0$; and the velocity thresholds are $V_{min} = 0.0$ and $V_{max} = 4.0$. Regarding the updating process, the velocity update is defined as follows:

$$v_{id}^{k+1} = \omega^k \cdot v_{id}^k + c_1 \cdot rand_1(P_{best,id}^k - x_{id}^k) + c_2 \cdot rand_2(G_{best} - x_{id}^k) \quad (3)$$

where c_1 and c_2 are acceleration coefficients, $rand_1$ and $rand_2$ are two random numbers in $[0, 1]$ and ω is the inertia weight which is updated with the following equation:

$$\omega^k = \omega_{max} - k \cdot \left(\frac{\omega_{max} - \omega_{min}}{k_{max}} \right) \quad (4)$$

where ω_{max} and ω_{min} the inertia weights, k is the current iteration and k_{max} is the maximum number of iterations. The velocity threshold control is applied as follows:

$$v_{id}^k = \begin{cases} V_{max}, & \text{if } v_{id}^k > V_{max} \\ V_{min}, & \text{if } v_{id}^k < V_{min} \\ v_{id}^k, & \text{otherwise} \end{cases} \quad (5)$$

Nevertheless, the velocity defined in Eq. 3 as a continuous value can not be directly applied to update the discrete space that represents the particle's position. Therefore, a V-shaped function [10] is used to re-define velocity in terms of probability, and it is defined as

$$f(v_{id}^k) = |\tanh(v_{id}^k)|. \quad (6)$$

Finally, the position update is defined as follows:

$$x_{id}^k = \begin{cases} 0, & \text{if } f(v_{id}^k) < rand \\ 1, & \text{if } f(v_{id}^k) \geq rand \end{cases} \quad (7)$$

where $rand$ is a random number in $[0, 1]$. Here, this work differs from the use that [10] gives to the V-shaped function so that the probability output from $f(v_{id}^k)$ is directly associated with the x_{id}^k value (the higher the probability, the higher the chance of x_{id}^k to be 1). Thus, the velocity is also directly associated with the value of x_{id}^k .

4 Experimentation

4.1 Methodology

Based on the nine scenarios described in Sect. 2 and the stochastic nature of the metaheuristics, 50 seeds for each type of scenario have been addressed in the experimentation². This ensures that all algorithms face the same set of problem instances. In order to obtain fair comparative results between algorithms, these use the same population/swarm size of 100 solutions and the same genetic operators: binary tournament selection, two points crossover with crossover rate of 0.9, and bit flip mutation with a mutation rate of $1/L$, being L the number of cells in the scenario. The BPSO is the exception, as it does not use a crossover operator. Regarding the specific operators [8], we use the application rates 0.1 and 0.01 to be consistent with previous work. The stopping condition is defined by the number of evaluations of the objective function but, in order to ensure that the algorithms reach convergence, this limit is linked to the density of the instances. Since the size of the search space lies in the density of BSs, the following stopping conditions have been defined: for $L\{X\}$ (being X the three values for the UEs densities), 100000 evaluations; for $M\{X\}$, 150000 evaluations; and for $H\{X\}$, 250000 evaluations. These numbers are the result of a preliminary analysis of the convergence of the algorithms. The quality of the Pareto front approximations has been measured with the Hypervolume [15] and the attainment surfaces [6]. Since the Hypervolume value is highly dependent on the arbitrary scaling of the objectives, a normalization process with respect to a reference front composed by all the non-dominated solutions found by all the algorithms for the same scenario has been carried out before calculating it.

4.2 Results

4.3 PSO Performance

In this new work, we start from a slightly different network modelling. Previously, we worked with omnidirectional SBSs, i.e., antennas radiating in all directions. Now, we use antennas that can generate very narrow beams, allowing them to be grouped into matrixes or arrays. This allows us to have much more precise control because these beams consume much less power. Due to this change, the density of SBSs has increased by three times, thus generating a larger search space. For this reason, the results of MOCcell and NSGA-II are different.

Table 2 in the supplementary material shows the HV performance for the nine scenarios and the three algorithms, where the cells with a grey background indicate the best result for each scenario. According to HV, the algorithm that best approximates the fronts is BPSO, followed by NSGA-II in seven scenarios, and MOCcell in the remaining two. The reason for this result can be better understood by looking at the Fig. 1. BPSO explores much more the solutions with lower power consumption, and the rest of the algorithms achieve a more

² The source code is available at https://github.com/galeanobra/CSO_BPSO.git

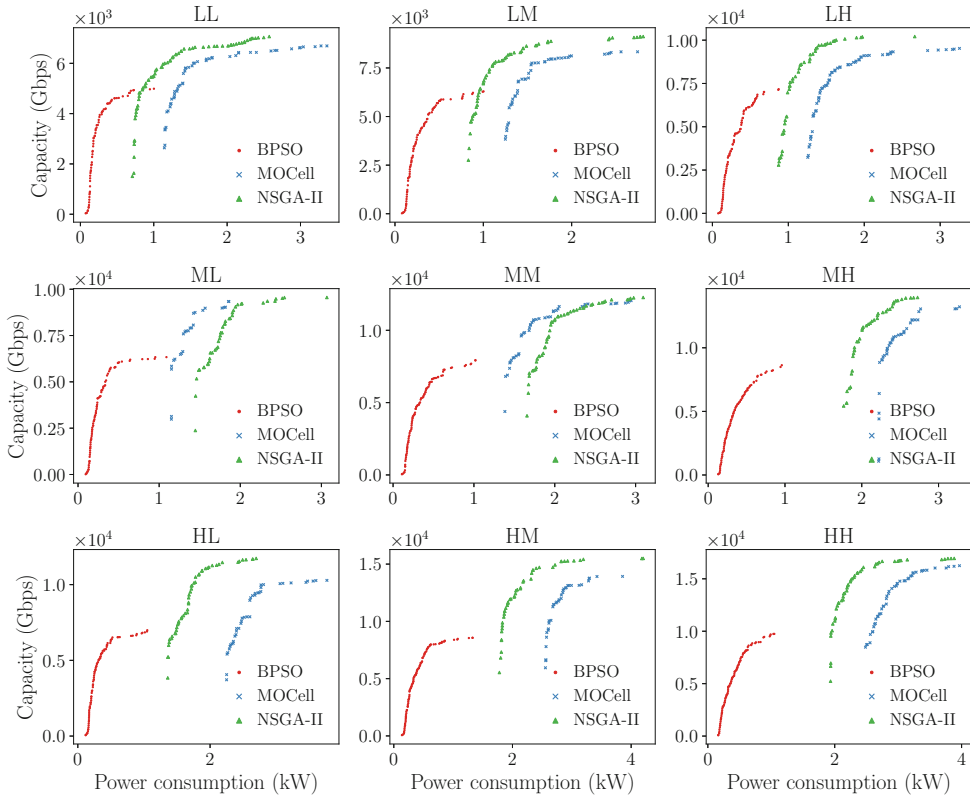


Fig. 1. Attainment surfaces of the three algorithms for each scenario.

equal compromise between both objectives. The reason for the difference in HV is due to the fact that the generated RPF is very vertical, i.e., it covers very little of the consumption objective, so BPSO is always covered by the RPF and the other two algorithms only partially. This can be seen in the MOCcell result from the MH scenario.

4.4 Specific Operators in PSO

As discussed above, in [8] we present the hybridization of MOCcell and NSGA-II with two specific operators that seek to bring expert knowledge of the problem to the search of the algorithms. We compare the performance of the operators directly with the algorithms without hybridization, using the same indicators as in this work. In the conference paper, we showed that the application of the operators contributed to the search by obtaining better solutions in both objectives. The HV results for each of the above-mentioned algorithms are shown in the Tables 3, 4 and 5 of the supplementary material. As we demonstrated in the previous work, MOCcell and NSGA-II obtain a very significant improvement in HV when hybridized with both specific operators. In the case of BPSO,

hybridization with these operators generates a less significant improvement. Of the nine density combinations with which we have experimented, in six, BPSO improves due to hybridization. Even so, the improvement obtained is slight and not very significant.

Finally, Fig. 2 shows the attainment surfaces for scenario HH. The results are similar for the nine scenarios, but for space reasons we only show the most relevant one. Thanks to this indicator, we can observe the results of HV directly extrapolated to fronts. Thus, it can be observed that the performance of MOCell and NSGA-II with hybridization is significantly better, while the improvement in BPSO is not significant. After analysing the solutions, we can conclude that the BPSO performance is caused because it reaches sparse solutions, i.e., solutions containing too few active SBSs. This makes it difficult for specific operators to switch off more cells, and therefore does not improve the performance of the algorithm. Regarding the statistical significance tests, we found that for BPSO there are no significant differences between the application or not of the hybridization. In contrast, both MOCell and NSGA-II obtain significantly better performance when hybridization is applied. For more information, please see the supplementary material³.

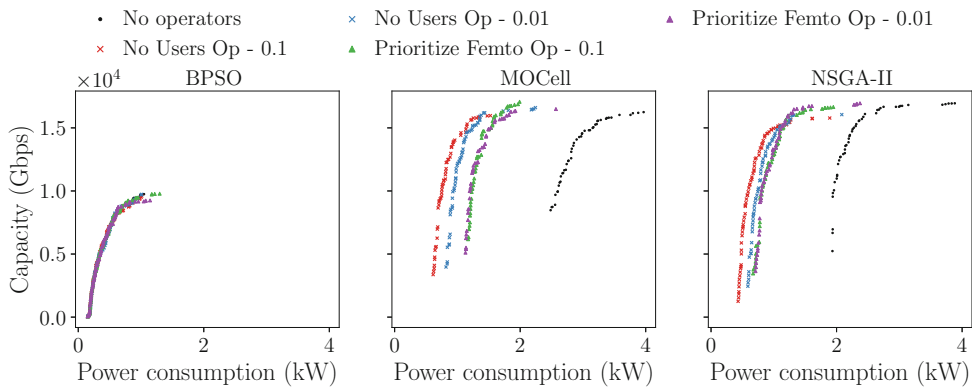


Fig. 2. Attainment surfaces of the three algorithms for scenario HH.

5 Conclusions

The Ultra-Dense Networks are a key building block for 5G and Beyond 5G networks, but they also have a power consumption problem that needs to be addressed. This problem has been formulated in the literature as a multi-objective optimization problem that selectively switches off a subset of Small Base Stations in these networks, aiming to reduce the power consumption while maximizing the QoS of the demands. This work continues a previous one, analysing the performance of the Binary PSO in this multi-objective problem,

³ <https://doi.org/10.6084/m9.figshare.19682955.v2>

as well as the hybridization with the previously proposed operators. The results show that this algorithm obtains solutions with larger energy savings, although worse QoS, and the hybridization with these specific operators improves the search, but not significantly. As future work, it is proposed to study different mechanisms for PSO to deal with binary codification, as well as its hybridization with new specific operators that would improve the algorithm search.

Acknowledgements. This research was funded in part by the Spanish Ministry of Science and Innovation, grant number PID2020-112545RB-C54, and the Regional Government of Extremadura, Spain, grant numbers IB18003 and GR21097.

References

1. 3GPP: small cell enhancements for E-UTRA and E-UTRAN-physical layer aspects. Technical report, 3rd Generation Partnership Project (3GPP) (2014)
2. Alsharif, M.H., Kelechi, A.H., Kim, J., Kim, J.H.: Energy efficiency and coverage trade-off in 5G for eco-friendly and sustainable cellular networks. *Symmetry* **11**(3), 408 (2019)
3. Deb, K., Pratap, A., Agarwal, S., Meyarivan, T.: A fast and elitist multiobjective genetic algorithm: NSGA-II. *IEEE Trans. Evol. Comput.* **6**(2), 182–197 (2002)
4. Ge, X., Tu, S., Mao, G., Wang, C.X., Han, T.: 5G ultra-dense cellular networks. *IEEE Wirel. Commun.* **23**(1), 72–79 (2016)
5. González, D.G., Hämäläinen, J., Yanikomeroglu, H., García-Lozano, M., Senarath, G.: A novel multiobjective cell switch-off framework for cellular networks. *IEEE Access* **4**, 7883–7898 (2016)
6. Knowles, J.: A summary-attainment-surface plotting method for visualizing the performance of stochastic multiobjective optimizers. In: 5th ISDA, pp. 552–557. IEEE (2005)
7. Luna, F., Luque-Baena, R., Martínez, J., Valenzuela-Valdés, J., Padilla, P.: Addressing the 5G cell switch-off problem with a multi-objective cellular genetic algorithm. In: IEEE 5G World Forum, 5GWF 2018 - Conference Proceedings, pp. 422–426 (2018)
8. Luna, F., Zapata-Cano, P.H., Palomares-Caballero, Á., Valenzuela-Valdés, J.F.: A capacity-enhanced local search for the 5G cell switch-off problem. In: Dorrnsoro, B., Ruiz, P., de la Torre, J.C., Urda, D., Talbi, E.-G. (eds.) OLA 2020. CCIS, vol. 1173, pp. 165–178. Springer, Cham (2020). https://doi.org/10.1007/978-3-030-41913-4_14
9. Mejia, V.D.L.: A modified binary particle swarm optimization algorithm to solve the thermal unit commitment problem. Master's thesis (2018)
10. Mirjalili, S., Lewis, A.: S-shaped versus V-shaped transfer functions for binary particle swarm optimization. *Swarm Evol. Comput.* **9**, 1–14 (2013)
11. Nebro, A.J., Durillo, J.J., Luna, F., Dorrnsoro, B., Alba, E.: MOCcell: a cellular genetic algorithm for multiobjective optimization. *Int. J. Intell. Syst.* **24**(7), 726–746 (2009)
12. Venkateswararao, K., Swain, P.: Binary-PSO-based energy-efficient small cell deployment in 5G ultra-dense network. *J. Supercomput.* **78**(1), 1071–1092 (2021). <https://doi.org/10.1007/s11227-021-03910-5>

13. Kang, M.W., Chung, Y.W.: An efficient energy saving scheme for base stations in 5G networks with separated data and control planes using particle swarm optimization. *Energies* **10**(9), 1417 (2017)
14. Zapata-Cano, P., Luna, F., Valenzuela-Valdés, J., Mora, A.M., Padilla, P.: Meta-heurísticas híbridas para el problema del apagado de celdas en redes 5G. In: XIII MAEB, pp. 665–670 (2018) (in Spanish)
15. Zitzler, E., Thiele, L.: Multiobjective evolutionary algorithms: a comparative case study and the strength pareto approach. *IEEE Trans. Evol. Comput.* **3**(4), 257–271 (1999)

3.2 Hybridization with Problem-Specific Operators

This article addresses the high energy consumption associated with the dense deployment of base stations in 5G networks through multi-objective metaheuristics. The paper introduces novel problem-specific operators to craft hybrid evolutionary metaheuristics that incorporate domain expertise into the algorithmic search process. This methodological advancement is shown to outperform canonical algorithms, validating the hypothesis that hybridization with multiple problem-specific operators can significantly enhance the search efficiency of multi-objective evolutionary algorithms.

THIS IS THE PUBLISHED VERSION OF THE PAPER:

J. Galeano-Brajones, F. Luna-Valero, J. Carmona-Murillo, P. H. Z. Cano, and J. F. Valenzuela-Valdés, “Designing problem-specific operators for solving the Cell Switch-Off problem in ultra-dense 5G networks with hybrid MOEAs,” *Swarm and Evolutionary Computation*, vol. 78, p. 101290, 2023.

- Journal Impact Factor (JIF) in JCR 2022: 10.0
- Category: COMPUTER SCIENCE, ARTIFICIAL INTELLIGENCE. JIF rank: 15/145 (Q1).
- Category: COMPUTER SCIENCE, THEORY & METHODS. JIF rank: 7/111 (D1).

Supplementary material is available in the Appendix C.

Disclaimer:

This work has been published in *Swarm and Evolutionary Computation*.
DOI: 10.1016/j.swevo.2023.101290

Copyright:

© 2023 The Authors. Published by Elsevier B.V. This is an open access article under the Creative Commons Attribution 4.0 International (CC-BY-4.0).



Contents lists available at ScienceDirect

Swarm and Evolutionary Computation

journal homepage: www.elsevier.com/locate/swevo

Designing problem-specific operators for solving the Cell Switch-Off problem in ultra-dense 5G networks with hybrid MOEAs

Jesús Galeano-Brajones^a, Francisco Luna-Valero^{b,c,*}, Javier Carmona-Murillo^a, Pablo H. Zapata Cano^d, Juan F. Valenzuela-Valdés^e

^a Dpto. de Ingeniería de Sistemas Informáticos y Telemáticos, Universidad de Extremadura, Centro Universitario de Mérida, Mérida, 06800, Spain

^b ITIS Software, Universidad de Málaga, Edificio de Investigación Ada Byron, Málaga, 29071, Spain

^c Dpto. de Lenguajes y Ciencias de la Computación, Universidad de Málaga, E.T.S.I. Informática, Málaga, 29071, Spain

^d School of Electrical and Computer Engineering, Aristotle University of Thessaloniki, Thessaloniki, 541 24, Greece

^e Dpto. de Teoría de la Señal, Telemática y Comunicaciones, CITIC, Universidad de Granada, Granada, 18014, Spain

ARTICLE INFO

Dataset link: https://github.com/galeanobra/C_SO_Hybrid, <https://doi.org/10.6084/m9.figshare.21378000>

Keywords:

Problem-specific operators
Hybridization
Multi-objective optimization
Ultra-dense networks
5G

ABSTRACT

The massive deployment of base stations is one of the key pillars of the fifth generation (5G) of mobile communications. However, this network densification entails high energy consumption that must be addressed to enhance the sustainability of this industry. This work faces this problem from a multi-objective optimization perspective, in which both energy efficiency and quality of service criteria are taken into account. To do so, several newly problem-specific operators have been designed so as to engineer hybrid multi-objective evolutionary metaheuristics (MOEAs) that bring expert knowledge of the domain to the search of the algorithms. These hybrid approaches have been able to improve upon canonical versions of the algorithms, clearly showing the contributions of our approach. Furthermore, this paper tests the hypothesis that the hybridization using several of those problem-specific operators simultaneously can enhance the search of MOEAs that are endowed only with a single one.

1. Introduction

Global mobile data traffic has increased massively, specially in the last decade, growing by 40% between Q1 2021 and Q1 2022. The high data transmission rates, along with other services that require ultra-low latency and reliable connections (e.g., autonomous driving, factory automation, etc.) or a massive number of narrowband Internet access (e.g., sensing and monitoring, Internet of Things, etc.), has promoted the development of a new generation of mobile communication systems, the fifth or 5G, to cope with such demanding scenarios and is currently under deployment. Indeed, 5G mobile subscriptions will surpass 1 billion in 2022, and are predicted to be 4.4 billion by the end of 2027, accounting for 48 percent of all mobile subscriptions [1]. 5G networks are expected to provide data rates 13 times higher than the average mobile connection by 2023, reaching 575 Mbps [2], as well as latencies below 1 ms and the support of more than one million devices per km². But this high performance must be achieved by saving 90% of power consumption, to make these new communication systems sustainable [3].

Three main paradigms have been identified to approach the challenging design requirements and expected performance indicators of 5G

networks [4,5]: (i) using the millimeter wave (mmWave) spectrum to enable larger bandwidths, (ii) increasing spectral efficiency by multi-antenna transmission (massive, collaborative MIMO), and (iii) also increasing spatial reuse through network densification [6] both in horizontal (streets, hotspots, etc.) and vertical dimensions of the network (apartments, offices, etc.) [7]. The bandwidth requirements of 5G networks force switching to mmWave spectrum, with carrier frequencies of 30–300 GHz [8]. In these bands, many antennas are needed to overcome the path losses [9]. The combination of both massive MIMO and mmWave in a single technology mixes the prospects of having a large mmWave bandwidth available and the gains provided by massive MIMO antenna arrays. Thus, enabling access to the 30–300 GHz bands will substantially improve the spectral efficiency [10,11]. Furthermore, this reinforces the necessity of having an Ultra-Dense Network (UDN), since transmitting at higher frequencies requires a reduction of the user-antenna distance, which translates into a smaller cell size, in order to overcome channel difficulties like blocking and path-loss [12]. This work aims at reducing the impact of these last two paradigms on the energy consumption of 5G networks.

* Corresponding author at: Dpto. de Lenguajes y Ciencias de la Computación, Universidad de Málaga, E.T.S.I. Informática, Málaga, 29071, Spain.
E-mail address: flv@cc.uma.es (F. Luna-Valero).

<https://doi.org/10.1016/j.swevo.2023.101290>

Received 21 October 2022; Received in revised form 4 January 2023; Accepted 3 March 2023

Available online 16 March 2023

2210-6502/© 2023 The Author(s). Published by Elsevier B.V. This is an open access article under the CC BY license (<http://creativecommons.org/licenses/by/4.0/>).

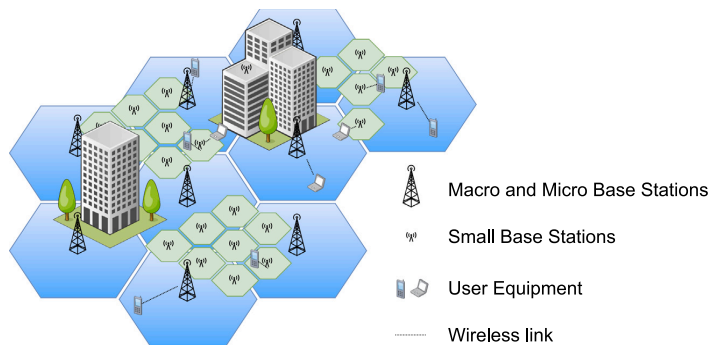


Fig. 1. An example of a UDN.

Several studies, such as [13], predict the density of 5G base stations (Small Base Stations, SBSs) to come up to 40–50 sites/km², but theoretical works exist in which SBS deployments with one-meter separation are characterized [6]. The main idea behind the network ultra-densification is to get the access nodes as close as possible to the end users. However, UDNs also lead to increased power consumption because of the large number of deployed SBSs (see Fig. 1). In fact, since the SBSs are responsible for 50 to 80 percent of the whole energy demand [14], densification will lead to unaffordable operational expenditures. In this context, an standardized approach by the 3rd Generation Partnership Project association [15] to save energy is the selective turning off of SBSs in periods in which the network is serving a low number of users. This problem, called the Cell Switch Off (CSO) problem [16], is NP-complete [17] and cannot only account for a reduction in energy consumption (a trivial solution might be to shut down the entire infrastructure), but also for any performance criterion that measures the Quality of Service (QoS) provided by the network. To this end, the network capacity has been considered in terms of the total bandwidth that can be served to users. Given the level of densification anticipated for real-world 5G networks, that is, the size of problem instances (the number of SBSs that could be switched on/off), a metaheuristic approach is used. Specifically, we elaborate on multi-objective metaheuristics that seek trade-off solutions between power consumption and network capacity [18,19].

This work is in the line of developing problem-specific search operators to improve the exploration of multi-objective metaheuristics, and significantly extends previous works [20,21]. Firstly, the problem modeling has been enhanced to incorporate additional real-world features of 5G networks, including a mmWave massive multiuser MIMO scenario in which several User Equipments (UEs) are communicating at the same time using connections towards high-frequency SBSs. Each of these SBSs now has several sectors, and each sector now installs multiple antennas grouped into radio frequency chains that define the cells (i.e., the area covered by the sector). Under this new modeling, two new search operators are proposed that take advantage of the network densification and sectorization of SBSs to reduce power consumption. The adaptation and extension of previously defined operators to the CSO problem in [20,21] have also been achieved. The effectiveness of all these operators has been evaluated by providing solid experimental evidence in nine different scenarios with different densification levels in the deployment of both SBS and UE. For each of these scenarios, 50 different instances have been randomly generated, thus considering 450 problem instances. We have engineered hybrid versions of multi-objective metaheuristics that encompass Pareto-based, indicator-based, and decomposition-based approaches to show that the problem-specific information introduced by the newly devised operators improves the search of the three main algorithmic groups within the domain. In particular, the solvers used are as follows: NSGA-II [22] and MOCcell [23]

(Pareto-based), as they have been used in our previous works [19–21], SMS-EMOA [24] (indicator-based), and MOEA/D [25]. Furthermore, since the solutions are represented by binary strings, where each bit corresponds to the state (on/off) of a cell, and we seek to reduce the power consumption over periods of low traffic demands (i.e., a small number of UEs), solutions may contain many bits set to zero. For this reason, we have also included in the comparison a recent and specialized algorithm called SparseEA [26], which targets precisely this kind of sparse optimization problems [27]. Using the Hypervolume (HV) [28], a Pareto-compliant quality indicator, the results have shown that newly devised operators have always improved the search of all the multi-objective metaheuristics considered, thus clearly enhancing their search capabilities for addressing the CSO problem.

The rest of the document is organized as follows: the next section elaborates on the work related to the CSO problem and how it has been addressed in the literature. Section 3 details the UDN system model and formulates the CSO problem objectives. The MOEAs used and the problem-specific operators designed for hybridization are described in Section 4. Section 5 develops the methodology used in the experimentation and analyzes the results obtained. The final section is devoted to summarizing the main conclusions of the work as well as the lines of future work.

2. Related work

The energy consumption of Information and Communication Technologies infrastructures (ICT) in general [29], and cellular networks in particular [30,31], has been an active research topic, specially in the last 20 years, in order to address the ever-increasing carbon footprint on the environment of this industry. The enabling technologies of 5G networks make the energy issue even worse, as has been clearly stated in recent surveys that have revised the different approaches proposed in the literature to reduce power consumption from different perspectives, ranging from advanced energy management strategies [32–37] to data-driven schemes based on Artificial Intelligence/Machine Learning [38, 39]. Sustainability in UDNs has also attracted a lot of attention, as the massive deployment of SBSs is a key factor in power consumption, with surveys specifically aimed at this 5G paradigm [40–42].

Cell activation/deactivation is a common and useful technique for reducing energy consumption in all previously comprehensive reviews of the literature. Determining which SBSs are switched on or off requires the network first to serve a traffic demand, and the decision can be made either in an online (dynamic) [43] or offline (static) manner [44]. This work focuses on the latter approach, as radio network engineers are usually reluctant to undertake frequent SBS switching (e.g., at locations with large traffic fluctuations) and require their approval. The underlying problem, named the Cell Switch-Off (CSO) problem [16], is known to be NP-complete [17], and it has been tackled

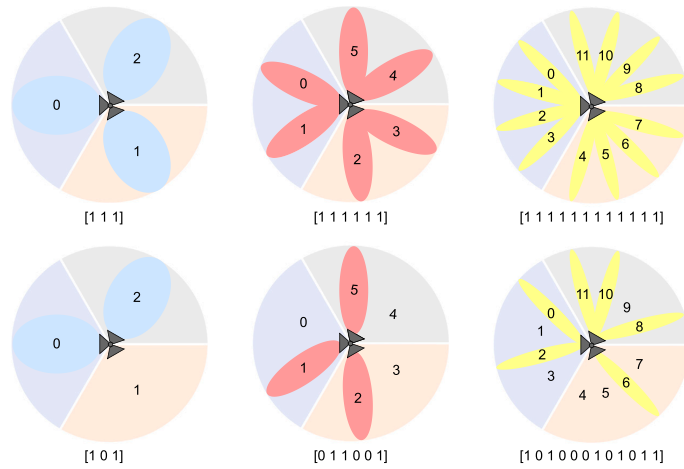


Fig. 2. Configuration of the SBSs, sectors and cells used in this work, as well as its mapping into a binary encoded representation.

Table 1

Model parameters for users and base stations.

Cell	Parameter	Eq.	LL	LM	LH	ML	MM	MH	HL	HM	HH	
Micro	G_{ix}	(2)	12									
	f	(5)	5 GHz (BW = 500 MHz)									
	α	(8)	15									
	β	(8)	10000									
	δ	(8)	1									
	ρ [W]	(8)	1									
	n_{ix}		8									
	n_{rx}		2									
	λ_p^{micro} [Cells/km ²]			300	300	300	600	600	600	900	900	900
	Pico	G_{ix}	(2)	20								
f		(5)	20 GHz (BW = 2000 MHz)									
α		(8)	9									
β		(8)	6800									
δ		(8)	0.5									
ρ [W]		(8)	1									
n_{ix}			64									
n_{rx}			4									
λ_p^{pico} [Cells/km ²]				1500	1500	1500	1800	1800	1800	2100	2100	2100
Femto		G_{ix}	(2)	28								
	f	(5)	68 GHz (BW = 6800 MHz)									
	α	(8)	5.5									
	β	(8)	4800									
	δ	(8)	0.2									
	ρ [W]	(8)	1									
	n_{ix}		256									
	n_{rx}		8									
	λ_p^{femto} [Cells/km ²]			3000	3000	3000	6000	6000	6000	9000	9000	9000
	UEs	λ_p^{UE} [UE/km ²]		1000	2000	3000	1000	2000	3000	1000	2000	3000

with different approaches in the domain, such as clustering [45–47] or game theory [48]. This decision problem has also been defined as an optimization problem [17] and, within this research field, it has been addressed with exact [49,50], heuristic [51–53] and metaheuristic techniques [18,54]. Our work relies on this last set of methods, which embrace both single [55,56] and multi-objective approaches [19,57]. However, in the context of the CSO problem, apart from previous works from the authors [20,21], only canonical versions of metaheuristics have been used. It is well known that hybridization is a powerful tool for improving the search of these algorithms [58] but, to the best of our knowledge, this topic is still unexplored in the CSO literature. Under the new and more accurate modeling of the CSO problem, this work improves upon our previously published material by devising additional local search operators aimed at reducing the power consumption and

also showing their suitability over MOEAs covering the most important trends in the domain, e.g., Pareto-based, decomposition-based, and indicator-based algorithms that, to the best of our knowledge, have never been hybridized (SMS-EMOA and MOEA/D, particularly) or even used before in the context of this problem (SparseEA). We have also evaluated the synergy between different operators, which also opens new promising lines of research.

3. The CSO problem

This section first introduces the modeling of the UDN and its parameters, and then describes the mathematical formulation of the CSO problem addressed.

3.1. UDN modeling

This work considers a service area of 500×500 meters, where ten different regions have been defined with different propagation conditions. To compute the received power at a given location of this area, P_{rx} [dBm], the following model has been used:

$$P_{rx} \text{ [dBm]} = P_{tx} \text{ [dBm]} + P_{Loss} \text{ [dB]} \quad (1)$$

where, P_{rx} is the received power in dBm, P_{tx} is the transmitted power in dBm, and P_{Loss} are the global signal losses, which depend on the given propagation region, and are computed as:

$$P_{Loss} \text{ [dB]} = GA + PA \quad (2)$$

where GA is the total gain of both antennas, and PA are the transmission losses in space, computed as:

$$PA \text{ [dB]} = \left(\frac{\lambda}{4 \cdot \pi \cdot d} \right)^K \quad (3)$$

where d is the Euclidean distance to the corresponding sector at the SBS, K is the exponent loss, which randomly ranges in $[2.0, 4.0]$ for each of the 10 different regions. The Signal-to-Interference plus Noise Ratio (SINR) for UE k , is computed as:

$$SINR_k = \frac{P_{rx,j,k} \text{ [mW]}}{\sum_{i=1}^M P_{rx,i,k} \text{ [mW]} - P_{rx,j,k} \text{ [mW]} + P_n \text{ [mW]}} \quad (4)$$

where $P_{rx,j,k}$ is the received power by UE k from the cell j , the summation is the total received power by UE k from all the cells operating at the same frequency that j , and P_n is the noise power, computed as:

$$P_n \text{ [dBm]} = -174 + 10 \cdot \log_{10} BW_j \quad (5)$$

being BW_j the bandwidth of cell j , defined as 10% of the SBS operating frequency, which is the same for all cells it deploys (see Table 1).

Finally, the UEs capacity has been calculated according to the MIMO depicted in [59]. Thus, we assume that the transmission power from each antenna is P_{tx}/n_{tx} , where n_{tx} indicates the number of transmitting antennas. Then, if we consider the subchannels to be uncoupled, their capacities can add up, and the overall channel capacity of the UE k can be estimated using the Shannon capacity formula:

$$C_k^j \text{ [bps]} = BW_k^j \text{ [Hz]} \cdot \sum_{i=1}^r \log_2 \left(1 + \frac{SINR_k \cdot \lambda_i}{n_{tx}} \right) \quad (6)$$

where $\sqrt{\lambda_i}$ is the singular value of the channel matrix \mathbf{H} , of dimensions $n_{rx} \times n_{tx}$ (i.e., # receiving antennas \times # transmitting antennas). Note that both n_{rx} and n_{tx} depend on the cell type (see Table 1). BW_k^j is the bandwidth assigned to UE k when connected to the cell j , assuming round-robin scheduling, that is:

$$BW_k^j = \frac{BW_j}{N_j} \quad (7)$$

where N_j is the number of UEs connected to a cell j , and the UEs are connected to the cell that provides the highest SINR, regardless of its type.

In order to build a heterogeneous network, three different types of cells of increasing size and decreasing frequency are considered: femtocells, picocells and microcells. Recall that these cells are generated by the antennas installed in a given sector of an SBS. Fig. 2 illustrates the three configurations used in our modeling. In the first row, the three SBSs have the three sectors and all their cells switched on (in operation), thus the mapping to the binary string that represents a tentative solution, included below each subfigure, does have all the genes set to 1. In the second row, we have included several solutions with a subset of cells switched off, with the corresponding genes set to 0. It should also be noted that the number of transmitting antennas of each cell type increases with frequency, being 8, 64 and 256 transmitting antennas, respectively, for micro, pico, and femtocells. In the same way, we assume that high-capacity UEs, which will preferably connect to

small cells (pico and femtocells), will implement a higher number of receiving antennas (4 and 8 for pico and femtocells, respectively).

With the system configuration described above, the actual deployment of the cells is carried out via the placement of SBSs in the working area, using a random rotation angle for the sectors, which determines the orientation of the different cell beams. Then, both SBSs and UEs are deployed using independent Poisson Point Processes (PPP) with different densities, defined by λ_p^{cells} and λ_p^{UE} , respectively. We have implemented in our software framework a discretization approach that uses a grid of 100×100 points (also called ‘‘pixels’’ or area elements), each covering a 25 m^2 area, where the signal power is assumed to be constant. In addition to that, vertical densification has been taken into account by considering 3 vertical area elements, i.e., 25 meters of height. The purpose of this mechanism is to reduce the computational cost of calculating the SINR values.

The power consumption of a transmitter is computed based on the model presented in [3], which considers that the device is transmitting over the fiber backhauling. Therefore, the regular power consumption of cell j , P_j , is expressed as:

$$P_j = \alpha \cdot P + \beta + \delta \cdot S + \rho \quad (8)$$

where P denotes the transmitted or radiated power of the transmitter, the coefficient α represents the efficiency of the transmission power produced by a radio frequency amplifier and feeder losses, the power dissipated due to signal processing and site cooling is denoted by β and the dynamic power consumption per unit of data is given by δ , being S the actual traffic demand provided by the serving cell. Finally, the power consumption of the transmitting device is represented by the coefficient ρ . However, in order to consider an accurate power consumption model, the power consumed by the air conditioning and power supply of the SBS should be also taken into account [60]. This has been called maintenance power and is set to $2W/SBS$ for any SBS containing at least one active cell.

The detailed parametrization of the scenarios addressed is included in Table 1, in which column Eq. links the parameter to the corresponding equation in the formulation detailed above. The names in the last nine columns, XY, represent the deployment densities of SBSs and UEs, respectively, so that $X = \{L, M, H\}$, meaning either low, medium, or high-density deployments (λ_p^{cells} parameter of the PPP), and $Y = \{L, M, H\}$, indicates a low, medium or high density of deployed UEs (λ_p^{UE} parameter of the PPP), in the last row of the table. The parameters G_{tx} and f of each type of cell refer to the transmission gain and the operating frequency (and its available bandwidth) of the antenna, respectively, being n_{tx} and n_{rx} the number of transmit and receive antennas. Finally, the parameters of the previously described power consumption model are also included. Nine instances have been therefore used in this work in order to assess the performance of the different metaheuristics and their hybridization with the problem-specific operators.

3.2. Problem formulation and objectives

Let \mathcal{B} be the set of randomly deployed SBSs and \mathcal{C}_b the set of cells installed in SBS b , with $b \in \mathcal{B}$. A solution to the CSO problem is a binary string s , where s_c^b indicates whether the cell c of a given SBS b is activated or not. The first objective to be minimized is, therefore, computed as:

$$\min f_{Power}(s) = \sum_b^{\mathcal{B}} P_b \sum_c^{\mathcal{C}_b} s_c^b \quad (9)$$

where P_b is the power consumption of SBS b (Eq. (8)). Note that P_b includes both the transmission power of every cell $c \in \mathcal{C}_b$ and its maintenance power.

Let \mathcal{U} be the set of UEs also deployed as described in the previous section, and \mathcal{U} the entire set of cells contained in \mathcal{B} . Subsequently, in order to compute the total capacity of the system, UEs are first

assigned to the active Cell that provides it with the highest SINR. Let $\mathcal{A}(s) \in \{0,1\}^{|\mathcal{U}^*| \times |\mathcal{C}|}$ be the matrix where $a_{ij} = 1$ if $s_j = 1$ and the Cell j serves UE i with the highest SINR, and $a_{ij} = 0$ otherwise. Then, the second objective to be maximized, which is the total capacity provided to all UEs, is calculated as:

$$\max f_{Cap}(s) = \sum_{i=1}^{|\mathcal{U}^*|} \sum_{j=1}^{|\mathcal{C}|} s_j \cdot a_{ij} \cdot C_i^j \quad (10)$$

where C_i^j is the capacity of Cell j provided to UE i (Eq. (7)). We would like to remark that these two problem objectives are clearly conflicting one each other, since switching off base stations leads to a reduction of the power consumption of the network, but it also damages the capacity received by the user, as the UE-Cell distance increases (rising the propagation losses) at the same time as the available bandwidth to serve users is reduced.

4. Hybridization: MOEAs used and newly developed operators for the CSO problem

This section first describes briefly the MOEAs used in this work. Then, the problem-specific operators devised for the CSO problem are detailed. The last part is devoted to showing how these operators are integrated within the evolutionary loop of the chosen multi-objective metaheuristics.

4.1. Multi-objective evolutionary algorithms

In the last decades, Evolutionary Algorithms (EAs) have shown their effectiveness in solving different optimization and search problems. In addition, one of the most interesting capabilities of these algorithms is the ability to deal with multi-objective optimization problems. Since its proposal in the 1990s, Multi-Objective Evolutionary Algorithms (MOEAs) have been widely used for the resolution of several complex problems with two or three conflicting objectives in various branches of engineering, science, and commerce. If the problems have more conflicting objectives, the research community has proposed different alternatives, since MOEAs lose performance when the number of conflicting objectives increases [61,62].

In order to address the optimization problem stated in this paper, the following five MOEAs have been chosen from the specialized literature: NSGA-II (*Non-dominated Sorting Genetic Algorithm II*) [22], MOCell (*Multi-Objective Cellular Genetic Algorithm*) [23], SMS-EMOA (*S Metric Selection Evolutionary Multi-Objective Algorithm*) [24], MOEA/D (*Multi-Objective Evolutionary Algorithm based on Decomposition*) [25] and SparseEA [26].

The first four algorithms are well known in the literature and have been selected to cover the three main paradigms for solving multi-objective optimization problems (MOPs), namely, Pareto-based, indicator-based, and decomposition-based. NSGA-II and MOCell are representative of Pareto-based approaches that have already been used in previous works by the authors in the context of the CSO problem. They use ranking to identify non-dominated solutions, and crowding as a density estimator to promote these non-dominated solutions of the less populated areas of the approximated Pareto fronts. This latter operator is rather computationally expensive, but improved implementations exist [63]. As an indicator-based algorithm, we have chosen SMS-EMOA, whose search engine is guided by Hypervolume. And finally, MOEA/D covers the decomposition-based paradigm. SparseEA deserves special attention, as it is a recent algorithmic proposal specifically aimed at solving sparse MOPs, i.e., large-scale binary-encoded MOPs in which most of the decision variables are zero [64]. This is potentially the context of the CSO problem, as it tries to switch off as many cells as possible in periods of low traffic demands to reduce power consumption. To do so, SparseEA uses a similar scheme as NSGA-II in terms of crossover, selection, ranking and crowding, but

it applies tailored strategies to generate the initial population and the offspring that aim at ensuring the sparsity of the solutions generated. This algorithm uses a hybrid representation of the solutions (real and binary vectors), where the real vector stores the best values of the decision variables found so far, and the binary vector stores the decision variables that should be set to zero to control the sparsity of solutions.

4.2. Hybridization with problem-specific operators

The integration of problem-specific operators in the evolutionary cycle is done after the application of the genetic operators, as shown in Algorithm 1. Each specific operator is applied with a probability $rate_{operator}$ defined in [0,1]. For multi-operator hybrids, the following order is used: EC^\downarrow , SC^\downarrow , PF^\uparrow , PSC^\uparrow and HF^\uparrow . Hence, all, some, or none could be potentially applied.

4.3. Problem-specific operators

We have defined five different local search operators that are aimed at exploiting problem-specific information that can guide the search of MOEAs towards regions of higher quality solutions. These operators mainly target switching cells either on or off, so their acronyms have used a superscript with a \uparrow or \downarrow , respectively, to better show this fact and enhance the reading. They all have linear computational complexity, thus not substantially increasing the runtime.

4.3.1. EC^\downarrow : Empty cell operator

As a consequence of SBS densification and sectorization, many cells may result to be empty, i.e., not providing service to any user, so that it can be switched off. In order to incorporate this useful information about the network into the algorithm search, the *Empty Cell* operator, or EC^\downarrow for short, has been designed. It explores all cells of the candidate solution, switching off those that are not serving any UE, as it is illustrated in Algorithm 2. Despite its apparent simplicity, this operator promotes a considerable intensification capacity. It is remarkable that, when applied without any restriction, the EC^\downarrow operator can disrupt the evolution of the algorithm, since it prevents the generation of solutions that reassign users to such empty cells, since they would all be switched off after the action of the operator. In order to address this issue, the operator is applied with a certain rate.

4.3.2. SC^\downarrow : Single cell operator

Having multiple sectors/cells within a single SBS introduces new optimization possibilities to improve the search capabilities of the algorithms. In particular, the *Single Cell* operator (SC^\downarrow) aims to explore low power consumption solutions by switching off base stations that have only one single active cell, saving in this way the power consumed by the air conditioning and power supply of the entire SBS. Again, when applied without restrictions, this operator might lead to solutions in which some important base stations might be switched off, regardless of the number of users that were assigned to them. This fact could significantly disrupt the search of the MOEAs. For that reason, this operator is applied with a given rate. Algorithm 3 sketches the pseudocode of the operator.

4.3.3. PF^\uparrow And PSC^\uparrow : Prioritize femto and prioritize small cells operators

In contrast to the previous specific operators, which aim to intensify the search in areas of low energy consumption, the *Prioritize Femto Cells* and *Prioritize Small Cells* operators aim to intensify it in the area of the highest capacity. These operators seek active cells that offer an SINR level higher than a threshold over the SINR of users with the cells to which they are assigned. After experiments with values from 1 dB to 9 dB, the threshold value was set at 1 dB, as it was the one with the best results. In addition, this value allows us to maintain consistency with previous works [21]. The difference between the two operators lies in the set of candidate UEs to participate in the search:

Algorithm 1: Pseudocode of the hybridization with problem-specific operators.

```

1:  $t \leftarrow 0$  // Generation counter
2:  $A(t) \leftarrow \emptyset$  // Archive for non-dominated solutions
3:  $S(t) \leftarrow \text{GenerateInitialPopulation}()$  // Current population
4:  $\text{Evaluate}(S(t))$  // Evaluate the problem objectives
5:  $A(t) \leftarrow \text{Update}(A(t), S(t))$  // Obtain the non-dominated solutions from  $S(0)$ 
6: while not  $\text{StoppingCondition}()$  do
7:    $t \leftarrow t + 1$ 
8:    $S(t) \leftarrow \text{Selection}(S(t-1), A(t-1))$  // Select solutions for mating
9:    $S(t) \leftarrow \text{Variation}(S(t), A(t-1))$  // Apply variation operators (crossover, mutation)
10:  // using the mating population and the archive
11:  for all  $s \in S(t)$  do
12:     $r_1 \leftarrow \text{Random}(0, 1)$  // Draw a random number in  $[0, 1]$ 
13:    if  $r_1 < \text{rate}_{\text{Operator1}}$  then
14:       $s \leftarrow \text{Operator1}(s)$  // Apply Operator1 to solution  $s$ 
15:    end if
16:     $r_2 \leftarrow \text{Random}(0, 1)$ 
17:    if  $r_2 < \text{rate}_{\text{Operator2}}$  then
18:       $s \leftarrow \text{Operator2}(s)$  // Apply Operator2 to solution  $s$ 
19:    end if
20:    ...
21:     $r_n \leftarrow \text{Random}(0, 1)$ 
22:    if  $r_n < \text{rate}_{\text{OperatorN}}$  then
23:       $s \leftarrow \text{OperatorN}(s)$  // Apply OperatorN to solution  $s$ 
24:    end if
25:  end for
26:   $\text{Evaluate}(S(t))$ 
27:   $A(t) \leftarrow \text{Update}(A(t-1), S(t))$  // Obtain the non-dominated solutions from the
28:  // current population  $S(t)$  and the archive  $A(t-1)$ 
29:   $S(t) \leftarrow \text{Replacement}(S(t), A(t))$  // Replace solutions in the current population
30: end while
31: Output:  $A(t)$ 

```

Algorithm 2: Pseudocode of the EC^\perp operator.

```

1:  $C \leftarrow \text{cells}(UDN)$ 
2: for  $c \in C$  do
3:   if  $\text{ConnectedUES}(c) == 0$  then
4:      $\text{SwitchOff}(c)$ 
5:   end if
6: end for

```

Algorithm 3: Pseudocode of the SC^\perp operator.

```

1:  $B \leftarrow \text{SBSs}(UDN)$ 
2: for  $b \in B$  do
3:   if  $\text{ActiveCells}(b) == 1$  then
4:      $c \leftarrow \text{ActiveCell}(b)$ 
5:      $\text{SwitchOff}(c)$ 
6:   end if
7: end for

```

Prioritize Femto Cells only concerns the UDN UEs that are not assigned to femtocells; *Prioritize Small Cells* is less restrictive, using the UEs that are not assigned to small cells, that is, microcells and macrocells. After switching on the cell that meets the SINR threshold, if any, the operator switches off all cells that have no UEs assigned to them. Therefore, the EC^\perp is likely to be applied as a final step. Algorithm 4 shows the pseudocode of the two operators, which differs only in the initial set of cells.

4.3.4. HF^\perp : Higher frequency operator

Similar to PF^\perp and PSC^\perp operators, the purpose of the *Higher Frequency* operator is to intensify the search towards the capacity objective. This operator seeks to take advantage of the capacity improvements that can be offered by smaller cells with a higher operating frequency than those serving UEs. Thus, this operator turns on cells of the same SBSs to which the UEs are assigned and that offer a higher SINR than the one they already have. Furthermore, if the cell to which the UEs are assigned only serves one, the cell is turned off to encourage the UEs to be assigned to the activated cell, thus promoting the increase

Algorithm 4: Pseudocode of the PF^\perp and PSC^\perp operators.

```

1: if  $PF^\perp$  then
2:    $U \leftarrow \text{UsersNotServedByFemtoCells}(UDN)$ 
3: else if  $PSC^\perp$  then
4:    $U \leftarrow \text{UsersNotServedBySmallCells}(UDN)$ 
5: end if
6:
7: for  $u \in U$  do
8:    $\text{current} \leftarrow \text{GetServingCell}(u)$ 
9:    $C \leftarrow \text{GetFemtoCellsWithHigherSINR}(u)$ 
10:  for  $c \in C$  do
11:    if  $\text{SINR}(u, c) > 1 \text{ dB}$  then
12:       $\text{SwitchOn}(c)$ 
13:      if  $\text{GetAssignedUsers}(\text{current}) == 1$  then
14:         $\text{SwitchOff}(\text{current})$ 
15:      end if
16:    break
17:  end if
18: end for
19: end for
20:  $\text{SwitchOffEmptyCells}()$ 

```

of capacity as well as the reduction of the power consumption, as illustrated in Algorithm 5.

5. Experimentation

This section describes the methodology used to conduct the experiments, showing the effectiveness of the new hybrid proposals, as well as the analysis of the results obtained.

5.1. Methodology

Based on the nine scenarios described in Section 3 and the stochastic nature of the metaheuristics, 50 seeds have been addressed in the experimentation for each type of scenario. This ensures that all algorithms face the same set of problem instances.

Algorithm 5: Pseudocode of the HF^1 operator.

```

1:  $U \leftarrow GetUsers(UDN)$ 
2: for  $u \in U$  do
3:    $b \leftarrow GetServingBTS(u)$ 
4:    $best \leftarrow GetServingCell(u)$ 
5:    $current \leftarrow best$ 
6:   for  $c \in GetCellsWithHigherOperatingFrequency(b)$  do
7:     if  $SINR(u,c) \geq SINR(u,best)$  then
8:        $best \leftarrow c$ 
9:     end if
10:  end for
11: end for
12:  $SwitchOn(best)$ 
13: if  $GetAssignedUsers(current) == 1$  then
14:    $SwitchOff(current)$ 
15: end if

```

In order to obtain fair comparative results between algorithms, they all use the same population size of 100 solutions and the same genetic operators: binary tournament selection, two-point crossover with a crossover rate of 0.9, and bit-flip mutation with a mutation rate of $1/L$, being L the number of cells in the scenario. SparseEA is the exception because its own framework is designed to maintain sparsity in solutions, and changing its genetic operators to general-purpose ones would cause the algorithm to lose its distinguishing features from the others. Moreover, MOEA/D has also used a binary tournament to select two parents for crossover.

The stopping condition is defined as a maximum number of function evaluations, which increases with the density of deployed SBSs, that is, with the size of the instance. The following values have been set up: 100,000 evaluations for $L\{X\}$; 150,000 evaluations for $M\{X\}$; and 250,000 evaluations for $H\{X\}$, (being $\{X\}$ the three densities of the UEs). These values are obtained after a preliminary study that has shown that they are enough to guarantee the convergence of the algorithms.

With respect to the specific operators, the first step has been to conduct experiments with them separately to clearly isolate their impact on the search of the different MOEAs. For this purpose, we have initially defined the following application rates: 0.1, 0.05, 0.01, 0.005 and 0.001. However, after briefly analyzing the results, the two smaller ones, 0.05 and 0.005, have not been considered anymore in this work, as they have provided negligible contributions to the quality of the solutions reached. We have also removed these two settings to increase the readability of the results. Bearing all this in mind, this part of the experiments accounted for a total of 67,500 runs. A final set of experiments carried out to analyze potential synergies between the problem-specific operators in the hybrid MOEAs has involved 5 MOEAs, 5 operators, 5 application rates, 14 combinations between operators, 9 scenarios, and 50 seeds, which amounts to 31,500 additional runs. All of them have required roughly about 18.4 years of CPU time. In order to afford such computational demands, the experiments have been deployed in the facilities of the Supercomputing and Bioinformatics Center of the Universidad de Málaga, named Picasso. It is a heterogeneous computing platform composed of several clusters with up to 30.616 computing cores. The full hardware description can be found in <http://www.scbi.uma.es/site/scbi/hardware>.

Two indicators have been used to measure the quality of the approximations to the Pareto front achieved by the different algorithms: the attainment surfaces [65] and Hypervolume (HV) [28]. The empirical attainment function (EAF) [65] allows undertaking a graphical analysis of the approximated fronts. Indeed, EAF graphically displays the expected performance and its variability of the approximated Pareto fronts obtained by the multi-objective algorithm over multiple runs. Informally, the 50%-attainment surface in the multi-objective domain, which is

Table 2
Median and IQR of HV for the canonical MOEAs.

	NSGA-II	MOCeII	SMS-EMOA	MOEA/D	SparseEA
LL	0.521 _{0,170}	0.296 _{0,188}	0.642 _{0,150}	0.000 _{0,000}	0.212 _{0,051}
LM	0.520 _{0,185}	0.266 _{0,193}	0.594 _{0,125}	0.000 _{0,000}	0.208 _{0,069}
LH	0.449 _{0,161}	0.258 _{0,198}	0.556 _{0,133}	0.000 _{0,000}	0.216 _{0,055}
ML	0.271 _{0,170}	0.434 _{0,212}	0.519 _{0,137}	0.000 _{0,000}	0.165 _{0,045}
MM	0.193 _{0,231}	0.303 _{0,183}	0.437 _{0,141}	0.000 _{0,000}	0.173 _{0,041}
MH	0.210 _{0,285}	0.036 _{0,194}	0.435 _{0,191}	0.000 _{0,000}	0.181 _{0,040}
HL	0.365 _{0,249}	0.005 _{0,199}	0.579 _{0,161}	0.000 _{0,000}	0.153 _{0,036}
HM	0.179 _{0,265}	0.000 _{0,035}	0.438 _{0,160}	0.000 _{0,000}	0.145 _{0,042}
HH	0.177 _{0,265}	0.000 _{0,075}	0.407 _{0,204}	0.000 _{0,000}	0.155 _{0,040}

chosen here, is analogous to the median value in the single-objective one. The HV, in turn, is a Pareto-compliant, single-value-based quality indicator considered in the multi-objective community as one of the most reliable measures to compare approximations to the Pareto front of different algorithms. Its values depend, however, on the arbitrary scale of the objective function values, so a normalization procedure is required to avoid misleading results. To do so, and since the problem addressed in this paper is a realistic NP-complete combinatorial optimization problem for which we do not have the true Pareto front, a reference Pareto front (RPF) has been built for each instance of the problem. This RPF is composed of all the non-dominated solutions found by all the algorithms involved in these experiments, and is used to normalize the approximated fronts reached by the algorithms prior to calculating the HV value. Non-dominated solutions outside of the limits of the corresponding RPF are discarded (i.e., their contribution to the HV is zero).

In order to provide these HV results with statistical significance [66], a Kolmogorov–Smirnov test is first performed to check whether the 50 samples are distributed according to a normal distribution or not. If so, an ANOVA I test is performed; otherwise, a Kruskal–Wallis test is performed. Since more than two algorithms are involved in the study, a post hoc testing phase that allows for multiple comparisons of samples (multicompare) has been conducted. All statistical tests are performed with a confidence level of 95%. The stats output is shown in a tabular form, as a head-to-head comparison between pairs of algorithms; a black upward triangle says that the setting of the row has statistically higher values than the configuration of the column, and a white downward triangle states that the configuration in the row has statistically lower values than the configuration in the column. When no statistically significant differences are found, the spot is left empty. We have also computed the Friedman rank sum test with Holm correction to support several rankings among the algorithms that are undertaken in the result analyses below.

Both the generated data and the statistical tests can be found as supplementary material at <https://doi.org/10.6084/m9.figshare.21378000>. All the software and the scenarios used can be also downloaded from https://github.com/galeanobra/CSO_Hybrid in order to guarantee the reproducibility of the experimentation. In the following sections, we have structured all this information in a readable form to ease the analysis of the results and to better support our conclusions.

5.2. Results

This scbi has been structured into two separated parts: the first one aims at showing how the problem-specific operators devised in this work (and described in Section 4.3) improve the search of the five MOEAs in which they have been incorporated; as these operators have different intensification capabilities towards a given objective (either the energy consumption or the network capacity), the second part is devoted to analyzing potential synergies between them, when applying several of such operators simultaneously.

Table 3
Median and IQR of the HV indicator for NSGA-II in the nine scenarios.

	Canonical	EC ¹			SC ¹			PF ¹			PSC ¹			HF ¹		
		0.1	0.01	0.001	0.1	0.01	0.001	0.1	0.01	0.001	0.1	0.01	0.001	0.1	0.01	0.001
LL	0.521 _{0,170}	0.766 _{0,076}	0.748 _{0,104}	0.668 _{0,219}	0.539 _{0,187}	0.608 _{0,119}	0.541 _{0,158}	0.744 _{0,079}	0.758 _{0,080}	0.589 _{0,211}	0.732 _{0,082}	0.735 _{0,100}	0.571 _{0,232}	0.528 _{0,226}	0.536 _{0,200}	0.505 _{0,162}
LM	0.520 _{0,185}	0.747 _{0,071}	0.720 _{0,081}	0.621 _{0,247}	0.510 _{0,149}	0.555 _{0,131}	0.519 _{0,130}	0.700 _{0,087}	0.693 _{0,092}	0.533 _{0,185}	0.687 _{0,121}	0.671 _{0,148}	0.530 _{0,184}	0.486 _{0,167}	0.467 _{0,160}	0.514 _{0,134}
LH	0.449 _{0,161}	0.719 _{0,086}	0.671 _{0,068}	0.546 _{0,228}	0.441 _{0,154}	0.504 _{0,147}	0.438 _{0,162}	0.648 _{0,122}	0.639 _{0,126}	0.479 _{0,227}	0.648 _{0,097}	0.644 _{0,082}	0.500 _{0,175}	0.413 _{0,164}	0.449 _{0,184}	0.452 _{0,165}
ML	0.271 _{0,170}	0.739 _{0,076}	0.713 _{0,102}	0.658 _{0,167}	0.261 _{0,191}	0.412 _{0,193}	0.327 _{0,222}	0.717 _{0,095}	0.717 _{0,105}	0.624 _{0,366}	0.710 _{0,109}	0.710 _{0,106}	0.572 _{0,466}	0.280 _{0,199}	0.262 _{0,141}	0.282 _{0,203}
MM	0.193 _{0,231}	0.707 _{0,070}	0.689 _{0,096}	0.617 _{0,243}	0.150 _{0,248}	0.286 _{0,204}	0.228 _{0,241}	0.668 _{0,103}	0.667 _{0,100}	0.362 _{0,493}	0.665 _{0,092}	0.640 _{0,126}	0.367 _{0,398}	0.183 _{0,260}	0.179 _{0,224}	0.207 _{0,219}
MH	0.210 _{0,285}	0.668 _{0,092}	0.657 _{0,129}	0.513 _{0,113}	0.210 _{0,279}	0.312 _{0,215}	0.266 _{0,263}	0.622 _{0,163}	0.606 _{0,147}	0.416 _{0,501}	0.589 _{0,155}	0.607 _{0,147}	0.295 _{0,356}	0.165 _{0,325}	0.191 _{0,298}	0.184 _{0,246}
HL	0.365 _{0,249}	0.714 _{0,082}	0.714 _{0,096}	0.683 _{0,146}	0.306 _{0,260}	0.480 _{0,218}	0.366 _{0,281}	0.712 _{0,106}	0.720 _{0,095}	0.697 _{0,187}	0.695 _{0,104}	0.709 _{0,090}	0.671 _{0,151}	0.320 _{0,201}	0.339 _{0,283}	0.334 _{0,294}
HM	0.179 _{0,265}	0.653 _{0,093}	0.630 _{0,119}	0.583 _{0,162}	0.189 _{0,226}	0.321 _{0,232}	0.253 _{0,188}	0.619 _{0,129}	0.613 _{0,133}	0.595 _{0,237}	0.616 _{0,100}	0.628 _{0,108}	0.584 _{0,172}	0.176 _{0,180}	0.186 _{0,250}	0.192 _{0,197}
HH	0.177 _{0,265}	0.633 _{0,088}	0.600 _{0,103}	0.539 _{0,187}	0.191 _{0,263}	0.276 _{0,229}	0.165 _{0,241}	0.603 _{0,134}	0.592 _{0,118}	0.400 _{0,418}	0.600 _{0,089}	0.598 _{0,125}	0.517 _{0,288}	0.160 _{0,260}	0.126 _{0,256}	0.158 _{0,302}

Table 4
Median and IQR of the HV indicator for MOCell in the nine scenarios.

	Canonical	EC ¹			SC ¹			PF ¹			PSC ¹			HF ¹		
		0.1	0.01	0.001	0.1	0.01	0.001	0.1	0.01	0.001	0.1	0.01	0.001	0.1	0.01	0.001
LL	0.296 _{0,188}	0.720 _{0,073}	0.672 _{0,114}	0.450 _{0,362}	0.276 _{0,221}	0.387 _{0,175}	0.318 _{0,201}	0.626 _{0,096}	0.612 _{0,153}	0.394 _{0,260}	0.615 _{0,110}	0.620 _{0,128}	0.428 _{0,308}	0.279 _{0,160}	0.291 _{0,204}	0.313 _{0,221}
LM	0.266 _{0,191}	0.677 _{0,094}	0.595 _{0,117}	0.472 _{0,226}	0.297 _{0,185}	0.366 _{0,164}	0.302 _{0,222}	0.557 _{0,134}	0.519 _{0,149}	0.385 _{0,267}	0.624 _{0,152}	0.607 _{0,119}	0.621 _{0,092}	0.477 _{0,173}	0.522 _{0,141}	0.523 _{0,137}
LH	0.258 _{0,198}	0.623 _{0,088}	0.567 _{0,117}	0.349 _{0,323}	0.256 _{0,229}	0.352 _{0,164}	0.300 _{0,266}	0.497 _{0,137}	0.448 _{0,278}	0.292 _{0,229}	0.563 _{0,155}	0.585 _{0,141}	0.568 _{0,109}	0.397 _{0,147}	0.464 _{0,149}	0.476 _{0,143}
ML	0.434 _{0,212}	0.691 _{0,101}	0.728 _{0,100}	0.511 _{0,430}	0.002 _{0,122}	0.531 _{0,167}	0.535 _{0,159}	0.457 _{0,127}	0.452 _{0,157}	0.450 _{0,116}	0.610 _{0,134}	0.611 _{0,131}	0.533 _{0,407}	0.004 _{0,099}	0.176 _{0,432}	0.423 _{0,201}
MM	0.303 _{0,183}	0.718 _{0,070}	0.680 _{0,078}	0.644 _{0,080}	0.305 _{0,154}	0.418 _{0,166}	0.407 _{0,160}	0.589 _{0,134}	0.571 _{0,138}	0.570 _{0,140}	0.552 _{0,156}	0.547 _{0,131}	0.568 _{0,126}	0.244 _{0,300}	0.292 _{0,242}	0.305 _{0,221}
MH	0.036 _{0,194}	0.591 _{0,132}	0.559 _{0,137}	0.305 _{0,438}	0.003 _{0,109}	0.125 _{0,245}	0.057 _{0,303}	0.467 _{0,184}	0.453 _{0,197}	0.278 _{0,440}	0.505 _{0,163}	0.485 _{0,223}	0.486 _{0,201}	0.195 _{0,257}	0.273 _{0,165}	0.291 _{0,229}
HL	0.005 _{0,199}	0.679 _{0,100}	0.656 _{0,128}	0.591 _{0,176}	0.000 _{0,159}	0.160 _{0,283}	0.046 _{0,341}	0.608 _{0,109}	0.610 _{0,114}	0.567 _{0,262}	0.620 _{0,113}	0.617 _{0,127}	0.552 _{0,176}	0.317 _{0,295}	0.362 _{0,282}	0.422 _{0,246}
HM	0.000 _{0,035}	0.583 _{0,094}	0.556 _{0,128}	0.453 _{0,346}	0.000 _{0,185}	0.077 _{0,173}	0.000 _{0,268}	0.488 _{0,156}	0.502 _{0,219}	0.290 _{0,199}	0.525 _{0,148}	0.495 _{0,124}	0.377 _{0,156}	0.150 _{0,245}	0.197 _{0,251}	0.217 _{0,228}
HH	0.000 _{0,075}	0.559 _{0,099}	0.507 _{0,120}	0.410 _{0,240}	0.000 _{0,073}	0.045 _{0,186}	0.000 _{0,131}	0.431 _{0,182}	0.437 _{0,206}	0.197 _{0,403}	0.453 _{0,137}	0.437 _{0,181}	0.381 _{0,258}	0.061 _{0,247}	0.146 _{0,264}	0.084 _{0,313}

Table 5
Median and IQR of the HV indicator for SMS-EMOA in the nine scenarios.

	Canonical	EC ¹			SC ¹			PF ¹			PSC ¹			HF ¹		
		0.1	0.01	0.001	0.1	0.01	0.001	0.1	0.01	0.001	0.1	0.01	0.001	0.1	0.01	0.001
		LL	0.642 _{0.150}	0.734 _{0.105}	0.720 _{0.108}	0.719 _{0.070}	0.641 _{0.135}	0.691 _{0.093}	0.683 _{0.086}	0.716 _{0.085}	0.706 _{0.072}	0.714 _{0.087}	0.714 _{0.110}	0.692 _{0.081}	0.703 _{0.106}	0.620 _{0.139}
LM	0.594 _{0.125}	0.721 _{0.074}	0.709 _{0.080}	0.714 _{0.090}	0.606 _{0.132}	0.672 _{0.104}	0.658 _{0.107}	0.697 _{0.078}	0.701 _{0.086}	0.699 _{0.117}	0.700 _{0.084}	0.682 _{0.109}	0.681 _{0.120}	0.562 _{0.141}	0.597 _{0.131}	0.633 _{0.154}
LH	0.556 _{0.133}	0.685 _{0.078}	0.679 _{0.108}	0.676 _{0.096}	0.547 _{0.100}	0.640 _{0.122}	0.633 _{0.117}	0.638 _{0.101}	0.646 _{0.095}	0.644 _{0.103}	0.646 _{0.110}	0.647 _{0.102}	0.629 _{0.116}	0.532 _{0.126}	0.542 _{0.146}	0.566 _{0.111}
ML	0.519 _{0.137}	0.725 _{0.132}	0.690 _{0.105}	0.698 _{0.066}	0.500 _{0.180}	0.624 _{0.073}	0.614 _{0.120}	0.691 _{0.098}	0.688 _{0.104}	0.688 _{0.160}	0.692 _{0.093}	0.682 _{0.095}	0.683 _{0.112}	0.456 _{0.208}	0.509 _{0.173}	0.500 _{0.151}
MM	0.437 _{0.141}	0.694 _{0.108}	0.694 _{0.086}	0.659 _{0.079}	0.446 _{0.173}	0.582 _{0.141}	0.565 _{0.101}	0.650 _{0.083}	0.668 _{0.092}	0.650 _{0.114}	0.668 _{0.064}	0.661 _{0.089}	0.646 _{0.098}	0.366 _{0.220}	0.431 _{0.217}	0.440 _{0.195}
MH	0.438 _{0.191}	0.653 _{0.101}	0.651 _{0.124}	0.666 _{0.095}	0.375 _{0.229}	0.553 _{0.144}	0.533 _{0.190}	0.632 _{0.112}	0.629 _{0.160}	0.642 _{0.130}	0.628 _{0.144}	0.622 _{0.116}	0.625 _{0.141}	0.360 _{0.238}	0.437 _{0.219}	0.407 _{0.231}
HL	0.579 _{0.161}	0.707 _{0.096}	0.689 _{0.094}	0.697 _{0.101}	0.565 _{0.136}	0.643 _{0.108}	0.652 _{0.110}	0.681 _{0.075}	0.678 _{0.079}	0.679 _{0.096}	0.683 _{0.099}	0.674 _{0.108}	0.679 _{0.078}	0.549 _{0.168}	0.584 _{0.147}	0.574 _{0.159}
HM	0.438 _{0.160}	0.616 _{0.108}	0.616 _{0.104}	0.629 _{0.101}	0.429 _{0.172}	0.553 _{0.134}	0.552 _{0.117}	0.627 _{0.087}	0.621 _{0.126}	0.594 _{0.095}	0.613 _{0.107}	0.609 _{0.085}	0.611 _{0.109}	0.348 _{0.168}	0.414 _{0.195}	0.415 _{0.166}
HH	0.407 _{0.204}	0.615 _{0.089}	0.604 _{0.110}	0.612 _{0.122}	0.402 _{0.199}	0.540 _{0.102}	0.522 _{0.139}	0.594 _{0.123}	0.585 _{0.124}	0.591 _{0.105}	0.575 _{0.120}	0.599 _{0.096}	0.569 _{0.124}	0.354 _{0.229}	0.388 _{0.158}	0.394 _{0.173}

6

Table 6
Median and IQR of the HV indicator for MOEA/D in the nine scenarios.

	Canonical	EC ¹			SC ¹			PF ¹			PSC ¹			HF ¹		
		0.1	0.01	0.001	0.1	0.01	0.001	0.1	0.01	0.001	0.1	0.01	0.001	0.1	0.01	0.001
		LL	0.000 _{0.000}	0.002 _{0.009}	0.000 _{0.000}	0.000 _{0.024}	0.000 _{0.000}	0.000 _{0.000}	0.000 _{0.022}	0.000 _{0.036}	0.000 _{0.066}	0.000 _{0.048}	0.011 _{0.143}	0.000 _{0.062}	0.000 _{0.063}	0.000 _{0.000}
LM	0.000 _{0.000}	0.000 _{0.032}	0.000 _{0.026}	0.000 _{0.000}	0.000 _{0.000}	0.000 _{0.012}	0.000 _{0.000}	0.000 _{0.000}	0.000 _{0.000}	0.000 _{0.000}	0.000 _{0.004}	0.000 _{0.000}	0.000 _{0.000}	0.000 _{0.000}	0.000 _{0.000}	0.000 _{0.000}
LH	0.000 _{0.000}	0.000 _{0.011}	0.000 _{0.002}	0.000 _{0.007}	0.000 _{0.000}	0.000 _{0.000}	0.000 _{0.000}	0.000 _{0.000}	0.000 _{0.000}	0.000 _{0.000}	0.000 _{0.000}	0.000 _{0.000}	0.000 _{0.000}	0.000 _{0.000}	0.000 _{0.000}	0.000 _{0.000}
ML	0.000 _{0.000}	0.043 _{0.125}	0.022 _{0.132}	0.027 _{0.097}	0.000 _{0.000}	0.000 _{0.000}	0.000 _{0.000}	0.004 _{0.074}	0.000 _{0.047}	0.000 _{0.045}	0.044 _{0.131}	0.008 _{0.106}	0.000 _{0.104}	0.000 _{0.000}	0.000 _{0.000}	0.000 _{0.000}
MM	0.000 _{0.000}	0.000 _{0.007}	0.000 _{0.039}	0.000 _{0.047}	0.000 _{0.000}	0.000 _{0.000}	0.000 _{0.000}	0.000 _{0.003}	0.000 _{0.015}	0.000 _{0.056}	0.000 _{0.084}	0.000 _{0.030}	0.000 _{0.020}	0.000 _{0.000}	0.000 _{0.000}	0.000 _{0.000}
MH	0.000 _{0.000}	0.000 _{0.042}	0.000 _{0.059}	0.000 _{0.028}	0.000 _{0.000}	0.000 _{0.018}	0.000 _{0.000}	0.000 _{0.015}	0.000 _{0.001}	0.000 _{0.000}	0.000 _{0.043}	0.000 _{0.030}	0.000 _{0.027}	0.000 _{0.000}	0.000 _{0.000}	0.000 _{0.000}
HL	0.000 _{0.000}	0.035 _{0.158}	0.043 _{0.170}	0.000 _{0.158}	0.000 _{0.000}	0.000 _{0.011}	0.000 _{0.009}	0.020 _{0.298}	0.003 _{0.121}	0.006 _{0.085}	0.030 _{0.170}	0.046 _{0.148}	0.024 _{0.142}	0.000 _{0.000}	0.000 _{0.000}	0.000 _{0.000}
HM	0.000 _{0.000}	0.036 _{0.134}	0.020 _{0.103}	0.000 _{0.105}	0.000 _{0.000}	0.000 _{0.014}	0.000 _{0.000}	0.000 _{0.076}	0.000 _{0.064}	0.000 _{0.047}	0.025 _{0.107}	0.006 _{0.087}	0.009 _{0.108}	0.000 _{0.000}	0.000 _{0.000}	0.000 _{0.000}
HH	0.000 _{0.000}	0.000 _{0.060}	0.000 _{0.034}	0.000 _{0.010}	0.000 _{0.000}	0.000 _{0.000}	0.000 _{0.000}	0.000 _{0.016}	0.000 _{0.001}	0.000 _{0.000}	0.014 _{0.077}	0.000 _{0.055}	0.000 _{0.026}	0.000 _{0.000}	0.000 _{0.000}	0.000 _{0.000}

Table 7
Median and IQR of the HV indicator for SparseEA in the nine scenarios.

	EC ¹			SC ¹			PF ¹			PSC ¹			HF ¹		
	0.1	0.01	0.001	0.1	0.01	0.001	0.1	0.01	0.001	0.1	0.01	0.001	0.1	0.01	0.001
LL	0.21 _{0.0051}	0.21 _{0.0053}	0.207 _{0.0051}	0.213 _{0.0052}	0.207 _{0.0051}	0.207 _{0.0051}	0.207 _{0.0051}	0.207 _{0.0051}	0.207 _{0.0051}	0.207 _{0.0051}	0.207 _{0.0051}	0.207 _{0.0051}	0.207 _{0.0051}	0.207 _{0.0051}	0.207 _{0.0051}
LM	0.208 _{0.0069}	0.234 _{0.0052}	0.232 _{0.0063}	0.237 _{0.0067}	0.209 _{0.0060}	0.210 _{0.0052}	0.211 _{0.0050}	0.212 _{0.0049}	0.213 _{0.0047}	0.214 _{0.0046}	0.215 _{0.0045}	0.216 _{0.0044}	0.217 _{0.0043}	0.218 _{0.0042}	0.219 _{0.0041}
LH	0.21 _{0.0055}	0.228 _{0.0063}	0.219 _{0.0058}	0.212 _{0.0067}	0.207 _{0.0057}	0.205 _{0.0054}	0.212 _{0.0049}	0.203 _{0.0057}	0.212 _{0.0051}	0.209 _{0.0054}	0.206 _{0.0055}	0.208 _{0.0054}	0.209 _{0.0055}	0.205 _{0.0054}	0.203 _{0.0057}
ML	0.165 _{0.0045}	0.200 _{0.0079}	0.189 _{0.0046}	0.192 _{0.0063}	0.165 _{0.0051}	0.165 _{0.0044}	0.161 _{0.0038}	0.169 _{0.0050}	0.170 _{0.0042}	0.179 _{0.0056}	0.171 _{0.0043}	0.171 _{0.0046}	0.178 _{0.0046}	0.165 _{0.0050}	0.159 _{0.0057}
MM	0.173 _{0.0041}	0.202 _{0.0043}	0.200 _{0.0042}	0.203 _{0.0043}	0.175 _{0.0047}	0.168 _{0.0035}	0.169 _{0.0025}	0.176 _{0.0033}	0.185 _{0.0041}	0.189 _{0.0035}	0.179 _{0.0043}	0.191 _{0.0035}	0.170 _{0.0039}	0.168 _{0.0044}	0.177 _{0.0040}
MH	0.181 _{0.0040}	0.204 _{0.0046}	0.202 _{0.0045}	0.211 _{0.0050}	0.185 _{0.0053}	0.184 _{0.0040}	0.181 _{0.0042}	0.185 _{0.0043}	0.185 _{0.0041}	0.192 _{0.0056}	0.188 _{0.0036}	0.195 _{0.0051}	0.191 _{0.0048}	0.178 _{0.0059}	0.182 _{0.0059}
HL	0.157 _{0.0056}	0.194 _{0.0056}	0.191 _{0.0059}	0.191 _{0.0049}	0.148 _{0.0041}	0.163 _{0.0043}	0.151 _{0.0034}	0.166 _{0.0052}	0.160 _{0.0053}	0.170 _{0.0050}	0.168 _{0.0050}	0.162 _{0.0049}	0.163 _{0.0047}	0.153 _{0.0046}	0.155 _{0.0041}
HM	0.147 _{0.0042}	0.183 _{0.0054}	0.183 _{0.0038}	0.194 _{0.0047}	0.149 _{0.0051}	0.151 _{0.0047}	0.150 _{0.0047}	0.168 _{0.0042}	0.156 _{0.0054}	0.163 _{0.0039}	0.168 _{0.0040}	0.171 _{0.0046}	0.175 _{0.0046}	0.142 _{0.0042}	0.141 _{0.0050}
HH	0.157 _{0.0040}	0.198 _{0.0055}	0.188 _{0.0053}	0.193 _{0.0042}	0.153 _{0.0039}	0.154 _{0.0047}	0.158 _{0.0038}	0.169 _{0.0038}	0.169 _{0.0036}	0.172 _{0.0036}	0.172 _{0.0037}	0.175 _{0.0044}	0.182 _{0.0038}	0.150 _{0.0042}	0.157 _{0.0041}

5.2.1. Impact of the problem-specific operators

Let us start by defining our baseline for the comparison. Table 2 includes the median and the Interquartile Range (IQR) of the HV values reached by the canonical MOEAs, that is, those with the default settings described above regarding population size, crossover/mutation operators and rates, etc., and without applying any of the problem-specific operators. A gray background is used in the table cell with the best (highest) HV value.

The starting point is that SMS-EMOA has reached the approximated Pareto fronts with the highest (best) HV indicator values. This is consistent across the nine scenarios and with statistical significance in most cases, as shown in Figure S.9 in the online supplementary material. This is the first relevant finding of this work, as SMS-EMOA has been scarcely used in the context of the CSO problem. To the best of our knowledge, this algorithm has been used in a preliminary study on multi-connectivity in the CSO problem, and no differences have been reported with respect to NSGA-II and MOCell [67].

A second conclusion of the results presented in Table 2 and Fig. 3 is the extremely bad performance of MOEA/D, for which the HV values in each scenario are always zero. This is the effect of the normalization procedure that discards non-dominated solutions out of the limits of the RPF. Fig. 3 graphically shows this fact with the attainment surfaces of the five canonical MOEAs and the RPF for the MM scenario (the same happens in all the other cases, as shown in the figures included in the supplementary material). Note that only those non-dominated solutions having a power consumption below roughly 2 kW (the highest extreme point of the RPF in this objective for this scenario) contribute to the HV value, that is, only NSGA-II, MOCell, SMS-EMOA and SparseEA have a median greater than zero in the row MM of Table 2. The reason for this is that the solutions reached by the hybrid MOEAs with the devised problem-specific operators clearly dominate those of the canonical versions, thus displacing the actual RPF far from the average approximations computed by the canonical versions. After a deep inspection of the MOEA/D implementation used, and available in the jMetal framework (<https://github.com/Mezcal/Metal>), we can explain this issue in that the evolutionary loop of this algorithm, for which the decomposition-based approach works well for real-coded problems and the Differential Evolution crossover operator, but fails when using binary strings with two-point crossover and bit-flip mutation. Recall that we have kept these common settings across the evolutionary-based MOEAs for comparison purposes. As it can be seen below in Table 6, this happens in most of the results reported by HV involving MOEA/D. As a consequence, from this point onward, we have decided to stop analyzing any results of this algorithm for this quality indicator (removing their contributions to the RPF of each scenario), in order to both reduce the length of the paper and ease its reading. In any case, we would like to point out that problem-specific operators have also improved the search of MOEA/D, as can be seen in the attainment functions reached by the approximated Pareto fronts for the HL scenario, taken as a representative one, in Fig. 4, where the hybrid versions with EC¹, PF¹, and PSC¹ clearly dominate that of the canonical version. The point is that these improvements are not enough to move the approximated Pareto fronts into the limits of the corresponding RPF.

Now, we turn to analyze the actual impact of the five problem-specific operators. Tables 3 to 7 include the median and IQR of the HV values over the 50 runs of NSGA-II, MOCell, SMS-EMOA, MOEA/D and SparseEA for both the canonical and the 15 hybrid versions (five operators applied at three different rates). We will be using the previous names to refer to the canonical MOEAs, and MOEA/D to mention a particular hybridization using a given application rate. The tables also use two different gray backgrounds in each row to highlight the best configuration over all settings (darker gray) and the best within a given operator (lighter gray) for each UDN scenario.

The first clear conclusion that can be drawn from all the tables is that hybrid MOEAs have outperformed canonical ones, thus showing

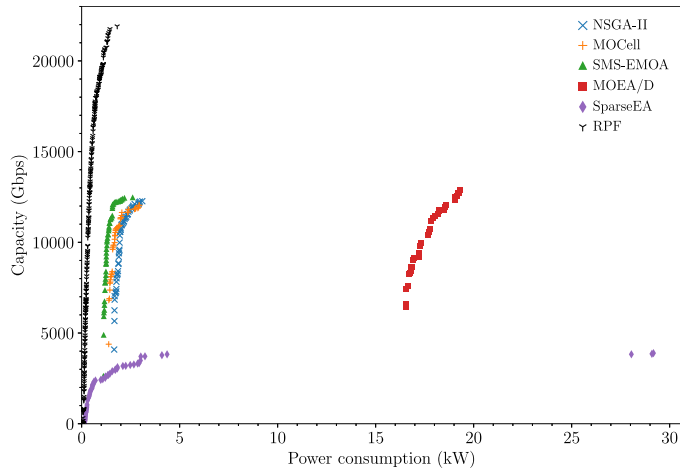


Fig. 3. Attainment functions of the five canonical MOEAs for the MM scenario, and the RPF used in the normalization procedure required to compute the HV indicator.

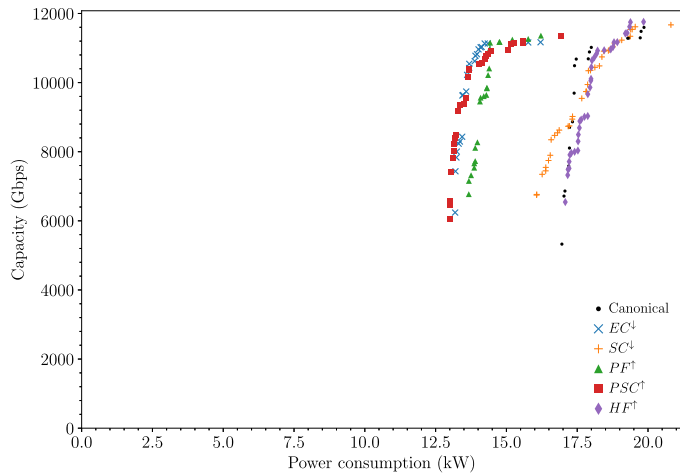


Fig. 4. Attainment functions of both the canonical and hybrid versions of MOEA/D for the HL scenario.

that there is at least one problem-specific operator that has been able to enhance the search capabilities of the algorithms. The dark gray background indicates that the EC^l operator at 0.1 has been able to obtain the best (highest) HV value in most scenarios for NSGA-II (8 out of 9), MOCell (8 out of 9) and SMS-EMOA (6 out of 9), and with statistical significance, as shown in Figures S.10 to S.13.

It is important to remark that most hybrid configurations have enhanced the search of NSGA-II, MOCell and SMS-EMOA, and to a lesser extent that of SparseEA. To better illustrate this fact, we have computed the gap between the HV value of the best application rate for a given operator and the HV value of the canonical MOEA, and have aggregated it over the nine UDN scenarios (LL to HH). The results are shown in Fig. 5, where it can be seen that the HV values have increased substantially, specially in NSGA-II and MOCell, with 0.23 and 0.31, on average, for the five problem-specific operators. Diving a bit deeper into the data reported in this figure, the columns corresponding to the EC^l operator show the maximum gap, that is, the largest increase in the HV value with respect to the canonical version, thus achieving the best-approximated fronts with respect to this indicator. Out of the

five devised problem-specific operators, HF^l has provided little-to-no contributions to the search capability of the MOEAs (except for MOCell), even obtaining a negative gap (i.e., the canonical MOEA has outperformed this hybrid version). In fact, averaging the nine scenarios and the three application rates, NSGA-II $_{HF^l}$ has a gap of -0.0013 . Despite these results, we will show below, in the next section, that this operator is still useful when combined with others by generating a synergy that enhances the search of MOEAs.

We want to complete our analysis with an operator-wise dimension, that is, how the different combinations of operators and application rates perform. To do so, we computed the average ranking of the HV value for each operator/rate over all the nine UDN scenarios within two different comparison baselines: Table 8 ranks hybrids among the three application rates (that is, the rank is between 1 and 3, which corresponds, respectively, to the best and worst HV value), and Table 9 ranks them among the fifteen hybrids (that is, the rank here ranges between 1 and 15). The first table aims at showing which application rates reached the best (highest) HV value for each operator, whereas the second one compares all the proposed hybrids. The two tables also include a final row that averages the rank over all the four considered

Table 8
Average rank at different application rates of the different hybrid MOEAs for the nine scenarios.

	EC^{\downarrow}			SC^{\downarrow}			PF^{\uparrow}			PSC^{\uparrow}			HF^{\uparrow}		
	0.1	0.01	0.001	0.1	0.01	0.001	0.1	0.01	0.001	0.1	0.01	0.001	0.1	0.01	0.001
NSGA-II	1.11	1.89	3.00	2.78	1.00	2.22	1.22	1.78	3.00	1.56	1.44	3.00	2.33	2.11	1.56
MOCcell	1.11	1.89	3.00	2.78	1.11	1.89	1.33	1.78	2.89	1.56	2.00	2.44	3.00	1.89	1.11
SMS-EMOA	1.44	2.44	2.11	3.00	1.11	1.89	1.67	2.22	2.11	1.22	2.33	2.44	3.00	1.67	1.33
SparseEA	1.56	2.78	1.67	2.11	1.89	2.00	2.56	2.11	1.33	2.44	2.33	1.22	2.22	1.78	2.00
Average	1.31	2.25	2.44	2.67	1.28	2.00	1.69	1.97	2.33	1.69	2.03	2.28	2.64	1.86	1.50

Table 9
Average rank of all the different hybrid MOEAs in all nine scenarios.

	EC^{\downarrow}			SC^{\downarrow}			PF^{\uparrow}			PSC^{\uparrow}			HF^{\uparrow}		
	0.1	0.01	0.001	0.1	0.01	0.001	0.1	0.01	0.001	0.1	0.01	0.001	0.1	0.01	0.001
NSGA-II	1.22	2.56	7.33	13.22	9.22	11.44	3.22	4.11	8.33	5.11	4.89	9.00	14.00	13.56	12.78
MOCcell	1.11	2.44	8.11	14.56	11.78	12.56	5.11	6.11	8.89	4.33	4.78	6.67	12.33	11.00	10.00
SMS-EMOA	1.67	2.89	2.44	12.89	9.89	10.78	5.22	5.56	6.56	5.33	7.33	8.33	15.00	13.33	12.78
SparseEA	1.56	3.11	1.67	11.00	10.67	11.00	9.44	8.22	6.33	7.00	7.33	5.44	13.33	11.11	12.78
Average	1.39	2.75	4.89	12.92	10.39	11.44	5.75	6.00	7.53	5.44	6.08	7.36	13.67	12.25	12.08

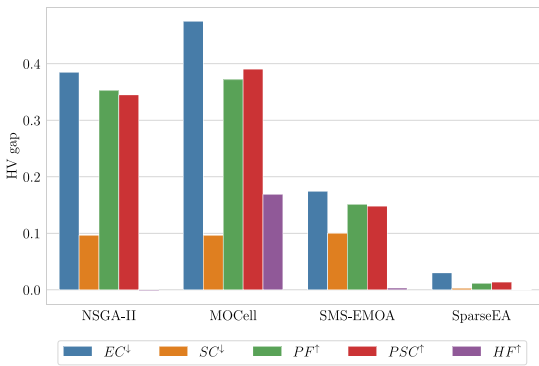


Fig. 5. HV gap between the canonical and the five hybrid MOEAs aggregated over the nine CSO scenarios.

hybrid MOEAs. In order to better support our claims, we have also included in Fig. 6 the attainment functions of both the canonical and the best hybrid versions of the four MOEAs for the scenarios LL, MM and HH, as representative cases with increasing levels of density for UEs and cells (for readability and room constraints, the remaining ones can be found in the supplementary material).

From Table 8, it can be seen that the application rate of 0.1 for EC^{\downarrow} has reported the best ranking (lowest) within the four algorithms separately. The switching off of the empty cells (i.e., not serving any UE) that promotes this problem-specific operator contributes to the search of all the evolutionary loops by introducing many 0's in the tentative solutions (deactivating useless cells) that are managed properly by the genetic operators. The gains in the HV values for NSGA-II, MOCcell, and SMS-EMOA are therefore clearly achieved by approximated fronts with non-dominated solutions in the regions of the search space with low power consumption, as can be seen with the blue \times in the left-hand side of the subplots in Fig. 6, because a smaller number of cells are operating in the UDN network. Although this is the main effect of the EC^{\downarrow} operator, turning the cells off also allows the removal of interference signals, which also increases SINR and, subsequently, network capacity.

The SC^{\downarrow} operator, which also aims to switch cells off, performs better when applied at a lower rate, 0.01, because it has a stronger effect on the network when applied. In fact, it may deactivate cells even with UEs connected to save energy by sleeping the entire SBS. As a consequence, these UEs have to be reallocated to a different cell,

which may cause: (i) that the cell will not to be deactivated on a later iteration, if it was already empty, or (ii) the network capacity is reduced, as the cell bandwidth is shared in a round-robin fashion among all the UEs connected to that cell. Nevertheless, the targeted cells on which the SC^{\downarrow} operator may act are scarce, as it could be difficult to find an SBS in the UDN network with one single cell activated. In any case, the SC^{\downarrow} -based hybrid MOEAs can improve on the canonical versions consistently in the nine UDN scenarios. This can be seen in the HV values of the column SC^{\downarrow} in Tables 3 to 7. What the shape of the approximated fronts shows with the attainment functions displayed in Fig. 6 is that in most of the cases for NSGA-II $_{SC^{\downarrow}}$, MOCcell $_{SC^{\downarrow}}$ and SMS-EMOA $_{SC^{\downarrow}}$, the canonical versions reach solutions with higher (better) capacity (the two attainments cross towards the right-hand side of the plots). Therefore, the operator is able to enhance the search towards regions with solutions having a lower power consumption in these three classical MOEAs. It has a little-to-no contribution to the search capability of SparseEA.

PF^{\uparrow} and PSC^{\uparrow} report similar results in Table 8: the best rate for NSGA-II, MOCcell and SMS-EMOA is 0.1, but the worst for SparseEA. The design goal of these two operators is to switch cells on so that they may serve UEs with higher bandwidth to enhance the second problem objective (capacity), but also with a final call to EC^{\downarrow} (Algorithm 4) to increase energy savings. Therefore, they have reached approximated Pareto fronts with better (higher) values in the network capacity than the EC^{\downarrow} -based hybrids, but also with higher power consumption. A clear example is SMS-EMOA and the HH scenario in Fig. 6.i, where the attainment functions with green triangles (PF^{\uparrow}) and red squares (PSC^{\uparrow}) cross with blue \times (EC^{\downarrow}) around 1.4 kW. The best application rate of the HF^{\uparrow} operator is 0.001, the smallest possible one, thus showing that, only by itself, the new genetic material introduced in the evolutionary loop is not enough to improve the search of the hybrid MOEAs.

SparseEA deserves special attention, as it is an algorithm specially designed to deal with sparse MOPs. This means that it has concentrated the exploration of the search space in the region with solutions having a very small number of SBSs switched on, thus saving much energy, but, on the contrary, it has not been able to find solutions with comparable values for the capacity objective. As a consequence, SparseEA has also suffered the issue of the HV computation because its approximated fronts are mostly outside the limits of the RPF (this justifies its low HV values in comparison with the other three MOEAs). The last row of Fig. 6 graphically displays this effect. Even though the differences are very tight in the smaller scenario (Fig. 6.j), there is a substantial improvement in the attained fronts when the instances become more complex (higher density). Indeed, the canonical SparseEA is not capable of reaching solutions over about 4000 and 5000 Gbps for the capacity

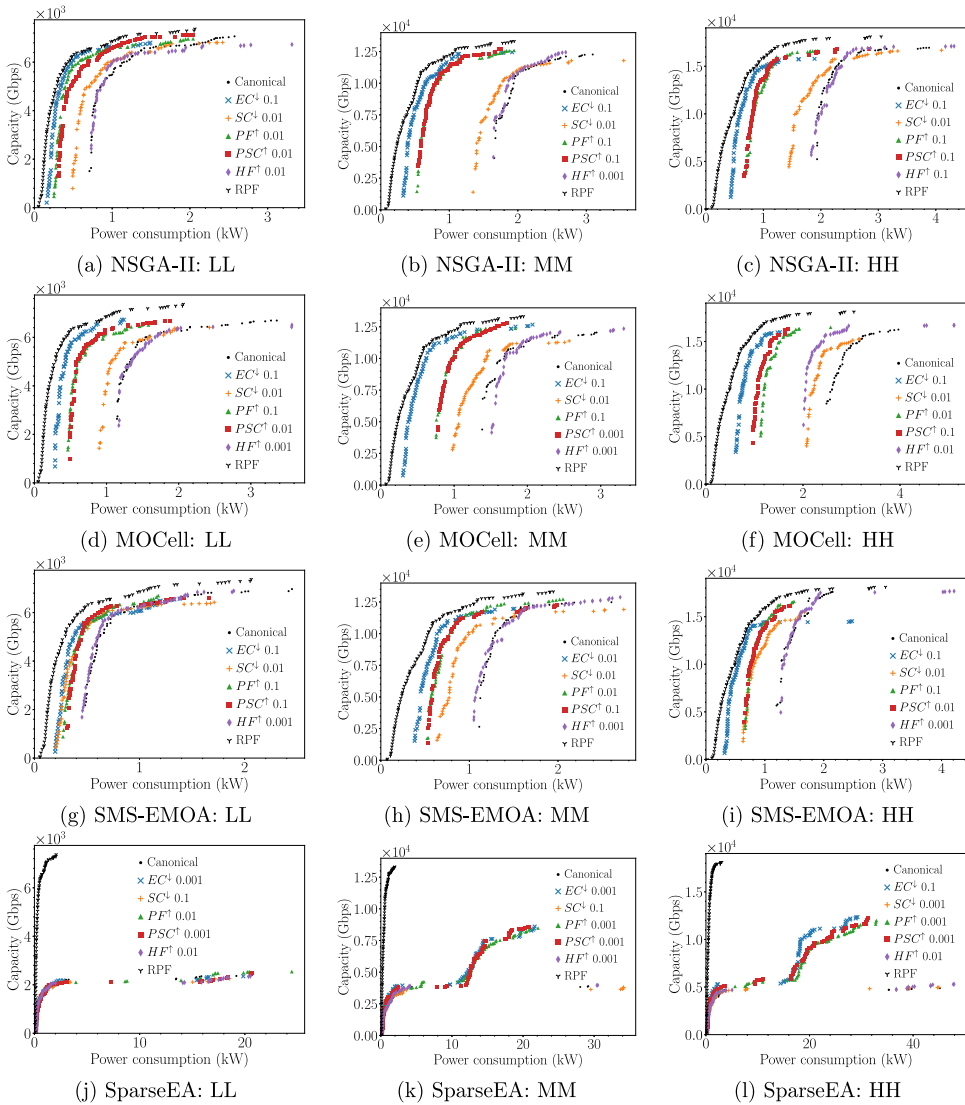


Fig. 6. Attainment functions of both the canonical and hybrid versions of the four MOEAs for three selected UDN scenarios: LL, MM and HH.

objective in the MM and HH scenarios, respectively (Fig. 6.k and Fig. 6.l), but the SparseEA_{EC^l} does, thus showing the advantages of the EC^l problem-specific operator. The point is that the HV computation has not properly captured this information because the extreme value of the power consumption objective in the RPF is fairly low, thus discarding most of the non-dominated solutions above this value.

If we focus on the global ranking among the hybrid versions with EC^l, PF^l, and PSC^l in Table 9, they have scored the best (lowest) with 3.01, 6.43 and 6.30 average ranks over the three application rates, respectively. The SC^l-based hybrid MOEAs can be considered as the fourth out of the five operators with an average rank of 11.58 over the 12.57 of HF^l. All these results are supported by the Friedman rank sum test included in the Supplementary material.

We do not want to finish this section without highlighting the actual impact of the improvements in the approximated Pareto fronts within the domain of the CSO problem. As stated above, this work has used

a static version of the problem [44], so the objective values can be considered as instantaneous power consumption and network capacity, so even small improvements have a profound impact, specially on the electricity bill over a month/year period for a network operator in their 5G deployments.

5.2.2. Exploring synergies between operators

The five problem-specific operators devised in this work try to exploit different features of the CSO problem so that they can be integrated into the search performed by the different MOEAs. Indeed, while two of them promote turning cells off (EC^l and SC^l), the other three aim at turning on (PF^l, PSC^l and HF^l). In the previous section, we have characterized the impact of all of them in an isolated manner, but our hypothesis is that a multi-operator approach in the hybrid MOEAs may generate synergies among them, and improve upon the single-operator ones.

Table 10
Combinations of operators and application rates.

	EC^1	SC^1	PSC^1	HF^1
$SY N_1^{11}$	0.100	0.100	0.100	0.010
$SY N_2^{11}$	0.100	0.100	0.010	0.010
$SY N_3^{11}$	0.100	0.100	0.010	0.001
$SY N_4^{11}$	0.100	0.010	0.010	0.010
$SY N_5^{11}$	0.100	0.010	0.001	0.001
$SY N_6^{11}$	0.100	0.001	0.100	0.010
$SY N_7^{11}$	0.100	0.001	0.100	0.001
$SY N_8^{11}$	0.100	0.001	0.010	0.100
$SY N_9^{11}$	0.100	0.001	0.010	0.010
$SY N_{10}^{11}$	0.010	0.001	0.100	0.010
$SY N_{11}^{11}$	0.001	0.100	0.100	0.010
$SY N_{12}^{11}$	0.001	0.100	0.010	0.001
$SY N_{13}^{11}$	0.001	0.010	0.100	0.010
$SY N_{14}^{11}$	0.001	0.010	0.100	0.001

Table 11
Median and IQR of HV for the canonical and both the best single- and multi-operator configurations for NSGA-II in the nine scenarios.

	Canonical	Best single	Best synergy
LL	0.52 _{0,170}	0.766 _{0,076}	0.766 _{0,074}
LM	0.520 _{0,185}	0.747 _{0,071}	0.746 _{0,068}
LH	0.449 _{0,161}	0.719 _{0,086}	0.712 _{0,083}
ML	0.277 _{0,170}	0.739 _{0,076}	0.736 _{0,077}
MM	0.193 _{0,231}	0.707 _{0,070}	0.713 _{0,059}
MH	0.210 _{0,285}	0.668 _{0,092}	0.677 _{0,084}
HL	0.365 _{0,249}	0.720 _{0,095}	0.722 _{0,092}
HM	0.179 _{0,265}	0.653 _{0,093}	0.667 _{0,075}
HH	0.177 _{0,265}	0.633 _{0,088}	0.643 _{0,084}

The first issue we have to deal with here is the combinatorial explosion of experiments. As a starting point, we have 9 scenarios \times 50 seeds \times 4 algorithms \times 5 operators \times $3^3 = 27$ possible combinations of the three application rates, which equals 243,000 independent executions. This is obviously not affordable in a reasonable amount of time. To reduce the number of experiments, we have first considered only the LL scenario (the smaller one), and the PSC^1 operator has been discarded because its results are fairly similar to those of PSC^1 (it is more restrictive since it only considers femtocells). From all these combinations, we have ranked them based on the HV value reached for the 50 seeds of the LL scenario, and we have selected those that surpass the median HV value of all the single-operator hybrid MOEAs separately. In total, 14 multi-operator hybrid MOEAs have resulted from this preliminary selection, whose application rates are included in Table 10, and have been used further in the experiments for the eight remaining scenarios (from LM to HH).

Under these experimental conditions, Tables 11 to 14 include the HV value of the approximated Pareto fronts of the canonical and both the best single-operator and best multi-operator hybrid versions of NSGA-II, MOCell, SMS-EMOA, and SparseEA, respectively. The columns aside the HV data link to the configuration that reached that value of Table 10. A gray background has also been used to highlight the best (highest) HV value.

For 20 out of the 36 settings (4 algorithms \times 9 scenarios), the multi-operator hybrid MOEAs have been able to improve upon the single-operator setting, thus showing that an effective synergy between operators has been reached. That is, problem-specific operators promoting both switching on and off strategies are useful for improving upon schemes based on a single approach. This synergy has been especially impacted in NSGA-II and MOCell, where $SY N^{11}$ has obtained a higher (better) HV value in 14 out of the 18 comparisons (with statistical significance for most cases in MOCell, as shown in Section 2 of the supplementary material). In order to better illustrate these benefits,

Table 12
Median and IQR of HV for the canonical and both the best single- and multi-operator configurations for MOCell in the nine scenarios.

	Canonical	Best single	Best synergy
LL	0.296 _{0,188}	0.720 _{0,073}	0.772 _{0,094}
LM	0.266 _{0,193}	0.677 _{0,094}	0.729 _{0,079}
LH	0.258 _{0,198}	0.623 _{0,088}	0.682 _{0,073}
ML	0.434 _{0,212}	0.725 _{0,100}	0.740 _{0,072}
MM	0.303 _{0,183}	0.718 _{0,070}	0.696 _{0,090}
MH	0.036 _{0,194}	0.591 _{0,132}	0.655 _{0,076}
HL	0.005 _{0,199}	0.679 _{0,103}	0.716 _{0,102}
HM	0.000 _{0,035}	0.583 _{0,094}	0.643 _{0,091}
HH	0.000 _{0,075}	0.559 _{0,109}	0.617 _{0,072}

Table 13
Median and IQR of HV for the canonical and both the best single- and multi-operator configurations for SMS-EMOA in the nine scenarios.

	Canonical	Best single	Best synergy
LL	0.642 _{0,150}	0.734 _{0,105}	0.747 _{0,091}
LM	0.594 _{0,125}	0.721 _{0,074}	0.718 _{0,089}
LH	0.556 _{0,133}	0.685 _{0,078}	0.677 _{0,082}
ML	0.519 _{0,137}	0.725 _{0,132}	0.680 _{0,128}
MM	0.437 _{0,141}	0.694 _{0,086}	0.673 _{0,085}
MH	0.435 _{0,191}	0.666 _{0,095}	0.652 _{0,112}
HL	0.579 _{0,161}	0.707 _{0,086}	0.618 _{0,145}
HM	0.438 _{0,160}	0.629 _{0,101}	0.588 _{0,094}
HH	0.407 _{0,204}	0.615 _{0,089}	0.582 _{0,072}

Table 14
Median and IQR of HV for the canonical and both the best single- and multi-operator configurations for SparseEA in the nine scenarios.

	Canonical	Best single	Best synergy
LL	0.212 _{0,051}	0.213 _{0,052}	0.237 _{0,057}
LM	0.208 _{0,069}	0.237 _{0,067}	0.239 _{0,060}
LH	0.216 _{0,055}	0.228 _{0,063}	0.226 _{0,054}
ML	0.165 _{0,045}	0.200 _{0,079}	0.209 _{0,057}
MM	0.173 _{0,041}	0.203 _{0,043}	0.206 _{0,043}
MH	0.181 _{0,040}	0.211 _{0,059}	0.211 _{0,053}
HL	0.153 _{0,036}	0.194 _{0,056}	0.208 _{0,068}
HM	0.145 _{0,042}	0.194 _{0,047}	0.191 _{0,045}
HH	0.155 _{0,040}	0.198 _{0,055}	0.197 _{0,070}

Fig. 7 displays the attainment functions of the best configurations for three scenarios with increasing density levels (i.e., complexity), namely LL, MM and HH. It can be seen that, for these two MOEAs, as long as the density gets larger, the multi-operator hybrids explore better the regions with non-dominated solutions with lower power consumption than that of the single-operator ones, but sacrificing slightly the capacity objective. It is important to note that the best single-operator hybrid is based on EC^1 , which promotes cell deactivation, but even in this case, the synergy between all can improve upon the power consumption. A problem-side explanation is that an UDN may have more cells switched on, but each consuming less energy (recall that the modeling used for the power consumption is not only based on whether a cell is activated or not, but also on its operating frequency, the traffic load, if it is installed in an SBS with other active cells, etc.). However, SMS-EMOA and SparseEA require further elaboration, as their HV results are again impacted by the normalization process. Indeed, the single-operator hybrid SMS-EMOA has reached the best (highest) value for this indicator in 8 of the 9 UDN scenarios (with very tight differences, actually), but if one analyzes the attainment functions in Figs. 7(g), (h) and (i), it can be seen that the same justification holds as for NSGA-II and MOCell. The only difference is that, on average, the approximated fronts of the SMS-EMOA multi-operator (the + marks) cover solutions with slightly lower network capacity, thus contributing very little to the HV indicator, while the SMS-EMOA single operator (the x marks). In fact, its attainment function seems to be the closest to the RPF in this region of the search space. Finally, by inspecting its attainment surfaces, SparseEA has been clearly the hybrid MOEA that has profited the most with the synergy between the different

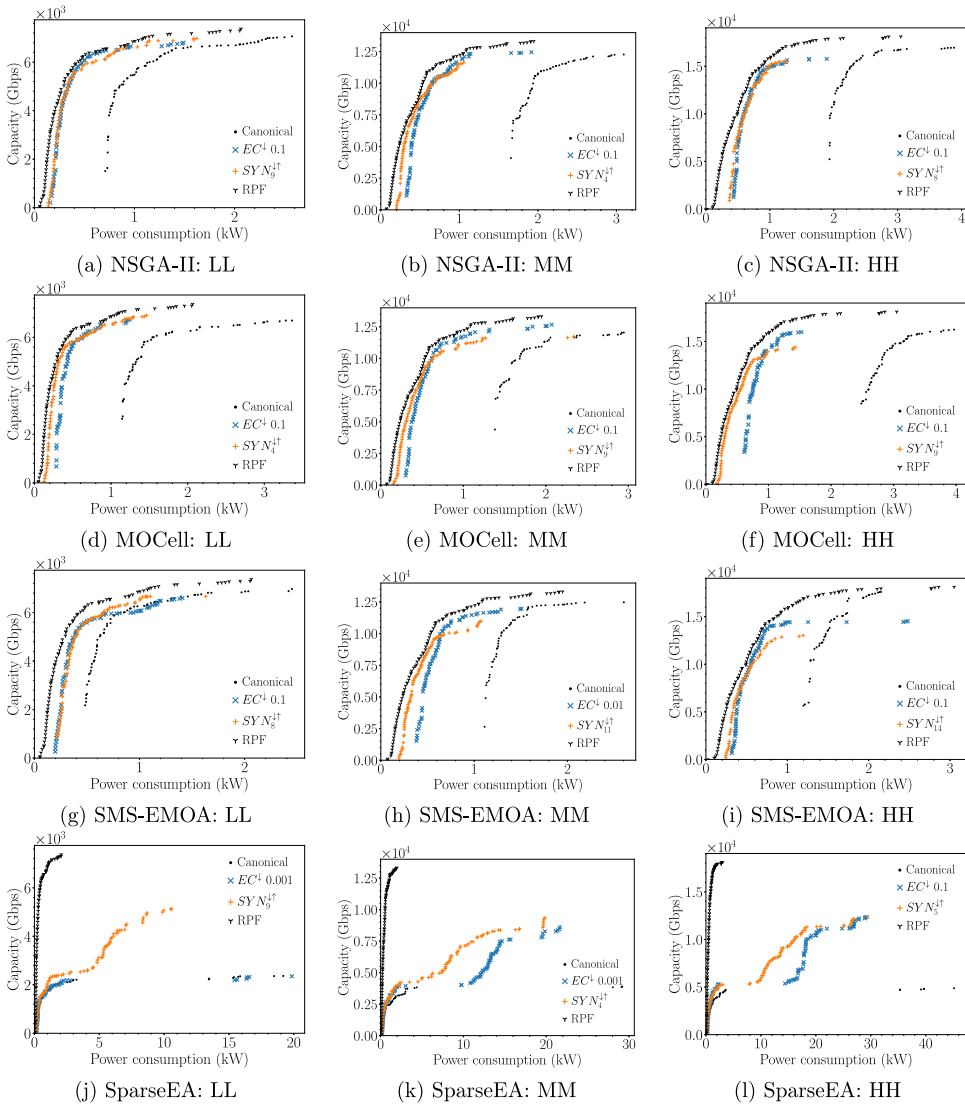


Fig. 7. Attainment functions of the canonical, the best single-operator, and the best multi-operator hybrid MOEAs for three selected UDN scenarios: LL, MM and HH.

problem-specific operators, an important finding not captured by the HV indicator as most of the non-dominated solutions of this MOEA are out of the limit of the RPF. Figs. 7 (j), (k) and (l) clearly show that the median approximated Pareto front of SYN^{41} clearly dominates that of EC^4 . Being SparseEA an algorithm that seeks solutions with a very small number of 1's (sparse MOP), combining problem-specific operators that not only promote the deactivation, but also the activation of cells has allowed the algorithm to better explore non-dominated solutions with a higher network capacity objective.

6. Conclusions and future work

Ultra-Dense Networks are a key enabler technology for 5G networks, bringing numerous advantages to new small base station deployments. Even so, the massive deployment of small base stations poses a power

consumption problem that is being addressed by the research community. This problem has been formulated here as a multi-objective optimization problem, which selectively switches off a subset of small base stations in order to reduce power consumption while maximizing the capacity of network users. In this context, this work proposes the use of hybrid MOEAs to address this issue, incorporating expert knowledge of the problem into the search engine of several algorithms. The results obtained allow us to conclude that hybridization with specific operators, which aim at switching cells on and off, significantly improves the approximated Pareto fronts reached, specially in the power consumption objective. We have also evaluated a multi-operator hybridization, demonstrating that synergies between the different operators can improve upon single-operator-based approaches. Further characterizing these synergies is a limitation of this work. Both all data and the developed software are publicly available

at <https://doi.org/10.6084/m9.figshare.21378000> and https://github.com/galeanobra/CSO_Hybrid, respectively.

This work opens up various lines of future work. First, we have worked with five MOEAs that have shown search patterns with different capabilities to explore different regions of the solution space. To exploit these capabilities, we will develop heterogeneous distributed models with several islands. Secondly, we will further seek synergies, not only at a problem-specific operator level, but also with helper objectives that may guide the search towards higher quality solutions. Also, we used for the first time a MOEA designed for sparse problems in the context of the CSO problem. This kind of algorithm is receiving much attention currently in the specialized literature, and deserves a thorough analysis of its performance in the context of our problem. Finally, the modeling of the problem can be evolved to incorporate Cell-Free Massive MIMO technology. This is based on the fact that there are more antennas than users in the scenario, abstracting from the concept “cell”, to serve each with multiple antennas. This implies new levels of complexity for the search space, incorporating many more antennas, and changing the allocation strategies between users and base stations.

CRedit authorship contribution statement

Jesús Galeano-Brajonos: Software, Investigation, Writing – original draft, Visualization. **Francisco Luna-Valero:** Conceptualization, Methodology, Formal analysis, Investigation, Writing – original draft, Project administration. **Javier Carmona-Murillo:** Validation, Writing – review & editing, Funding acquisition. **Pablo H. Zapata Cano:** Software, Validation, Writing – review & editing. **Juan F. Valenzuela-Valdés:** Conceptualization, Investigation, Writing – review & editing, Funding acquisition.

Declaration of competing interest

The authors declare that they have no known competing financial interests or personal relationships that could have appeared to influence the work reported in this paper.

Data availability

Source code available at https://github.com/galeanobra/CSO_Hybrid and data available at <https://doi.org/10.6084/m9.figshare.21378000>.

Acknowledgments

This work has been partially funded by the Spanish Ministry of Science and Innovation via grant PID2020-112545RB-C54, by the European Union NextGenerationEU/PRTR under grants TED2021-131699B-I00 and TED2021-129938B-I00 (MCIN/AEI/10.13039/501100011033, FEDER) and the Andalusian PAIDI program with grants A-TIC-608-UGR20, P18.RT.4830, and PYC20-RE-012-UGR. The authors also thank the Supercomputing and Bioinformatics Center of the Universidad de Málaga, for providing its services and the Picasso supercomputer facilities to perform the experiments (<http://www.scbi.uma.es/>). Funding for open access charge: Universidad de Málaga/CBUA.

Appendix A. Supplementary data

Supplementary material related to this article can be found online at <https://doi.org/10.1016/j.swevo.2023.101290>.

References

- [1] Ericsson, Mobility report, 2022, URL <https://www.ericsson.com/49d3a0/assets/local/reports-papers/mobility-report/documents/2022/ericsson-mobility-report-june-2022.pdf>.
- [2] Cisco, Cisco Annual Internet Report (2018–2023), White Paper, 2020, 2020, URL <https://www.cisco.com/c/en/us/solutions/collateral/executive-perspectives/annual-internet-report/white-paper-c11-741490.pdf>.
- [3] N. Piovesan, A. Fernandez Gambin, M. Miozzo, M. Rossi, P. Dini, Energy sustainable paradigms and methods for future mobile networks: A survey, *Comput. Commun.* 119 (December 2017) (2018) 101–117, <http://dx.doi.org/10.1016/j.comcom.2018.01.005>.
- [4] J.G. Andrews, S. Buzzi, W. Choi, S.V. Hanly, A. Lozano, A.C.K. Soong, J.C. Zhang, What will 5G be? *IEEE J. Sel. Areas Commun.* 32 (6) (2014) 1065–1082, <http://dx.doi.org/10.1109/JSAC.2014.2328098>.
- [5] A. Bohlj, R. Bouallegue, How to meet increased capacities by future green 5G networks: A survey, *IEEE Access* 7 (2019) 42220–42237, <http://dx.doi.org/10.1109/ACCESS.2019.2907284>.
- [6] D. Lopez-Perez, M. Ding, H. Claussen, A.H. Jafari, Towards 1 Gbps/UE in cellular systems: Understanding ultra-dense small cell deployments, *IEEE Commun. Surv. Tutor.* 17 (4) (2015) 2078–2101, <http://dx.doi.org/10.1109/COMST.2015.2439636>.
- [7] M. Kamel, W. Hamouda, A. Youssef, Ultra-dense networks: A survey, *IEEE Commun. Surv. Tutor.* 18 (4) (2016) 2522–2545, <http://dx.doi.org/10.1109/COMST.2016.2571730>.
- [8] P.K. Agyapong, M. Iwamura, D. Staehle, W. Kiess, A. Benjebbour, Design considerations for a 5G network architecture, *IEEE Commun. Mag.* 52 (11) (2014) 65–75, <http://dx.doi.org/10.1109/MCOM.2014.6957145>.
- [9] S.A. Busari, K.M.S. Huq, S. Mumtaz, L. Dai, J. Rodriguez, Millimeter-wave massive MIMO communication for future wireless systems: A survey, *IEEE Commun. Surv. Tutor.* 20 (2) (2018) 836–869, <http://dx.doi.org/10.1109/COMST.2017.2787460>.
- [10] A.L. Swindlehurst, E. Ayanoglu, P. Heydari, F. Capolino, Millimeter-wave massive MIMO: The next wireless revolution? *IEEE Commun. Mag.* 52 (9) (2014) 56–62, <http://dx.doi.org/10.1109/MCOM.2014.6894453>.
- [11] R.W. Heath, N. González-Prelcic, S. Rangan, W. Roh, A.M. Sayeed, An overview of signal processing techniques for millimeter wave MIMO systems, *IEEE J. Sel. Top. Signal. Process.* 10 (3) (2016) 436–453, <http://dx.doi.org/10.1109/JSTSP.2016.2523924>.
- [12] Q.C. Li, H. Niu, A.T. Papanthanasios, G. Wu, 5G network capacity: Key elements and technologies, *IEEE Veh. Technol. Mag.* 9 (1) (2014) 71–78, <http://dx.doi.org/10.1109/MVT.2013.2295070>.
- [13] X. Ge, S. Tu, G. Mao, C.X. Wang, T. Han, 5G ultra-dense cellular networks, *IEEE Wirel. Commun.* 23 (1) (2016) 72–79, <http://dx.doi.org/10.1109/MWC.2016.7422408>.
- [14] M. Yao, M.M. Sohel, X. Ma, V. Marojevic, J.H. Reed, Sustainable green networking: exploiting degrees of freedom towards energy-efficient 5G systems, *Wirel. Netw.* 25 (3) (2019) 951–960, <http://dx.doi.org/10.1007/s11276-017-1626-7>.
- [15] 3GPP, Small Cell Enhancements for E-UTRA and E-UTRAN—Physical Layer Aspects, Tech. Rep., 3rd Generation Partnership Project (3GPP), 2014, URL <http://www.3gpp.org/ftp/Specs/html-info/36872.htm>.
- [16] M. Feng, S. Mao, T. Jiang, Base station ON-OFF switching in 5G wireless networks: Approaches and challenges, *IEEE Wirel. Commun.* 24 (4) (2017) 46–54, <http://dx.doi.org/10.1109/MWC.2017.1600353>.
- [17] D. Gonzalez G., J. Hamalainen, H. Yanikomeroglu, M. Garcia-Lozano, G. Senarath, A novel multiobjective cell switch-off framework for cellular networks, *IEEE Access* 4 (2016) 7883–7898.
- [18] D. González González, E. Mutafungwa, B. Haile, J. Hämäläinen, H. Poveda, A planning and optimization framework for ultra dense cellular deployments, *Mob. Inf. Syst.* 2017 (2017) 1–17, <http://dx.doi.org/10.1155/2017/9242058>.
- [19] F. Luna, R. Luque-Baena, J. Martínez, J. Valenzuela-Valdés, P. Padilla, Addressing the 5G cell switch-off problem with a multi-objective cellular genetic algorithm, in: *IEEE 5G World Forum, 5GWF 2018 - Conference Proceedings*, 2018, pp. 422–426.
- [20] P. Zapata-Cano, F. Luna, J. Valenzuela-Valdés, A.M. Mora, P. Padilla, Metaheurísticas híbridas para el problema del apagado de celdas en redes 5G (in spanish), in: *XIII Congreso Español En Metaheurísticas Y Algoritmos Evolutivos Y Bioinspirados, MAEB'18*, 2018, pp. 665–670.
- [21] F. Luna, P. Zapata-Cano, A. Palomares-Caballero, F. Valenzuela-Valdés, A capacity-enhanced local search for the 5G cell switch-off problem, in: *Communications in Computer and Information Science*, Vol. 1173, CCIS, 2020, pp. 165–178.
- [22] K. Deb, A. Pratap, S. Agarwal, T. Meyarivan, A fast and elitist multiobjective genetic algorithm: NSGA-II, *IEEE Trans. Evol. Comput.* 6 (2) (2002) 182–197.
- [23] A.J. Nebro, J.J. Durillo, F. Luna, B. Dorronsoro, E. Alba, MoeCell: A cellular genetic algorithm for multiobjective optimization, *Int. J. Intell. Syst.* 24 (7) (2009) 726–746.
- [24] N. Beume, B. Naujoks, M. Emmerich, SMS-EMOA: Multiobjective selection based on dominated hypervolume, *European J. Oper. Res.* 181 (3) (2007) 1653–1669.

- [25] Q. Zhang, H. Li, MOEA/D: A multiobjective evolutionary algorithm based on decomposition, *IEEE Trans. Evol. Comput.* 11 (6) (2007) 712–731.
- [26] Y. Tian, X. Zhang, C. Wang, Y. Jin, An evolutionary algorithm for large-scale sparse multiobjective optimization problems, *IEEE Trans. Evol. Comput.* 24 (2) (2020) 380–393.
- [27] I. Kropp, A.P. Nejadhashemi, K. Deb, Benefits of sparse population sampling in multi-objective evolutionary computing for large-scale sparse optimization problems, *Swarm Evol. Comput.* 69 (2022) 101025, <http://dx.doi.org/10.1016/j.swevo.2021.101025>.
- [28] E. Zitzler, L. Thiele, Multiobjective evolutionary algorithms: A comparative case study and the strength Pareto approach, *IEEE Trans. Evol. Comput.* 3 (4) (1999) 257–271.
- [29] E. Hossain, V. Bhargava, G. Fettweis, *Green Radio Communication Networks*, Cambridge University Press, 2012, <http://dx.doi.org/10.1017/CBO9781139084284>.
- [30] G. Miao, G. Song, *Energy and Spectrum Efficient Wireless Network Design*, Cambridge University Press, 2014.
- [31] M. Ismail, M. Shakir, K. Qaraqe, E. Serpedin, *Green Heterogeneous Wireless Networks*, Wiley, 2016.
- [32] S. Buzzi, C.-L. I, T.E. Klein, H.V. Poor, C. Yang, A. Zappone, A survey of energy-efficient techniques for 5G networks and challenges ahead, *IEEE J. Sel. Areas Commun.* 34 (4) (2016) 697–709, <http://dx.doi.org/10.1109/JSAC.2016.2550338>.
- [33] I.B. Sofi, A. Gupta, A survey on energy efficient 5G green network with a planned multi-tier architecture, *J. Netw. Comput. Appl.* 118 (2018) 1–28.
- [34] M. Usama, M. Erol-Kantarci, A survey on recent trends and open issues in energy efficiency of 5G, *Sensors (Switzerland)* 19 (14) (2019).
- [35] S. Zhang, X. Cai, W. Zhou, Y. Wang, Green 5G enabling technologies: An overview, *IET Commun.* 13 (2) (2019) 135–143.
- [36] P. Karmakar, R. Rajakumar, R. Roy, A survey on energy efficient cellular mobile communication, *Wirel. Pers. Commun.* 120 (2) (2021) 1475–1500, <http://dx.doi.org/10.1007/s11277-021-08520-1>.
- [37] S. Malathy, P. Jayarajan, H. Ojukwu, F. Qamar, M.N. Hindia, K. Dimiyati, K.A. Noordin, I.S. Amiri, A review on energy management issues for future 5G and beyond network, *Wirel. Netw.* 27 (4) (2021) 2691–2718, <http://dx.doi.org/10.1007/s11276-021-02616-z>.
- [38] A. Mughees, M. Tahir, M.A. Sheikh, A. Ahad, Towards energy efficient 5G networks using machine learning: Taxonomy, research challenges, and future research directions, *IEEE Access* 8 (2020) 187498–187522, <http://dx.doi.org/10.1109/ACCESS.2020.3029903>.
- [39] I. Chochliouras, M.-A. Kourti, A. Spiliopoulou, P. Lazaridis, Z. Zaharis, C. Zarakovitis, A. Kourti, Energy efficiency concerns and trends in future 5G network infrastructures, *Energies* 14 (17) (2021) <http://dx.doi.org/10.3390/en14175392>.
- [40] O. Alamu, A. Gbenga-Ilori, M. Adelabu, A. Imoize, O. Ladipo, Energy efficiency techniques in ultra-dense wireless heterogeneous networks: An overview and outlook, *Eng. Sci. Technol. Int. J.* (2020).
- [41] G. Premsankar, G. Piao, P.K. Nicholson, M.D. Francesco, D. Lugones, Data-driven energy conservation in cellular networks: A systems approach, *IEEE Trans. Netw. Serv. Manag.* 18 (3) (2021) 3567–3582, <http://dx.doi.org/10.1109/TNSM.2021.3083073>.
- [42] H.I. Obakhena, A.L. Imoize, F.I. Anyasi, K.V.N. Kavitha, Application of cell-free massive MIMO in 5G and beyond 5G wireless networks: A survey, *J. Eng. Appl. Sci.* 68 (1) (2021) 13, <http://dx.doi.org/10.1186/s44147-021-00014-y>.
- [43] F. Luna, P.H. Zapata-Cano, J.C. Gonzalez-Macias, J.F. Valenzuela-Valdés, Approaching the cell switch-off problem in 5G ultra-dense networks with dynamic multi-objective optimization, *Future Gener. Comput. Syst.* 110 (2020) 876–891.
- [44] T. Beitelmal, S.S. Szyszkowicz, G. David González, H. Yanikomeroglu, Sector and site switch-off regular patterns for energy saving in cellular networks, *IEEE Trans. Wireless Commun.* 17 (5) (2018) 2932–2945, <http://dx.doi.org/10.1109/TWC.2018.2804397>.
- [45] W. Lai, C.-S. Shieh, C.-S. Ho, Y.-R. Chen, A clustering-based energy saving scheme for dense small cell networks, *IEEE Access* 7 (2019) 2880–2893, <http://dx.doi.org/10.1109/ACCESS.2018.2886274>.
- [46] J. Li, H. Wang, X. Wang, Z. Li, Optimized sleep strategy based on clustering in dense heterogeneous networks, *Eurasip J. Wirel. Commun. Netw.* 2018 (1) (2018) <http://dx.doi.org/10.1186/s13638-018-1311-2>.
- [47] F. Ding, Y. Lu, Z. Pan, D. Zhang, H. Zhu, Performance analysis of an energy-efficient clustering algorithm for coordination networks, *Mob. Netw. Appl.* 25 (5) (2020) 1632–1643.
- [48] A. Hajijamali Arani, M.J. Omid, A. Mehbodiyi, F. Adachi, Minimizing base stations' ON/OFF switchings in self-organizing heterogeneous networks: A distributed satisfactory framework, *IEEE Access* 5 (2017) 26267–26278, <http://dx.doi.org/10.1109/ACCESS.2017.2777914>.
- [49] M. Dolfi, C. Cavdar, S. Morosi, P. Piuanti, J. Zander, E. Del Re, On the trade-off between energy saving and number of switchings in green cellular networks, *Trans. Emerg. Telecommun. Technol.* 28 (11) (2017) e3193, <http://dx.doi.org/10.1002/ett.3193>.
- [50] F. Ahmed, M. Naem, W. Ejaz, M. Iqbal, A. Anpalagan, M. Haneef, Energy cooperation with sleep mechanism in renewable energy assisted cellular hetnets, *Wirel. Pers. Commun.* 116 (1) (2021) 105–124.
- [51] Q.-N. Le-The, T. Beitelmal, F. Lagum, S.S. Szyszkowicz, H. Yanikomeroglu, Cell switch-off algorithms for spatially irregular base station deployments, *IEEE Wirel. Commun. Lett.* 6 (3) (2017) 354–357, <http://dx.doi.org/10.1109/LWC.2017.2690677>.
- [52] F. Lagum, Q.-N. Le-The, T. Beitelmal, S.S. Szyszkowicz, H. Yanikomeroglu, Cell switch-off for networks deployed with variable spatial regularity, *IEEE Wirel. Commun. Lett.* 6 (2) (2017) 234–237, <http://dx.doi.org/10.1109/LWC.2017.2665472>.
- [53] G. Femenias, N. Lassoued, F. Riera-Palou, Access point switch ON/OFF strategies for green cell-free massive MIMO networking, *IEEE Access* 8 (2020) 21788–21803.
- [54] H. Fourati, R. Maaloul, L. Fourati, M. Jmaïel, An efficient energy-saving scheme using genetic algorithm for 5G heterogeneous networks, *IEEE Syst. J.* (2022).
- [55] A. Salem, S. El-Rabaie, M. Shokair, Energy efficient ultra-dense networks (UDNs) based on joint optimisation evolutionary algorithm, *IET Commun.* 13 (1) (2019) 99–107.
- [56] K. Venkateswararao, P. Swain, Binary-PSO-based energy-efficient small cell deployment in 5g ultra-dense network, *J. Supercomput.* (2021) 1–22.
- [57] D.G. González, J. Hämäläinen, H. Yanikomeroglu, M. García-Lozano, G. Senarath, A novel multiobjective cell switch-off framework for cellular networks, *IEEE Access* 4 (2016) 7883–7898.
- [58] E.-G. Talbi (Ed.), *Hybrid Metaheuristics, Studies in Computational Intelligence*, vol. 434, Springer Berlin Heidelberg, Berlin, Heidelberg, 2013, <http://dx.doi.org/10.1007/978-3-642-30671-6>.
- [59] Performance limits of multiple-input multiple-output wireless communication systems, in: *Space-Time Coding*, John Wiley & Sons, Ltd, 2005, pp. 1–47.
- [60] J. Son, S. Kim, B. Shim, Energy efficient ultra-dense network using long short-term memory, in: *2020 IEEE Wireless Communications and Networking Conference, WCNC, 2020*, pp. 1–6.
- [61] C. Von Lücken, B. Barán, C. Brizuela, A survey on multi-objective evolutionary algorithms for many-objective problems, *Comput. Optim. Appl.* 58 (3) (2014) 707–756.
- [62] T. Liu, Z. Wang, M. Wei, A many-objective optimization algorithm using a two-space interactive evolutionary framework, *Swarm Evol. Comput.* 75 (2022) 101185, <http://dx.doi.org/10.1016/j.swevo.2022.101185>.
- [63] C. Yue, P. Suganthan, J. Liang, B. Qu, K. Yu, Y. Zhu, L. Yan, Differential evolution using improved crowding distance for multimodal multiobjective optimization, *Swarm Evol. Comput.* 62 (2021) 100849, <http://dx.doi.org/10.1016/j.swevo.2021.100849>.
- [64] Z. Ding, L. Chen, D. Sun, X. Zhang, A multi-stage knowledge-guided evolutionary algorithm for large-scale sparse multi-objective optimization problems, *Swarm Evol. Comput.* 73 (2022) 101119, <http://dx.doi.org/10.1016/j.swevo.2022.101119>.
- [65] J. Knowles, A summary-attainment-surface plotting method for visualizing the performance of stochastic multiobjective optimizers, in: *5th International Conference on Intelligent Systems Design and Applications, ISDA'05, IEEE, 2005*, pp. 552–557.
- [66] E. Osaba, E. Villar-Rodríguez, J. Del Ser, A.J. Nebro, D. Molina, A. LaTorre, P.N. Suganthan, C.A. Coello Coello, F. Herrera, A tutorial on the design, experimentation and application of metaheuristic algorithms to real-world optimization problems, *Swarm Evol. Comput.* 64 (2021) 100888, <http://dx.doi.org/10.1016/j.swevo.2021.100888>.
- [67] A. Quinones-García, J. Galeano-Brajones, P.H. Zapata-Cano, F. Luna-Valero, J. Carmona-Murillo, J.F. Valenzuela-Valdés, El efecto de la multicongruencia en el problema del apagado selectivo de redes 5G ultradensas [In Spanish], in: *XIV Congreso Español De Metaheurísticas, Algoritmos Evolutivos Y Bioinspirados, 2021*, pp. 446–451.

4

EXTENDING OPTIMIZATION TO OTHER 5G NETWORK PROBLEMS

This chapter presents an article to achieve O3. This article introduces a novel methodology that uses L-moment theory and ML algorithms for network traffic analysis and classification in the context of 5G networks, emphasizing intelligent system integration for enhanced management and security. Following this, the next section progresses to optimizing the methodology using an asynchronous steady-state version of the NSGA-II algorithm. This optimization aims to reduce the number of samples needed to estimate standard L-moments, perform feature selection, and maximize balanced accuracy. This approach demonstrates the efficacy of L-moments in network flow processing and highlights their potential to improve feature selection for similar challenges.x

Contents

4.1	Flow Analysis Using L-moments Theory	88
4.2	Optimization of the L-moments	96
4.2.1	Problem Modeling	96
4.2.2	Results	97

4.1 Flow Analysis Using L-moments Theory

To extend the expertise in optimization to other challenges within 5G/6G networks, this section introduces a cutting-edge methodology that takes advantage of L-moments theory and ML for network traffic analysis. This approach not only facilitates the integration of intelligent systems for enhanced network management and security, but also demonstrates robustness against outliers, requiring minimal data to accurately characterize traffic flows. The subsequent results underline the effectiveness of L-moments in network flow processing and the high-quality outcomes achievable with classification algorithms, paving the way for improved feature selection to address similar network issues.

THIS IS THE PUBLISHED VERSION OF THE PAPER:

J. Galeano-Brajones, M. I. Chidean, F. Luna, and J. Carmona-Murillo, "A novel approach for flow analysis in software-based networks using L-moments theory," *Computer Communications*, vol. 201, pp. 116–122, 2023.

- Journal Impact Factor (JIF) in JCR 2022: 6.0
- Category: COMPUTER SCIENCE, INFORMATION SYSTEMS. JIF rank: 33/158 (Q1).
- Category: ENGINEERING, ELECTRICAL & ELECTRONIC. JIF rank: 52/275 (Q1).
- Category: TELECOMMUNICATIONS. JIF rank: 18/88 (Q1).

Supplementary material is available in the Appendix D.

Disclaimer:

This work has been published in *Computer Communications*.

DOI: 10.1016/j.comcom.2023.01.022

Copyright:

© 2023 The Authors. Published by Elsevier B.V. This is an open access article under the Creative Commons Attribution 4.0 International (CC-BY-4.0).



Contents lists available at ScienceDirect

Computer Communications

journal homepage: www.elsevier.com/locate/comcom

A novel approach for flow analysis in software-based networks using L-moments theory

Jesús Galeano-Brajones^{a,*}, Mihaela I. Chidean^b, Francisco Luna^c, Javier Carmona-Murillo^a

^a Department of Computing and Telematics System Engineering, Universidad de Extremadura, Mérida, 06800, Extremadura, Spain

^b Department of Signal Theory and Communications, Universidad Rey Juan Carlos, Fuenlabrada, 28942, Madrid, Spain

^c School of Computer Science and Engineering, Universidad de Málaga, Málaga, 29071, Andalucía, Spain

ARTICLE INFO

Keywords:

Network traffic analysis

L-moments theory

Intelligent network management

6G

Machine Learning

ABSTRACT

The continuous increase in the number of devices connected to the Internet, together with the growth of applications and services, has made the tasks of network traffic analysis and classification essential in any environment. The deployment of 5G networks has prompted the research community to establish the pillars of Next-Generation Networks. These include intelligent systems, providing the network with intelligence in management and security tasks. In addition, these tasks require mechanisms capable of characterizing traffic in order to make network decisions. In this context, this paper proposes a novel methodology for processing network traffic using the L-moments theory and Machine Learning algorithms. This methodology is robust to outliers, requires few data to characterize the flows and subsequently fit the classification models. The results show that L-moments are particularly useful for processing network flows, and the classification algorithms obtain very high-quality results. Moreover, we show that the considered statistical tools also allow for a better understanding of the attack behaviour, leading the way to the improvement of the feature selection in similar problems.

1. Introduction

The major leap towards intelligent network management is thanks to 5G, mainly due to the introduction of software-defined, virtualization and slicing, among other techniques. These techniques allow services and applications to be virtualized on the network so that intelligent systems can be deployed as applications for both network management and security purposes. Moreover, the massive and continuous increase in network traffic makes the need to analyse and classify it even more essential. The sixth generation (6G) is not yet completely defined, but the research community agrees that these technologies will remain crucial. Furthermore, as intelligent systems evolve towards network self-management, Artificial Intelligence (AI) becomes much more important in Next-Generation Networks (NGNs) being the key characteristic of 6G autonomous networks [1].

Network and service management in 5G, Beyond 5G and especially 6G networks, including network security, are expected to be completely autonomous [2]. To achieve this, these networks will be driven on the Zero-touch network and Service Management (ZSM) concept defined by *European Telecommunications Standards Institute* [3]. This paradigm aims to integrate AI into the network as a key technology supported by software-defined and virtualization techniques. In this way, networks

will be able to manage themselves by taking decisions without the need for human intervention [4], thereby optimizing capital expenditure and operating expenses [5]. For achieving this automation, network traffic analysis and classification techniques are crucial to provide networks with relevant information to guide them in taking accurate decisions.

In this scenario, network traffic analysis is a hot topic for the scientific community, specifically from the network security assessment point of view. In this area, different techniques have been employed for threat detection by analysing network traffic and flows: (i) port-based analysis is the simplest and no longer useful technique due to the large proliferation of new services and applications using non-IANA well-defined ports [6]; (ii) Deep Packet Inspection (DPI) emerges as an alternative, but its major limitations are that it is only applicable to non-encrypted packets and the problems regarding the user's privacy, leading the way for the proposal of Machine Learning (ML) or Deep Learning (DL) techniques to mitigate these drawbacks [7]; (iii) payload-based technique uses only the information contained in the application layer payload and is usually deployed together with DPI [6]; (iv) statistical-based approaches use payload-independent parameters (e.g., flow duration, inter-arrival time, header length, etc.), which can be used as input to different statistical, ML or DL

* Corresponding author.

E-mail addresses: jgaleanobra@unex.es (J. Galeano-Brajones), mihaela.chidean@urjc.es (M.I. Chidean), flv@cc.uma.es (F. Luna), jcarmur@unex.es (J. Carmona-Murillo).

<https://doi.org/10.1016/j.comcom.2023.01.022>

Received 6 September 2022; Received in revised form 16 December 2022; Accepted 31 January 2023

Available online 2 February 2023

0140-3664/© 2023 The Author(s). Published by Elsevier B.V. This is an open access article under the CC BY license (<http://creativecommons.org/licenses/by/4.0/>).

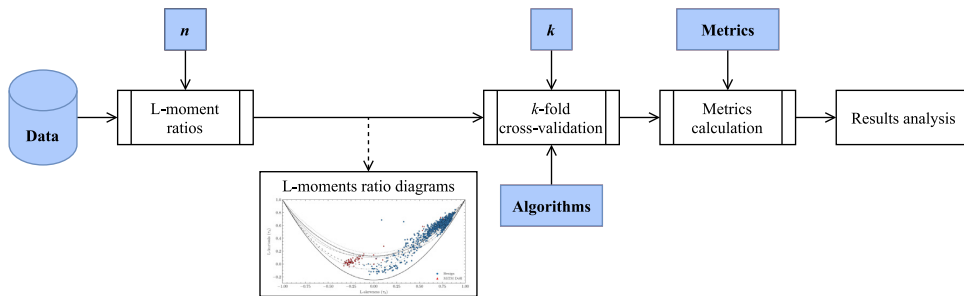


Fig. 1. Complete framework. The stages of the proposed methodology are represented with rectangles connected with arrows. Blue elements represent the modifiable parameters in this framework.

models. Finally, in recent years, there has been a growth in DL models applied to the network traffic classification [8].

L-moments have been widely used in different research fields since their proposal in 1990 [9], and network security and management has not been one of the most significant ones. The field with the most applications is climate analysis, especially regional frequency analysis [10]. Some specific examples include modelling probability distributions of wind and precipitation [11]. However, they have also been used in other fields like bioengineering for target classification in radar applications [12] and in the context of complex network theory [13]. Some additional examples include financial data and stock analysis [14,15], reliability disciplines [16], mathematical modelling of mechanical processes [17] or medical data [18]. Finally, as far as authors know, L-moments have only been used in two works related to network traffic analysis: (i) in [19] L-moments are used to fit the generalized Pareto distribution to network traffic data, especially to a heavy-tailed data sample; (ii) in [20] L-moments are used to characterize network flows. The latter is one of the first approaches of the authors to this methodology and a preliminary work of the present article.

This article proposes a novel methodology to classify network traffic data using L-moments and ML algorithms. L-moments allow the use of higher-order statistical moments avoiding the restrictions regarding the required amount of data for the estimation procedure. This advantage, together with the requirement of low computational resources, allows real-time data processing. Being this the first formal proposal of this methodology, the ML algorithms considered are k-Nearest Neighbours (kNN) and Support Vector Machines (SVM). In order to show the applicability of the proposed methodology, the experimentation has been performed with the CIC-DDoS2019 dataset [21]. This dataset contains scenarios with different up-to-date realistic DDoS and DrDoS attacks.

There are significant differences between [20] and the present work: (i) in this work, traffic data are analysed in a realistic way, i.e. data flows are not previously divided into benign/attack flows; (ii) in this work, we actually analyse and classify the traffic data using different state-of-the-art algorithms; (iii) in this work we consider a more realistic and state-of-the-art database, focusing on a specific attack. In short, [20] is just an exploratory work where the authors shown that network traffic data could be analysed with the L-moment statistical theory, while this is a complete analysis in a realistic scenario.

The rest of the document is organized as follows. Section 2 focuses on the theoretical background and technological basis of the proposed methodology; Section 3 details the set-up and the experimental evaluation conducted to validate our proposal; Section 4 shows and discusses some results obtained after the application of the proposed methodology, and also provides future directions for research. Finally, Section 5 concludes this article.

2. Framework and methods

This section describes the complete framework as well as each stage of the proposed methodology. Fig. 1 shows these stages, indicating in blue the inputs that can be modified. These inputs are described as follows:

- **Data** — input dataset. A cybersecurity-related dataset in this work, however, this methodology can be applied in other fields.
- **n** — amount of samples used to estimate each L-moment ratio, i.e., each point of the L-moment ratio diagram (LmomRD).
- **k** — number of folds used in cross-validation.
- **Algorithms** — network traffic classification algorithm. This meth-

odology allows the usage of multiple algorithms for the classification task.

- **Metrics** — evaluation metrics used for results analysis.

The following subsections provide a more in-depth description of each of the stages of this methodology. First, L-moments and LmomRD are briefly described. Then, the two ML algorithms used in this article are defined, although any type of classification or clustering algorithms can be used in this methodology.

2.1. L-moments

In data analysis, statistical moments are used to characterize the geometry of distributions and summarize samples. Standard statistical practise is based on “classical” or “conventional” moments, also known in the literature as product moments. However, product moments are just one of the available moment definitions, being the L-moments theory [9] the selected framework for this work.

In short, the L-moments are calculated by means of a linear combination of the expected values of order statistics. L-moments are suitable for data with large skew, large or long tails, or outliers [10, 22], characteristics that several variables obtained from network flow data fulfil [20]. Furthermore, L-moment estimators are unbiased, robust to outliers and with low sampling variability [9,10], leading to more accurate and precise estimations than product moments. Also, the sample size required to accurately estimate L-moments is significantly lower than for the product moments [9]. Further details regarding L-moments, such as their formal definition as well as their basic properties and estimators, can be found in [9].

Another great benefit of using L-moments is that this theory is parallel to the product moment theory also in terms of interpretation. That is, the first L-moment (λ_1) is defined as *L-location* and equals the mean of the distribution or average value of the dataset; this is the only case where the values are the same for both statistical theories. The second L-moment (λ_2) is known as *L-scale* and gives insight into the scale of dispersion, the third one (λ_3) describes the asymmetry, the

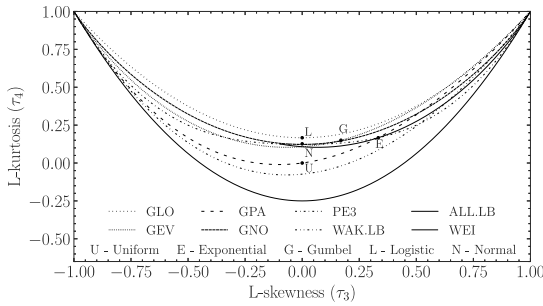


Fig. 2. LmomRD of some common distributions (GLO: Generalized Logistic; GEV: Generalized Extreme Value; GPA: Generalized Pareto; GNO: Generalized Normal; PE3: Pearson Type 3 or Gamma; WEI: Weibull; WAK.LB: Lower bound of the Wakeby distribution; ALLLB: Lower threshold for any distribution) [9].

fourth L-moment (λ_4) is related to the tails of a given distribution, and so on.

The standardized versions of λ_3 and λ_4 are named as *L-skewness* (τ_3) and *L-kurtosis* (τ_4), respectively. They also have the same interpretation as the skewness and kurtosis in classical statistics, e.g., $\tau_3 > 0$ (< 0) indicates positive (negative) symmetry and $\tau_4 > 0$ (< 0) indicate positive (negative) kurtosis. L-skewness and L-kurtosis are both lower and upper-bounded by definition for all distributions, a very interesting property that allows, for example, the direct comparison between distributions with significantly different locations and scales.

In this work, τ_3 and τ_4 will be estimated for the selected network traffic parameters and will be the input to the classification algorithms.

2.2. LmomRD

The L-moment theory provides also an extremely useful graphical tool: the L-moments ratio diagram, previously defined as the acronym LmomRD. This tool is mainly used for exploratory analysis as well as for distribution selection tasks, however in this work enables a visual result presentation, interpretation and comparison.

The LmomRD plots tuples (usually pairs) of L-moment ratios, each element in one axis. The most common pair of L-moment ratios to be related using this diagram is the $\{\tau_3, \tau_4\}$ one. It is also common to include in the LmomRD the theoretical L-moment ratios for some common distributions (see Fig. 2). In order to facilitate the interpretation and result comparison, all figures presented in this work will also include these theoretical lines, following the same legend.

2.3. Algorithms

As previously mentioned, the proposed methodology can include any clustering algorithm, classification technique, and even more complex ML or DL models. Basically, this framework can include any type of algorithm capable of classifying the points of the LmomRD. Given all available algorithms that fulfil the previous requirement, in this work two different yet state of the art representative algorithms are considered. In the following, these are briefly described; please refer to the original publications for further details.

The first considered algorithm is kNN, the non-parametric classification method proposed in 1951 [23]. kNN is a method used for both regression and classification since in both cases the algorithm takes as input the k samples closest to the dataset. If used for regression, the output of the algorithm is the average of the values of the k nearest neighbours. If used for classification, the output is a property class of the object based on its k neighbours.

The second considered algorithm is SVM. These are a set of supervised learning algorithms that analyse data in order to perform

classification or regression tasks and outliers detection. Proposed in 1992 [24], it has become one of the most robust prediction methods available currently. An SVM is a model that represents the data samples in space, separating the classes by a hyperplane or set of hyperplanes. Each hyperplane is defined as the vector between the points of the two nearest classes, which is called the support vector.

2.4. Evaluation metrics

In this work, results are quantitatively analysed using the *balanced accuracy* metric, which is defined as follows:

$$\text{Balanced Accuracy} = \frac{1}{2} \left(\frac{TP}{TP + FN} + \frac{TN}{TN + FP} \right) \quad (1)$$

where *TP* is the number of true positives, *FN* is the number of false negatives, *TN* is the number of true negatives and *FP* is the number of false positives. The balanced accuracy is a widely accepted metric in the scientific literature and it is suitable for unbalanced datasets, like the one considered in this work (see Section 3.1 for details regarding the dataset). Recall that the proposed framework allows any evaluation metric.

3. Experimental setting

In order to validate the usefulness of the proposed framework, we evaluate it using a state-of-the-art cybersecurity-related dataset. This section describes the experimental setting and the considered dataset.

3.1. CIC-DDoS2019 dataset

There are multiple network traffic datasets available for the research community, each considering specific scenarios and applications, and even with a variety of DDoS attacks. As the attacks are continuously evolving and presenting new challenges, new datasets are created that contain the latest information about the attacks.

In this work, we use the CIC-DDoS2019 dataset [21], as nowadays can be considered as the state-of-the-art dataset for any work that analyses network threats, specifically DDoS threats. This dataset has been generated by the Canadian Institute for Cybersecurity (CIC) with the aim of remedying all current deficiencies related to DDoS attacks. The dataset contains traffic flows belonging to different types of DDoS attacks that resemble actual real-world data.

In addition to the captured traffic, the authors of the dataset provide labelled CSV files generated by the CICFlowMeter-V3 tool. CICFlowMeter-V3 is a tool designed by CIC to perform analysis of the captured flows. The flow features obtained by this tool are based on the time stamp, source and destination IPs and ports, protocols, packets, inter-arrival time between packets, etc.

The CIC-DDoS2019 dataset contains an abstract behaviour of 25 users using the HTTP, HTTPS, FTP, SSH and email protocols. It includes network flows and CSV files for 10 DrDoS and 12 DDoS attacks captured in two days.

3.2. Experimental application

The experimental application implements all the stages included in the considered framework, starting from the initial parameters configuration and ending with the result representation. It automates the process of analysing the network flows of the input dataset. Besides calculating the L-moments and L-moment ratios to train classification algorithms, the application can perform an automatic analysis to establish which features of the dataset are the most promising to obtain the best classifications. This approach is very useful before deploying the trained models in the intelligent network since these models will be trained with the most promising features and will be as efficient as possible.

Table 1

Balance accuracy scores obtained for all the considered scenarios. Columns indicate the scenario and rows indicate the classification algorithm. The last row includes accuracy results from [26] for comparison purposes.

	(a)	(b)	(c)	(d)	(e)	(f)
kNN-unif	.9994	.8708	.9991	.9989	.6660	.9370
kNN-dist	.9995	.9666	.9991	.9800	.7549	.9545
SVM-lin	.9995	.9791	.9991	.8584	.8438	.6125
SVM_RBF	.9994	.9791	.9991	.9795	.9556	.9995
SVM-poly	.9924	.9916	.9978	.9784	.6660	.9820
DIDDOS [26]	.9952	.9997	.9997	.9987	.9996*	.9998

First, the CIC-DDoS2019 dataset is loaded and properly organized using the Python available variable representation. Following, the L-moment ratios are calculated using the $n = 200$ value, meaning that for each point of the LmomRD a total of 200 data packets are used. The data packets are analysed by means of a non-overlapping sliding window. The $n = 200$ value was empirically determined during the initial tests and it is a trade-off between moment estimation accuracy and delay. Using lower n values lead to less accurate moment estimation, while using larger n values imply larger delays in the analysis. Recall that the considered L-moments are third and fourth-order statistical moments, therefore using such a low amount of data packets to properly estimate them is one of the main reasons the L-moment theory was included in this methodology.

At this point, the LmomRDs are plotted. This step is used mainly as an auxiliary step to visually observe the input to the classification algorithms increasing the user-friendliness of the application. Afterwards, the classification task is performed with either kNN and SVM algorithm, together with the cross-validation technique [25]. In this work, 5-fold cross-validation is performed (input parameter $k = 5$) and the folds are made by preserving the percentage of samples for each class. Finally, the balanced accuracy metric of the classifications for the trained models is computed with the test subset.

Regarding the algorithm-related parameters, both kNN and SVM are configured attending their particular features. For kNN, we consider $k = \sqrt{N}/2$, being N is the size of the training set. The choice of an adjustable value for k is a consequence of the dataset characteristics, where each scenario has a different amount of data. With this k the kNN algorithm is able to properly adapt to each scenario, obtaining better accuracy and avoiding both under and over-fitting. We also consider the following weights functions: uniform and distance. The first one considers the same distance between neighbours, and the second one takes into account the distance between points in the classification space. These two cases will be labelled as “kNN-unif” and “kNN-dist”, respectively, in the rest of this document.

On the other hand, for SVM we consider the following three kernels: linear, polynomial and Radial Basis Function (RBF). The first one creates a linear hyperplane; the second one uses a polynomial (degree 3) function; the last one uses $\gamma = 1/(n_features \cdot \sigma^2)$, where γ is a scalar that defines how much influence a single training example has, $n_features$ is the number of features and, σ is the variance. These three cases will be labelled as “SVM-lin”, “SVM-poly” and “SVM-RBF”, respectively, in the rest of this document.

4. Results and discussion

This section includes the presentation and discussion of the results, as well as a brief analysis of the main benefits and drawbacks of the proposed methodology.

The experimentation has been conducted with the complete CIC-DDoS2019 dataset. In this work, we show the results for a total of six different scenarios, in order to show the potential of this methodology. These scenarios differentiate one from another in terms of the considered attack (either DDoS or DrDoS), the flow feature and/or different traffic capture of the dataset, i.e., different capture days. The following list details the characteristics of each scenario:

- (a) DrDoS attack using a Network Time Protocol (NTP) vulnerability to amplify UDP traffic to the victim and benign traffic; *packet length mean* feature; attack captured on the first day of the dataset.
- (b) DrDoS attack amplified by the Trivial File Transfer Protocol (TFTP) and benign traffic; *destination port* feature; attack captured on the first day of the dataset.
- (c) Scenario with the same characteristics as scenario (b) except for the feature; in this case, the feature is *maximum packet length*.
- (d) DrDoS attack amplified by Portmap and benign traffic; *packet length mean* feature; attack captured on the second day of the dataset.
- (e) DrDoS, amplified by NetBIOS and by LDAP, and benign traffic; *packet length mean* feature; attack captured on the second day of the dataset. This is a scenario where two different attacks are considered and multi-class classification is applied.
- (f) DDoS attack with TCP SYN flood, where the attackers initiate massive TCP connections to the victim without terminating the connection consuming the victim’s resources hindering the ability to not respond to legitimate traffic; *minimum forwarding inter-arrival time* feature; attack captured on the second day of the dataset.

The obtained results are represented in Fig. 3, where each inset represents an LmomRD (τ_3 vs. τ_4), calculated using n data packets, identifying benign flows and attacks with different colours and markers. In order to better understand the classification results, each point is labelled as benign (attack) when the majority of the n data packets used for each L-moment calculation are labelled as benign (attack). These points are the input to each considered classification algorithm, and the obtained balanced accuracy scores for all cases are showed in Table 1. In both figures, each scenario is identified by the label used in the previous list and, in the following, we discuss the results for each scenario.

4.1. LmomRD

In most cases, benign and attack markers are blended in the LmomRD. In particular, these are the points where the proportion of n benign and attack data flows used to estimate each L-moment are similar. This mix will be the source of errors for the classification algorithms, an expected situation in these kinds of problems.

Starting with the considered features, let us start with scenarios (a), (d) and (e) where the same feature (*packet length mean*) is used to analyse different attacks. This feature selection is not casual and helps with the method validation. We can observe that, as expected, clusters corresponding to benign traffic, although with a small number of points, are concentrated around similar values of τ_3 and τ_4 across the three insets.

Regarding the cluster localization and shape in general, they entirely depend on the traffic type (attack or benign) and the selected feature. In general, benign traffic tends to have positive L-skewness, indicating that the data distribution follows a probability distribution where most of the data are concentrated in the lower range. Also, benign traffic tends to have positive L-kurtosis, indicating that distribution tails are heavier than for a Normal distribution, therefore outliers are more likely.

Attack behaviour in terms of the LmomRD shows two quite some different situations: low and high cluster dispersion. On one hand, scenarios (c), (d) and DrDoS-NetBIOS from (e) reveal a significantly high range for L-skewness. This fact indicates that the values of the measured feature do not necessarily concentrate around a “gravity point” and can also indicate changes in the data statistics over time. The dispersed cluster behaviour can be explained by the way DrDoS works and its impact on the considered features, as through the network travel both short-length request packets as long-length response packets. The

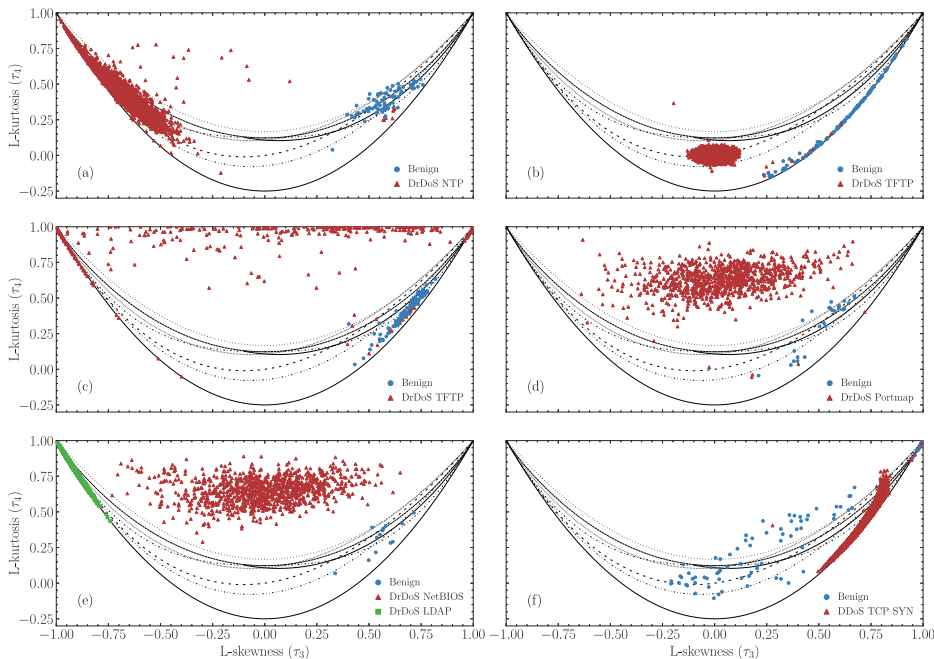


Fig. 3. LmomRD for the six considered scenarios. Each inset identifies the corresponding scenario in the left-lower corner. Attack and benign data are identified with different markers and colours, see legend for each scenario in the right-lower corner.

temporal behaviour would be very interesting to be analysed with more detail in future work, searching for example if there is some kind of relation between L-skewness and the duration of the attack and/or the temporal organization of the attack. In these three cases, the L-kurtosis is positive in all cases with rather high values, revealing heavy tails and therefore high outlier probability.

On the other hand, scenarios (a), (b), DrDoS-LDAP from (e) and (f) show less dispersion in the obtained clusters for attack traffic, but also with different behaviour. For example, DrDoS-NTP from (a) and DrDoS-LDAP from (e) show high negative L-skewness, while DrDoS-TCP-SYN from (f) reveal high positive L-skewness, while the tree cases show slightly high positive L-kurtosis. These facts reveal that these features for these specific attacks concentrate around a “gravity point” (either at the lower or the higher side of the range) and have quite some heavier tails than the Normal distribution, i.e., high probability for outliers. The extreme values obtained for the L-skewness in the three cases are also due to the attack/feature combination: (i) attacks from scenarios (a) and DrDoS-LDAP from (e) do not get any response from the victim and only long-length packets generated by the amplification mechanism travel through the network; (ii) attack from scenario (f) establishes a high amount of connections with the victim that lead to a significant increase in the packet transmission rate and this fact is reflected in the considered feature. Finally, DrDoS-TFTP from (b) has both low L-skewness and low L-kurtosis, meaning that these features could be easily adjusted to a Uniform distribution. Again, this statistical behaviour is the expected one for this feature, as the DrDoS attack tries to collapse a device by flooding a specific port. The variation around the (0, 0) point is due to the mix of benign and attack in the n packets used to estimate each L-moment.

4.2. Balanced accuracy

Once understood the scenario behaviours, the classification results are now analysed in terms of the balanced accuracy metric. These results are shown in Table 1 for all the considered algorithms (with their

respective settings) and scenarios. Precision, recall, and F_1 -score values have also been obtained to validate the results of the accuracy and can be found in the supplementary material. Best scores are marked in bold font, however, it can be observed that the balanced accuracy is quite high for the majority of the cases. From all considered scenarios, the SVM-RBF algorithm is the one that obtains a better-balanced accuracy score, even for the (e) scenario where other algorithms perform rather poor.

Table 1 also shows the results obtained for the accuracy score in a different work from the literature that analyses the same CIC-DDoS2019 dataset, but with a Gated Recurrent Unit (GRU), a type of Recurrent Neural Network (RNN) [26]. In order to properly compare these scores, recall that in [26] the authors balance the dataset by means of Synthetic Minority Oversampling Technique (SMOTE) and compute the accuracy, while in this work we analyse the original dataset and compute the balanced accuracy. Also note that the * in scenario (e) of Table 1 is due to the fact that DIDDOS classifies the two attacks involved individually, while our proposal performs a multi-class classification considering both attacks at the same time.

The approach followed [26] requires significantly higher computational resources for the RNN model compared with the methodology proposed in this work. However, it can be observed that their accuracy results differ quite little from the ones obtained in this work. Therefore, we can conclude that the methodology proposed in this work obtains results comparable in quality with more complex solutions published in the literature, with the clear benefit of requiring less computational resources for its implementation.

The previous results show a total of six scenarios, although the considered database includes other attacks and each flow has many other features. The presented results show some positive cases, where the combination of attack and feature leads to an adequate classification. However, there are also cases where the balanced accuracy is not high enough to properly separate attack from benign traffic. This situation is common in this type of problem with datasets where the amount

of available features is high and in an actual implementation, an initial analysis and feature selection is unavoidable. Nevertheless, we consider that the present results show a sufficient variety of cases to properly validate the proposed methodology.

4.3. Drawbacks and benefits

Regarding the main pros and cons of the presented methodology, in the following, we summarize them and propose several future research lines.

On the drawback part, one of the most relevant ones is the requirement to perform feature selection in order to obtain high-quality results, and therefore high attack detection accuracy. However, this also occurs in most classification problems, and it can be resolved by either using information about the attack characteristics, performing exploratory analysis over the available database or even with automated procedures. Another drawback of this methodology is that categorical features would require preprocessing in order to define numerical values that would allow computing the corresponding L-moments. In any case, network traffic databases usually include many more numerical than categorical features and, depending on the scenario, this drawback could be ignored. Finally, this is a new method that we validated using a limited amount of scenarios and a specific database. For a full validation and therefore usefulness, this method should be also validated in an actual 5G scenario in a real-time operation, being this one of our main future research and work lines.

On the positive part, this methodology has lower computational complexity compared to other state-of-the-art procedures, as both the L-moment estimation and the considered classification algorithms (kNN and SVM) have low computational requirements [10,23,24]. It is worth to mention that the total computational complexity depends on the considered classification algorithm, however, we have shown that even simple algorithms like kNN lead to high-quality classifications. This methodology also allows a better understanding of the statistical behaviour of the data and even to study the temporal attack behaviour, thanks to the usage of the LmomRD. This information can be useful for the proposal of mitigation actions in an actual software-defined scenario. Another benefit is that this methodology can be easily adapted to include multi-feature analysis. This can be achieved by either including a multivariate classification algorithm or by introducing the L-comoments [10], e.g., L-correlation, in the framework, being this idea another of our main future research lines. The last pro that we would like to mention is the possibility to introduce in the framework higher-order L-moments. This additional characteristic is straightforward from a programming point of view, however, it would require some additional theoretical support for the result interpretation. When considering higher-order L-moments, also multidimensional classification will be enabled and LmomRDs with more than two dimensions could be considered.

5. Conclusions

In 5G networks, the increase in connected devices and traffic volume has highlighted the need to analyse network traffic and classify it for both intelligent management and security purposes. Therefore, and in order to contribute to the progress towards Zero-touch networks, this article proposes a novel methodology for analysing and classifying network traffic. This methodology is based on the use of the L-moment ratios, a tool that has proven to be very useful for this task and that, to the best of our knowledge, has not been previously explored for this application. In order to validate the methodology, experimentation has been performed with the most up-to-date realistic dataset. The results allow us to validate the methodology, showing comparative results with another current proposal in the literature, and to propose various lines of future research.

CRedit authorship contribution statement

Jesús Galeano-Brajones: Methodology, Software, Investigation, Writing – original draft, Writing – review & editing, Visualization. **Mihaela I. Chidean:** Conceptualization, Methodology, Formal analysis, Writing – original draft, Writing – review & editing, Supervision. **Francois Luna:** Conceptualization, Validation, Writing – review & editing. **Javier Carmona-Murillo:** Conceptualization, Validation, Writing – review & editing, Project administration, Funding acquisition.

Declaration of competing interest

The authors declare that they have no known competing financial interests or personal relationships that could have appeared to influence the work reported in this paper.

Data availability

The dataset used is referenced in the document.

Acknowledgements

This research was funded in part by the European Union NextGenerationEU/PRTR, grant TED2021-131699B-I00 (AEI/FEDER/UE), by the Spanish Ministry of Science and Innovation, grant numbers PID2020-112545RB-C54 and PDC2022-133900-I00, by the Regional Government of Extremadura, Spain, grant IB18003, and by the Univ. Rey Juan Carlos Program for Research Promotion and Development (Ref. F920 and “AYUDA PUENTE 2022, URJC” Ref. F931).

Appendix A. Supplementary data

Supplementary material related to this article can be found online at <https://doi.org/10.1016/j.comcom.2023.01.022>. It contains the tables with the results of the evaluation metrics of the classifications as a complement to Table 1.

References

- [1] Z. Zhang, Y. Xiao, Z. Ma, M. Xiao, Z. Ding, X. Lei, G.K. Karagiannidis, P. Fan, 6G wireless networks: Vision, requirements, architecture, and key technologies, *IEEE Veh. Technol. Mag.* 14 (3) (2019) 28–41.
- [2] M. Bunyakitanon, X. Vasilakos, R. Nejabati, D. Simeonidou, End-to-end performance-based autonomous VNF placement with adopted reinforcement learning, *IEEE Trans. Cognit. Commun. Netw.* 6 (2) (2020) 534–547.
- [3] ETSI, GSZS, Zero-touch network and Service Management (ZSM); Reference Architecture, Tech. Rep, 2019.
- [4] C. Benzaid, T. Taleb, AI-driven zero touch network and service management in 5G and beyond: Challenges and research directions, *IEEE Netw.* 34 (2) (2020) 186–194.
- [5] M. Bagaa, T. Taleb, J.B. Bernabe, A. Skarmeta, Qos and resource-aware security orchestration and life cycle management, *IEEE Trans. Mob. Comput.* (2020).
- [6] H.-K. Lim, J.-B. Kim, K. Kim, Y.-G. Hong, Y.-H. Han, Payload-based traffic classification using multi-layer LSTM in Software Defined Networks, *Appl. Sci.* 9 (12) (2019) 2550.
- [7] F. Pacheco, E. Exposito, M. Gineste, C. Baudoin, J. Aguilar, Towards the Deployment of Machine Learning Solutions in Network Traffic Classification: A Systematic Survey, *IEEE Commun. Surv. Tutor.* 21 (2) (2018) 1988–2014.
- [8] S. Rezaei, X. Liu, Deep Learning for Encrypted Traffic Classification: An Overview, *IEEE Commun. Mag.* 57 (5) (2019) 76–81.
- [9] J.R. Hosking, L-moments: Analysis and estimation of distributions using linear combinations of order statistics, *J. R. Stat. Soc. Ser. B Stat. Methodol.* 52 (1) (1990) 105–124.
- [10] W.H. Asquith, *Univariate Distributional Analysis with L-Moment Statistics using R* (Ph.D. thesis), 2011.
- [11] M. Fawad, T. Yan, L. Chen, K. Huang, V.P. Singh, Multiparameter probability distributions for at-site frequency analysis of annual maximum wind speed with L-moments for parameter estimation, *Energy* 181 (2019) 724–737.
- [12] R. Ginoulhac, F. Barbaresco, J.-Y. Schneider, J.-M. Pannier, S. Savary, Target Classification Based On Kinematic Data From AIS/ADS-B, Using Statistical Features Extraction and Boosting, in: 2019 20th International Radar Symposium, IRS, IEEE, 2019, pp. 1–10.

- [13] F. Mohd-Zaid, C.M. Schubert Kabban, R.F. Deckro, A test on the L-moments of the degree distribution of a Barabási–Albert network for detecting nodal and edge degradation, *J. Complex Netw.* 6 (1) (2018) 24–53.
- [14] J.R.M. Hosking, *L-Moments and their Applications in the Analysis of Financial Data*, IBM Thomas J. Watson Research Division, 1999.
- [15] E. Jurczenko, B. Maillat, P. Merlin, *Efficient frontier for robust higher-order moment portfolio selection*, 2008.
- [16] N.U. Nair, B. Vineshkumar, L-moments of residual life, *J. Statist. Plann. Inference* 140 (9) (2010) 2618–2631.
- [17] S. Cao, H. Lu, Y. Peng, F. Ren, A novel fourth-order L-moment reliability method for L-correlated variables, *Appl. Math. Model.* 95 (2021) 806–823.
- [18] P. Royston, Which measures of skewness and kurtosis are best? *Stat. Med.* 11 (3) (1992) 333–343.
- [19] J. Hosking, Some theory and practical uses of trimmed L-moments, *J. Statist. Plann. Inference* 137 (9) (2007) 3024–3039.
- [20] M.I. Chidean, J. Carmona-Murillo, R.H. Jacobsen, Q. Zhang, Network Traffic Characterization Using L-moment Ratio Diagrams, in: 2019 Sixth International Conference on Internet of Things: Systems, Management and Security, IOTSMS, IEEE, 2019, pp. 555–560.
- [21] I. Sharafaldin, A.H. Lashkari, S. Hakak, A.A. Ghorbani, Developing realistic distributed denial of service (DDoS) attack dataset and taxonomy, in: 2019 International Carnahan Conference on Security Technology, ICCST, IEEE, 2019, pp. 1–8.
- [22] R.M. Vogel, N.M. Fennessey, L moment diagrams should replace product moment diagrams, *Water Resour. Res.* 29 (6) (1993) 1745–1752.
- [23] E. Fix, *Discriminatory Analysis: Nonparametric Discrimination, Consistency Properties*, vol. 1, USAF school of Aviation Medicine, 1985.
- [24] B.E. Boser, I.M. Guyon, V.N. Vapnik, A Training Algorithm for Optimal Margin Classifiers, in: *Proceedings of the Fifth Annual Workshop on Computational Learning Theory*, 1992, pp. 144–152.
- [25] F. Mosteller, J.W. Tukey, Data analysis, including statistics, in: *Handbook of Social Psychology*, vol. 2, 1968, pp. 80–203.
- [26] S. ur Rehman, M. Khaliq, S.I. Imtiaz, A. Rasool, M. Shafiq, A.R. Javed, Z. Jalil, A.K. Bashir, DIDDOS: An approach for detection and identification of distributed denial of service (DDoS) cyberattacks using gated recurrent units (GRU), *Future Gener. Comput. Syst.* 118 (2021) 453–466.

4.2 Optimization of the L-moments

Building on the methodology based on the theory of L-moments proposed in the previous article [58] (see Section 4.1), this section addresses a multi-objective optimization problem. The goals are threefold: to reduce the sample size n required to estimate the standard L-moments, to decrease the number of selected flow features, and to improve the balanced accuracy of the system. Therefore, the overarching goal of the optimization problem is to fine-tune ML models to minimize the resources required for their deployment in the network. This involves selecting features from flows and choosing the value of n to achieve the highest quality of classifications. Given that the problem has three objectives, a decision-making process is necessary after experimentation to evaluate which solution to the optimization problem is the most feasible for the network.

This section first outlines the modeling of the multi-objective problem. Following this, it details the experimental approach adopted and discusses the outcomes achieved from the optimization process.

4.2.1 Problem Modeling

The first objective of the problem is to minimize the number of flow features. Let $x_i = [x_0, x_1, \dots, x_n]$ be the binary array where each element x_i can take values 0 or 1. The objective is formalized as minimizing the sum of the elements of the array (see Eq. 4.1). This objective is subject to the constraint that at least one element of the array must be 1, which can be expressed as Eq. 4.4.

The second objective aims to minimize the number of samples required to estimate the L-moments, n (see Eq. 4.2). As explained in Section 4.1, a lower value results in more dispersed clusters, while a higher value leads to more concentrated clusters, facilitating easier clustering but with a higher probability of misclassifying some flows. The associated constraint for this objective is that n must be strictly greater than zero, as defined in Eq 4.5.

The third objective in Eq. 4.3 is to maximize a function $f(x, n)$ that depends both on the binary feature array x and the sample value n . This function calculates the balanced accuracy using the features x and the sample size n for the test part of the dataset used.

Therefore, the complete formulation of the multi-objective optimization problem is as follows:

$$\min \sum_{i=1}^m x_i, \quad (4.1)$$

$$\min n, \quad (4.2)$$

$$\max f(x, n) = \frac{1}{2} \left(\frac{TP}{TP + FN} + \frac{TN}{TN + FP} \right), \quad (4.3)$$

$$\text{subject to } \sum_{i=1}^m x_i \geq 1, \quad (4.4)$$

$$n > 0, \quad (4.5)$$

$$x_i \in \{0, 1\} \quad \forall i = 1, 2, \dots, m. \quad (4.6)$$

where TP represents true positives, TN represents true negatives, FP denotes false positives, and FN signifies false negatives. Therefore, $\frac{TP}{TP+FN}$ calculates the average true positive rate, and $\frac{TN}{TN+FP}$ calculates the average true negative rate, providing a more informative measure of accuracy on unbalanced datasets compared to overall accuracy.

4.2.2 Results

The following section outlines the experimental methodology adopted for this study. Subsequently, the results for two specific attacks are compared with those obtained in Section 4.1.

4.2.2.1 Experimental Methodology

Given the computational complexity in terms of time and memory resources required to optimize the L-moments methodology, an asynchronous steady-state version of the NSGA-II algorithm has been used, based on the one published in [59], NSGA-II_{ss}^{asy}. The evolutionary cycle of NSGA-II_{ss}^{asy} runs on a main node and is responsible for sending candidate solutions to the evaluation nodes to calculate the objectives of the problem and the constraints. These solutions are returned back to the main node, which processes the solution within the algorithm framework. Thus, the optimization of the methodology can be carried out in reasonable computing times, reducing the execution time of the algorithm from approximately 87 days which requires a sequential run, to about 7 hours using 300 evaluation nodes.

Regarding NSGA-II_{ss}^{asy} parameterization, 25,000 maximum evaluations have been used as stopping condition with a population of 100 solutions. The

encoding of the solution is composite, featuring a binary array for the selection of features and an integer value for n . Selection occurs through a binary tournament. Regarding the crossover and mutation processes, the algorithm uses a two-point crossover. For mutation, it uses bit flip in the binary feature selection array and polynomial mutation for n .

The dataset used for this study, CIC-DDoS2019 [60], is identical to that used in the previous article, facilitating a direct comparison. For predictions on the test segment of the dataset and calculating balanced accuracy, the same ML models from the previous study are employed: k-Nearest Neighbors with a uniform weighting function (kNN-unif), kNN with a distance-based weighting function (kNN-dist), a Linear Support Vector Machine (SVM-lin), an SVM with a Radial Basis Function (RBF) kernel (SVM-RBF), and an SVM with a 3rd-degree polynomial kernel (SVM-poly). These models are integrated into an ensemble that collaboratively determines the classification of each prediction. A soft voting classifier mechanism is used for decision-making, which selects the class by identifying *argmax* among the summed probabilities predicted by the ensemble models. That is, for a set of N models $\{M_1, M_2, \dots, M_N\}$ and a set of K classes $\{C_1, C_2, \dots, C_K\}$, where each model M_i provides a probability vector $P_i(c_k)$ for each class c_k with $i = 1, 2, \dots, N$ and $k = 1, 2, \dots, K$, the class predicted by the ensemble is defined by $\operatorname{argmax}_{c_k} \left(\sum_{i=1}^N P_i(c_k) \right)$.

4.2.2.2 Approximations to the Pareto Front

Given the size of the dataset and the computational resource costs of optimization, the methodology has been optimized for two types of DrDoS attacks: NTP and Portmap. Both attacks have been analyzed and discussed in Section 4.1, but the results of the optimized methodology are presented below.

In Figure 4.1, the approximation to the Pareto front by NSGA-II^{asy} is observed. In Section 4.1, the best balanced accuracy value was achieved with the kNN-dist and SVM-lin algorithms, reaching 0.9995 for a value of $n = 200$ and analyzing a single feature, the *packet length mean*. After optimizing the methodology, we obtain solutions that balance the three objectives of the problem, as well as solutions that exploit a specific objective. For example, there is a solution with a balanced accuracy of 1.0, two selected flow features, and an $n = 374$. Solutions are also obtained with low values n at the cost of a slight loss in classification quality or requiring more selected features. An example is a solution with a balanced accuracy of 0.91, a selected characteristic, and $n = 10$. Such low n values mean that the clusters of standard L-moments are not as concentrated, yet very good results can still be achieved. After a thorough

study of the involved features, these types of solutions could be very good candidates for implementation in real-time networks due to the low number of samples required. The figure also highlights the knee point as a red circle, which represents the solution that best balances the three objectives, situated at the shortest Euclidean distance to the point $[0, 0, 1.0]$. This origin point symbolizes the optimal objective values (minimum for the objectives to be minimized and maximum for those to be maximized). In this scenario, the value of the knee point is $[51, 3, 0.9992]$, suggesting it as the most balanced solution for deploying models in an online network.

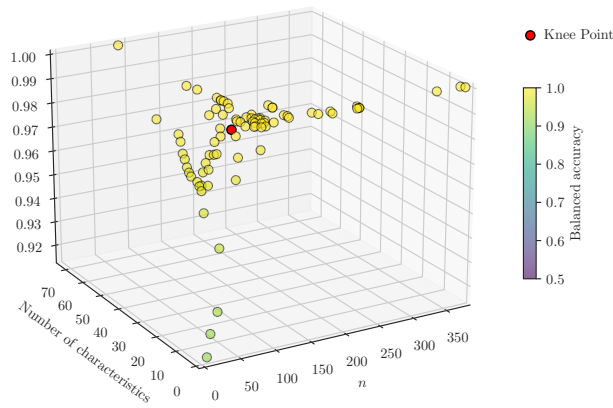


Figure 4.1: Approximation to the 3D Pareto front for the NTP DrDoS attack.

Regarding the Portmap DrDoS attack, whose approximation to the Pareto front can be seen in Figure 4.2, the situation is similar to the previous one. We start with a balanced accuracy of 0.9989 with $n = 200$ and one selected feature, again, the *packet length mean*. In this case, we find solutions with a worse balanced accuracy, 0.5, but with minimal values for the rest of the objectives, as it only selects one feature of the flows and $n = 10$. Regarding the knee point, in this instance, it has achieved values of $[32, 7, 0.9989]$.

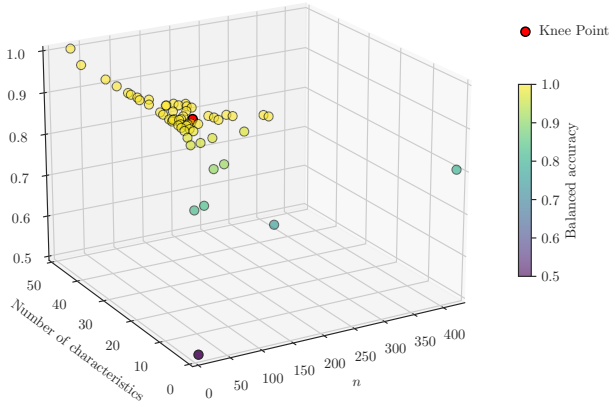


Figure 4.2: Approximation to the 3D Pareto front for the Portmap DrDoS attack.

Given that we start with very high-quality classifications in Section 4.1, the optimization of the methodology for these attacks makes sense to reduce the number of samples n to estimate the L-moments while compromising the classification quality as little as possible. Therefore, in these cases, the application of this optimization may be more focused on obtaining optimized methodologies for deployment in real-time networks rather than improving the classifications obtained.

5

CONCLUSIONS AND FUTURE WORK

The concluding chapter synthesizes the thesis findings and outlines avenues for future research. It reflects on the significant advancements made towards enhancing energy efficiency in 5G/6G networks through advanced optimization techniques. In addition, it presents a detailed roadmap for extending this research, highlighting potential improvements in optimization algorithms and the exploration of new problem areas within the domain of next-generation networks. This chapter serves as both a capstone to the research undertaken and a bridge to future explorations in the field.

Contents

5.1	Conclusions	102
5.2	Future Work	103

5.1 Conclusions

Following the development of this thesis, it can be concluded that advanced optimization techniques in multi-objective metaheuristics are crucial for both optimizing the CSO problem to reduce the energy consumption of 5G/6G networks and addressing other next-generation network challenges, such as optimizing the L-moments-based methodology for flow analysis and classification. Building on the objectives outlined in Section 1.2, the specific conclusions reached are enumerated as follows:

- Upon delving into the landscape of the CSO problem and examining the intricate relationships among various features, it has become evident that the spatial heterogeneity of traffic not only simplifies the landscape for exploration but also enhances the potential for a more effective algorithmic search. The introduction of a specialized search operator is a strategic response to the challenges presented in less heterogeneous, and consequently more complex, areas of 5G/6G networks. This operator, which uses detailed insights from landscape analysis, markedly improves the ability of metaheuristics to approximate the Pareto front of the CSO problem. The empirical evidence gathered supports the efficacy of the operator in refining search strategies, demonstrating a noteworthy advancement in utilizing landscape characteristics to achieve more precise and efficient optimization results.
- The design and integration of problem-specific operators, particularly those focusing on the strategic deactivation of cells, combined with the hybridization of multi-objective evolutionary algorithms, have significantly pushed forward the capabilities in optimizing network energy efficiency. This approach has led to marked advancements in achieving closer approximations to the Pareto front of the CSO problem, especially in the scope of reducing energy consumption. Moreover, the venture into multi-operator hybridization has opened new avenues, showcasing the potential to eclipse the performance of single-operator methods. This methodological evolution indicates a promising direction for further refining network optimization strategies, highlighting the intricate balance between operational efficiency and energy sustainability.
- The flow analysis methodology in 5G/6G networks utilizing L-moments has demonstrated its utility through effective classification capabilities and minimal resource requirements for simple ML models. The optimization process of this approach plays an important role in the practical deployment of trained models within next-generation networks. It facilitates a reduction in the number of flow samples needed for L-moment

calculations, consequently decreasing the time required for classification tasks, thereby streamlining the process for more efficient network management and operation.

5.2 Future Work

Given the focus of this thesis on current topics in the literature related to energy efficiency in 5G/6G and intelligent networks, various and extensive lines of work are proposed for each objective outlined in Section 1.2:

- Future work on spatial traffic heterogeneity and landscape analysis can be categorized into three main areas. First, conducting a thorough analysis of additional problem descriptors, such as UE-cell association mechanisms. Second, further development of landscape-aware genetic operators to utilize landscape information within the evolutionary cycle. Third, apply landscape insights to closely related problems, such as optimizing the deployment of base station locations, and extend the applicability of CSO problem insights to broader network optimization challenges.
- Several future research directions emerge regarding the hybridization with problem-specific operators. Initially, leveraging the diverse exploration capabilities of five MOEAs, the next step involves creating heterogeneous distributed models to enhance the coverage of the solution space. Additionally, efforts will focus on discovering synergies not only through problem-specific operators, but also through auxiliary objectives to refine solution quality. The application of a MOEA tailored for sparse problems to the CSO challenge, a novel approach that warrants in-depth performance analysis, is another critical work. Lastly, evolving the problem model to include Cell-Free Massive MIMO technology introduces a paradigm shift, increasing complexity and necessitating new user-base station allocation strategies, given the high number of antennas required.
- The L-moments-based methodology opens up several future research directions. First, expanding the order of standard L-moments to higher values, such as τ_5 or τ_6 , could offer new insight into the data for better classifications. Second, characterizing different types of flows, such as various types of attacks or service types, could further refine the analysis. Lastly, enhancing the optimization of the ML model ensemble is also of interest, incorporating model hyperparameters as optimization variables to potentially boost performance, and proposing problem-specific operators to hybridize the metaheuristics.

BIBLIOGRAPHY

- [1] M. Giordani, M. Polese, M. Mezzavilla, S. Rangan, and M. Zorzi, “Toward 6G Networks: Use Cases and Technologies,” *IEEE Communications Magazine*, vol. 58, pp. 55–61, 2019.
- [2] I. Akyildiz, A. Kak, and S. Nie, “6G and Beyond: The Future of Wireless Communications Systems,” *IEEE Access*, vol. 8, pp. 133995–134030, 2020.
- [3] H. Tataria, M. Shafi, A. Molisch, M. Dohler, H. Sjöland, and F. Tufvesson, “6G Wireless Systems: Vision, Requirements, Challenges, Insights, and Opportunities,” *Proceedings of the IEEE*, vol. 109, pp. 1166–1199, 2020.
- [4] S. Alraih, I. Shayea, M. Behjati, R. Nordin, N. Abdullah, A. Abu-Samah, and D. Nandi, “Revolution or Evolution? Technical Requirements and Considerations towards 6G Mobile Communications,” *Sensors (Basel, Switzerland)*, vol. 22, 2022.
- [5] F. Hu, Y. Deng, W. Saad, M. Bennis, and H. Aghvami, “Cellular-Connected Wireless Virtual Reality: Requirements, Challenges, and Solutions,” *IEEE Communications Magazine*, vol. 58, pp. 105–111, 2020.
- [6] S. Vitturi, C. Zunino, and T. Sauter, “Industrial Communication Systems and Their Future Challenges: Next-Generation Ethernet, IIoT, and 5G,” *Proceedings of the IEEE*, vol. 107, pp. 944–961, 2019.
- [7] Ericsson, “Ericsson Mobility Report November 2023,” 2023.
- [8] W. Saad, M. Bennis, and M. Chen, “A Vision of 6G Wireless Systems: Applications, Trends, Technologies, and Open Research Problems,” *IEEE Network*, vol. 34, pp. 134–142, 2019.
- [9] P. Yang, Y. Xiao, M. Xiao, and S. Li, “6G Wireless Communications: Vision and Potential Techniques,” *IEEE Network*, vol. 33, pp. 70–75, 2019.
- [10] A. Srivastava, M. Gupta, and G. Kaur, “Energy efficient transmission trends towards future green cognitive radio networks (5G): Progress, taxonomy and open challenges,” *Journal of Network and Computer Application*, vol. 168, p. 102760, 2020.
- [11] C. I. S. Han, and S. Bian, “Energy-efficient 5G for a greener future,” *Nature Electronics*, vol. 3, pp. 182–184, 2020.
- [12] Ericsson, “Ericsson Mobility Report November 2021,” 2021.
- [13] Cisco, “Cisco Annual Internet Report (2018–2023) White Paper,” 2023.
- [14] N. Piovesan, A. Fernandez Gambin, M. Miozzo, M. Rossi, and P. Dini, “Energy sustainable paradigms and methods for future mobile networks: A survey,” *Computer Communications*, vol. 119, no. December 2017, pp. 101–117, 2018.
- [15] A. Bohli and R. Bouallegue, “How to meet increased capacities by future green 5G networks: A survey,” *IEEE Access*, vol. 7, pp. 42220–42237, 2019.
- [16] D. López-Pérez, M. Ding, H. Claussen, and A. H. Jafari, “Towards 1 Gbps/UE in cellular systems: Understanding ultra-dense small cell deployments,” *IEEE Communications Surveys & Tutorials*, vol. 17, no. 4, pp. 2078–2101, 2015.
- [17] M. Kamel, W. Hamouda, and A. Youssef, “Ultra-dense networks: A survey,” *IEEE Communications surveys & tutorials*, vol. 18, no. 4, pp. 2522–2545, 2016.

- [18] S. Ju, Y. Xing, O. Kanhere, and T. Rappaport, "Millimeter Wave and Sub-Terahertz Spatial Statistical Channel Model for an Indoor Office Building," *IEEE Journal on Selected Areas in Communications*, vol. 39, pp. 1561–1575, 2021.
- [19] S. A. Busari, K. M. S. Huq, S. Mumtaz, L. Dai, and J. Rodriguez, "Millimeter-wave massive MIMO communication for future wireless systems: A survey," *IEEE Communications Surveys & Tutorials*, vol. 20, no. 2, pp. 836–869, 2017.
- [20] H. Huang, Y. Song, J. Yang, G. Gui, and F. Adachi, "Deep-Learning-Based Millimeter-Wave Massive MIMO for Hybrid Precoding," *IEEE Transactions on Vehicular Technology*, vol. 68, pp. 3027–3032, 2019.
- [21] GSMA, "Mobile Net Zero State of the Industry on Climate Action 2021," 2021.
- [22] H. Khaled, I. Ahmad, D. Habibi, and Q. V. Phung, "A Green Traffic Steering Solution for Next Generation Communication Networks," *IEEE Transactions on Cognitive Communications and Networking*, vol. 7, pp. 222–238, 2021.
- [23] GSMA, "Mobile Net Zero State of the Industry on Climate Action 2023," 2023.
- [24] HEXA-X-II, "Deliverable D1.1 Environmental, social, and economic drivers and goals for 6G," 2023.
- [25] H. Viswanathan, S. Wesemann, J. Du, and H. Holma, "Energy Efficiency in Next-generation Mobile Networks (White Paper)," 2022.
- [26] P. Lahdekorpi, M. Hronec, P. Jolma, and J. Moilanen, "Energy efficiency of 5G mobile networks with base station sleep modes," *2017 IEEE Conference on Standards for Communications and Networking, CSCN 2017*, pp. 163–168, 2017.
- [27] T. Islam, D. Lee, and S. S. Lim, "Enabling Network Power Savings in 5G-Advanced and Beyond," *IEEE Journal on Selected Areas in Communications*, 2023.
- [28] P. Frenger and R. Tano, "More capacity and less power: How 5G NR can reduce network energy consumption," in *IEEE Vehicular Technology Conference 2019*, 2019.
- [29] F. E. Salem, T. Chahed, E. Altman, A. Gati, and Z. Altman, "Optimal Policies of Advanced Sleep Modes for Energy-Efficient 5G networks," in *2019 IEEE 18th International Symposium on Network Computing and Applications, NCA 2019*, 2019.
- [30] P. Frenger and K. W. Helmersson, "Massive MIMO Muting using Dual-polarized and Array-size Invariant Beamforming," in *IEEE Vehicular Technology Conference 2021*, 2021.
- [31] K. N. V. Prasad, E. Hossain, and V. K. Bhargava, "Energy Efficiency in Massive MIMO-Based 5G Networks: Opportunities and Challenges," *IEEE Wireless Communications*, vol. 24, pp. 86–94, 2017.
- [32] E. Björnson, L. Sanguinetti, J. Hoydis, and M. Debbah, "Optimal design of energy-efficient multi-user MIMO systems: Is massive MIMO the answer?," *IEEE Transactions on Wireless Communications*, vol. 14, pp. 3059–3075, 2015.
- [33] R. Tao, W. Liu, X. Chu, and J. Zhang, "An Energy Saving Small Cell Sleeping Mechanism with Cell Range Expansion in Heterogeneous Networks," *IEEE Transactions on Wireless Communications*, vol. 18, pp. 2451–2463, 2019.
- [34] G. Jang, N. Kim, T. Ha, C. Lee, and S. Cho, "Base Station Switching and Sleep Mode Optimization with LSTM-Based User Prediction," *IEEE Access*, vol. 8, pp. 711–723, 2020.

- [35] C. Peng, S. B. Lee, S. Lu, and H. Luo, "GreenBSN: Enabling Energy-Proportional Cellular Base Station Networks," *IEEE Transactions on Mobile Computing*, vol. 13, pp. 2537–2551, 2014.
- [36] W. Teng, M. Sheng, X. Chu, K. Guo, J. Wen, and Z. Qiu, "Joint Optimization of Base Station Activation and User Association in Ultra Dense Networks under Traffic Uncertainty," *IEEE Transactions on Communications*, vol. 69, pp. 6079–6092, 2021.
- [37] D. Gonzalez G., J. Hamalainen, H. Yanikomeroglu, M. Garcia-Lozano, and G. Senarath, "A Novel Multiobjective Cell Switch-Off Framework for Cellular Networks," *IEEE Access*, vol. 4, pp. 7883–7898, 2016.
- [38] W. K. Lai, C.-S. Shieh, C.-S. Ho, and Y.-R. Chen, "A clustering-based energy saving scheme for dense small cell networks," *IEEE Access*, vol. 7, pp. 2880–2893, 2018.
- [39] J. Li, H. Wang, X. Wang, and Z. Li, "Optimized sleep strategy based on clustering in dense heterogeneous networks," *EURASIP Journal on Wireless Communications and Networking*, vol. 2018, pp. 1–10, 2018.
- [40] F. Ding, Y. Lu, Z. Pan, D. Zhang, and H. Zhu, "Performance Analysis of an Energy-Efficient Clustering Algorithm for Coordination Networks," *Mobile Networks and Applications*, vol. 25, pp. 1632–1643, 2020.
- [41] A. H. Arani, M. J. Omid, A. Mehdodniya, and F. Adachi, "Minimizing base stations' ON/OFF switchings in self-organizing heterogeneous networks: A distributed satisfactory framework," *IEEE Access*, vol. 5, pp. 26267–26278, 2017.
- [42] M. Dolfi, C. Cavdar, S. Morosi, P. Piunti, J. Zander, and E. Del Re, "On the trade-off between energy saving and number of switchings in green cellular networks," *Transactions on Emerging Telecommunications Technologies*, vol. 28, no. 11, p. e3193, 2017.
- [43] F. Ahmed, M. Naeem, W. Ejaz, M. Iqbal, A. Anpalagan, and M. Haneef, "Energy cooperation with sleep mechanism in renewable energy assisted cellular hetnets," *Wireless Personal Communications*, vol. 116, pp. 105–124, 2021.
- [44] Q.-N. Le-The, T. Beitelmal, F. Lagum, S. S. Szyszkowicz, and H. Yanikomeroglu, "Cell switch-off algorithms for spatially irregular base station deployments," *IEEE Wireless Communications Letters*, vol. 6, no. 3, pp. 354–357, 2017.
- [45] F. Lagum, Q.-N. Le-The, T. Beitelmal, S. S. Szyszkowicz, and H. Yanikomeroglu, "Cell switch-off for networks deployed with variable spatial regularity," *IEEE Wireless Communications Letters*, vol. 6, no. 2, pp. 234–237, 2017.
- [46] G. Femenias, N. Lassoued, and F. Riera-Palou, "Access point switch ON/OFF strategies for green cell-free massive MIMO networking," *IEEE access*, vol. 8, pp. 21788–21803, 2020.
- [47] D. González González, E. Mutafungwa, B. Haile, J. Hämäläinen, H. Poveda, *et al.*, "A planning and optimization framework for ultra dense cellular deployments," *Mobile Information Systems*, vol. 2017, 2017.
- [48] H. Fourati, R. Maaloul, L. Fourati, and M. Jmaiel, "An efficient energy-saving scheme using genetic algorithm for 5G heterogeneous networks," *IEEE Systems Journal*, vol. 17, no. 1, pp. 589–600, 2022.
- [49] A. A. Salem, S. El-Rabaie, and M. Shokair, "Energy efficient ultra-dense networks (UDNs) based on joint optimisation evolutionary algorithm," *IET Communications*, vol. 13, no. 1, pp. 99–107, 2019.

- [50] K. Venkateswararao and P. Swain, "Binary-PSO-based energy-efficient small cell deployment in 5G ultra-dense network," *The Journal of Supercomputing*, vol. 78, no. 1, pp. 1071–1092, 2022.
- [51] F. Luna, R. M. Luque-Baena, J. Martinez, J. F. Valenzuela-Valdés, and P. Padilla, "Addressing the 5g cell switch-off problem with a multi-objective cellular genetic algorithm," in *2018 IEEE 5G World Forum (5GWF)*, pp. 422–426, IEEE, 2018.
- [52] D. G. González, J. Hämäläinen, H. Yanikomeroglu, M. García-Lozano, and G. Senarath, "A novel multiobjective cell switch-off framework for cellular networks," *IEEE access*, vol. 4, pp. 7883–7898, 2016.
- [53] H. Liu, J. Zhang, X. Zhang, A. Kurniawan, T. Juhana, and B. Ai, "Tabu-Search-Based Pilot Assignment for Cell-Free Massive MIMO Systems," *IEEE Transactions on Vehicular Technology*, vol. 69, pp. 2286–2290, 2020.
- [54] D. K. Luong, M. Ali, Y. F. Hu, J. P. Li, R. Asif, and K. Abdo, "Simulated annealing-based multilink selection algorithm in SDN-enabled avionic networks," *Ieee Access*, vol. 9, pp. 145301–145316, 2021.
- [55] E.-G. Talbi, "Machine Learning into Metaheuristics," *ACM Computing Surveys (CSUR)*, vol. 54, pp. 1 – 32, 2021.
- [56] A. Liefvooghe, F. Daolio, S. Verel, B. Derbel, H. Aguirre, and K. Tanaka, "Landscape-Aware Performance Prediction for Evolutionary Multiobjective Optimization," *IEEE Transactions on Evolutionary Computation*, vol. 24, pp. 1063–1077, dec 2020.
- [57] G. R. Raidl, J. Puchinger, and C. Blum, "Metaheuristic hybrids," *Handbook of metaheuristics*, pp. 385–417, 2019.
- [58] J. Galeano-Brajones, M. I. Chidean, F. Luna, and J. Carmona-Murillo, "A novel approach for flow analysis in software-based networks using L-moments theory," *Computer Communications*, vol. 201, pp. 116–122, 2023.
- [59] J. J. Durillo, A. J. Nebro, F. Luna, and E. Alba, "A study of master-slave approaches to parallelize NSGA-II," in *2008 IEEE international symposium on parallel and distributed processing*, pp. 1–8, IEEE, 2008.
- [60] I. Sharafaldin, A. H. Lashkari, S. Hakak, and A. A. Ghorbani, "Developing realistic distributed denial of service (DDoS) attack dataset and taxonomy," in *2019 International Carnahan Conference on Security Technology (ICCST)*, pp. 1–8, IEEE, 2019.
- [61] J. Y. Branka Vucetic, *Performance Limits of Multiple-Input Multiple-Output Wireless Communication Systems*, ch. 1, pp. 1–47. John Wiley & Sons, Ltd, 2005.
- [62] J. Son, S. Kim, and B. Shim, "Energy efficient ultra-dense network using long short-term memory," in *2020 IEEE Wireless Communications and Networking Conference (WCNC)*, pp. 1–6, IEEE, 2020.

A

ANTS22 SUPPLEMENTARY MATERIAL

This supplementary material for ANTS22 (Section 3.1) contains the UDN modeling used for the article, the HV results and the average comparison of the algorithms.

Contents:

A.1 UDN Modeling

A.2 Hypervolume

A.3 Average Comparison of All Algorithms

A.1 UDN Modeling

This work considers a service area of 500×500 meters, which has been discretized using a grid of 100×100 points (also called “pixels” or area elements), each covering a 25 m^2 area, where the signal power is assumed to be constant. In addition to that, vertical densification has been taken into account by considering 3 vertical area elements, i.e., 25 meters of height. Ten different regions have been defined with different propagation conditions. In order to compute the received power at each point, the model used is $P_{rx}[dBm] = P_{tx}[dBm] + P_{Loss}[dB]$, where, P_{rx} is the received power in dBm, P_{tx} is the transmitted power in dBm, and P_{Loss} are the global signal losses, which depend on the given propagation region, and are computed as $P_{Loss}[dB] = GA + PA$ (A.1), where GA is the total gain of both antennas, and PA are the transmission losses in space, computed as:

$$PA[dB] = \left(\frac{\lambda}{2 \cdot \pi \cdot d} \right)^K \quad (\text{A.2})$$

where d is the Euclidean distance to the SBS, K is the exponent loss, which ranges randomly in $[2.0, 4.0]$ for each of the 10 different regions. The signal-to-interference plus noise ratio (SINR) for User Equipment (UE) k , is computed as:

$$SINR_k = \frac{P_{rx,j,k}[mW]}{\sum_{i=1}^M P_{rx,i,k}[mW] - P_{rx,j,k}[mW] + P_n[mW]} \quad (\text{A.3})$$

where $P_{rx,j,k}$ is the received power by UE k from the cell j , the summation is the total received power by UE k from all the cells operating at the same frequency that j , and $P_n[dBm] = -174 + 10 \cdot \log_{10} BW_j$ (A.4) is the noise power, being BW_j the bandwidth of SBS j , defined as 10% of the SBS operating frequency (see Table A.1).

Finally, the UE’s capacity has been calculated according to the MIMO depicted in [61]. Thus, we assume that the transmission power from each antenna is P_{tx}/n_{tx} , where n_{tx} indicates the number of transmit antennas. Then, if we consider the sub-channels to be uncoupled, their capacities can add up, and the overall channel capacity of the UE k can be estimated using the Shannon capacity formula:

$$C_k^j[bps] = BW_k^j[Hz] \cdot \sum_{i=1}^r \log_2 \left(1 + \frac{SINR_k \cdot \lambda_i}{n_{tx}} \right) \quad (\text{A.5})$$

where $\sqrt{\lambda_i}$ is the singular value of the channel matrix \mathbf{H} , of dimensions $n_{rx} \times n_{tx}$ (i.e., # receive antennas \times # transmit antennas). Note that both n_{rx} and n_{tx} depend on the cell type (see Table A.1). BW_k^j is the bandwidth assigned to UE k when connected to cell j , assuming a round-robin scheduling, that is $BW_k^j = \frac{BW_j}{N_j}$ (A.6), where N_j is the number of UEs connected to a cell j , and UEs are connected to the cell that provides the highest SINR, regardless of its type.

In order to build a heterogeneous network, three different types of cells of increasing size and decreasing frequency are considered: femtocells, picocells, and microcells. It should be noted that the number of transmit antennas of each cell type increases with frequency, going from 8 transmit antennas (microcell) to 256 (femtocell). In the same way, we assume that ‘‘high capacity’’ UEs, which will preferably connect to small cells (picocells and femtocells), will implement a higher number of receive antennas (4 for picocells and 8 for femtocells). Both cells and UEs are deployed using independent Poisson Point Processes (PPP) with different densities, defined by λ_P^{Cells} and λ_P^{UE} , respectively.

The power consumption of a transmitter is computed based on the model presented in [14], which considers that the device is transmitting over the fiber backhauling. Hence, the regular power consumption of SBS j is $P_j = \alpha \cdot P + \beta + \delta \cdot S + \rho$ (A.7), where P denotes the transmitted or radiated power of the transmitter, the coefficient α represents the efficiency of transmit power produced by a radio-frequency amplifier and feeder losses, the power dissipated owing to signal processing and site cooling is denoted by β and the dynamic power consumption per unit data is given by δ , being S the actual traffic demand provided by the serving cell. Finally, the power consumption of the transmitting device is represented by the coefficient ρ . However, in order to consider an accurate power consumption model, the power consumed by the air conditioning and power supply of the base station should be also taken into account [62]. This has been called maintenance power, and it is set to 2W/SBS for any SBS containing at least one active cell.

The detailed parametrization of the scenarios addressed is included in Table A.1, in which column Eq. links the parameter to the corresponding equation in the formulation detailed above. The names in the last nine columns, XY, stand for the deployment densities of SBSs and UEs, respectively, so that $X = \{L, M, H\}$, meaning either low, medium, or high-density deployments (λ_P^{Cell} parameter of the PPP) and $Y = \{L, M, H\}$, indicates a low, medium or high density of deployed UEs (λ_P^{UE} parameter of the PPP), in the last row of the table. The parameters G_{tx} and f of each type of cell refer to the transmission gain and the operating frequency (and its available bandwidth) of the antenna, respectively, being n_{tx} and n_{rx} the number of transmit and receive antennas. Finally, the parameters of the previously described power consumption model are also

included. Nine instances have been therefore used in this work in order to assess the performance of the different metaheuristics and specific operators.

Table A.1: Model parameters for users and base stations.

Cell	Parameter	Eq.	LL	LM	LH	ML	MM	MH	HL	HM	HH
Micro	G_{tx}	(A.1)	12								
	f	(A.4)	5 GHz (BW = 500 MHz)								
	α	(A.7)	15								
	β	(A.7)	10000								
	δ	(A.7)	1								
	$\rho[W]$	(A.7)	8								
	n_{tx}		2								
	λ_P^{micro} [Cells/km ²]		300	300	300	600	600	600	900	900	900
Pico	G_{tx}	(A.1)	20								
	f	(A.4)	20 GHz (BW = 2000 MHz)								
	α	(A.7)	9								
	β	(A.7)	6800								
	δ	(A.7)	0.5								
	$\rho[W]$	(A.7)	1								
	n_{tx}		64								
	λ_P^{pico} [Cells/km ²]		1500	1500	1500	1800	1800	1800	2100	2100	2100
Femto	G_{tx}	(A.1)	28								
	f	(A.4)	68 GHz (BW = 6800 MHz)								
	α	(A.7)	5.5								
	β	(A.7)	4800								
	δ	(A.7)	0.2								
	$\rho[W]$	(A.7)	1								
	n_{tx}		256								
	λ_P^{femto} [Cells/km ²]		3000	3000	3000	6000	6000	6000	9000	9000	9000
UEs	λ_P^{UE} [UE/km ²]		1000	2000	3000	1000	2000	3000	1000	2000	3000

A.2 Hypervolume

A.2.1 PSO Performance

Table A.2: Hypervolume indicator (Mean \pm Standard deviation).

	BPSO	MOCeII	NSGA-II
LL	0.631 \pm 0.077	0.279 \pm 0.164	0.497 \pm 0.158
LM	0.578 \pm 0.068	0.260 \pm 0.163	0.468 \pm 0.142
LH	0.564 \pm 0.061	0.241 \pm 0.157	0.441 \pm 0.130
ML	0.572 \pm 0.067	0.350 \pm 0.174	0.185 \pm 0.172
MM	0.518 \pm 0.056	0.254 \pm 0.163	0.153 \pm 0.161
MH	0.487 \pm 0.055	0.074 \pm 0.108	0.170 \pm 0.161
HL	0.546 \pm 0.070	0.086 \pm 0.129	0.298 \pm 0.223
HM	0.465 \pm 0.069	0.081 \pm 0.115	0.238 \pm 0.194
HH	0.472 \pm 0.053	0.068 \pm 0.105	0.219 \pm 0.168

A.2.2 Specific Operators in PSO

Table A.3: Hypervolume indicator for BPSO (Mean \pm Standard deviation).

	No Operators	No Users Op.		Prioritize Femto Op.	
		0.10	0.01	0.10	0.01
LL	0.631 \pm 0.077	0.636 \pm 0.064	0.627 \pm 0.075	0.634 \pm 0.063	0.626 \pm 0.066
LM	0.578 \pm 0.068	0.576 \pm 0.065	0.577 \pm 0.065	0.590 \pm 0.064	0.578 \pm 0.065
LH	0.564 \pm 0.061	0.551 \pm 0.055	0.557 \pm 0.057	0.561 \pm 0.059	0.554 \pm 0.053
ML	0.572 \pm 0.067	0.561 \pm 0.065	0.569 \pm 0.065	0.553 \pm 0.072	0.568 \pm 0.068
MM	0.518 \pm 0.056	0.522 \pm 0.068	0.520 \pm 0.074	0.523 \pm 0.067	0.523 \pm 0.053
MH	0.487 \pm 0.055	0.493 \pm 0.041	0.502 \pm 0.058	0.502 \pm 0.049	0.493 \pm 0.053
HL	0.546 \pm 0.070	0.545 \pm 0.062	0.550 \pm 0.070	0.544 \pm 0.064	0.544 \pm 0.066
HM	0.465 \pm 0.069	0.469 \pm 0.062	0.460 \pm 0.067	0.466 \pm 0.070	0.466 \pm 0.067
HH	0.472 \pm 0.053	0.462 \pm 0.051	0.458 \pm 0.046	0.466 \pm 0.042	0.464 \pm 0.049

Table A.4: Hypervolume indicator for MOCeII (Mean \pm Standard deviation).

	No Operators	No Users Op.		Prioritize Femto Op.	
		0.10	0.01	0.10	0.01
LL	0.279 \pm 0.164	0.720 \pm 0.059	0.661 \pm 0.079	0.614 \pm 0.085	0.585 \pm 0.117
LM	0.260 \pm 0.163	0.675 \pm 0.072	0.591 \pm 0.105	0.533 \pm 0.102	0.510 \pm 0.128
LH	0.241 \pm 0.157	0.641 \pm 0.075	0.570 \pm 0.101	0.511 \pm 0.120	0.385 \pm 0.215
ML	0.350 \pm 0.174	0.675 \pm 0.076	0.712 \pm 0.066	0.623 \pm 0.108	0.604 \pm 0.119
MM	0.254 \pm 0.163	0.714 \pm 0.071	0.681 \pm 0.075	0.548 \pm 0.125	0.535 \pm 0.131
MH	0.074 \pm 0.108	0.604 \pm 0.092	0.540 \pm 0.115	0.415 \pm 0.150	0.416 \pm 0.145
HL	0.086 \pm 0.129	0.685 \pm 0.096	0.637 \pm 0.110	0.593 \pm 0.125	0.592 \pm 0.127
HM	0.081 \pm 0.115	0.608 \pm 0.105	0.576 \pm 0.120	0.502 \pm 0.138	0.503 \pm 0.153
HH	0.068 \pm 0.105	0.611 \pm 0.081	0.570 \pm 0.106	0.464 \pm 0.146	0.475 \pm 0.140

Table A.5: Hypervolume indicator for NSGA-II (Mean \pm Standard deviation).

	No Operators	No Users Op.		Prioritize Femto Op.	
		0.10	0.01	0.10	0.01
LL	0.497 \pm 0.158	0.785 \pm 0.051	0.760 \pm 0.070	0.759 \pm 0.059	0.758 \pm 0.065
LM	0.468 \pm 0.142	0.742 \pm 0.059	0.715 \pm 0.072	0.693 \pm 0.083	0.673 \pm 0.110
LH	0.441 \pm 0.130	0.738 \pm 0.055	0.690 \pm 0.076	0.659 \pm 0.091	0.642 \pm 0.125
ML	0.185 \pm 0.172	0.741 \pm 0.062	0.717 \pm 0.076	0.701 \pm 0.088	0.705 \pm 0.079
MM	0.153 \pm 0.161	0.711 \pm 0.071	0.669 \pm 0.097	0.642 \pm 0.104	0.646 \pm 0.109
MH	0.170 \pm 0.161	0.683 \pm 0.066	0.649 \pm 0.091	0.611 \pm 0.112	0.606 \pm 0.114
HL	0.298 \pm 0.223	0.741 \pm 0.069	0.734 \pm 0.082	0.721 \pm 0.082	0.727 \pm 0.082
HM	0.238 \pm 0.194	0.684 \pm 0.096	0.673 \pm 0.104	0.649 \pm 0.105	0.639 \pm 0.123
HH	0.219 \pm 0.168	0.697 \pm 0.073	0.663 \pm 0.096	0.636 \pm 0.105	0.642 \pm 0.112

A.3 Average Comparison: Algorithm and Scenario

First, the comparison between the averages for each algorithm and scenario is shown. Secondly, the comparison of all algorithms for each scenario. The stats output is shown in tabular form: a black upward triangle (\blacktriangle) states that the setting of the row has statistically higher values than the configuration of the column, a white downward triangle (\blacktriangledown) states that the configuration in the row has statistically lower values than the configuration in the column. When no statistically significant differences are found, the spot is left empty.

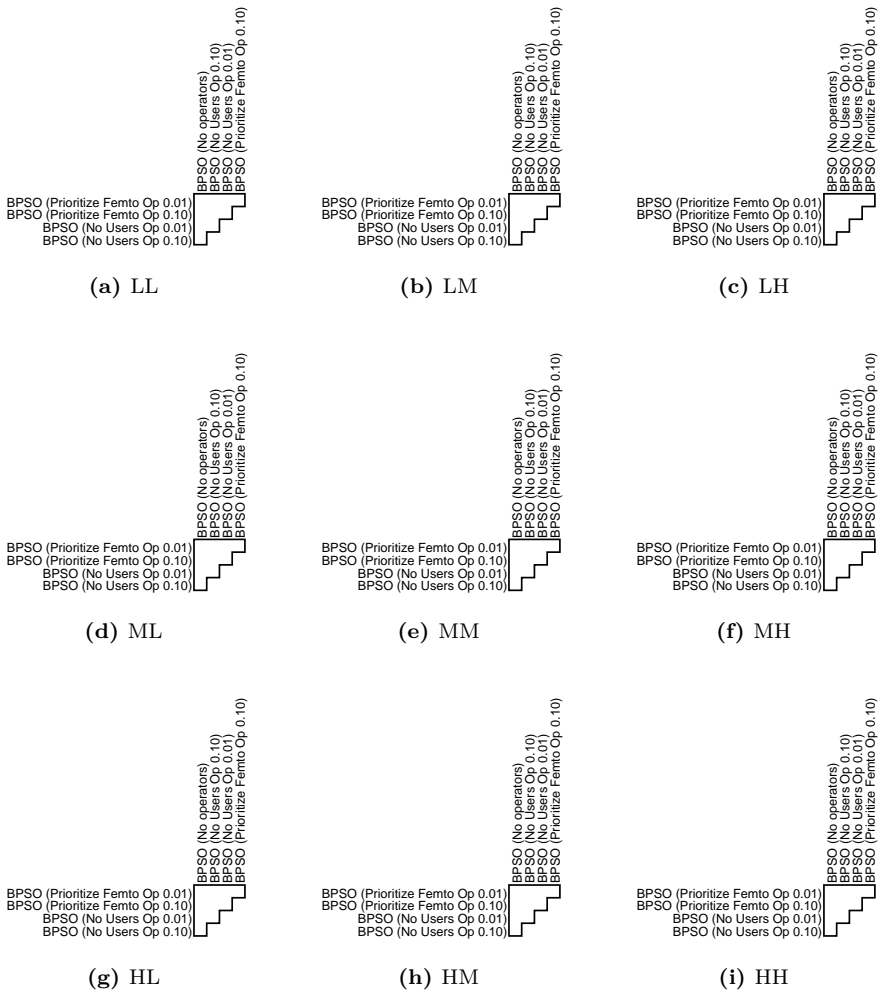


Figure A.1: Comparison of BPSO averages for each scenario.

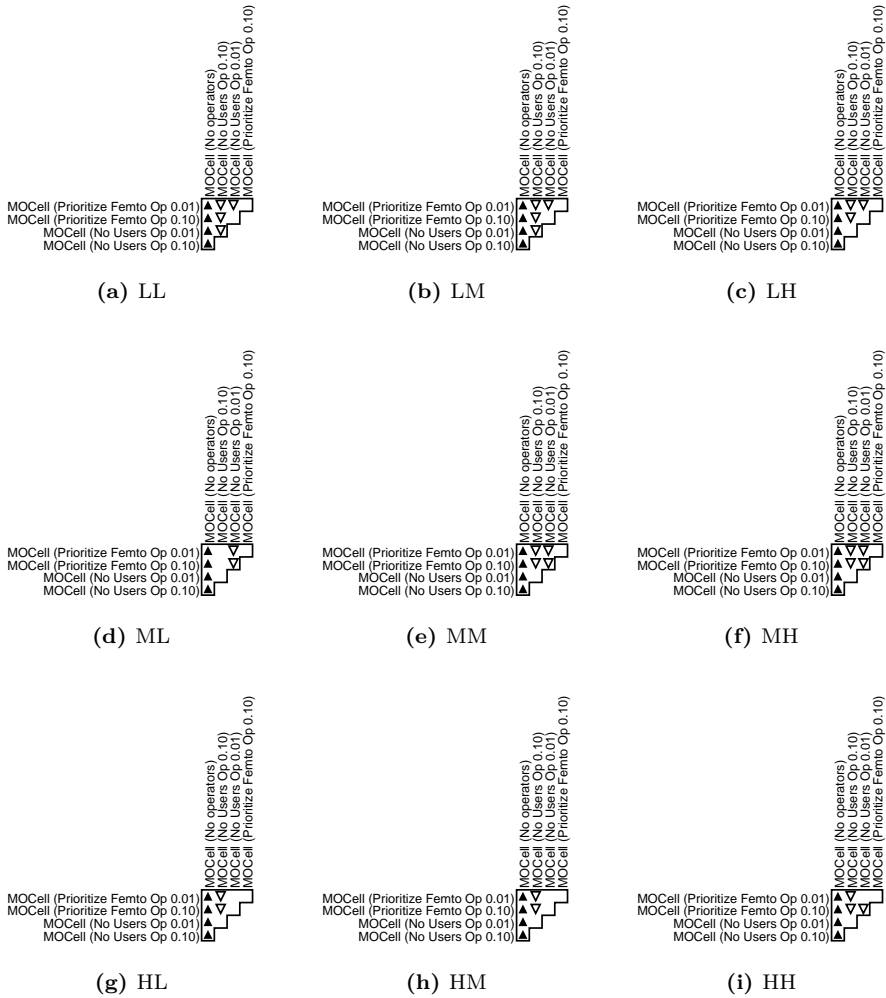


Figure A.2: Comparison of MOCcell averages for each scenario.

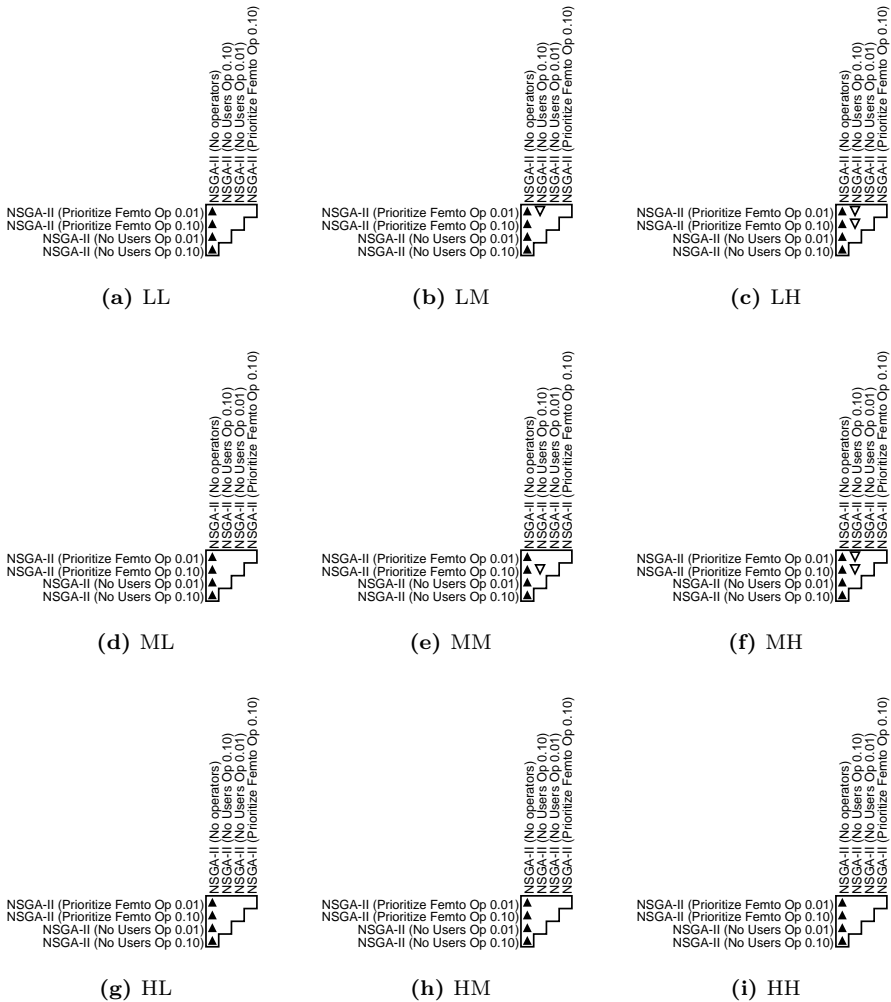


Figure A.3: Comparison of NSGA-II averages for each scenario.

A.4 Average Comparison of All Algorithms

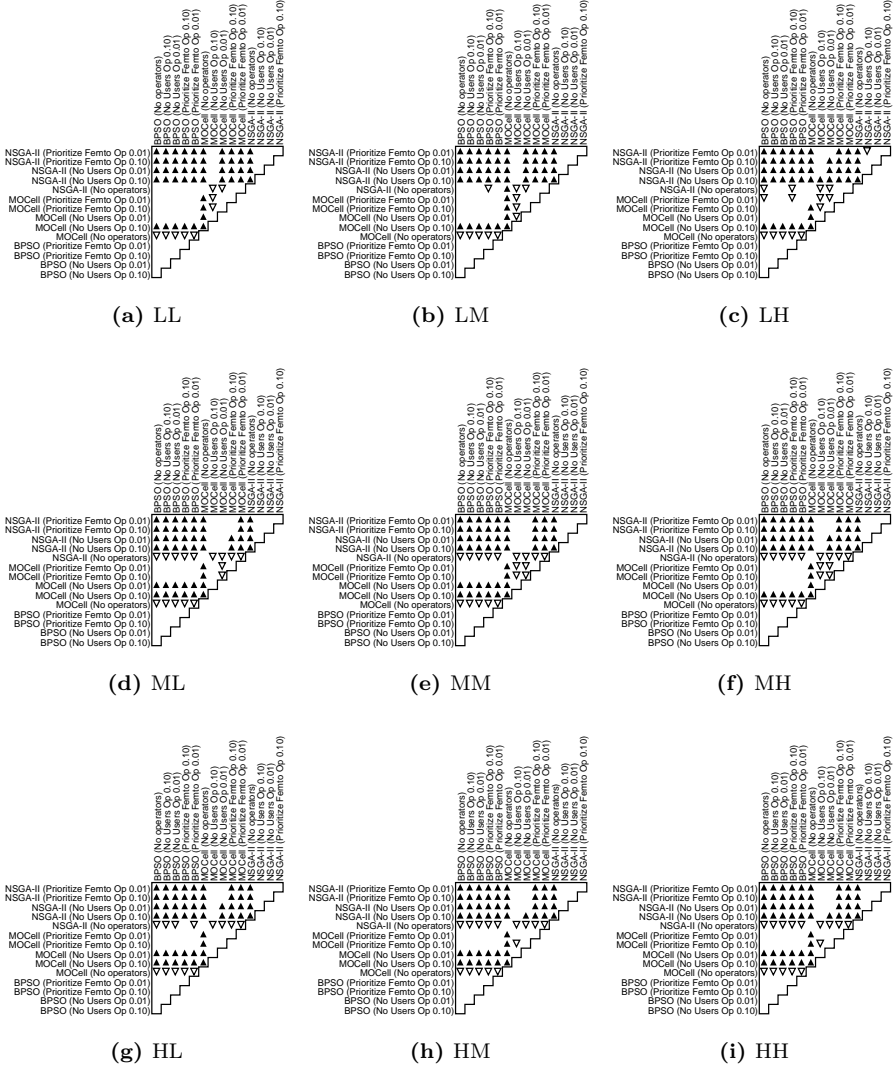


Figure A.4: Comparison of all algorithms averages for each scenario.

B

GENO SUPPLEMENTARY MATERIAL

This supplementary material for GENO article (Section 2.1) contains the network modeling used in this paper, the results of the approximations to the Pareto Front, and the HV values obtained.

Contents:

B.1 Network Modeling

B.2 Approximations to the Pareto Front

B.3 HV Values

B.1 Network Modeling

In this study, a service area measuring 500×500 meters is considered, within which ten distinct regions are defined, each with different propagation conditions. To calculate the received power, P_{rx} in dBm , at any given location within this area, the following model has been employed:

$$P_{rx}[dBm] = P_{tx}[dBm] + P_{loss}[dB] \quad (B.1)$$

where P_{rx} denotes the received power in dBm , P_{tx} represents the transmitted power in dBm , and P_{loss} refers to the global signal losses. These losses are contingent upon the specific propagation region and are computed as follows:

$$P_{loss}[dB] = GA + PA \quad (B.2)$$

where GA is the total gain of both antennas, and PA are the transmission losses in space, computed as:

$$PA[dB] = \left(\frac{\lambda}{4 \cdot \pi \cdot d} \right)^K \quad (B.3)$$

where d is the Euclidean distance to the corresponding sector in the SBS, K denotes the exponent loss, which randomly ranges in $[2.0, 4.0]$ for each of the 10 different regions. The Signal-to-Noise Ratio (SNR) for UE k , is computed as:

$$SNR_k = \frac{P_{rx,j,k}[mW]}{P_n[mW]} \quad (B.4)$$

where $P_{rx,j,k}$ is the received power by UE k from the cell j , and P_n is the noise power, computed as:

$$P_n[dBm] = -174 + 10 \cdot \log_{10} BW_j \quad (B.5)$$

being BW_j the bandwidth of cell j , defined as 10% of the operating frequency of SBS, which is the same for all cells it deploys (see Table B.1).

In the final analysis, the UE capacity is determined based on the Multiple Input Multiple Output (MIMO) model as described in [61]. It is assumed that the transmission power from each antenna is $P_{tx}/n_t x$, with $n_t x$ representing

the number of transmitting antennas. When considering the subchannels as uncoupled, their capacities can be summarized. Therefore, the total channel capacity for UE k is estimated using the Shannon capacity formula as follows:

$$C_k^j [bps] = BW_k^j [Hz] \cdot \sum_{i=1}^r \log_2 \left(1 + \frac{SNR_k \cdot \lambda_i}{n_{tx}} \right) \quad (\text{B.6})$$

where $\sqrt{\lambda_i}$ represents the singular value of the channel matrix \mathbf{H} , which has dimensions $n_{rx} \times n_{tx}$, indicating the number of receiving antennas times the number of transmitting antennas. The values of both n_{rx} and n_{tx} are contingent upon the type of cell, as detailed in Table B.1. The term BW_k^j denotes the bandwidth allocated to UE k when it is connected to cell j , under the assumption of round-robin scheduling, which implies:

$$BW_k^j = \frac{BW_j}{N_j} \quad (\text{B.7})$$

where N_j denotes the number of UEs connected to a cell j .

To build a heterogeneous network, three types of cells are considered, varying in size and frequency: femtocells, picocells, and microcells. These cells originate from antennas within a sector of a SBS. Figure B.1 illustrates the configurations used in our model. The first row shows three SBSs, each with three sectors and all cells in operation, represented by binary strings with all genes set to 1. The second row presents several solutions where a subset of cells are switched off, reflected in the binary strings with genes set to 0. Notably, the number of transmitting antennas for each cell type increases with frequency: 8 for microcells, 64 for picocells, and 256 for femtocells. Similarly, high-capacity UEs, likely to connect to smaller cells (picocells and femtocells), are assumed to have a larger number of receiving antennas, with 4 and 8 antennas for picocells and femtocells, respectively.

The deployment of cells in this system is achieved by placing SBSs within the work area, each having a random rotation angle for its sectors. This angle determines the orientation of the cell beams. Both SBSs and UEs are deployed using independent Poisson Point Processes (PPP) with different densities, denoted by λ_P^{Cells} for cells and λ_P^{UE} for UEs. Our software framework incorporates a discretization method that uses a grid comprising 100×100 points, also called ‘‘pixels’’ or area elements, each covering 25 m^2 where the signal power is considered uniform. Furthermore, vertical densification is addressed by considering 3 vertical area elements, equivalent to 25 meters of height. This approach is designed to reduce the computation cost of the SNR values.

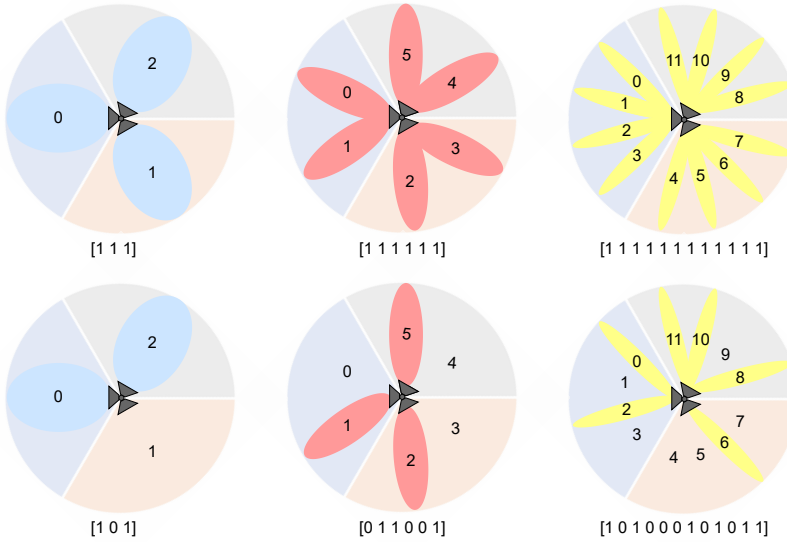


Figure B.1: Configuration of the SBSs, sectors, and cells used in this work, along with their mapping into a binary encoded representation.

The power consumption of a transmitter is computed using the model outlined in [14], which assumes the device transmits over fiber backhauling. Consequently, the standard power consumption of cell j , denoted as P_j , is expressed as follows:

$$P_j = \alpha \cdot P + \beta + \delta \cdot S + \rho \quad (\text{B.8})$$

where P denotes the transmitted or radiated power of the transmitter, the coefficient α represents the efficiency of the transmission power produced in the radio frequency amplifier and feeder losses. The term β refers to the power dissipated due to signal processing and site cooling, and δ indicates the dynamic power consumption per unit of data, with S being the actual traffic demand served by the cell. The power consumption of the transmitting device itself is denoted by the coefficient ρ . However, for a more accurate power consumption model, the power consumed by air conditioning and the SBS power supply is also considered [62]. This aspect, referred to as maintenance power, is set to 2W per SBS, applicable for any SBS with at least one active cell.

The parameterization of the scenarios addressed in this study is detailed in Table B.1. This table links the parameter to its corresponding equation in the formulation described above. The names in the last nine columns, XY,

Cell	Parameter	Eq.	LL	LM	LH	ML	MM	MH	HL	HM	HH
Micro	G_{tx}	(B.2)	12								
	f	(B.5)	5 GHz (BW = 500 MHz)								
	α	(B.8)	15								
	β	(B.8)	10000								
	δ	(B.8)	1								
	$\rho[W]$	(B.8)	1								
	n_{tx}		8								
	n_{rx}		2								
	$\lambda_P^{micro} [Cells/km^2]$		300	300	300	600	600	600	900	900	900
Pico	G_{tx}	(B.2)	20								
	f	(B.5)	20 GHz (BW = 2000 MHz)								
	α	(B.8)	9								
	β	(B.8)	6800								
	δ	(B.8)	0.5								
	$\rho[W]$	(B.8)	1								
	n_{tx}		64								
	n_{rx}		4								
	$\lambda_P^{pico} [Cells/km^2]$		1500	1500	1500	1800	1800	1800	2100	2100	2100
Femto	G_{tx}	(B.2)	28								
	f	(B.5)	68 GHz (BW = 6800 MHz)								
	α	(B.8)	5.5								
	β	(B.8)	4800								
	δ	(B.8)	0.2								
	$\rho[W]$	(B.8)	1								
	n_{tx}		256								
	n_{rx}		8								
	$\lambda_P^{femto} [Cells/km^2]$		3000	3000	3000	6000	6000	6000	9000	9000	9000
UEs	$\lambda_P^{UE} [UE/km^2]$		1000	2000	3000	1000	2000	3000	1000	2000	3000

Table B.1: Model parameters for UEs and SBSs.

represent the deployment densities of SBSs and UEs, respectively, so that $X = \{L, M, H\}$, meaning either low, medium, or high-density deployments (λ_P^{Cell} parameter of the PPP) and $Y = \{L, M, H\}$, indicates a low, medium, or high density of deployed UEs (λ_P^{UE} parameter of the PPP), in the last row of the table. The parameters G_{tx} and f for each type of cell refer to the transmission gain and the operating frequency (including the available bandwidth) of the antenna, with n_{tx} and n_{rx} representing the number of transmit and receive antennas. Finally, the parameters of the power consumption model described previously are also included in the table. Therefore, nine different scenarios have been used in this work.

B.2 Approximations to the Pareto Front

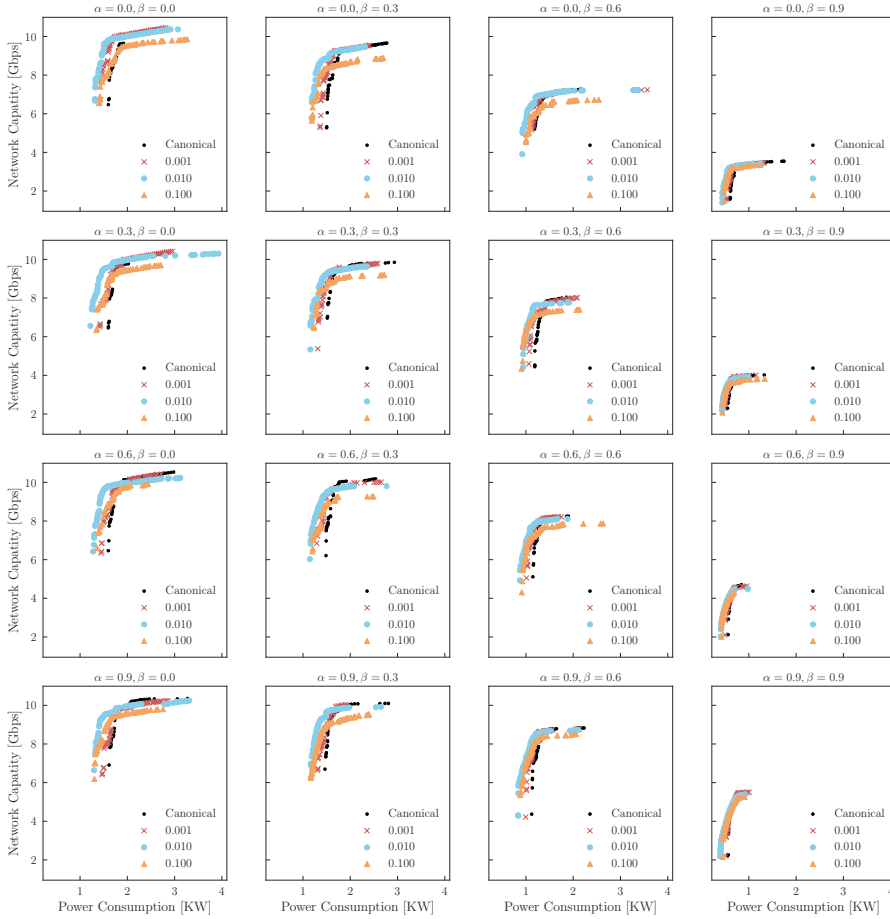


Figure B.2: Approximations to the Pareto front for the different rates of application of the landscape-aware local search operator in the LL scenario.

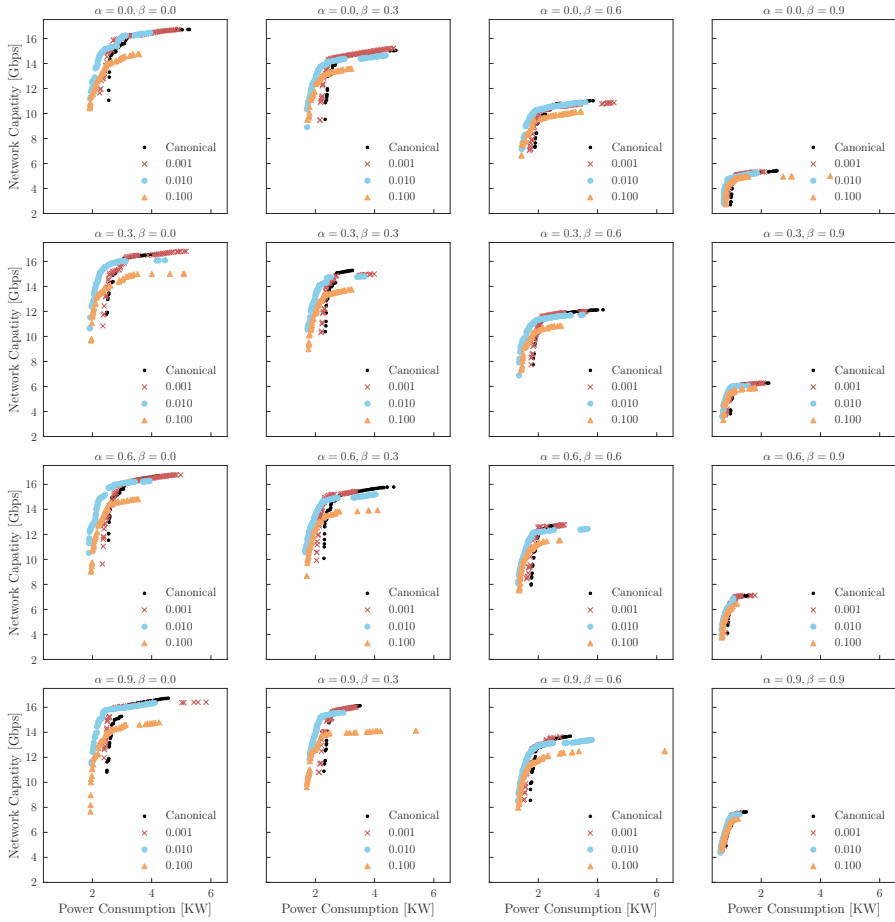


Figure B.3: Approximations to the Pareto front for the different rates of application of the landscape-aware local search operator in the LM scenario.

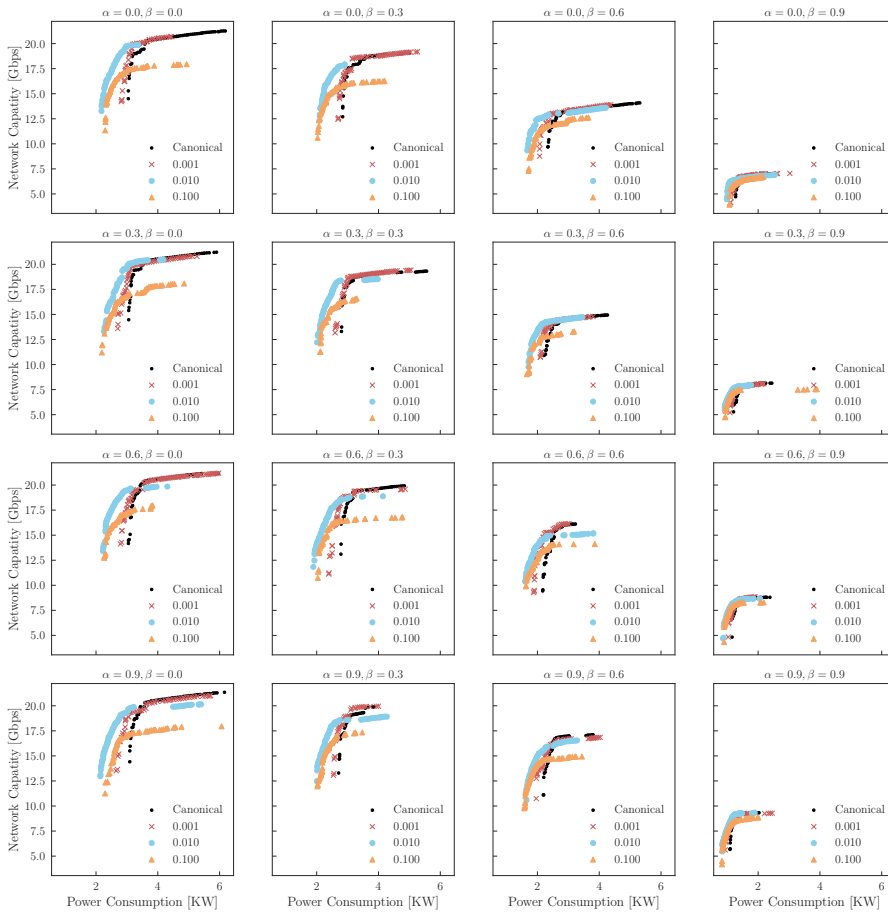


Figure B.4: Approximations to the Pareto front for the different rates of application of the landscape-aware local search operator in the LH scenario.

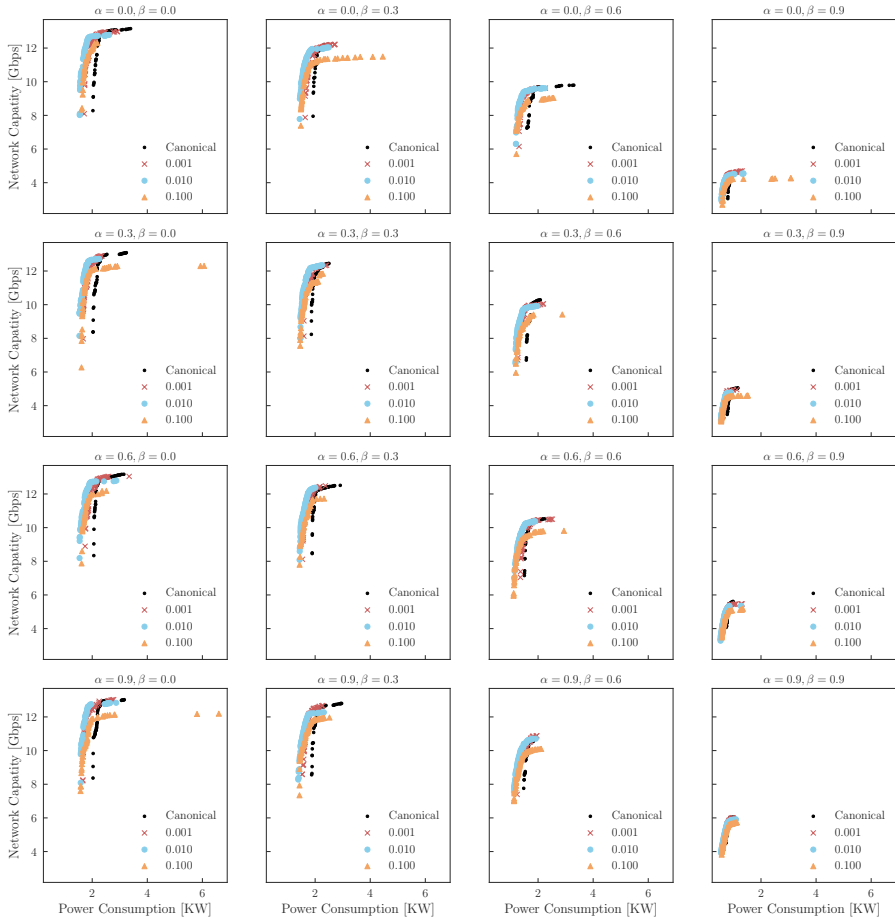


Figure B.5: Approximations to the Pareto front for the different rates of application of the landscape-aware local search operator in the ML scenario.

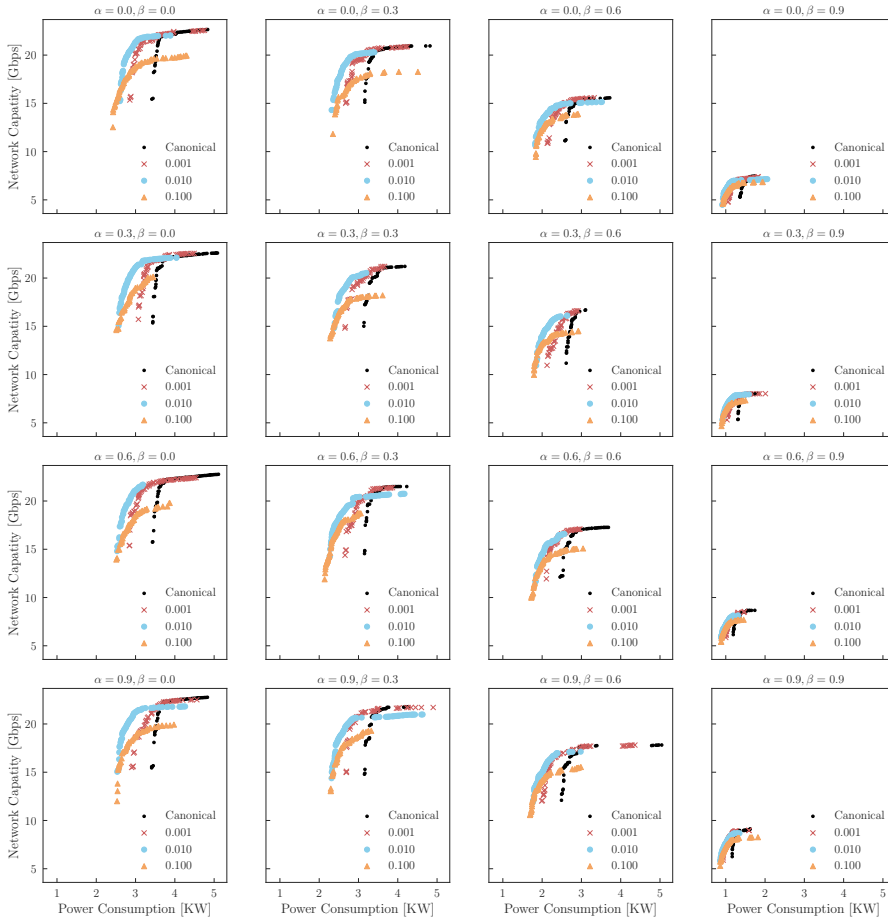


Figure B.6: Approximations to the Pareto front for the different rates of application of the landscape-aware local search operator in the MM scenario.

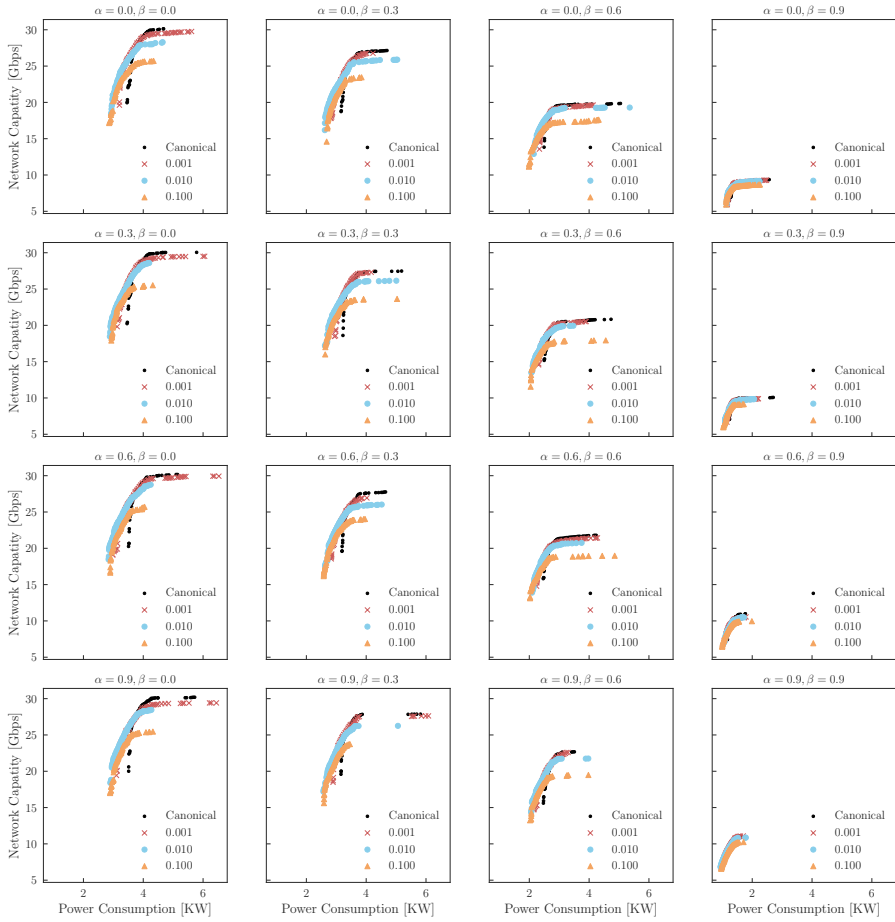


Figure B.7: Approximations to the Pareto front for the different rates of application of the landscape-aware local search operator in the MH scenario.

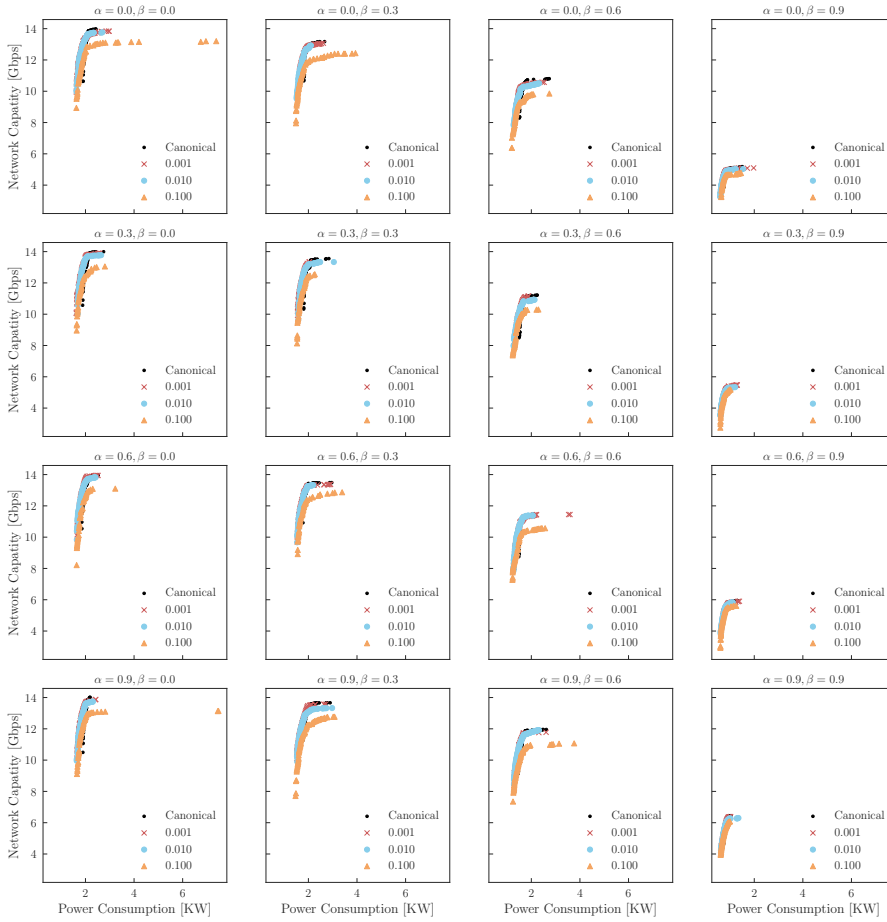


Figure B.8: Approximations to the Pareto front for the different rates of application of the landscape-aware local search operator in the HL scenario.

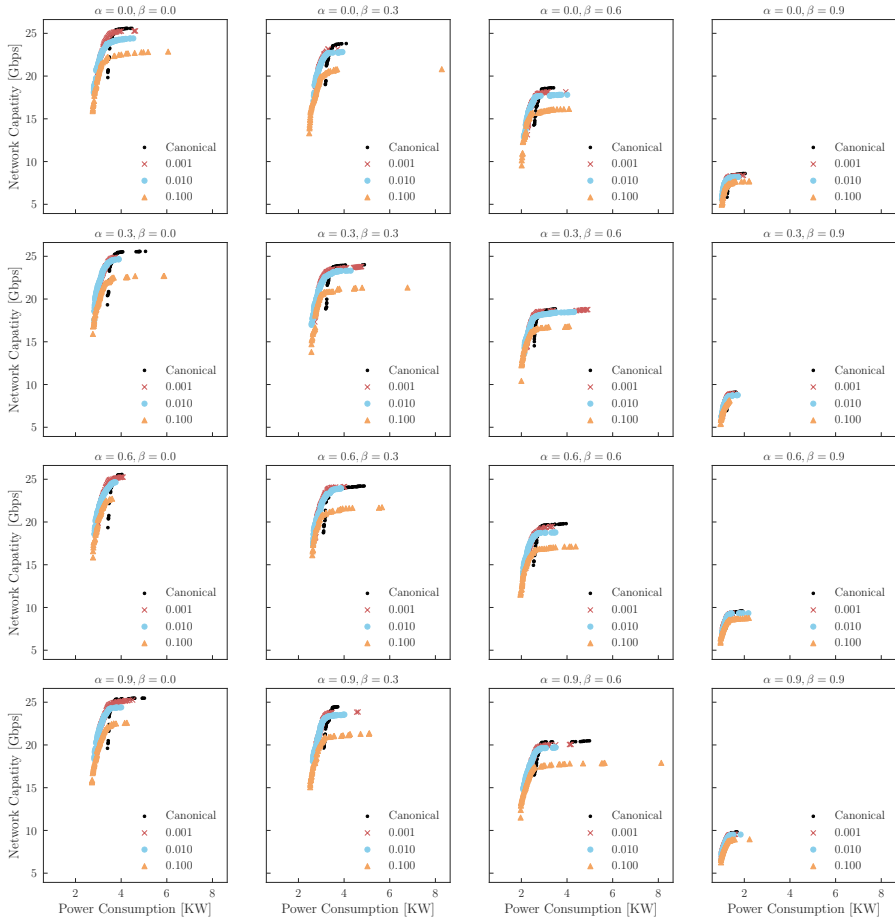


Figure B.9: Approximations to the Pareto front for the different rates of application of the landscape-aware local search operator in the HM scenario.

B.3 HV Values

α, β	Application rate			
	0.000	0.001	0.010	0.100
0.0, 0.0	0.3679	0.4240	0.4561	0.3926
0.0, 0.3	0.3585	0.4015	0.4519	0.4127
0.0, 0.6	0.3716	0.3974	0.4518	0.3979
0.0, 0.9	0.3582	0.4032	0.4349	0.4002
0.3, 0.0	0.3710	0.4102	0.4580	0.4023
0.3, 0.3	0.3525	0.4081	0.4496	0.4028
0.3, 0.6	0.3453	0.3859	0.4358	0.4119
0.3, 0.9	0.3444	0.3991	0.4303	0.4053
0.6, 0.0	0.3787	0.4081	0.4582	0.4098
0.6, 0.3	0.3546	0.4017	0.4497	0.3920
0.6, 0.6	0.3361	0.3894	0.4429	0.4064
0.6, 0.9	0.3184	0.3696	0.4141	0.3970
0.9, 0.0	0.3749	0.3990	0.4534	0.4204
0.9, 0.3	0.3518	0.3916	0.4483	0.4103
0.9, 0.6	0.3284	0.3761	0.4410	0.4034
0.9, 0.9	0.2944	0.3173	0.3997	0.3683

Table B.2: LL

α, β	Application rate			
	0.000	0.001	0.010	0.100
0.0, 0.0	0.3396	0.3813	0.4365	0.4032
0.0, 0.3	0.3348	0.3770	0.4442	0.3992
0.0, 0.6	0.3512	0.3830	0.4424	0.3933
0.0, 0.9	0.3721	0.4119	0.4405	0.4078
0.3, 0.0	0.3406	0.3754	0.4452	0.3902
0.3, 0.3	0.3430	0.3767	0.4439	0.4033
0.3, 0.6	0.3365	0.3663	0.4436	0.4027
0.3, 0.9	0.3365	0.3918	0.4433	0.4079
0.6, 0.0	0.3390	0.3827	0.4463	0.3959
0.6, 0.3	0.3237	0.3876	0.4357	0.3916
0.6, 0.6	0.3197	0.3597	0.4387	0.3934
0.6, 0.9	0.3142	0.3708	0.4304	0.3960
0.9, 0.0	0.3383	0.3816	0.4436	0.3895
0.9, 0.3	0.3306	0.3606	0.4414	0.3894
0.9, 0.6	0.3116	0.3704	0.4289	0.3936
0.9, 0.9	0.3043	0.3457	0.4220	0.3839

Table B.3: LM

α, β	Application rate			
	0.000	0.001	0.010	0.100
0.0, 0.0	0.3353	0.3721	0.4394	0.3824
0.0, 0.3	0.3209	0.3634	0.4348	0.3951
0.0, 0.6	0.3355	0.3895	0.4446	0.3940
0.0, 0.9	0.3603	0.4057	0.4371	0.3949
0.3, 0.0	0.3313	0.3815	0.4313	0.3865
0.3, 0.3	0.3288	0.3637	0.4394	0.3838
0.3, 0.6	0.3198	0.3611	0.4355	0.3915
0.3, 0.9	0.3361	0.3787	0.4393	0.4066
0.6, 0.0	0.3325	0.3689	0.4359	0.3783
0.6, 0.3	0.3173	0.3698	0.4403	0.3792
0.6, 0.6	0.3104	0.3703	0.4355	0.3882
0.6, 0.9	0.3204	0.3591	0.3281	0.3992
0.9, 0.0	0.3240	0.3712	0.4397	0.3778
0.9, 0.3	0.3235	0.3687	0.4371	0.3843
0.9, 0.6	0.3027	0.3565	0.4242	0.3957
0.9, 0.9	0.2850	0.3523	0.4063	0.3781

Table B.4: LH

α, β	Application rate			
	0.000	0.001	0.010	0.100
0.0, 0.0	0.2800	0.3959	0.4512	0.4087
0.0, 0.3	0.2654	0.3665	0.4504	0.4011
0.0, 0.6	0.2780	0.3986	0.4463	0.4108
0.0, 0.9	0.2847	0.4104	0.4353	0.3985
0.3, 0.0	0.2746	0.4062	0.4520	0.4094
0.3, 0.3	0.2795	0.3822	0.4477	0.4047
0.3, 0.6	0.2526	0.3891	0.4360	0.4000
0.3, 0.9	0.2581	0.3805	0.4222	0.3832
0.6, 0.0	0.2853	0.3826	0.4514	0.4057
0.6, 0.3	0.2557	0.3901	0.4460	0.4041
0.6, 0.6	0.2520	0.3313	0.4318	0.4008
0.6, 0.9	0.2508	0.3637	0.4192	0.3731
0.9, 0.0	0.2783	0.4098	0.4469	0.4068
0.9, 0.3	0.2438	0.3888	0.4476	0.3986
0.9, 0.6	0.2366	0.3489	0.4239	0.3877
0.9, 0.9	0.2499	0.3365	0.3998	0.3579

Table B.5: ML

α, β	Application rate			
	0.000	0.001	0.010	0.100
0.0, 0.0	0.2579	0.3715	0.4381	0.4026
0.0, 0.3	0.2568	0.3693	0.4379	0.3814
0.0, 0.6	0.2599	0.3647	0.4331	0.3953
0.0, 0.9	0.2604	0.3748	0.4309	0.3992
0.3, 0.0	0.2542	0.3438	0.4368	0.3979
0.3, 0.3	0.2430	0.3533	0.4302	0.3963
0.3, 0.6	0.2389	0.3515	0.4311	0.3934
0.3, 0.9	0.2497	0.3599	0.4265	0.4038
0.6, 0.0	0.2612	0.3735	0.4394	0.3901
0.6, 0.3	0.2259	0.3337	0.4232	0.3990
0.6, 0.6	0.2183	0.3421	0.4130	0.3940
0.6, 0.9	0.2118	0.3258	0.4138	0.3901
0.9, 0.0	0.2524	0.3558	0.4460	0.3907
0.9, 0.3	0.2346	0.3436	0.4330	0.3960
0.9, 0.6	0.2120	0.3497	0.4192	0.3984
0.9, 0.9	0.2337	0.3574	0.4116	0.3814

Table B.6: MM

α, β	Application rate			
	0.000	0.001	0.010	0.100
0.0, 0.0	0.3418	0.3897	0.4182	0.3841
0.0, 0.3	0.3390	0.3974	0.4164	0.3798
0.0, 0.6	0.3599	0.3966	0.4163	0.3987
0.0, 0.9	0.3842	0.4148	0.4206	0.4065
0.3, 0.0	0.3312	0.3851	0.4161	0.3785
0.3, 0.3	0.3274	0.3749	0.4161	0.3798
0.3, 0.6	0.3413	0.3797	0.4149	0.3890
0.3, 0.9	0.3683	0.4055	0.4105	0.4060
0.6, 0.0	0.3375	0.3976	0.4256	0.3806
0.6, 0.3	0.3235	0.3829	0.4158	0.3843
0.6, 0.6	0.3332	0.3802	0.4120	0.3876
0.6, 0.9	0.3535	0.3875	0.4016	0.3946
0.9, 0.0	0.3456	0.3976	0.4261	0.3847
0.9, 0.3	0.3250	0.3774	0.4157	0.3830
0.9, 0.6	0.3349	0.3839	0.4094	0.3852
0.9, 0.9	0.3497	0.3815	0.4073	0.3771

Table B.7: MH

α, β	Application rate				α, β	Application rate			
	0.000	0.001	0.010	0.100		0.000	0.001	0.010	0.100
0.0, 0.0	0.3231	0.4389	0.4298	0.3928	0.0, 0.0	0.2576	0.3895	0.4200	0.3876
0.0, 0.3	0.3182	0.4174	0.4218	0.3999	0.0, 0.3	0.2564	0.3901	0.4004	0.3874
0.0, 0.6	0.3095	0.4044	0.4183	0.3883	0.0, 0.6	0.2869	0.3940	0.4168	0.3917
0.0, 0.9	0.3569	0.4291	0.4268	0.3948	0.0, 0.9	0.3179	0.4075	0.4155	0.3837
0.3, 0.0	0.3292	0.4374	0.4275	0.3949	0.3, 0.0	0.2763	0.4097	0.4235	0.3926
0.3, 0.3	0.3176	0.4284	0.4151	0.4008	0.3, 0.3	0.2648	0.3998	0.4173	0.3912
0.3, 0.6	0.3149	0.4067	0.4152	0.3975	0.3, 0.6	0.2771	0.3764	0.4030	0.3926
0.3, 0.9	0.3535	0.4101	0.4187	0.3974	0.3, 0.9	0.3031	0.3969	0.4065	0.3878
0.6, 0.0	0.3368	0.4274	0.4314	0.3972	0.6, 0.0	0.2651	0.3962	0.4248	0.3971
0.6, 0.3	0.3171	0.4331	0.4283	0.3817	0.6, 0.3	0.2631	0.3849	0.4128	0.3855
0.6, 0.6	0.3081	0.4046	0.4132	0.3871	0.6, 0.6	0.2498	0.3620	0.3967	0.3852
0.6, 0.9	0.3352	0.3936	0.4934	0.3899	0.6, 0.9	0.2972	0.3840	0.3907	0.3869
0.9, 0.0	0.3251	0.4368	0.4285	0.3929	0.9, 0.0	0.2661	0.3840	0.4211	0.3901
0.9, 0.3	0.3039	0.4237	0.4188	0.3906	0.9, 0.3	0.2455	0.3847	0.3925	0.3857
0.9, 0.6	0.3120	0.4082	0.4189	0.3872	0.9, 0.6	0.2577	0.3704	0.4036	0.3832
0.9, 0.9	0.3184	0.3941	0.3996	0.3764	0.9, 0.9	0.2991	0.3858	0.3952	0.3858

Table B.8: HL

Table B.9: HM

α, β	Application rate			
	0.000	0.001	0.010	0.100
0.0, 0.0	0.2272	0.3698	0.4049	0.3687
0.0, 0.3	0.2360	0.3701	0.4033	0.3812
0.0, 0.6	0.2579	0.3584	0.4098	0.3807
0.0, 0.9	0.3117	0.3938	0.4118	0.4003
0.3, 0.0	0.2346	0.3904	0.4207	0.3798
0.3, 0.3	0.2318	0.3750	0.4101	0.3828
0.3, 0.6	0.2459	0.3511	0.4023	0.3880
0.3, 0.9	0.2775	0.3801	0.3944	0.3842
0.6, 0.0	0.2371	0.3724	0.4163	0.3879
0.6, 0.3	0.2176	0.3642	0.3955	0.3813
0.6, 0.6	0.2344	0.3512	0.3958	0.3867
0.6, 0.9	0.2742	0.3822	0.3906	0.3896
0.9, 0.0	0.2359	0.3670	0.4173	0.3869
0.9, 0.3	0.2257	0.3646	0.4029	0.3798
0.9, 0.6	0.2364	0.3572	0.4027	0.3824
0.9, 0.9	0.2786	0.3794	0.4002	0.3956

Table B.10: HH

C

SWEVO SUPPLEMENTARY MATERIAL

This supplementary material for SWEVO article (Section 3.2) includes the full data generated to test the behavior of both canonical and hybrid MOEAs in the CSO problem. The information has been divided into three sections. The first one contains the HV tables that could not be included in the main document due to space constraints. The second one shows the attainment surfaces plots that complement those shown in the main document. The last section contains the results of the statistical tests performed on the experimental results comparing MOEAs and problem-specific operators.

Contents:

C.1 HV Results

C.2 Attainment Surfaces

C.3 Results of the Statistical Tests

C.1 HV Results

The main document shows the tables with the HV obtained by the problem-specific operators in an isolated form (Tables 3 to 7). In this supplementary material, the tables with the HV results for the operator combinations in Table 10 are shown. Cells with a dark gray background indicate that this $SYN^{\downarrow\uparrow}$ has obtained the highest (best) global HV value for the algorithm (indicated in the table caption) and scenario (first column), that is, also taking into account the tables with the HV values for the operators separately. Those with a light gray background indicate that $SYN^{\downarrow\uparrow}$ is the best combination of specific operators, but the best HV value is obtained by an isolated operator (which can be seen in the tables of the main document).

Table C.1: Median and IQR of the HV indicator of the $SYN^{\downarrow\uparrow}$ combinations for NSGA-II in the nine scenarios.

	1	2	3	4	5	6	7	8	9	10	11	12	13	14
LL	0.743 _{0.093}	0.715 _{0.098}	0.715 _{0.087}	0.762 _{0.076}	0.742 _{0.103}	0.752 _{0.071}	0.750 _{0.056}	0.757 _{0.064}	0.776 _{0.074}	0.751 _{0.103}	0.753 _{0.088}	0.721 _{0.103}	0.757 _{0.099}	0.737 _{0.070}
LM	0.727 _{0.113}	0.714 _{0.109}	0.723 _{0.099}	0.740 _{0.070}	0.729 _{0.102}	0.721 _{0.080}	0.726 _{0.091}	0.721 _{0.099}	0.746 _{0.068}	0.716 _{0.074}	0.705 _{0.081}	0.704 _{0.081}	0.709 _{0.100}	0.695 _{0.083}
LH	0.700 _{0.077}	0.696 _{0.076}	0.689 _{0.070}	0.696 _{0.091}	0.711 _{0.088}	0.683 _{0.074}	0.685 _{0.093}	0.693 _{0.072}	0.712 _{0.083}	0.643 _{0.082}	0.666 _{0.099}	0.662 _{0.099}	0.656 _{0.105}	0.655 _{0.116}
ML	0.724 _{0.106}	0.672 _{0.130}	0.691 _{0.146}	0.718 _{0.101}	0.712 _{0.091}	0.736 _{0.077}	0.708 _{0.100}	0.725 _{0.085}	0.735 _{0.085}	0.719 _{0.104}	0.709 _{0.091}	0.643 _{0.111}	0.732 _{0.083}	0.717 _{0.094}
MM	0.704 _{0.058}	0.676 _{0.096}	0.694 _{0.055}	0.713 _{0.059}	0.696 _{0.075}	0.706 _{0.072}	0.703 _{0.076}	0.711 _{0.069}	0.712 _{0.068}	0.696 _{0.073}	0.695 _{0.063}	0.693 _{0.092}	0.694 _{0.091}	0.706 _{0.078}
MH	0.676 _{0.084}	0.667 _{0.094}	0.653 _{0.093}	0.677 _{0.096}	0.662 _{0.105}	0.656 _{0.106}	0.674 _{0.103}	0.667 _{0.095}	0.677 _{0.084}	0.627 _{0.143}	0.649 _{0.106}	0.668 _{0.112}	0.638 _{0.113}	0.659 _{0.135}
HL	0.701 _{0.111}	0.654 _{0.182}	0.645 _{0.128}	0.712 _{0.095}	0.693 _{0.139}	0.710 _{0.108}	0.722 _{0.092}	0.709 _{0.102}	0.717 _{0.121}	0.705 _{0.091}	0.703 _{0.105}	0.649 _{0.124}	0.713 _{0.080}	0.719 _{0.103}
HM	0.638 _{0.083}	0.627 _{0.106}	0.638 _{0.099}	0.658 _{0.071}	0.640 _{0.128}	0.663 _{0.085}	0.660 _{0.099}	0.653 _{0.107}	0.667 _{0.075}	0.646 _{0.091}	0.658 _{0.095}	0.648 _{0.083}	0.665 _{0.080}	0.663 _{0.094}
HH	0.632 _{0.087}	0.619 _{0.081}	0.614 _{0.107}	0.615 _{0.087}	0.626 _{0.092}	0.625 _{0.086}	0.630 _{0.092}	0.643 _{0.084}	0.641 _{0.101}	0.630 _{0.121}	0.630 _{0.092}	0.612 _{0.101}	0.630 _{0.115}	0.629 _{0.095}

Table C.2: Median and IQR of the HV indicator of the $SYN^{\downarrow\uparrow}$ combinations for MOCell in the nine scenarios.

	1	2	3	4	5	6	7	8	9	10	11	12	13	14
LL	0.736 _{0.039}	0.688 _{0.063}	0.691 _{0.087}	0.772 _{0.094}	0.733 _{0.086}	0.737 _{0.079}	0.729 _{0.095}	0.728 _{0.095}	0.763 _{0.082}	0.721 _{0.081}	0.731 _{0.093}	0.691 _{0.085}	0.696 _{0.086}	0.729 _{0.095}
LM	0.692 _{0.083}	0.665 _{0.078}	0.666 _{0.073}	0.722 _{0.067}	0.706 _{0.073}	0.701 _{0.088}	0.706 _{0.094}	0.715 _{0.083}	0.729 _{0.079}	0.690 _{0.087}	0.697 _{0.108}	0.668 _{0.067}	0.669 _{0.109}	0.692 _{0.107}
LH	0.659 _{0.058}	0.648 _{0.099}	0.629 _{0.081}	0.675 _{0.076}	0.664 _{0.084}	0.668 _{0.066}	0.665 _{0.069}	0.676 _{0.062}	0.682 _{0.073}	0.654 _{0.075}	0.652 _{0.083}	0.645 _{0.071}	0.632 _{0.098}	0.640 _{0.088}
ML	0.701 _{0.101}	0.652 _{0.079}	0.657 _{0.092}	0.722 _{0.082}	0.692 _{0.081}	0.711 _{0.104}	0.718 _{0.099}	0.724 _{0.091}	0.740 _{0.072}	0.696 _{0.080}	0.687 _{0.081}	0.663 _{0.080}	0.708 _{0.096}	0.709 _{0.082}
MM	0.651 _{0.078}	0.631 _{0.068}	0.617 _{0.072}	0.668 _{0.096}	0.661 _{0.074}	0.678 _{0.060}	0.679 _{0.079}	0.679 _{0.063}	0.696 _{0.090}	0.687 _{0.060}	0.650 _{0.061}	0.639 _{0.076}	0.647 _{0.093}	0.658 _{0.088}
MH	0.611 _{0.104}	0.581 _{0.075}	0.591 _{0.087}	0.624 _{0.108}	0.626 _{0.084}	0.643 _{0.115}	0.653 _{0.113}	0.644 _{0.091}	0.659 _{0.076}	0.645 _{0.117}	0.615 _{0.107}	0.601 _{0.079}	0.619 _{0.128}	0.618 _{0.101}
HL	0.688 _{0.089}	0.645 _{0.070}	0.645 _{0.073}	0.707 _{0.081}	0.685 _{0.088}	0.701 _{0.073}	0.707 _{0.086}	0.716 _{0.102}	0.711 _{0.088}	0.700 _{0.085}	0.686 _{0.078}	0.639 _{0.094}	0.701 _{0.077}	0.703 _{0.090}
HM	0.603 _{0.089}	0.572 _{0.073}	0.575 _{0.077}	0.624 _{0.089}	0.619 _{0.096}	0.631 _{0.095}	0.639 _{0.088}	0.634 _{0.099}	0.643 _{0.091}	0.632 _{0.100}	0.599 _{0.086}	0.581 _{0.069}	0.599 _{0.097}	0.610 _{0.096}
HH	0.581 _{0.069}	0.558 _{0.085}	0.565 _{0.079}	0.587 _{0.087}	0.570 _{0.067}	0.612 _{0.091}	0.606 _{0.089}	0.611 _{0.096}	0.617 _{0.072}	0.612 _{0.082}	0.563 _{0.104}	0.581 _{0.086}	0.588 _{0.099}	0.571 _{0.116}

Table C.3: Median and IQR of the HV indicator of the $SYN^{\downarrow\uparrow}$ combinations for SMS-EMOA in the nine scenarios.

	1	2	3	4	5	6	7	8	9	10	11	12	13	14
LL	0.701 _{0.129}	0.568 _{0.210}	0.575 _{0.194}	0.746 _{0.097}	0.649 _{0.124}	0.739 _{0.087}	0.740 _{0.087}	0.747 _{0.091}	0.729 _{0.119}	0.721 _{0.095}	0.721 _{0.088}	0.546 _{0.119}	0.738 _{0.075}	0.722 _{0.076}
LM	0.679 _{0.127}	0.569 _{0.166}	0.587 _{0.145}	0.663 _{0.132}	0.654 _{0.110}	0.696 _{0.103}	0.702 _{0.107}	0.699 _{0.084}	0.700 _{0.127}	0.718 _{0.089}	0.704 _{0.089}	0.593 _{0.117}	0.706 _{0.100}	0.695 _{0.086}
LH	0.675 _{0.100}	0.598 _{0.121}	0.586 _{0.127}	0.640 _{0.115}	0.647 _{0.108}	0.672 _{0.085}	0.673 _{0.073}	0.664 _{0.106}	0.675 _{0.100}	0.673 _{0.096}	0.677 _{0.082}	0.614 _{0.106}	0.660 _{0.088}	0.665 _{0.081}
ML	0.634 _{0.157}	0.473 _{0.183}	0.519 _{0.144}	0.676 _{0.161}	0.592 _{0.127}	0.672 _{0.116}	0.680 _{0.128}	0.671 _{0.117}	0.679 _{0.132}	0.675 _{0.113}	0.647 _{0.145}	0.493 _{0.211}	0.675 _{0.153}	0.672 _{0.126}
MM	0.644 _{0.090}	0.537 _{0.150}	0.535 _{0.135}	0.623 _{0.099}	0.618 _{0.125}	0.645 _{0.094}	0.661 _{0.084}	0.669 _{0.129}	0.648 _{0.103}	0.668 _{0.100}	0.673 _{0.085}	0.565 _{0.104}	0.667 _{0.087}	0.667 _{0.096}
MH	0.612 _{0.112}	0.553 _{0.097}	0.537 _{0.119}	0.598 _{0.113}	0.578 _{0.131}	0.626 _{0.140}	0.622 _{0.081}	0.629 _{0.105}	0.624 _{0.108}	0.631 _{0.122}	0.635 _{0.116}	0.547 _{0.099}	0.652 _{0.112}	0.645 _{0.105}
HL	0.579 _{0.189}	0.461 _{0.223}	0.470 _{0.183}	0.570 _{0.175}	0.543 _{0.184}	0.613 _{0.204}	0.610 _{0.121}	0.584 _{0.171}	0.602 _{0.214}	0.609 _{0.160}	0.581 _{0.148}	0.424 _{0.182}	0.618 _{0.145}	0.600 _{0.165}
HM	0.568 _{0.154}	0.502 _{0.173}	0.454 _{0.153}	0.561 _{0.122}	0.557 _{0.148}	0.566 _{0.149}	0.565 _{0.145}	0.548 _{0.125}	0.563 _{0.126}	0.588 _{0.094}	0.579 _{0.120}	0.459 _{0.143}	0.576 _{0.082}	0.579 _{0.118}
HH	0.548 _{0.104}	0.466 _{0.093}	0.483 _{0.150}	0.529 _{0.093}	0.551 _{0.121}	0.561 _{0.105}	0.531 _{0.102}	0.555 _{0.088}	0.552 _{0.079}	0.562 _{0.074}	0.572 _{0.105}	0.480 _{0.116}	0.582 _{0.090}	0.582 _{0.072}

Table C.4: Median and IQR of the HV indicator of the $SYN^{\downarrow\uparrow}$ combinations for SparseEA in the nine scenarios.

	1	2	3	4	5	6	7	8	9	10	11	12	13	14
LL	0.216 _{0.060}	0.213 _{0.052}	0.214 _{0.045}	0.233 _{0.062}	0.236 _{0.057}	0.221 _{0.073}	0.229 _{0.065}	0.226 _{0.062}	0.237 _{0.057}	0.224 _{0.047}	0.212 _{0.056}	0.221 _{0.048}	0.211 _{0.060}	0.222 _{0.079}
LM	0.219 _{0.063}	0.215 _{0.066}	0.212 _{0.056}	0.222 _{0.064}	0.236 _{0.059}	0.212 _{0.066}	0.224 _{0.054}	0.220 _{0.071}	0.239 _{0.060}	0.227 _{0.057}	0.210 _{0.052}	0.213 _{0.060}	0.222 _{0.055}	0.216 _{0.057}
LH	0.214 _{0.053}	0.210 _{0.048}	0.212 _{0.060}	0.226 _{0.072}	0.224 _{0.067}	0.218 _{0.062}	0.226 _{0.054}	0.224 _{0.053}	0.223 _{0.050}	0.210 _{0.058}	0.211 _{0.060}	0.207 _{0.045}	0.210 _{0.052}	0.211 _{0.046}
ML	0.180 _{0.055}	0.183 _{0.068}	0.185 _{0.055}	0.209 _{0.057}	0.202 _{0.071}	0.192 _{0.060}	0.189 _{0.060}	0.198 _{0.056}	0.199 _{0.063}	0.183 _{0.052}	0.172 _{0.050}	0.177 _{0.054}	0.179 _{0.048}	0.176 _{0.048}
MM	0.186 _{0.043}	0.195 _{0.049}	0.188 _{0.038}	0.206 _{0.043}	0.200 _{0.045}	0.200 _{0.052}	0.204 _{0.051}	0.201 _{0.048}	0.199 _{0.029}	0.196 _{0.043}	0.192 _{0.040}	0.187 _{0.044}	0.191 _{0.040}	0.195 _{0.053}
MH	0.183 _{0.055}	0.191 _{0.056}	0.191 _{0.048}	0.211 _{0.053}	0.207 _{0.049}	0.207 _{0.058}	0.207 _{0.065}	0.199 _{0.058}	0.207 _{0.054}	0.208 _{0.054}	0.198 _{0.047}	0.193 _{0.053}	0.191 _{0.048}	0.187 _{0.040}
HL	0.174 _{0.069}	0.183 _{0.065}	0.187 _{0.053}	0.203 _{0.069}	0.199 _{0.064}	0.202 _{0.055}	0.189 _{0.054}	0.194 _{0.056}	0.198 _{0.060}	0.208 _{0.068}	0.167 _{0.050}	0.182 _{0.063}	0.183 _{0.062}	0.170 _{0.062}
HM	0.175 _{0.051}	0.173 _{0.046}	0.173 _{0.052}	0.183 _{0.044}	0.191 _{0.045}	0.184 _{0.037}	0.187 _{0.044}	0.174 _{0.053}	0.186 _{0.044}	0.180 _{0.042}	0.176 _{0.046}	0.172 _{0.042}	0.165 _{0.058}	0.174 _{0.050}
HH	0.178 _{0.050}	0.178 _{0.044}	0.169 _{0.054}	0.196 _{0.064}	0.197 _{0.070}	0.190 _{0.042}	0.185 _{0.056}	0.186 _{0.062}	0.194 _{0.066}	0.192 _{0.044}	0.190 _{0.048}	0.176 _{0.038}	0.180 _{0.041}	0.174 _{0.041}

C.2 Attainment Surfaces

This section is divided into two parts. First, the canonical and the best hybrid versions for each algorithm in the nine scenarios are shown as complements for Figure 6. Second, the canonical, the best hybrid, and best $SYN^{\downarrow\uparrow}$ are shown as complements for Figure 7.

C.2.1 The Canonical and the Best Hybrid Versions

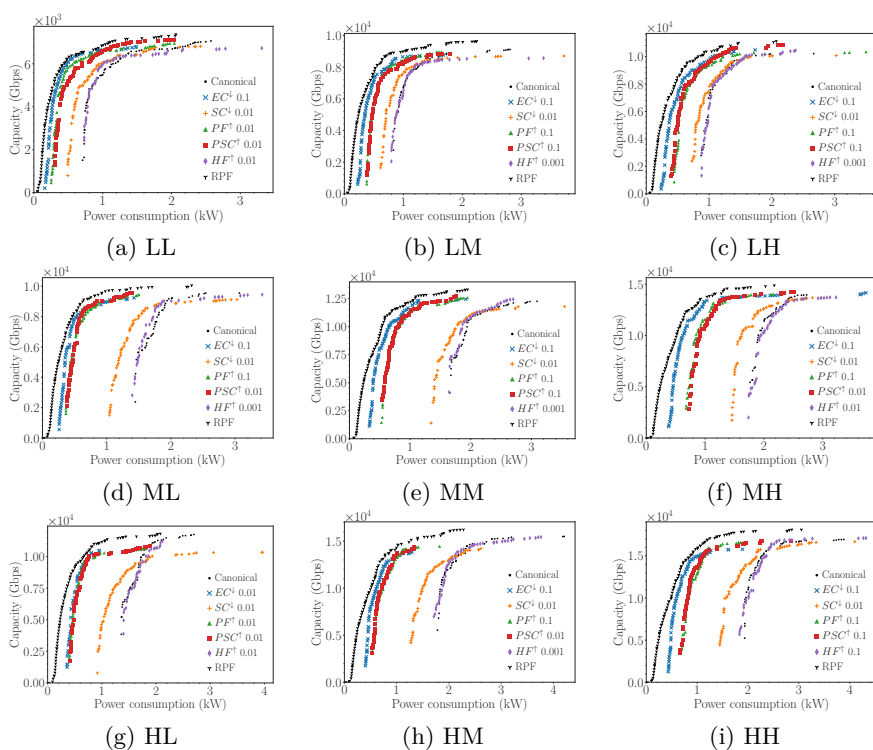


Figure C.1: Attainment functions of both the canonical and the best hybrid versions of NSGA-II for nine UDN scenarios.

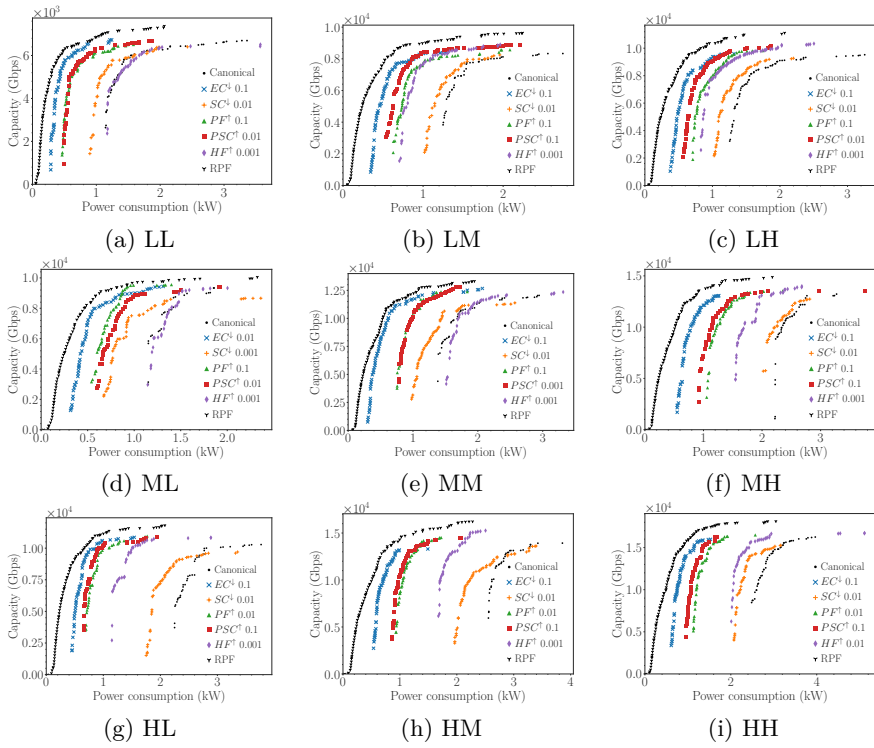


Figure C.2: Attainment functions of both the canonical and the best hybrid versions of MOCeII for nine UDN scenarios.

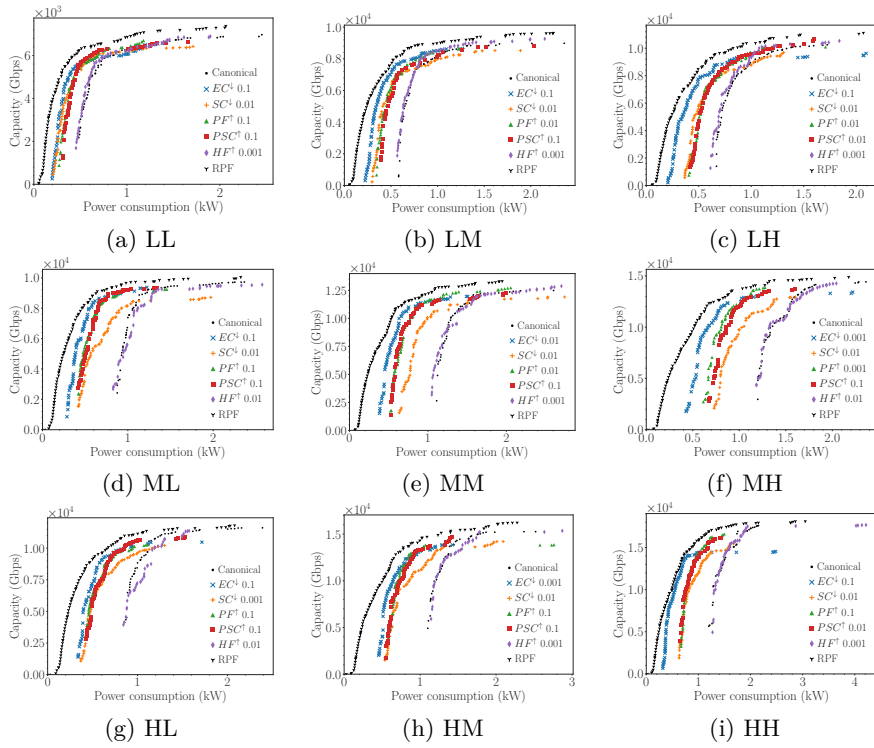


Figure C.3: Attainment functions of both the canonical and the best hybrid versions of SMS-EMOA for nine UDN scenarios.

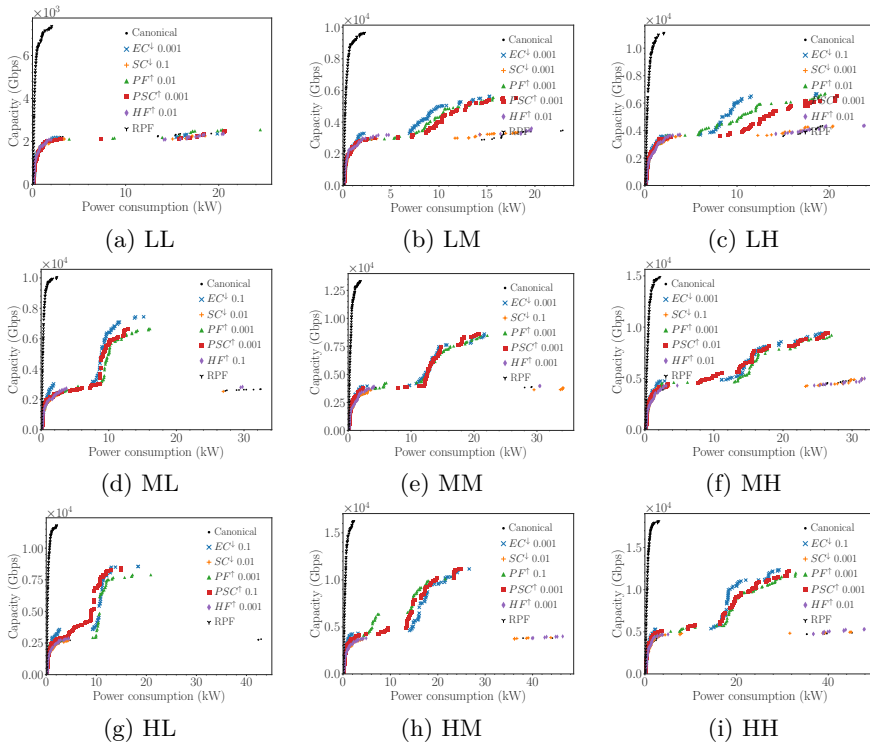


Figure C.4: Attainment functions of both the canonical and the best versions of SparseEA for nine UDN scenarios.

C.2.2 Canonical, Best Hybrid and Best $SYN^{\downarrow\uparrow}$

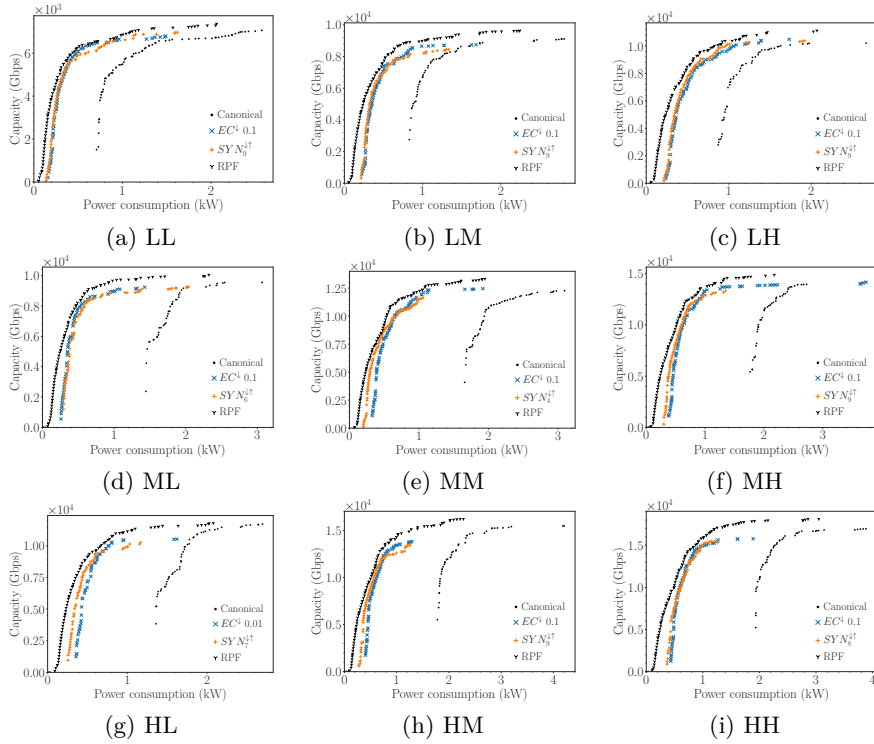


Figure C.5: Attainment functions of the canonical, the best hybrid and the best $SYN^{\downarrow\uparrow}$ of NSGA-II for nine UDN scenarios.

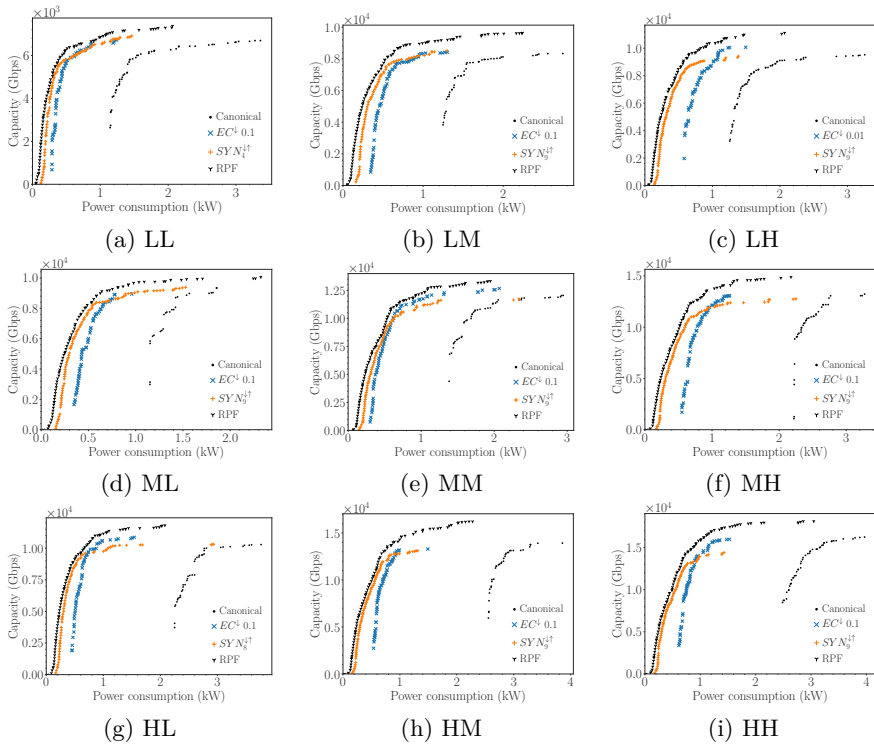


Figure C.6: Attainment functions of the canonical, the best hybrid and the best $SYN^{\downarrow\uparrow}$ of MOCcell for nine UDN scenarios.

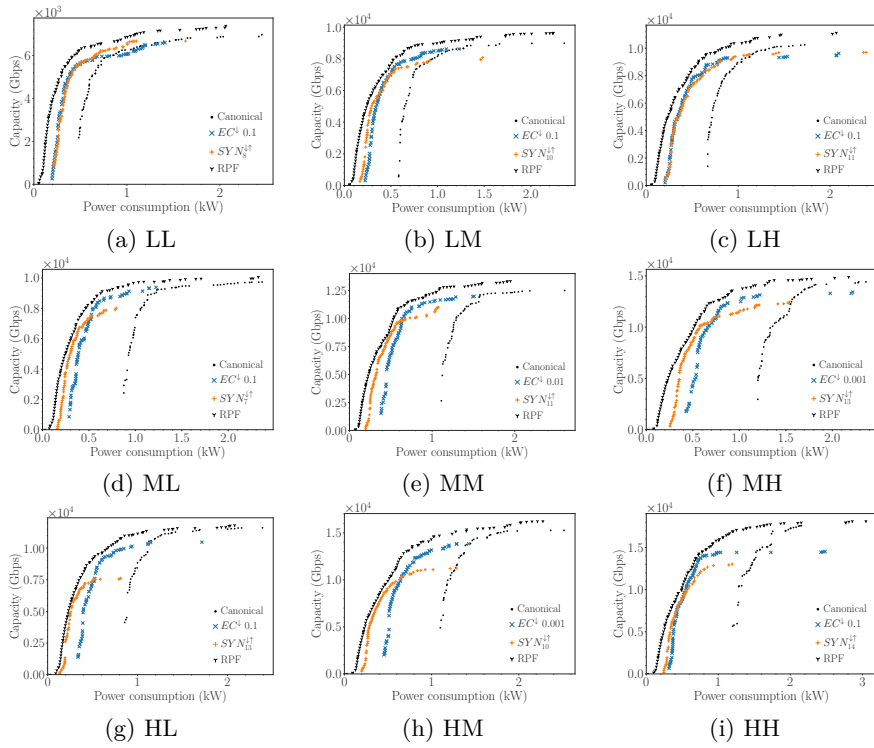


Figure C.7: Attainment functions of the canonical, the best hybrid and the best $SYN^{\downarrow\uparrow}$ of SMS-EMOA for nine UDN scenarios.

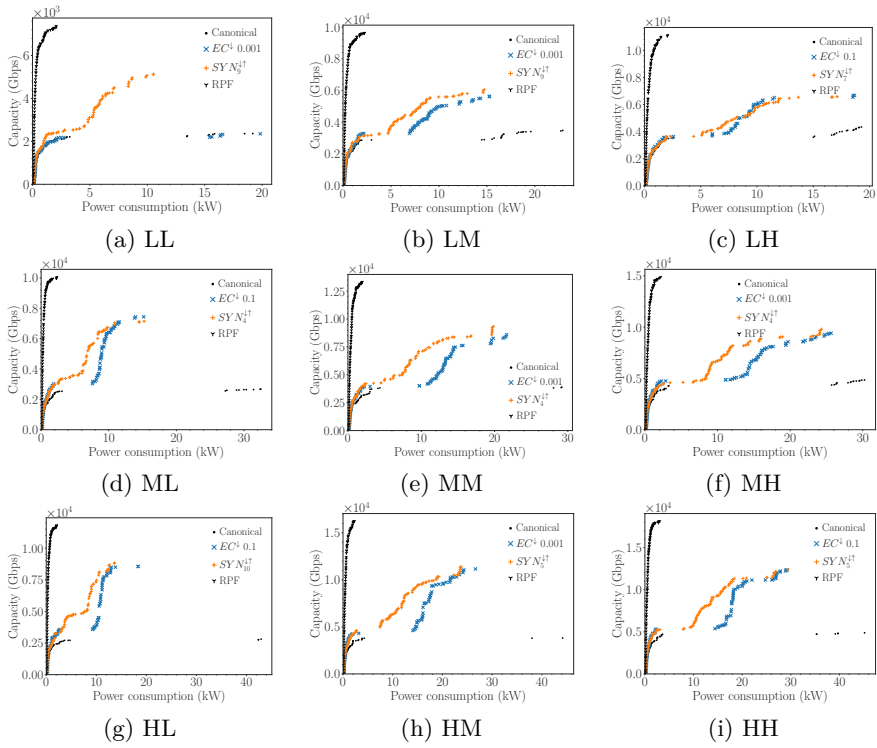


Figure C.8: Attainment functions of the canonical, the best hybrid and the best $SYN^{\downarrow\uparrow}$ of SparseEA for nine UDN scenarios.

C.3 Results of the Statistical Tests

This section contains the results obtained for three different statistical tests. The first subsection shows the results of a Kolmogorov-Smirnov test to distinguish between Gaussian and non-Gaussian distributions; for Gaussian distributions, the homoscedasticity of the samples is checked; if these two conditions hold, then a parametric ANOVA test is performed, which is the more reliable under these conditions. For non-Gaussian or Gaussian samples but without homoscedasticity, a non-parametric test is applied, Kruskal-Wallis in our case, because it allows comparing more than two samples. The second performs a Wilcoxon test. And the last, a Friedman test.

C.3.1 Pairwise Comparison

This subsection shows comparisons between the averages of the HV results for the different problem-specific operators and combinations ($SYN^{\downarrow\uparrow}$). The stats output is shown in tabular form: a black upward triangle (\blacktriangle) states that the setting of the row has statistically higher values than the configuration of the column, and a white downward triangle (\blacktriangledown) states that the configuration in the row has statistically lower values than the configuration in the column. When no statistically significant differences are found, the spot is left empty.

C.3.1.0.1

 Canonical MOEAs Comparison

First, the comparison between the averages of the four algorithms considered for each type of scenario is shown.

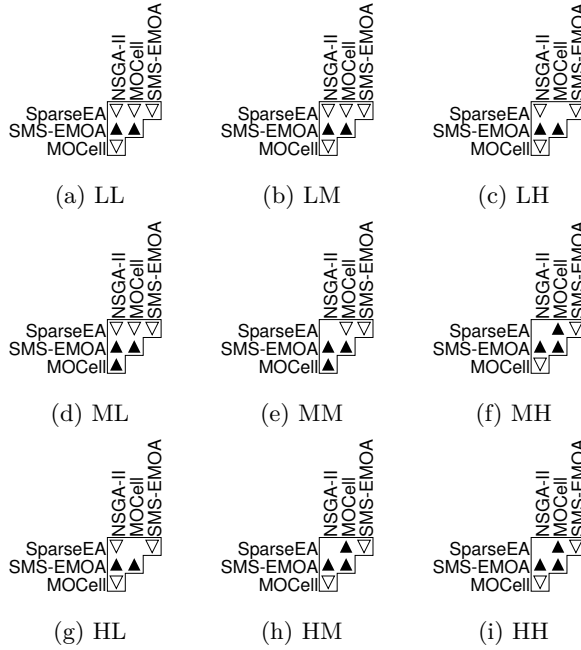


Figure C.9: Statistical analysis of the canonical MOEAs for the nine scenarios.

C.3.1.0.2 Problem-Specific Operators Comparison

Second, Figures C.10 to C.13 show the comparison between the different operator-rate configurations for each MOEA (indicated in the figure caption).

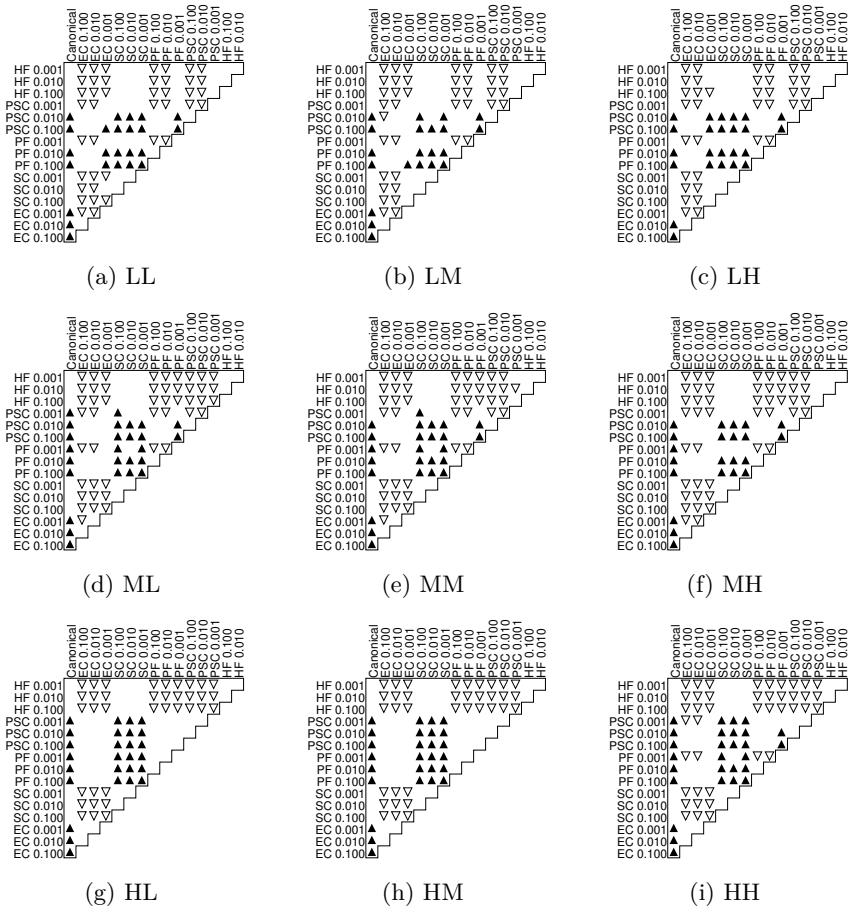


Figure C.10: Statistical analysis of NSGA-II for the nine scenarios.

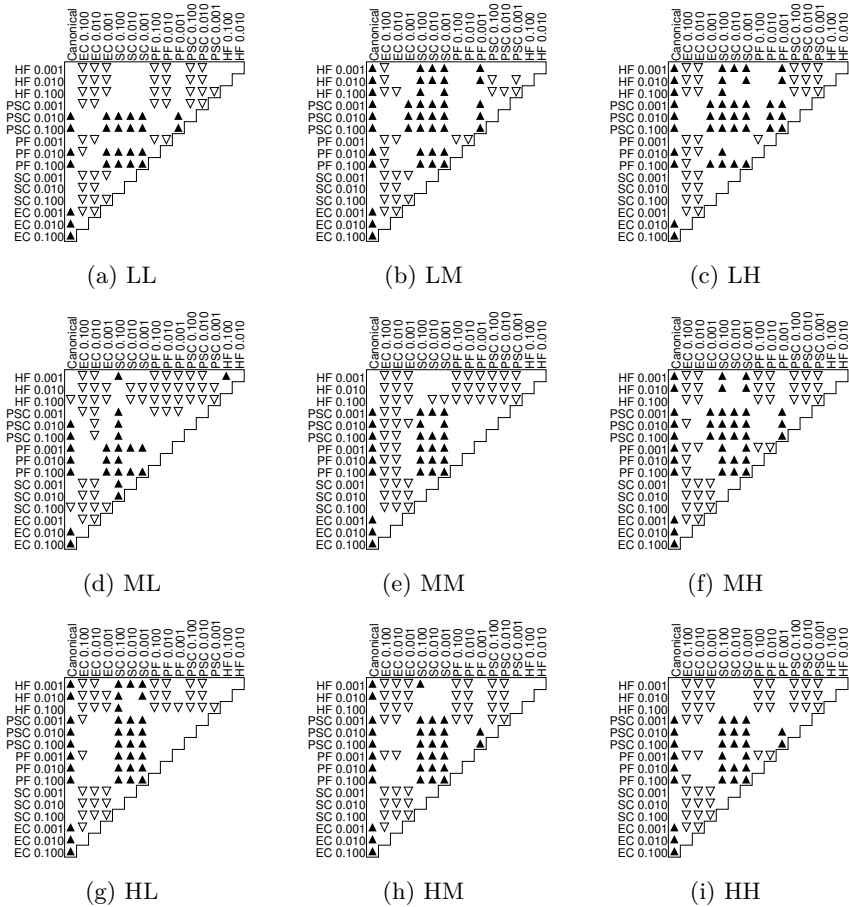


Figure C.11: Statistical analysis of MOCcell for the nine scenarios.

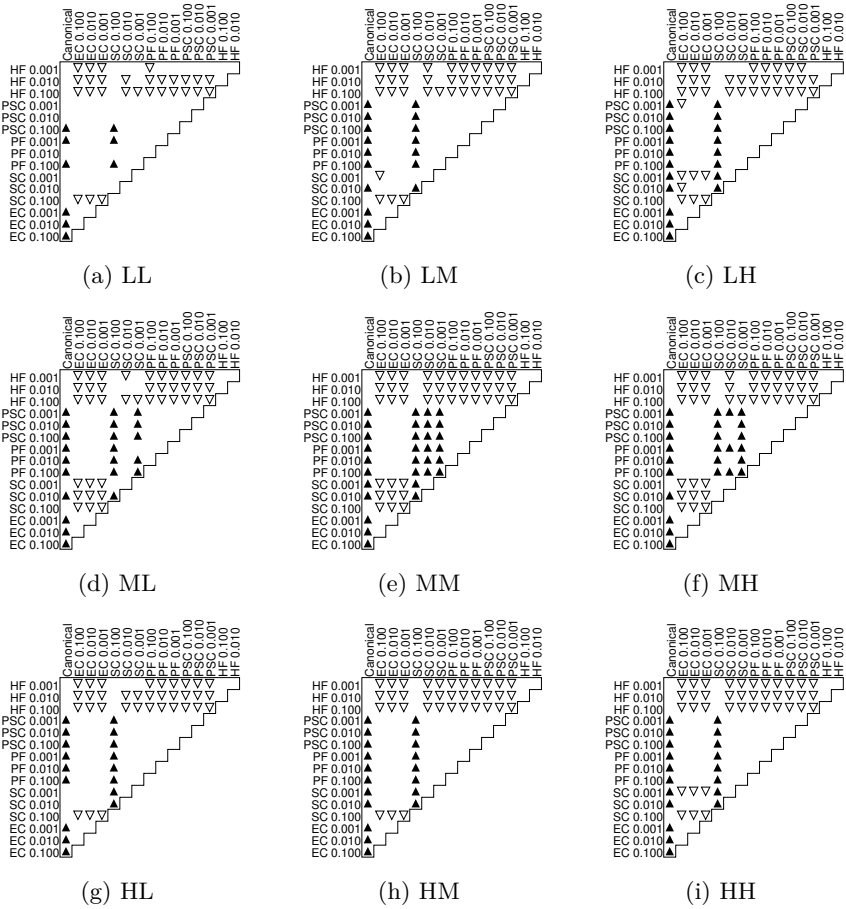


Figure C.12: Statistical analysis of SMS-EMOA for the nine scenarios.

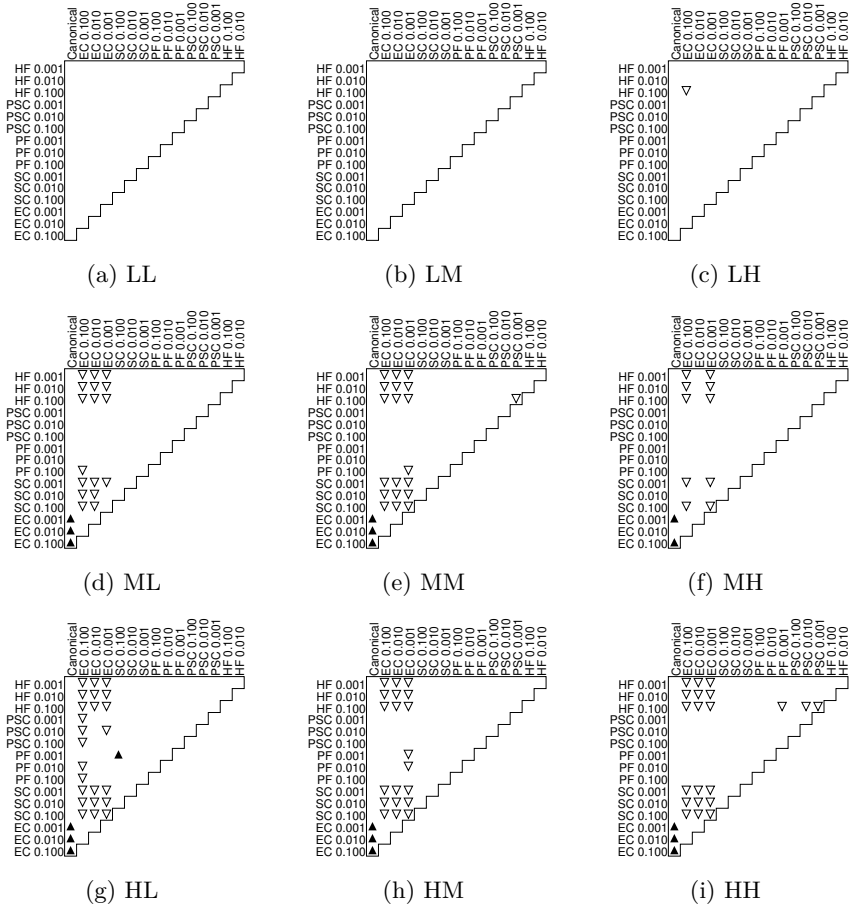


Figure C.13: Statistical analysis of SparseEA for the nine scenarios.

C.3.1.0.3 $SYN^{\downarrow\uparrow}$ Combinations Comparison

Finally, Figures C.14 to C.22 show the comparison between the canonical MOEAs, the best single-operator for the pair algorithm-scenario and the 14 $SYN^{\downarrow\uparrow}$ combinations. In this case, a figure is shown for each type of scenario, containing the results for the four MOEAs.

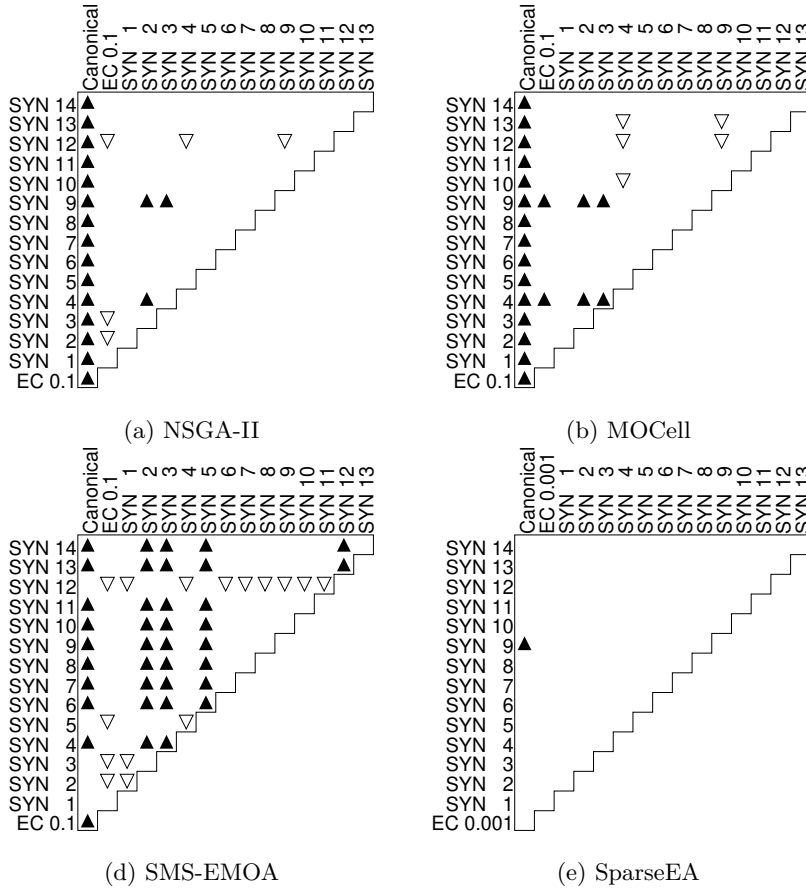


Figure C.14: Statistical analysis of the MOEAs synergies for LL.

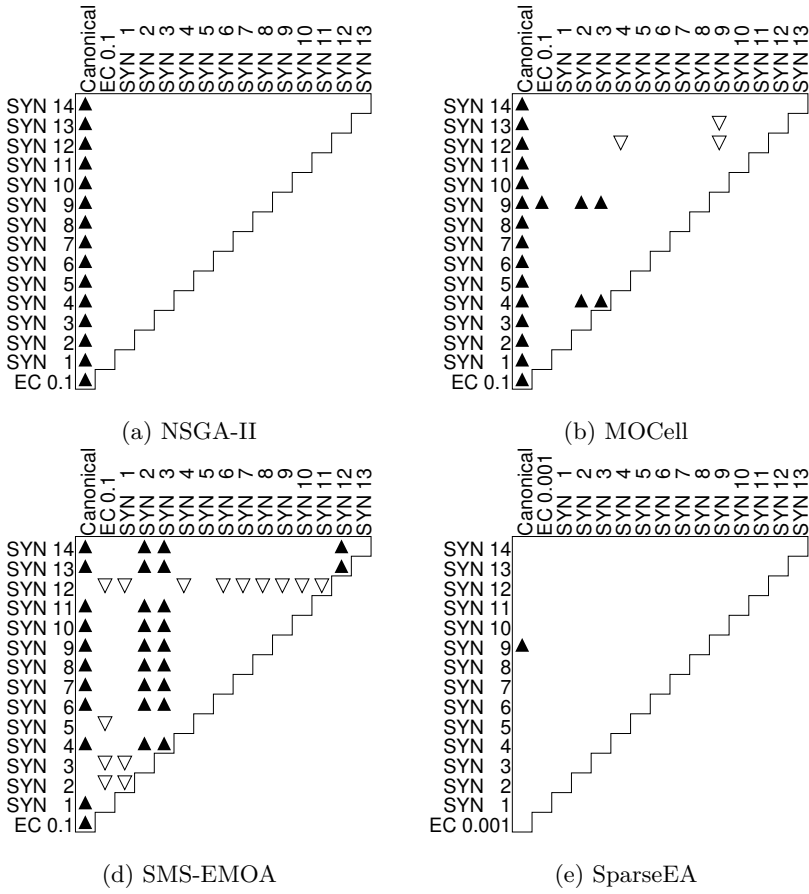


Figure C.15: Statistical analysis of the MOEAs synergies for LM.

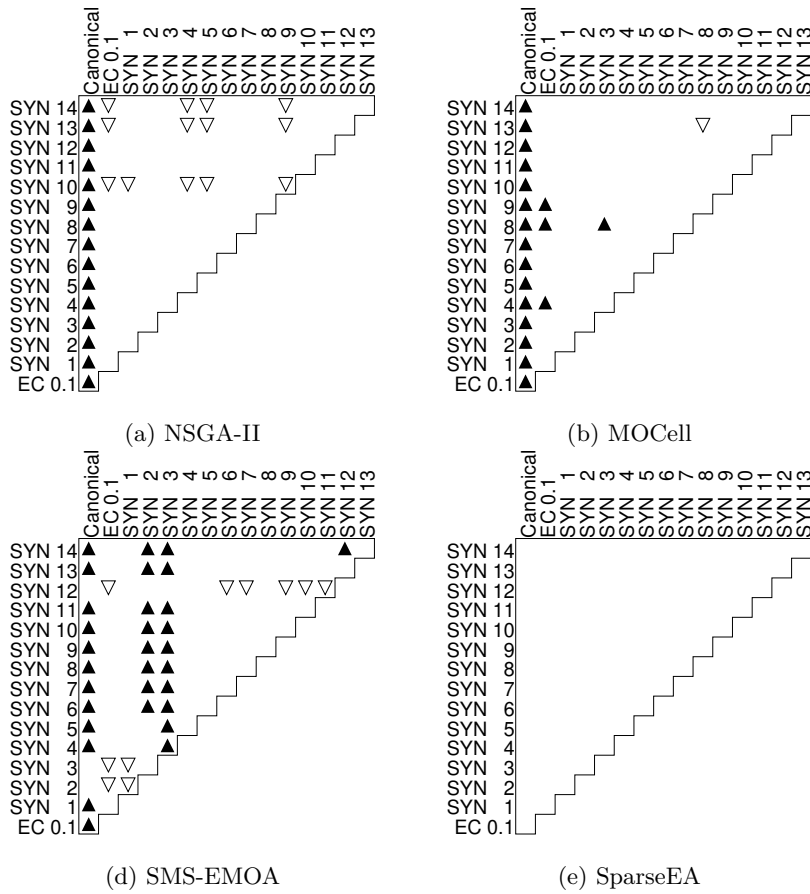


Figure C.16: Statistical analysis of the MOEAs synergies for LH.

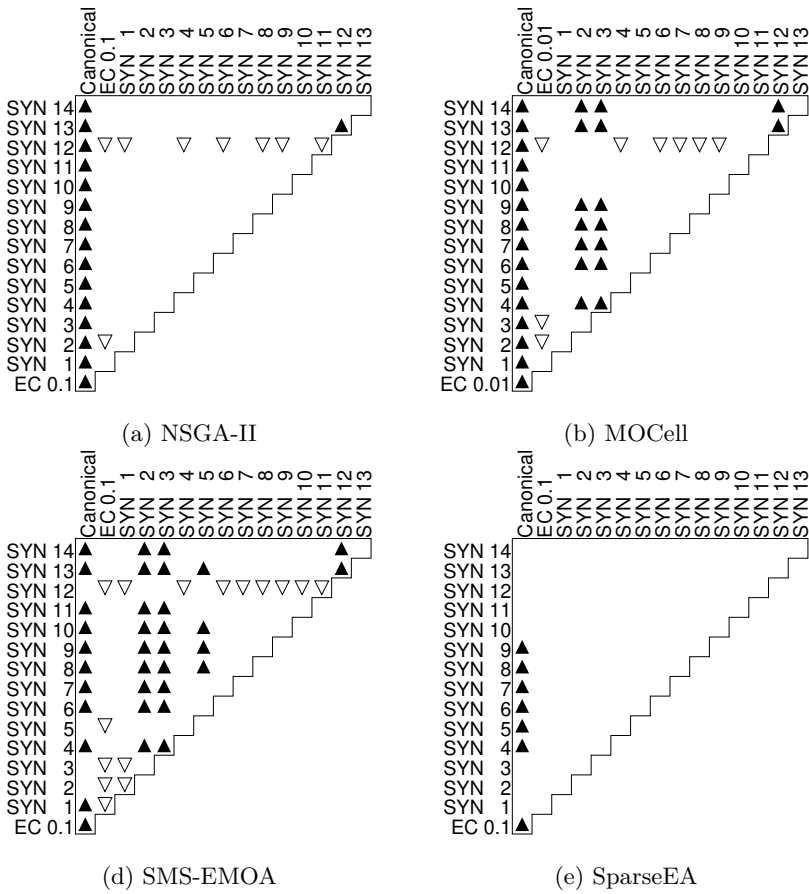


Figure C.17: Statistical analysis of the MOEAs synergies for ML.

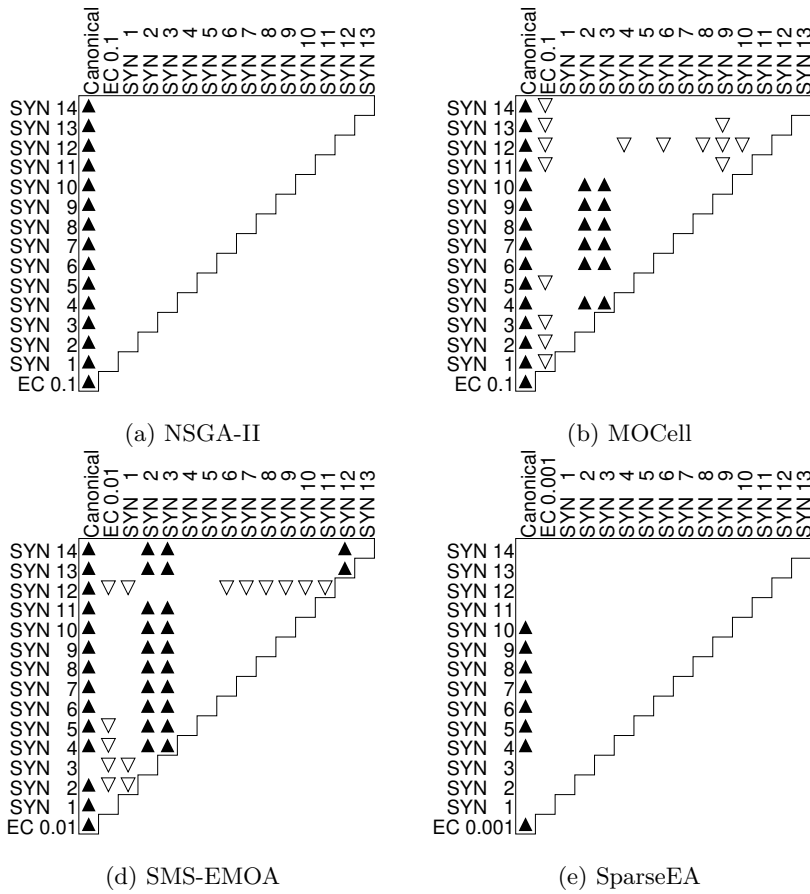


Figure C.18: Statistical analysis of the MOEAs synergies for MM.

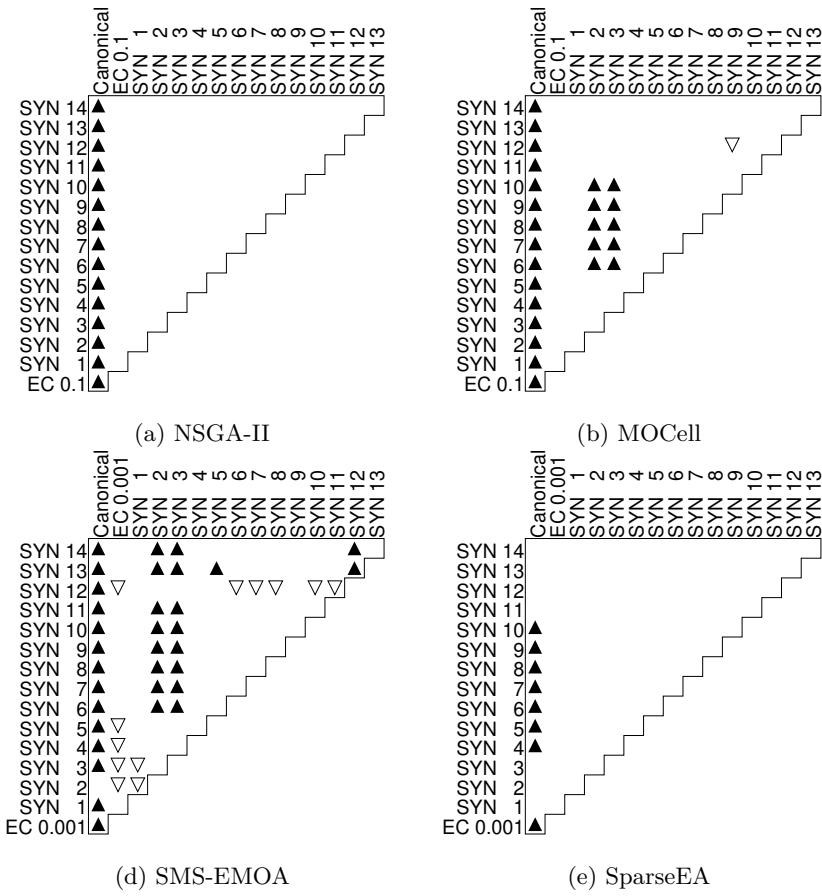


Figure C.19: Statistical analysis of the MOEAs synergies for MH.

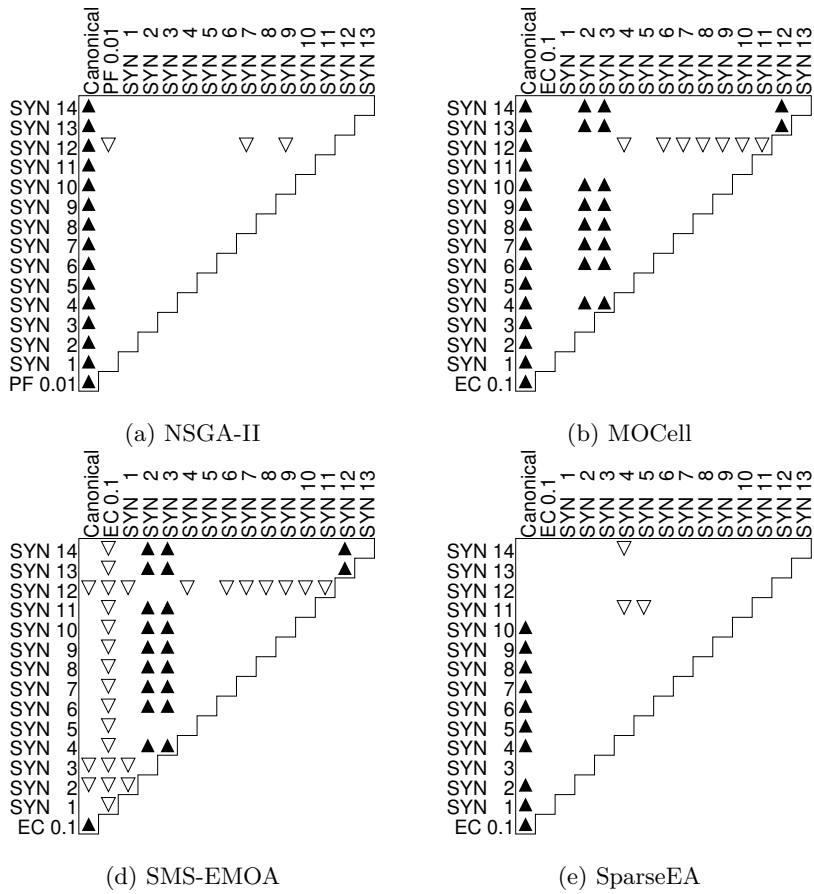


Figure C.20: Statistical analysis of the MOEAs synergies for HL.

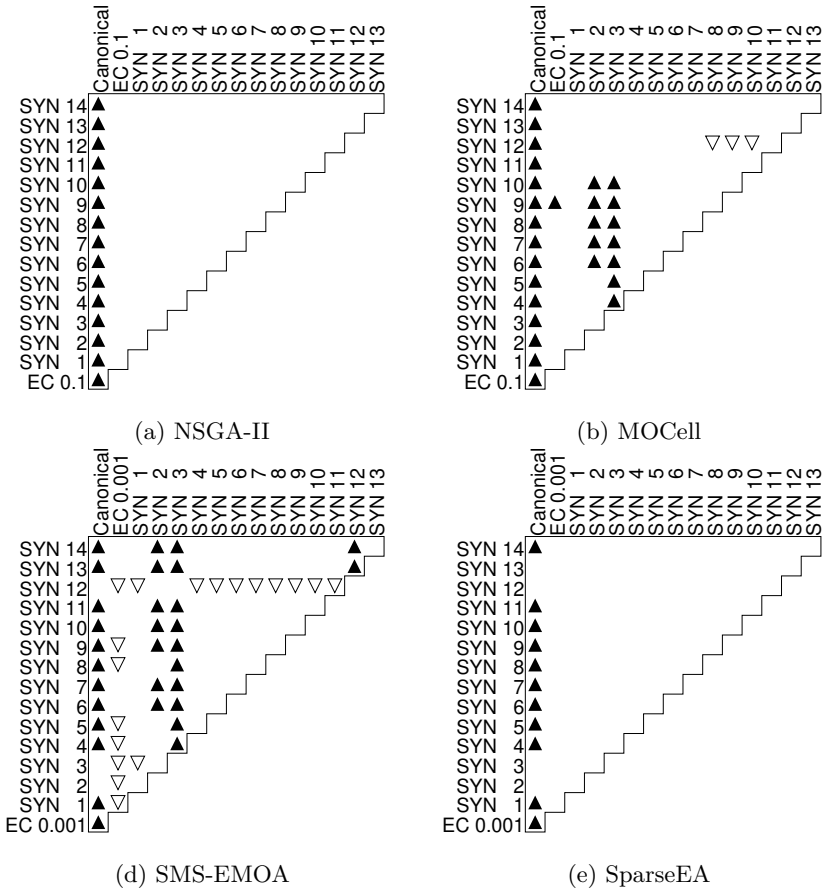


Figure C.21: Statistical analysis of the MOEAs synergies for HM.

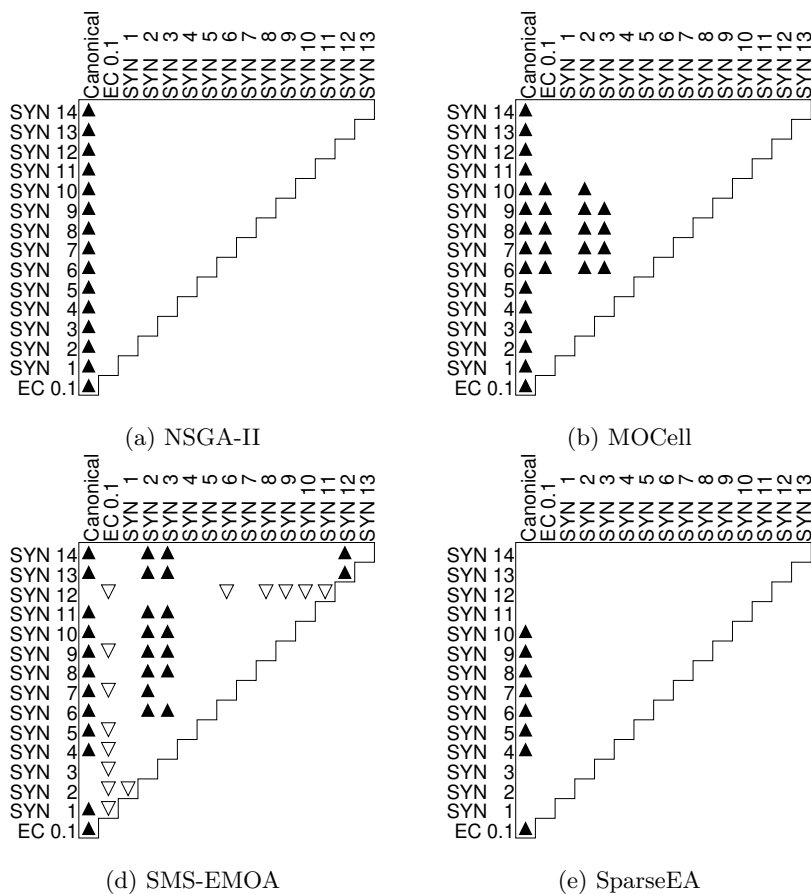


Figure C.22: Statistical analysis of the MOEAs synergies for HH.

C.3.3	Friedman Test
--------------	---------------

Algorithm	Ranking	p-value	Holm	Hypothesis
$SYN_9^{\downarrow\uparrow}$	1	0E0	0	-
$EC_{0.1}^{\downarrow}$	2	1,865E-3	0,05	Rejected
$SYN_4^{\downarrow\uparrow}$	3	4,918E-10	0,025	Rejected
$SYN_1^{\downarrow\uparrow}$	4	1,033E-20	0,017	Rejected
$SYN_{11}^{\downarrow\uparrow}$	5	1,519E-35	0,013	Rejected
$SYN_8^{\downarrow\uparrow}$	6	1,488E-54	0,01	Rejected
$PF_{0.1}^{\uparrow}$	7	9,514E-78	0,008	Rejected
$SYN_6^{\downarrow\uparrow}$	8	3,919E-105	0,007	Rejected
$SYN_{13}^{\downarrow\uparrow}$	9	1,033E-136	0,006	Rejected
$PF_{0.01}^{\uparrow}$	10	1,733E-172	0,006	Rejected
$SYN_5^{\downarrow\uparrow}$	11	1,846E-212	0,005	Rejected
$SYN_7^{\downarrow\uparrow}$	12	1,244E-256	0,005	Rejected
$EC_{0.01}^{\downarrow}$	13	0E0	0,004	Rejected
$SYN_{10}^{\downarrow\uparrow}$	14	0E0	0,004	Rejected
$SYN_{14}^{\downarrow\uparrow}$	15	0E0	0,004	Rejected
$PSC_{0.1}^{\uparrow}$	16	0E0	0,003	Rejected
$PSC_{0.01}^{\uparrow}$	17	0E0	0,003	Rejected
$SYN_3^{\downarrow\uparrow}$	18	0E0	0,003	Rejected
$SYN_2^{\downarrow\uparrow}$	19	0E0	0,003	Rejected
$SYN_{12}^{\downarrow\uparrow}$	20	0E0	0,003	Rejected
$EC_{0.001}^{\downarrow}$	21	0E0	0,003	Rejected
$SC_{0.01}^{\downarrow}$	22	0E0	0,002	Rejected
$PF_{0.001}^{\uparrow}$	23	0E0	0,002	Rejected
$PSC_{0.001}^{\uparrow}$	24	0E0	0,002	Rejected
$SC_{0.001}^{\downarrow}$	25	0E0	0,002	Rejected
$HF_{0.01}^{\uparrow}$	26	0E0	0,002	Rejected
$SC_{0.1}^{\downarrow}$	27	0E0	0,002	Rejected
$HF_{0.1}^{\uparrow}$	28	0E0	0,002	Rejected
Canonical	29	0E0	0,002	Rejected
$HF_{0.001}^{\uparrow}$	30	0E0	0,002	Rejected

Table C.77: Average ranking of NSGA-II in LL.

Algorithm	Ranking	p-value	Holm	Hypothesis
$SYN_4^{\downarrow\uparrow}$	1	0E0	0	-
$SYN_9^{\downarrow\uparrow}$	2	1,865E-3	0,05	Rejected
$SYN_5^{\downarrow\uparrow}$	3	4,918E-10	0,025	Rejected
$SYN_8^{\downarrow\uparrow}$	4	1,033E-20	0,017	Rejected
$SYN_1^{\downarrow\uparrow}$	5	1,519E-35	0,013	Rejected
$SYN_{11}^{\downarrow\uparrow}$	6	1,488E-54	0,01	Rejected
$SYN_6^{\downarrow\uparrow}$	7	9,514E-78	0,008	Rejected
$SYN_7^{\downarrow\uparrow}$	8	3,919E-105	0,007	Rejected
$SYN_{14}^{\downarrow\uparrow}$	9	1,033E-136	0,006	Rejected
$SYN_{10}^{\downarrow\uparrow}$	10	1,733E-172	0,006	Rejected
$EC_{0,1}^{\downarrow}$	11	1,846E-212	0,005	Rejected
$SYN_{13}^{\downarrow\uparrow}$	12	1,244E-256	0,005	Rejected
$SYN_3^{\downarrow\uparrow}$	13	0E0	0,004	Rejected
$SYN_{12}^{\downarrow\uparrow}$	14	0E0	0,004	Rejected
$SYN_2^{\downarrow\uparrow}$	15	0E0	0,004	Rejected
$EC_{0,01}^{\downarrow}$	16	0E0	0,003	Rejected
$PF_{0,1}^{\uparrow}$	17	0E0	0,003	Rejected
$PSC_{0,1}^{\uparrow}$	18	0E0	0,003	Rejected
$PSC_{0,01}^{\uparrow}$	19	0E0	0,003	Rejected
$PF_{0,01}^{\uparrow}$	20	0E0	0,003	Rejected
$EC_{0,001}^{\downarrow}$	21	0E0	0,003	Rejected
$PSC_{0,001}^{\uparrow}$	22	0E0	0,002	Rejected
$PF_{0,001}^{\uparrow}$	23	0E0	0,002	Rejected
$SC_{0,01}^{\downarrow}$	24	0E0	0,002	Rejected
Canonical	25	0E0	0,002	Rejected
$SC_{0,001}^{\downarrow}$	26	0E0	0,002	Rejected
$SC_{0,1}^{\downarrow}$	27	0E0	0,002	Rejected
$HF_{0,01}^{\uparrow}$	28	0E0	0,002	Rejected
$HF_{0,001}^{\uparrow}$	29	0E0	0,002	Rejected
$HF_{0,1}^{\uparrow}$	30	0E0	0,002	Rejected

Table C.78: Average ranking of MOCcell in LL.

Algorithm	Ranking	p-value	Holm	Hypothesis
$SYN_4^{\downarrow\uparrow}$	1	0E0	0	-
$SYN_{13}^{\downarrow\uparrow}$	2	1,865E-3	0,05	Rejected
$SYN_6^{\downarrow\uparrow}$	3	4,918E-10	0,025	Rejected
$SYN_8^{\downarrow\uparrow}$	4	1,033E-20	0,017	Rejected
$SYN_{14}^{\downarrow\uparrow}$	5	1,519E-35	0,013	Rejected
$SYN_7^{\downarrow\uparrow}$	6	1,488E-54	0,01	Rejected
$EC_{0.1}^{\downarrow}$	7	9,514E-78	0,008	Rejected
$SYN_9^{\downarrow\uparrow}$	8	3,919E-105	0,007	Rejected
$EC_{0.01}^{\downarrow}$	9	1,033E-136	0,006	Rejected
$SYN_{11}^{\downarrow\uparrow}$	10	1,733E-172	0,006	Rejected
$PF_{0.1}^{\uparrow}$	11	1,846E-212	0,005	Rejected
$SYN_{10}^{\downarrow\uparrow}$	12	1,244E-256	0,005	Rejected
$EC_{0.001}^{\downarrow}$	13	0E0	0,004	Rejected
$PF_{0.001}^{\uparrow}$	14	0E0	0,004	Rejected
$PSC_{0.1}^{\uparrow}$	15	0E0	0,004	Rejected
$PF_{0.01}^{\uparrow}$	16	0E0	0,003	Rejected
$SC_{0.01}^{\downarrow}$	17	0E0	0,003	Rejected
$SYN_1^{\downarrow\uparrow}$	18	0E0	0,003	Rejected
$PSC_{0.01}^{\uparrow}$	19	0E0	0,003	Rejected
$PSC_{0.001}^{\uparrow}$	20	0E0	0,003	Rejected
$SC_{0.001}^{\downarrow}$	21	0E0	0,003	Rejected
$SYN_5^{\downarrow\uparrow}$	22	0E0	0,002	Rejected
$HF_{0.001}^{\uparrow}$	23	0E0	0,002	Rejected
Canonical	24	0E0	0,002	Rejected
$SC_{0.1}^{\downarrow}$	25	0E0	0,002	Rejected
$HF_{0.01}^{\uparrow}$	26	0E0	0,002	Rejected
$HF_{0.1}^{\uparrow}$	27	0E0	0,002	Rejected
$SYN_{12}^{\downarrow\uparrow}$	28	0E0	0,002	Rejected
$SYN_3^{\downarrow\uparrow}$	29	0E0	0,002	Rejected
$SYN_2^{\downarrow\uparrow}$	30	0E0	0,002	Rejected

Table C.79: Average ranking of SMS-EMOA in LL.

Algorithm	Ranking	p-value	Holm	Hypothesis
$SYN_9^{\downarrow\uparrow}$	1	0E0	0	-
$SYN_5^{\downarrow\uparrow}$	2	1,865E-3	0,05	Rejected
$SYN_4^{\downarrow\uparrow}$	3	4,918E-10	0,025	Rejected
$SYN_8^{\downarrow\uparrow}$	4	1,033E-20	0,017	Rejected
$SYN_7^{\downarrow\uparrow}$	5	1,519E-35	0,013	Rejected
$SYN_6^{\downarrow\uparrow}$	6	1,488E-54	0,01	Rejected
$SYN_2^{\downarrow\uparrow}$	7	9,514E-78	0,008	Rejected
$SYN_{14}^{\downarrow\uparrow}$	8	3,919E-105	0,007	Rejected
$SYN_{10}^{\downarrow\uparrow}$	9	1,033E-136	0,006	Rejected
$SYN_{12}^{\downarrow\uparrow}$	10	1,733E-172	0,006	Rejected
$SYN_3^{\downarrow\uparrow}$	11	1,846E-212	0,005	Rejected
$SYN_{13}^{\downarrow\uparrow}$	12	1,244E-256	0,005	Rejected
$SYN_1^{\downarrow\uparrow}$	13	0E0	0,004	Rejected
$SYN_{11}^{\downarrow\uparrow}$	14	0E0	0,004	Rejected
$EC_{0.1}^{\downarrow}$	15	0E0	0,004	Rejected
$EC_{0.001}^{\downarrow}$	16	0E0	0,003	Rejected
$PF_{0.01}^{\uparrow}$	17	0E0	0,003	Rejected
$HF_{0.01}^{\uparrow}$	18	0E0	0,003	Rejected
$EC_{0.01}^{\downarrow}$	19	0E0	0,003	Rejected
Canonical	20	0E0	0,003	Rejected
$SC_{0.01}^{\downarrow}$	21	0E0	0,003	Rejected
$PSC_{0.001}^{\uparrow}$	22	0E0	0,002	Rejected
$SC_{0.1}^{\downarrow}$	23	0E0	0,002	Rejected
$HF_{0.001}^{\uparrow}$	24	0E0	0,002	Rejected
$PF_{0.1}^{\uparrow}$	25	0E0	0,002	Rejected
$PSC_{0.1}^{\uparrow}$	26	0E0	0,002	Rejected
$HF_{0.1}^{\uparrow}$	27	0E0	0,002	Rejected
$PSC_{0.01}^{\uparrow}$	28	0E0	0,002	Rejected
$SC_{0.001}^{\downarrow}$	29	0E0	0,002	Rejected
$PF_{0.001}^{\uparrow}$	30	0E0	0,002	Rejected

Table C.80: Average ranking of SparseEA in LL.

Algorithm	Ranking	p-value	Holm	Hypothesis
$SYN_4^{\downarrow\uparrow}$	1	0E0	0	-
$SYN_9^{\downarrow\uparrow}$	2	1,865E-3	0,05	Rejected
$EC_{0,1}^{\downarrow}$	3	4,918E-10	0,025	Rejected
$SYN_6^{\downarrow\uparrow}$	4	1,033E-20	0,017	Rejected
$SYN_1^{\downarrow\uparrow}$	5	1,519E-35	0,013	Rejected
$SYN_8^{\downarrow\uparrow}$	6	1,488E-54	0,01	Rejected
$SYN_7^{\downarrow\uparrow}$	7	9,514E-78	0,008	Rejected
$SYN_3^{\downarrow\uparrow}$	8	3,919E-105	0,007	Rejected
$SYN_5^{\downarrow\uparrow}$	9	1,033E-136	0,006	Rejected
$EC_{0,01}^{\downarrow}$	10	1,733E-172	0,006	Rejected
$SYN_2^{\downarrow\uparrow}$	11	1,846E-212	0,005	Rejected
$SYN_{11}^{\downarrow\uparrow}$	12	1,244E-256	0,005	Rejected
$SYN_{10}^{\downarrow\uparrow}$	13	0E0	0,004	Rejected
$SYN_{13}^{\downarrow\uparrow}$	14	0E0	0,004	Rejected
$SYN_{12}^{\downarrow\uparrow}$	15	0E0	0,004	Rejected
$SYN_{14}^{\downarrow\uparrow}$	16	0E0	0,003	Rejected
$PF_{0,1}^{\uparrow}$	17	0E0	0,003	Rejected
$PSC_{0,1}^{\uparrow}$	18	0E0	0,003	Rejected
$PF_{0,01}^{\uparrow}$	19	0E0	0,003	Rejected
$PSC_{0,01}^{\uparrow}$	20	0E0	0,003	Rejected
$EC_{0,001}^{\downarrow}$	21	0E0	0,003	Rejected
$SC_{0,01}^{\downarrow}$	22	0E0	0,002	Rejected
$PF_{0,001}^{\uparrow}$	23	0E0	0,002	Rejected
$PSC_{0,001}^{\uparrow}$	24	0E0	0,002	Rejected
$SC_{0,001}^{\downarrow}$	25	0E0	0,002	Rejected
$SC_{0,1}^{\downarrow}$	26	0E0	0,002	Rejected
Canonical	27	0E0	0,002	Rejected
$HF_{0,01}^{\uparrow}$	28	0E0	0,002	Rejected
$HF_{0,001}^{\uparrow}$	29	0E0	0,002	Rejected
$HF_{0,1}^{\uparrow}$	30	0E0	0,002	Rejected

Table C.81: Average ranking of NSGA-II in LM.

Algorithm	Ranking	p-value	Holm	Hypothesis
$SYN_9^{\downarrow\uparrow}$	1	0E0	0	-
$SYN_4^{\downarrow\uparrow}$	2	1,865E-3	0,05	Rejected
$SYN_8^{\downarrow\uparrow}$	3	4,918E-10	0,025	Rejected
$SYN_5^{\downarrow\uparrow}$	4	1,033E-20	0,017	Rejected
$SYN_6^{\downarrow\uparrow}$	5	1,519E-35	0,013	Rejected
$SYN_7^{\downarrow\uparrow}$	6	1,488E-54	0,01	Rejected
$SYN_1^{\downarrow\uparrow}$	7	9,514E-78	0,008	Rejected
$SYN_{10}^{\downarrow\uparrow}$	8	3,919E-105	0,007	Rejected
$SYN_{11}^{\downarrow\uparrow}$	9	1,033E-136	0,006	Rejected
$SYN_{14}^{\downarrow\uparrow}$	10	1,733E-172	0,006	Rejected
$SYN_{13}^{\downarrow\uparrow}$	11	1,846E-212	0,005	Rejected
$EC_{0,1}^{\downarrow}$	12	1,244E-256	0,005	Rejected
$SYN_{12}^{\downarrow\uparrow}$	13	0E0	0,004	Rejected
$SYN_2^{\downarrow\uparrow}$	14	0E0	0,004	Rejected
$SYN_3^{\downarrow\uparrow}$	15	0E0	0,004	Rejected
$PSC_{0,001}^{\uparrow}$	16	0E0	0,003	Rejected
$PSC_{0,1}^{\uparrow}$	17	0E0	0,003	Rejected
$EC_{0,01}^{\downarrow}$	18	0E0	0,003	Rejected
$PSC_{0,01}^{\uparrow}$	19	0E0	0,003	Rejected
$PF_{0,1}^{\uparrow}$	20	0E0	0,003	Rejected
$HF_{0,001}^{\uparrow}$	21	0E0	0,003	Rejected
$PF_{0,01}^{\uparrow}$	22	0E0	0,002	Rejected
$HF_{0,01}^{\uparrow}$	23	0E0	0,002	Rejected
$HF_{0,1}^{\uparrow}$	24	0E0	0,002	Rejected
$EC_{0,001}^{\downarrow}$	25	0E0	0,002	Rejected
$PF_{0,001}^{\uparrow}$	26	0E0	0,002	Rejected
$SC_{0,01}^{\downarrow}$	27	0E0	0,002	Rejected
$SC_{0,001}^{\downarrow}$	28	0E0	0,002	Rejected
Canonical	29	0E0	0,002	Rejected
$SC_{0,1}^{\downarrow}$	30	0E0	0,002	Rejected

Table C.82: Average ranking of MOCcell in LM.

Algorithm	Ranking	p-value	Holm	Hypothesis
$EC_{0,1}^{\downarrow}$	1	0E0	0	-
$EC_{0,01}^{\downarrow}$	2	1,865E-3	0,05	Rejected
$SYN_{10}^{\downarrow\uparrow}$	3	4,918E-10	0,025	Rejected
$SYN_{13}^{\downarrow\uparrow}$	4	1,033E-20	0,017	Rejected
$SYN_{8}^{\downarrow\uparrow}$	5	1,519E-35	0,013	Rejected
$EC_{0,001}^{\downarrow}$	6	1,488E-54	0,01	Rejected
$SYN_{9}^{\downarrow\uparrow}$	7	9,514E-78	0,008	Rejected
$SYN_{11}^{\downarrow\uparrow}$	8	3,919E-105	0,007	Rejected
$SYN_{14}^{\downarrow\uparrow}$	9	1,033E-136	0,006	Rejected
$SYN_{6}^{\downarrow\uparrow}$	10	1,733E-172	0,006	Rejected
$SYN_{7}^{\downarrow\uparrow}$	11	1,846E-212	0,005	Rejected
$PF_{0,1}^{\uparrow}$	12	1,244E-256	0,005	Rejected
$PF_{0,001}^{\uparrow}$	13	0E0	0,004	Rejected
$PF_{0,01}^{\uparrow}$	14	0E0	0,004	Rejected
$SC_{0,01}^{\downarrow}$	15	0E0	0,004	Rejected
$PSC_{0,001}^{\uparrow}$	16	0E0	0,003	Rejected
$SYN_{1}^{\downarrow\uparrow}$	17	0E0	0,003	Rejected
$PSC_{0,01}^{\uparrow}$	18	0E0	0,003	Rejected
$SYN_{4}^{\downarrow\uparrow}$	19	0E0	0,003	Rejected
$SC_{0,001}^{\downarrow}$	20	0E0	0,003	Rejected
$SYN_{5}^{\downarrow\uparrow}$	21	0E0	0,003	Rejected
$PSC_{0,1}^{\uparrow}$	22	0E0	0,002	Rejected
$HF_{0,001}^{\uparrow}$	23	0E0	0,002	Rejected
Canonical	24	0E0	0,002	Rejected
$SC_{0,1}^{\downarrow}$	25	0E0	0,002	Rejected
$SYN_{12}^{\downarrow\uparrow}$	26	0E0	0,002	Rejected
$HF_{0,01}^{\uparrow}$	27	0E0	0,002	Rejected
$SYN_{2}^{\downarrow\uparrow}$	28	0E0	0,002	Rejected
$SYN_{3}^{\downarrow\uparrow}$	29	0E0	0,002	Rejected
$HF_{0,1}^{\uparrow}$	30	0E0	0,002	Rejected

Table C.83: Average ranking of SMS-EMOA in LM.

Algorithm	Ranking	p-value	Holm	Hypothesis
$SYN_9^{\downarrow\uparrow}$	1	0E0	0	-
$SYN_5^{\downarrow\uparrow}$	2	1,865E-3	0,05	Rejected
$SYN_4^{\downarrow\uparrow}$	3	4,918E-10	0,025	Rejected
$EC_{0,001}^{\downarrow}$	4	1,033E-20	0,017	Rejected
$EC_{0,1}^{\downarrow}$	5	1,519E-35	0,013	Rejected
$EC_{0,01}^{\downarrow}$	6	1,488E-54	0,01	Rejected
$SYN_7^{\downarrow\uparrow}$	7	9,514E-78	0,008	Rejected
$SYN_8^{\downarrow\uparrow}$	8	3,919E-105	0,007	Rejected
$SYN_{10}^{\downarrow\uparrow}$	9	1,033E-136	0,006	Rejected
$SYN_6^{\downarrow\uparrow}$	10	1,733E-172	0,006	Rejected
$PSC_{0,1}^{\uparrow}$	11	1,846E-212	0,005	Rejected
$SYN_1^{\downarrow\uparrow}$	12	1,244E-256	0,005	Rejected
$SYN_{12}^{\downarrow\uparrow}$	13	0E0	0,004	Rejected
$PSC_{0,001}^{\uparrow}$	14	0E0	0,004	Rejected
$PF_{0,001}^{\uparrow}$	15	0E0	0,004	Rejected
$SYN_{11}^{\downarrow\uparrow}$	16	0E0	0,003	Rejected
$SYN_2^{\downarrow\uparrow}$	17	0E0	0,003	Rejected
$SYN_{13}^{\downarrow\uparrow}$	18	0E0	0,003	Rejected
$SYN_3^{\downarrow\uparrow}$	19	0E0	0,003	Rejected
$HF_{0,001}^{\uparrow}$	20	0E0	0,003	Rejected
$SC_{0,01}^{\downarrow}$	21	0E0	0,003	Rejected
$PSC_{0,01}^{\uparrow}$	22	0E0	0,002	Rejected
$HF_{0,01}^{\uparrow}$	23	0E0	0,002	Rejected
$SYN_{14}^{\downarrow\uparrow}$	24	0E0	0,002	Rejected
$SC_{0,001}^{\downarrow}$	25	0E0	0,002	Rejected
$HF_{0,1}^{\uparrow}$	26	0E0	0,002	Rejected
$SC_{0,1}^{\downarrow}$	27	0E0	0,002	Rejected
$PF_{0,1}^{\uparrow}$	28	0E0	0,002	Rejected
$PF_{0,01}^{\uparrow}$	29	0E0	0,002	Rejected
Canonical	30	0E0	0,002	Rejected

Table C.84: Average ranking of SparseEA in LM.

Algorithm	Ranking	p-value	Holm	Hypothesis
$SYN_5^{\downarrow\uparrow}$	1	0E0	0	-
$EC_{0,1}^{\downarrow}$	2	1,865E-3	0,05	Rejected
$SYN_9^{\downarrow\uparrow}$	3	4,918E-10	0,025	Rejected
$SYN_4^{\downarrow\uparrow}$	4	1,033E-20	0,017	Rejected
$SYN_1^{\downarrow\uparrow}$	5	1,519E-35	0,013	Rejected
$SYN_2^{\downarrow\uparrow}$	6	1,488E-54	0,01	Rejected
$SYN_8^{\downarrow\uparrow}$	7	9,514E-78	0,008	Rejected
$SYN_3^{\downarrow\uparrow}$	8	3,919E-105	0,007	Rejected
$SYN_7^{\downarrow\uparrow}$	9	1,033E-136	0,006	Rejected
$SYN_6^{\downarrow\uparrow}$	10	1,733E-172	0,006	Rejected
$SYN_{11}^{\downarrow\uparrow}$	11	1,846E-212	0,005	Rejected
$EC_{0,01}^{\downarrow}$	12	1,244E-256	0,005	Rejected
$SYN_{12}^{\downarrow\uparrow}$	13	0E0	0,004	Rejected
$SYN_{10}^{\downarrow\uparrow}$	14	0E0	0,004	Rejected
$SYN_{13}^{\downarrow\uparrow}$	15	0E0	0,004	Rejected
$SYN_{14}^{\downarrow\uparrow}$	16	0E0	0,003	Rejected
$PSC_{0,01}^{\uparrow}$	17	0E0	0,003	Rejected
$PSC_{0,1}^{\uparrow}$	18	0E0	0,003	Rejected
$PF_{0,1}^{\uparrow}$	19	0E0	0,003	Rejected
$PF_{0,01}^{\uparrow}$	20	0E0	0,003	Rejected
$EC_{0,001}^{\downarrow}$	21	0E0	0,003	Rejected
$SC_{0,01}^{\downarrow}$	22	0E0	0,002	Rejected
$PSC_{0,001}^{\uparrow}$	23	0E0	0,002	Rejected
$PF_{0,001}^{\uparrow}$	24	0E0	0,002	Rejected
$SC_{0,001}^{\downarrow}$	25	0E0	0,002	Rejected
$HF_{0,01}^{\uparrow}$	26	0E0	0,002	Rejected
Canonical	27	0E0	0,002	Rejected
$SC_{0,1}^{\downarrow}$	28	0E0	0,002	Rejected
$HF_{0,001}^{\uparrow}$	29	0E0	0,002	Rejected
$HF_{0,1}^{\uparrow}$	30	0E0	0,002	Rejected

Table C.85: Average ranking of NSGA-II in LH.

Algorithm	Ranking	p-value	Holm	Hypothesis
$SYN_8^{\downarrow\uparrow}$	1	0E0	0	-
$SYN_4^{\downarrow\uparrow}$	2	1,865E-3	0,05	Rejected
$SYN_9^{\downarrow\uparrow}$	3	4,918E-10	0,025	Rejected
$SYN_6^{\downarrow\uparrow}$	4	1,033E-20	0,017	Rejected
$SYN_5^{\downarrow\uparrow}$	5	1,519E-35	0,013	Rejected
$SYN_1^{\downarrow\uparrow}$	6	1,488E-54	0,01	Rejected
$SYN_7^{\downarrow\uparrow}$	7	9,514E-78	0,008	Rejected
$SYN_{10}^{\downarrow\uparrow}$	8	3,919E-105	0,007	Rejected
$SYN_2^{\downarrow\uparrow}$	9	1,033E-136	0,006	Rejected
$SYN_{12}^{\downarrow\uparrow}$	10	1,733E-172	0,006	Rejected
$SYN_{11}^{\downarrow\uparrow}$	11	1,846E-212	0,005	Rejected
$SYN_3^{\downarrow\uparrow}$	12	1,244E-256	0,005	Rejected
$SYN_{14}^{\downarrow\uparrow}$	13	0E0	0,004	Rejected
$SYN_{13}^{\downarrow\uparrow}$	14	0E0	0,004	Rejected
$EC_{0,1}^{\downarrow}$	15	0E0	0,004	Rejected
$PSC_{0,01}^{\uparrow}$	16	0E0	0,003	Rejected
$PSC_{0,1}^{\uparrow}$	17	0E0	0,003	Rejected
$PSC_{0,001}^{\uparrow}$	18	0E0	0,003	Rejected
$EC_{0,01}^{\downarrow}$	19	0E0	0,003	Rejected
$PF_{0,1}^{\uparrow}$	20	0E0	0,003	Rejected
$HF_{0,01}^{\uparrow}$	21	0E0	0,003	Rejected
$HF_{0,001}^{\uparrow}$	22	0E0	0,002	Rejected
$HF_{0,1}^{\uparrow}$	23	0E0	0,002	Rejected
$PF_{0,01}^{\uparrow}$	24	0E0	0,002	Rejected
$EC_{0,001}^{\downarrow}$	25	0E0	0,002	Rejected
$SC_{0,01}^{\downarrow}$	26	0E0	0,002	Rejected
$PF_{0,001}^{\uparrow}$	27	0E0	0,002	Rejected
$SC_{0,001}^{\downarrow}$	28	0E0	0,002	Rejected
$SC_{0,1}^{\downarrow}$	29	0E0	0,002	Rejected
Canonical	30	0E0	0,002	Rejected

Table C.86: Average ranking of MOCcell in LH.

Algorithm	Ranking	p-value	Holm	Hypothesis
$EC_{0,1}^{\downarrow}$	1	0E0	0	-
$EC_{0,001}^{\downarrow}$	2	1,865E-3	0,05	Rejected
$SYN_{14}^{\downarrow\uparrow}$	3	4,918E-10	0,025	Rejected
$EC_{0,01}^{\downarrow}$	4	1,033E-20	0,017	Rejected
$SYN_9^{\downarrow\uparrow}$	5	1,519E-35	0,013	Rejected
$SYN_6^{\downarrow\uparrow}$	6	1,488E-54	0,01	Rejected
$SYN_7^{\downarrow\uparrow}$	7	9,514E-78	0,008	Rejected
$SYN_{13}^{\downarrow\uparrow}$	8	3,919E-105	0,007	Rejected
$SYN_{11}^{\downarrow\uparrow}$	9	1,033E-136	0,006	Rejected
$SYN_{10}^{\downarrow\uparrow}$	10	1,733E-172	0,006	Rejected
$SYN_8^{\downarrow\uparrow}$	11	1,846E-212	0,005	Rejected
$SYN_1^{\downarrow\uparrow}$	12	1,244E-256	0,005	Rejected
$SYN_5^{\downarrow\uparrow}$	13	0E0	0,004	Rejected
$SYN_4^{\downarrow\uparrow}$	14	0E0	0,004	Rejected
$PF_{0,001}^{\uparrow}$	15	0E0	0,004	Rejected
$PF_{0,1}^{\uparrow}$	16	0E0	0,003	Rejected
$PF_{0,01}^{\uparrow}$	17	0E0	0,003	Rejected
$PSC_{0,01}^{\uparrow}$	18	0E0	0,003	Rejected
$PSC_{0,1}^{\uparrow}$	19	0E0	0,003	Rejected
$PSC_{0,001}^{\uparrow}$	20	0E0	0,003	Rejected
$SC_{0,01}^{\downarrow}$	21	0E0	0,003	Rejected
$SC_{0,001}^{\downarrow}$	22	0E0	0,002	Rejected
$SYN_{12}^{\downarrow\uparrow}$	23	0E0	0,002	Rejected
$SYN_2^{\downarrow\uparrow}$	24	0E0	0,002	Rejected
$SYN_3^{\downarrow\uparrow}$	25	0E0	0,002	Rejected
$HF_{0,001}^{\uparrow}$	26	0E0	0,002	Rejected
$SC_{0,1}^{\downarrow}$	27	0E0	0,002	Rejected
Canonical	28	0E0	0,002	Rejected
$HF_{0,01}^{\uparrow}$	29	0E0	0,002	Rejected
$HF_{0,1}^{\uparrow}$	30	0E0	0,002	Rejected

Table C.87: Average ranking of SMS-EMOA in LH.

Algorithm	Ranking	p-value	Holm	Hypothesis
$SYN_5^{\downarrow\uparrow}$	1	0E0	0	-
$EC_{0.1}^{\downarrow}$	2	1,865E-3	0,05	Rejected
$SYN_4^{\downarrow\uparrow}$	3	4,918E-10	0,025	Rejected
$SYN_9^{\downarrow\uparrow}$	4	1,033E-20	0,017	Rejected
$SYN_8^{\downarrow\uparrow}$	5	1,519E-35	0,013	Rejected
$SYN_7^{\downarrow\uparrow}$	6	1,488E-54	0,01	Rejected
$EC_{0.01}^{\downarrow}$	7	9,514E-78	0,008	Rejected
$EC_{0.001}^{\downarrow}$	8	3,919E-105	0,007	Rejected
$SYN_6^{\downarrow\uparrow}$	9	1,033E-136	0,006	Rejected
$SYN_{10}^{\downarrow\uparrow}$	10	1,733E-172	0,006	Rejected
$SYN_{12}^{\downarrow\uparrow}$	11	1,846E-212	0,005	Rejected
Canonical	12	1,244E-256	0,005	Rejected
$PF_{0.01}^{\uparrow}$	13	0E0	0,004	Rejected
$SYN_1^{\downarrow\uparrow}$	14	0E0	0,004	Rejected
$SYN_{13}^{\downarrow\uparrow}$	15	0E0	0,004	Rejected
$SYN_{11}^{\downarrow\uparrow}$	16	0E0	0,003	Rejected
$PSC_{0.01}^{\uparrow}$	17	0E0	0,003	Rejected
$SYN_3^{\downarrow\uparrow}$	18	0E0	0,003	Rejected
$SYN_{14}^{\downarrow\uparrow}$	19	0E0	0,003	Rejected
$PF_{0.001}^{\uparrow}$	20	0E0	0,003	Rejected
$PSC_{0.001}^{\uparrow}$	21	0E0	0,003	Rejected
$PSC_{0.1}^{\uparrow}$	22	0E0	0,002	Rejected
$HF_{0.001}^{\uparrow}$	23	0E0	0,002	Rejected
$SC_{0.01}^{\downarrow}$	24	0E0	0,002	Rejected
$SC_{0.001}^{\downarrow}$	25	0E0	0,002	Rejected
$SC_{0.1}^{\downarrow}$	26	0E0	0,002	Rejected
$SYN_2^{\downarrow\uparrow}$	27	0E0	0,002	Rejected
$HF_{0.01}^{\uparrow}$	28	0E0	0,002	Rejected
$PF_{0.1}^{\uparrow}$	29	0E0	0,002	Rejected
$HF_{0.1}^{\uparrow}$	30	0E0	0,002	Rejected

Table C.88: Average ranking of SparseEA in LH.

Algorithm	Ranking	p-value	Holm	Hypothesis
$EC_{0,1}^{\downarrow}$	1	0E0	0	-
$SYN_9^{\downarrow\uparrow}$	2	1,865E-3	0,05	Rejected
$SYN_4^{\downarrow\uparrow}$	3	4,918E-10	0,025	Rejected
$SYN_{13}^{\downarrow\uparrow}$	4	1,033E-20	0,017	Rejected
$SYN_6^{\downarrow\uparrow}$	5	1,519E-35	0,013	Rejected
$SYN_1^{\downarrow\uparrow}$	6	1,488E-54	0,01	Rejected
$SYN_8^{\downarrow\uparrow}$	7	9,514E-78	0,008	Rejected
$EC_{0,01}^{\downarrow}$	8	3,919E-105	0,007	Rejected
$SYN_{11}^{\downarrow\uparrow}$	9	1,033E-136	0,006	Rejected
$SYN_{10}^{\downarrow\uparrow}$	10	1,733E-172	0,006	Rejected
$SYN_5^{\downarrow\uparrow}$	11	1,846E-212	0,005	Rejected
$SYN_{14}^{\downarrow\uparrow}$	12	1,244E-256	0,005	Rejected
$PSC_{0,01}^{\uparrow}$	13	0E0	0,004	Rejected
$SYN_7^{\downarrow\uparrow}$	14	0E0	0,004	Rejected
$PF_{0,01}^{\uparrow}$	15	0E0	0,004	Rejected
$PF_{0,1}^{\uparrow}$	16	0E0	0,003	Rejected
$PSC_{0,1}^{\uparrow}$	17	0E0	0,003	Rejected
$SYN_{2}^{\downarrow\uparrow}$	18	0E0	0,003	Rejected
$SYN_3^{\downarrow\uparrow}$	19	0E0	0,003	Rejected
$SYN_{12}^{\downarrow\uparrow}$	20	0E0	0,003	Rejected
$EC_{0,001}^{\downarrow}$	21	0E0	0,003	Rejected
$PF_{0,001}^{\uparrow}$	22	0E0	0,002	Rejected
$PSC_{0,001}^{\uparrow}$	23	0E0	0,002	Rejected
$SC_{0,01}^{\downarrow}$	24	0E0	0,002	Rejected
$SC_{0,001}^{\downarrow}$	25	0E0	0,002	Rejected
$HF_{0,001}^{\uparrow}$	26	0E0	0,002	Rejected
Canonical	27	0E0	0,002	Rejected
$HF_{0,1}^{\uparrow}$	28	0E0	0,002	Rejected
$SC_{0,1}^{\downarrow}$	29	0E0	0,002	Rejected
$HF_{0,01}^{\uparrow}$	30	0E0	0,002	Rejected

Table C.89: Average ranking of NSGA-II in ML.

Algorithm	Ranking	p-value	Holm	Hypothesis
$SYN_9^{\downarrow\uparrow}$	1	0E0	0	-
$SYN_4^{\downarrow\uparrow}$	2	1,865E-3	0,05	Rejected
$SYN_8^{\downarrow\uparrow}$	3	4,918E-10	0,025	Rejected
$SYN_7^{\downarrow\uparrow}$	4	1,033E-20	0,017	Rejected
$SYN_6^{\downarrow\uparrow}$	5	1,519E-35	0,013	Rejected
$EC_{0.01}^{\downarrow}$	6	1,488E-54	0,01	Rejected
$SYN_{13}^{\downarrow\uparrow}$	7	9,514E-78	0,008	Rejected
$SYN_{14}^{\downarrow\uparrow}$	8	3,919E-105	0,007	Rejected
$SYN_{10}^{\downarrow\uparrow}$	9	1,033E-136	0,006	Rejected
$SYN_1^{\downarrow\uparrow}$	10	1,733E-172	0,006	Rejected
$SYN_{11}^{\downarrow\uparrow}$	11	1,846E-212	0,005	Rejected
$SYN_5^{\downarrow\uparrow}$	12	1,244E-256	0,005	Rejected
$EC_{0.1}^{\downarrow}$	13	0E0	0,004	Rejected
$SYN_3^{\downarrow\uparrow}$	14	0E0	0,004	Rejected
$SYN_2^{\downarrow\uparrow}$	15	0E0	0,004	Rejected
$SYN_{12}^{\downarrow\uparrow}$	16	0E0	0,003	Rejected
$PF_{0.001}^{\uparrow}$	17	0E0	0,003	Rejected
$PF_{0.1}^{\uparrow}$	18	0E0	0,003	Rejected
$PF_{0.01}^{\uparrow}$	19	0E0	0,003	Rejected
$PSC_{0.1}^{\uparrow}$	20	0E0	0,003	Rejected
$PSC_{0.01}^{\uparrow}$	21	0E0	0,003	Rejected
$SC_{0.01}^{\downarrow}$	22	0E0	0,002	Rejected
$SC_{0.001}^{\downarrow}$	23	0E0	0,002	Rejected
$PSC_{0.001}^{\uparrow}$	24	0E0	0,002	Rejected
$EC_{0.001}^{\downarrow}$	25	0E0	0,002	Rejected
Canonical	26	0E0	0,002	Rejected
$HF_{0.001}^{\uparrow}$	27	0E0	0,002	Rejected
$HF_{0.01}^{\uparrow}$	28	0E0	0,002	Rejected
$SC_{0.1}^{\downarrow}$	29	0E0	0,002	Rejected
$HF_{0.1}^{\uparrow}$	30	0E0	0,002	Rejected

Table C.90: Average ranking of MOCcell in ML.

Algorithm	Ranking	p-value	Holm	Hypothesis
$EC_{0,1}^{\downarrow}$	1	0E0	0	-
$EC_{0,001}^{\downarrow}$	2	1,865E-3	0,05	Rejected
$EC_{0,01}^{\downarrow}$	3	4,918E-10	0,025	Rejected
$SYN_9^{\downarrow\uparrow}$	4	1,033E-20	0,017	Rejected
$PF_{0,1}^{\uparrow}$	5	1,519E-35	0,013	Rejected
$SYN_{10}^{\downarrow\uparrow}$	6	1,488E-54	0,01	Rejected
$PF_{0,01}^{\uparrow}$	7	9,514E-78	0,008	Rejected
$SYN_{13}^{\downarrow\uparrow}$	8	3,919E-105	0,007	Rejected
$PSC_{0,01}^{\uparrow}$	9	1,033E-136	0,006	Rejected
$PSC_{0,1}^{\uparrow}$	10	1,733E-172	0,006	Rejected
$SYN_8^{\downarrow\uparrow}$	11	1,846E-212	0,005	Rejected
$PSC_{0,001}^{\uparrow}$	12	1,244E-256	0,005	Rejected
$SYN_7^{\downarrow\uparrow}$	13	0E0	0,004	Rejected
$SYN_4^{\downarrow\uparrow}$	14	0E0	0,004	Rejected
$SYN_{14}^{\downarrow\uparrow}$	15	0E0	0,004	Rejected
$SYN_6^{\downarrow\uparrow}$	16	0E0	0,003	Rejected
$PF_{0,001}^{\uparrow}$	17	0E0	0,003	Rejected
$SYN_{11}^{\downarrow\uparrow}$	18	0E0	0,003	Rejected
$SYN_1^{\downarrow\uparrow}$	19	0E0	0,003	Rejected
$SC_{0,01}^{\downarrow}$	20	0E0	0,003	Rejected
$SC_{0,001}^{\downarrow}$	21	0E0	0,003	Rejected
$SYN_5^{\downarrow\uparrow}$	22	0E0	0,002	Rejected
$SYN_3^{\downarrow\uparrow}$	23	0E0	0,002	Rejected
Canonical	24	0E0	0,002	Rejected
$SYN_{12}^{\downarrow\uparrow}$	25	0E0	0,002	Rejected
$HF_{0,01}^{\uparrow}$	26	0E0	0,002	Rejected
$SC_{0,1}^{\downarrow}$	27	0E0	0,002	Rejected
$HF_{0,001}^{\uparrow}$	28	0E0	0,002	Rejected
$SYN_2^{\downarrow\uparrow}$	29	0E0	0,002	Rejected
$HF_{0,1}^{\uparrow}$	30	0E0	0,002	Rejected

Table C.91: Average ranking of SMS-EMOA in ML.

Algorithm	Ranking	p-value	Holm	Hypothesis
$SYN_4^{\downarrow\uparrow}$	1	0E0	0	-
$EC_{0,1}^{\downarrow}$	2	1,865E-3	0,05	Rejected
$SYN_5^{\downarrow\uparrow}$	3	4,918E-10	0,025	Rejected
$SYN_9^{\downarrow\uparrow}$	4	1,033E-20	0,017	Rejected
$EC_{0,01}^{\downarrow}$	5	1,519E-35	0,013	Rejected
$SYN_6^{\downarrow\uparrow}$	6	1,488E-54	0,01	Rejected
$SYN_8^{\downarrow\uparrow}$	7	9,514E-78	0,008	Rejected
$EC_{0,001}^{\downarrow}$	8	3,919E-105	0,007	Rejected
$SYN_7^{\downarrow\uparrow}$	9	1,033E-136	0,006	Rejected
$SYN_{10}^{\downarrow\uparrow}$	10	1,733E-172	0,006	Rejected
$SYN_2^{\downarrow\uparrow}$	11	1,846E-212	0,005	Rejected
$SYN_1^{\downarrow\uparrow}$	12	1,244E-256	0,005	Rejected
$SYN_{12}^{\downarrow\uparrow}$	13	0E0	0,004	Rejected
$SYN_{13}^{\downarrow\uparrow}$	14	0E0	0,004	Rejected
$SYN_3^{\downarrow\uparrow}$	15	0E0	0,004	Rejected
$SYN_{14}^{\downarrow\uparrow}$	16	0E0	0,003	Rejected
$SYN_{11}^{\downarrow\uparrow}$	17	0E0	0,003	Rejected
$PSC_{0,001}^{\uparrow}$	18	0E0	0,003	Rejected
$PF_{0,001}^{\uparrow}$	19	0E0	0,003	Rejected
$PF_{0,01}^{\uparrow}$	20	0E0	0,003	Rejected
$PSC_{0,01}^{\uparrow}$	21	0E0	0,003	Rejected
$PSC_{0,1}^{\uparrow}$	22	0E0	0,002	Rejected
$PF_{0,1}^{\uparrow}$	23	0E0	0,002	Rejected
$SC_{0,1}^{\downarrow}$	24	0E0	0,002	Rejected
$HF_{0,01}^{\uparrow}$	25	0E0	0,002	Rejected
$SC_{0,01}^{\downarrow}$	26	0E0	0,002	Rejected
$SC_{0,001}^{\downarrow}$	27	0E0	0,002	Rejected
$HF_{0,1}^{\uparrow}$	28	0E0	0,002	Rejected
Canonical	29	0E0	0,002	Rejected
$HF_{0,001}^{\uparrow}$	30	0E0	0,002	Rejected

Table C.92: Average ranking of SparseEA in ML.

Algorithm	Ranking	p-value	Holm	Hypothesis
$SYN_4^{\downarrow\uparrow}$	1	0E0	0	-
$SYN_9^{\downarrow\uparrow}$	2	1,865E-3	0,05	Rejected
$EC_{0,1}^{\downarrow}$	3	4,918E-10	0,025	Rejected
$SYN_8^{\downarrow\uparrow}$	4	1,033E-20	0,017	Rejected
$SYN_3^{\downarrow\uparrow}$	5	1,519E-35	0,013	Rejected
$SYN_7^{\downarrow\uparrow}$	6	1,488E-54	0,01	Rejected
$SYN_5^{\downarrow\uparrow}$	7	9,514E-78	0,008	Rejected
$SYN_1^{\downarrow\uparrow}$	8	3,919E-105	0,007	Rejected
$SYN_{11}^{\downarrow\uparrow}$	9	1,033E-136	0,006	Rejected
$SYN_6^{\downarrow\uparrow}$	10	1,733E-172	0,006	Rejected
$SYN_{14}^{\downarrow\uparrow}$	11	1,846E-212	0,005	Rejected
$SYN_{12}^{\downarrow\uparrow}$	12	1,244E-256	0,005	Rejected
$SYN_2^{\downarrow\uparrow}$	13	0E0	0,004	Rejected
$SYN_{13}^{\downarrow\uparrow}$	14	0E0	0,004	Rejected
$SYN_{10}^{\downarrow\uparrow}$	15	0E0	0,004	Rejected
$EC_{0,01}^{\downarrow}$	16	0E0	0,003	Rejected
$PF_{0,01}^{\uparrow}$	17	0E0	0,003	Rejected
$PSC_{0,1}^{\uparrow}$	18	0E0	0,003	Rejected
$PF_{0,1}^{\uparrow}$	19	0E0	0,003	Rejected
$PSC_{0,01}^{\uparrow}$	20	0E0	0,003	Rejected
$EC_{0,001}^{\downarrow}$	21	0E0	0,003	Rejected
$PF_{0,001}^{\uparrow}$	22	0E0	0,002	Rejected
$PSC_{0,001}^{\uparrow}$	23	0E0	0,002	Rejected
$SC_{0,01}^{\downarrow}$	24	0E0	0,002	Rejected
$SC_{0,001}^{\downarrow}$	25	0E0	0,002	Rejected
Canonical	26	0E0	0,002	Rejected
$HF_{0,001}^{\uparrow}$	27	0E0	0,002	Rejected
$HF_{0,1}^{\uparrow}$	28	0E0	0,002	Rejected
$HF_{0,01}^{\uparrow}$	29	0E0	0,002	Rejected
$SC_{0,1}^{\downarrow}$	30	0E0	0,002	Rejected

Table C.93: Average ranking of NSGA-II in MM.

Algorithm	Ranking	p-value	Holm	Hypothesis
$EC_{0,1}^{\downarrow}$	1	0E0	0	-
$SYN_9^{\downarrow\uparrow}$	2	1,865E-3	0,05	Rejected
$SYN_8^{\downarrow\uparrow}$	3	4,918E-10	0,025	Rejected
$SYN_4^{\downarrow\uparrow}$	4	1,033E-20	0,017	Rejected
$SYN_{10}^{\downarrow\uparrow}$	5	1,519E-35	0,013	Rejected
$EC_{0,01}^{\downarrow}$	6	1,488E-54	0,01	Rejected
$SYN_6^{\downarrow\uparrow}$	7	9,514E-78	0,008	Rejected
$SYN_7^{\downarrow\uparrow}$	8	3,919E-105	0,007	Rejected
$SYN_5^{\downarrow\uparrow}$	9	1,033E-136	0,006	Rejected
$SYN_1^{\downarrow\uparrow}$	10	1,733E-172	0,006	Rejected
$SYN_{14}^{\downarrow\uparrow}$	11	1,846E-212	0,005	Rejected
$EC_{0,001}^{\downarrow}$	12	1,244E-256	0,005	Rejected
$SYN_{13}^{\downarrow\uparrow}$	13	0E0	0,004	Rejected
$SYN_{11}^{\downarrow\uparrow}$	14	0E0	0,004	Rejected
$SYN_{12}^{\downarrow\uparrow}$	15	0E0	0,004	Rejected
$SYN_{12}^{\downarrow\uparrow}$	16	0E0	0,003	Rejected
$SYN_2^{\downarrow\uparrow}$	17	0E0	0,003	Rejected
$PF_{0,1}^{\uparrow}$	18	0E0	0,003	Rejected
$PSC_{0,001}^{\uparrow}$	19	0E0	0,003	Rejected
$PF_{0,001}^{\uparrow}$	20	0E0	0,003	Rejected
$PSC_{0,1}^{\uparrow}$	21	0E0	0,003	Rejected
$PF_{0,01}^{\uparrow}$	22	0E0	0,002	Rejected
$PSC_{0,01}^{\uparrow}$	23	0E0	0,002	Rejected
$SC_{0,01}^{\downarrow}$	24	0E0	0,002	Rejected
$SC_{0,001}^{\downarrow}$	25	0E0	0,002	Rejected
Canonical	26	0E0	0,002	Rejected
$SC_{0,1}^{\downarrow}$	27	0E0	0,002	Rejected
$HF_{0,01}^{\uparrow}$	28	0E0	0,002	Rejected
$HF_{0,001}^{\uparrow}$	29	0E0	0,002	Rejected
$HF_{0,1}^{\uparrow}$	30	0E0	0,002	Rejected

Table C.94: Average ranking of MOCcell in MM.

Algorithm	Ranking	p-value	Holm	Hypothesis
$EC_{0,1}^{\downarrow}$	1	0E0	0	-
$EC_{0,01}^{\downarrow}$	2	1,865E-3	0,05	Rejected
$SYN_{14}^{\downarrow\uparrow}$	3	4,918E-10	0,025	Rejected
$SYN_{13}^{\downarrow\uparrow}$	4	1,033E-20	0,017	Rejected
$SYN_{11}^{\downarrow\uparrow}$	5	1,519E-35	0,013	Rejected
$EC_{0,001}^{\downarrow}$	6	1,488E-54	0,01	Rejected
$PSC_{0,1}^{\uparrow}$	7	9,514E-78	0,008	Rejected
$PF_{0,01}^{\uparrow}$	8	3,919E-105	0,007	Rejected
$SYN_{7}^{\downarrow\uparrow}$	9	1,033E-136	0,006	Rejected
$SYN_{8}^{\downarrow\uparrow}$	10	1,733E-172	0,006	Rejected
$SYN_{6}^{\downarrow\uparrow}$	11	1,846E-212	0,005	Rejected
$PSC_{0,01}^{\uparrow}$	12	1,244E-256	0,005	Rejected
$SYN_{10}^{\downarrow\uparrow}$	13	0E0	0,004	Rejected
$PF_{0,1}^{\uparrow}$	14	0E0	0,004	Rejected
$SYN_{9}^{\downarrow\uparrow}$	15	0E0	0,004	Rejected
$PSC_{0,001}^{\uparrow}$	16	0E0	0,003	Rejected
$SYN_{1}^{\downarrow\uparrow}$	17	0E0	0,003	Rejected
$PF_{0,001}^{\uparrow}$	18	0E0	0,003	Rejected
$SYN_{4}^{\downarrow\uparrow}$	19	0E0	0,003	Rejected
$SYN_{5}^{\downarrow\uparrow}$	20	0E0	0,003	Rejected
$SYN_{12}^{\downarrow\uparrow}$	21	0E0	0,003	Rejected
$SC_{0,001}^{\downarrow}$	22	0E0	0,002	Rejected
$SC_{0,01}^{\downarrow}$	23	0E0	0,002	Rejected
$SYN_{3}^{\downarrow\uparrow}$	24	0E0	0,002	Rejected
$SYN_{2}^{\downarrow\uparrow}$	25	0E0	0,002	Rejected
$HF_{0,001}^{\uparrow}$	26	0E0	0,002	Rejected
$SC_{0,1}^{\downarrow}$	27	0E0	0,002	Rejected
Canonical	28	0E0	0,002	Rejected
$HF_{0,01}^{\uparrow}$	29	0E0	0,002	Rejected
$HF_{0,1}^{\uparrow}$	30	0E0	0,002	Rejected

Table C.95: Average ranking of SMS-EMOA in MM.

Algorithm	Ranking	p-value	Holm	Hypothesis
$SYN_4^{\downarrow\uparrow}$	1	0E0	0	-
$EC_{0,001}^{\downarrow}$	2	1,865E-3	0,05	Rejected
$SYN_5^{\downarrow\uparrow}$	3	4,918E-10	0,025	Rejected
$SYN_9^{\downarrow\uparrow}$	4	1,033E-20	0,017	Rejected
$SYN_7^{\downarrow\uparrow}$	5	1,519E-35	0,013	Rejected
$EC_{0,01}^{\downarrow}$	6	1,488E-54	0,01	Rejected
$EC_{0,1}^{\downarrow}$	7	9,514E-78	0,008	Rejected
$SYN_6^{\downarrow\uparrow}$	8	3,919E-105	0,007	Rejected
$SYN_8^{\downarrow\uparrow}$	9	1,033E-136	0,006	Rejected
$SYN_{10}^{\downarrow\uparrow}$	10	1,733E-172	0,006	Rejected
$SYN_2^{\downarrow\uparrow}$	11	1,846E-212	0,005	Rejected
$SYN_{11}^{\downarrow\uparrow}$	12	1,244E-256	0,005	Rejected
$SYN_{12}^{\downarrow\uparrow}$	13	0E0	0,004	Rejected
$SYN_{13}^{\downarrow\uparrow}$	14	0E0	0,004	Rejected
$PSC_{0,001}^{\uparrow}$	15	0E0	0,004	Rejected
$SYN_3^{\downarrow\uparrow}$	16	0E0	0,003	Rejected
$SYN_{14}^{\downarrow\uparrow}$	17	0E0	0,003	Rejected
$PSC_{0,01}^{\uparrow}$	18	0E0	0,003	Rejected
$SYN_1^{\downarrow\uparrow}$	19	0E0	0,003	Rejected
$PF_{0,001}^{\uparrow}$	20	0E0	0,003	Rejected
$PSC_{0,1}^{\uparrow}$	21	0E0	0,003	Rejected
$PF_{0,01}^{\uparrow}$	22	0E0	0,002	Rejected
$PF_{0,1}^{\uparrow}$	23	0E0	0,002	Rejected
$SC_{0,01}^{\downarrow}$	24	0E0	0,002	Rejected
$HF_{0,001}^{\uparrow}$	25	0E0	0,002	Rejected
$SC_{0,1}^{\downarrow}$	26	0E0	0,002	Rejected
Canonical	27	0E0	0,002	Rejected
$SC_{0,001}^{\downarrow}$	28	0E0	0,002	Rejected
$HF_{0,01}^{\uparrow}$	29	0E0	0,002	Rejected
$HF_{0,1}^{\uparrow}$	30	0E0	0,002	Rejected

Table C.96: Average ranking of SparseEA in MM.

Algorithm	Ranking	p-value	Holm	Hypothesis
$SYN_9^{\downarrow\uparrow}$	1	0E0	0	-
$SYN_4^{\downarrow\uparrow}$	2	1,865E-3	0,05	Rejected
$SYN_1^{\downarrow\uparrow}$	3	4,918E-10	0,025	Rejected
$SYN_5^{\downarrow\uparrow}$	4	1,033E-20	0,017	Rejected
$EC_{0,1}^{\downarrow}$	5	1,519E-35	0,013	Rejected
$SYN_7^{\downarrow\uparrow}$	6	1,488E-54	0,01	Rejected
$SYN_6^{\downarrow\uparrow}$	7	9,514E-78	0,008	Rejected
$SYN_8^{\downarrow\uparrow}$	8	3,919E-105	0,007	Rejected
$SYN_{12}^{\downarrow\uparrow}$	9	1,033E-136	0,006	Rejected
$SYN_2^{\downarrow\uparrow}$	10	1,733E-172	0,006	Rejected
$SYN_3^{\downarrow\uparrow}$	11	1,846E-212	0,005	Rejected
$SYN_{11}^{\downarrow\uparrow}$	12	1,244E-256	0,005	Rejected
$SYN_{14}^{\downarrow\uparrow}$	13	0E0	0,004	Rejected
$SYN_{13}^{\downarrow\uparrow}$	14	0E0	0,004	Rejected
$EC_{0,01}^{\downarrow}$	15	0E0	0,004	Rejected
$SYN_{10}^{\downarrow\uparrow}$	16	0E0	0,003	Rejected
$PF_{0,1}^{\uparrow}$	17	0E0	0,003	Rejected
$PF_{0,01}^{\uparrow}$	18	0E0	0,003	Rejected
$PSC_{0,1}^{\uparrow}$	19	0E0	0,003	Rejected
$PSC_{0,01}^{\uparrow}$	20	0E0	0,003	Rejected
$EC_{0,001}^{\downarrow}$	21	0E0	0,003	Rejected
$PF_{0,001}^{\uparrow}$	22	0E0	0,002	Rejected
$PSC_{0,001}^{\uparrow}$	23	0E0	0,002	Rejected
$SC_{0,01}^{\downarrow}$	24	0E0	0,002	Rejected
$SC_{0,001}^{\downarrow}$	25	0E0	0,002	Rejected
$SC_{0,1}^{\downarrow}$	26	0E0	0,002	Rejected
$HF_{0,001}^{\uparrow}$	27	0E0	0,002	Rejected
Canonical	28	0E0	0,002	Rejected
$HF_{0,01}^{\uparrow}$	29	0E0	0,002	Rejected
$HF_{0,1}^{\uparrow}$	30	0E0	0,002	Rejected

Table C.97: Average ranking of NSGA-II in MH.

Algorithm	Ranking	p-value	Holm	Hypothesis
$SYN_9^{\downarrow\uparrow}$	1	0E0	0	-
$SYN_8^{\downarrow\uparrow}$	2	1,865E-3	0,05	Rejected
$SYN_{10}^{\downarrow\uparrow}$	3	4,918E-10	0,025	Rejected
$SYN_6^{\downarrow\uparrow}$	4	1,033E-20	0,017	Rejected
$SYN_7^{\downarrow\uparrow}$	5	1,519E-35	0,013	Rejected
$SYN_5^{\downarrow\uparrow}$	6	1,488E-54	0,01	Rejected
$SYN_4^{\downarrow\uparrow}$	7	9,514E-78	0,008	Rejected
$SYN_{11}^{\downarrow\uparrow}$	8	3,919E-105	0,007	Rejected
$SYN_{14}^{\downarrow\uparrow}$	9	1,033E-136	0,006	Rejected
$SYN_1^{\downarrow\uparrow}$	10	1,733E-172	0,006	Rejected
$SYN_{13}^{\downarrow\uparrow}$	11	1,846E-212	0,005	Rejected
$SYN_{12}^{\downarrow\uparrow}$	12	1,244E-256	0,005	Rejected
$EC_{0,1}^{\downarrow}$	13	0E0	0,004	Rejected
$SYN_3^{\downarrow\uparrow}$	14	0E0	0,004	Rejected
$SYN_2^{\downarrow\uparrow}$	15	0E0	0,004	Rejected
$EC_{0,01}^{\downarrow}$	16	0E0	0,003	Rejected
$PSC_{0,1}^{\uparrow}$	17	0E0	0,003	Rejected
$PSC_{0,001}^{\uparrow}$	18	0E0	0,003	Rejected
$PSC_{0,01}^{\uparrow}$	19	0E0	0,003	Rejected
$PF_{0,1}^{\uparrow}$	20	0E0	0,003	Rejected
$PF_{0,01}^{\uparrow}$	21	0E0	0,003	Rejected
$EC_{0,001}^{\downarrow}$	22	0E0	0,002	Rejected
$HF_{0,01}^{\uparrow}$	23	0E0	0,002	Rejected
$HF_{0,001}^{\uparrow}$	24	0E0	0,002	Rejected
$PF_{0,001}^{\uparrow}$	25	0E0	0,002	Rejected
$HF_{0,1}^{\uparrow}$	26	0E0	0,002	Rejected
$SC_{0,01}^{\downarrow}$	27	0E0	0,002	Rejected
$SC_{0,001}^{\downarrow}$	28	0E0	0,002	Rejected
Canonical	29	0E0	0,002	Rejected
$SC_{0,1}^{\downarrow}$	30	0E0	0,002	Rejected

Table C.98: Average ranking of MOCcell in MH.

Algorithm	Ranking	p-value	Holm	Hypothesis
$EC_{0.1}^{\downarrow}$	1	0E0	0	-
$EC_{0.01}^{\downarrow}$	2	1,865E-3	0,05	Rejected
$EC_{0.001}^{\downarrow}$	3	4,918E-10	0,025	Rejected
$SYN_{13}^{\downarrow\uparrow}$	4	1,033E-20	0,017	Rejected
$SYN_{14}^{\downarrow\uparrow}$	5	1,519E-35	0,013	Rejected
$SYN_{11}^{\downarrow\uparrow}$	6	1,488E-54	0,01	Rejected
$SYN_{10}^{\downarrow\uparrow}$	7	9,514E-78	0,008	Rejected
$PF_{0.001}^{\uparrow}$	8	3,919E-105	0,007	Rejected
$SYN_{7}^{\downarrow\uparrow}$	9	1,033E-136	0,006	Rejected
$SYN_{8}^{\downarrow\uparrow}$	10	1,733E-172	0,006	Rejected
$SYN_{6}^{\downarrow\uparrow}$	11	1,846E-212	0,005	Rejected
$PF_{0.1}^{\uparrow}$	12	1,244E-256	0,005	Rejected
$PSC_{0.001}^{\uparrow}$	13	0E0	0,004	Rejected
$PSC_{0.01}^{\uparrow}$	14	0E0	0,004	Rejected
$PF_{0.01}^{\uparrow}$	15	0E0	0,004	Rejected
$SYN_{9}^{\downarrow\uparrow}$	16	0E0	0,003	Rejected
$SYN_{1}^{\downarrow\uparrow}$	17	0E0	0,003	Rejected
$PSC_{0.1}^{\uparrow}$	18	0E0	0,003	Rejected
$SYN_{4}^{\downarrow\uparrow}$	19	0E0	0,003	Rejected
$SYN_{5}^{\downarrow\uparrow}$	20	0E0	0,003	Rejected
$SYN_{12}^{\downarrow\uparrow}$	21	0E0	0,003	Rejected
$SYN_{3}^{\downarrow\uparrow}$	22	0E0	0,002	Rejected
$SYN_{2}^{\downarrow\uparrow}$	23	0E0	0,002	Rejected
$SC_{0.01}^{\downarrow}$	24	0E0	0,002	Rejected
$SC_{0.001}^{\downarrow}$	25	0E0	0,002	Rejected
$SC_{0.1}^{\downarrow}$	26	0E0	0,002	Rejected
Canonical	27	0E0	0,002	Rejected
$HF_{0.01}^{\uparrow}$	28	0E0	0,002	Rejected
$HF_{0.001}^{\uparrow}$	29	0E0	0,002	Rejected
$HF_{0.1}^{\uparrow}$	30	0E0	0,002	Rejected

Table C.99: Average ranking of SMS-EMOA in MH.

Algorithm	Ranking	p-value	Holm	Hypothesis
$SYN_4^{\downarrow\uparrow}$	1	0E0	0	-
$SYN_{10}^{\downarrow\uparrow}$	2	1,865E-3	0,05	Rejected
$SYN_9^{\downarrow\uparrow}$	3	4,918E-10	0,025	Rejected
$SYN_7^{\downarrow\uparrow}$	4	1,033E-20	0,017	Rejected
$EC_{0,001}^{\downarrow}$	5	1,519E-35	0,013	Rejected
$EC_{0,1}^{\downarrow}$	6	1,488E-54	0,01	Rejected
$SYN_8^{\downarrow\uparrow}$	7	9,514E-78	0,008	Rejected
$SYN_5^{\downarrow\uparrow}$	8	3,919E-105	0,007	Rejected
$SYN_6^{\downarrow\uparrow}$	9	1,033E-136	0,006	Rejected
$EC_{0,01}^{\downarrow}$	10	1,733E-172	0,006	Rejected
$SYN_{11}^{\downarrow\uparrow}$	11	1,846E-212	0,005	Rejected
$PSC_{0,01}^{\uparrow}$	12	1,244E-256	0,005	Rejected
$PF_{0,01}^{\uparrow}$	13	0E0	0,004	Rejected
$SYN_{12}^{\downarrow\uparrow}$	14	0E0	0,004	Rejected
$SYN_{13}^{\downarrow\uparrow}$	15	0E0	0,004	Rejected
$PF_{0,001}^{\uparrow}$	16	0E0	0,003	Rejected
$PSC_{0,1}^{\uparrow}$	17	0E0	0,003	Rejected
$PSC_{0,001}^{\uparrow}$	18	0E0	0,003	Rejected
$SYN_3^{\downarrow\uparrow}$	19	0E0	0,003	Rejected
$SYN_2^{\downarrow\uparrow}$	20	0E0	0,003	Rejected
$SYN_1^{\downarrow\uparrow}$	21	0E0	0,003	Rejected
$SYN_{14}^{\downarrow\uparrow}$	22	0E0	0,002	Rejected
$SC_{0,01}^{\downarrow}$	23	0E0	0,002	Rejected
$PF_{0,1}^{\uparrow}$	24	0E0	0,002	Rejected
$HF_{0,01}^{\uparrow}$	25	0E0	0,002	Rejected
$SC_{0,1}^{\downarrow}$	26	0E0	0,002	Rejected
$SC_{0,001}^{\downarrow}$	27	0E0	0,002	Rejected
Canonical	28	0E0	0,002	Rejected
$HF_{0,001}^{\uparrow}$	29	0E0	0,002	Rejected
$HF_{0,1}^{\uparrow}$	30	0E0	0,002	Rejected

Table C.100: Average ranking of SparseEA in MH.

Algorithm	Ranking	p-value	Holm	Hypothesis
$EC_{0,01}^{\downarrow}$	1	0E0	0	-
$EC_{0,1}^{\downarrow}$	2	1,865E-3	0,05	Rejected
$SYN_9^{\downarrow\uparrow}$	3	4,918E-10	0,025	Rejected
$SYN_7^{\downarrow\uparrow}$	4	1,033E-20	0,017	Rejected
$SYN_{14}^{\downarrow\uparrow}$	5	1,519E-35	0,013	Rejected
$PF_{0,01}^{\uparrow}$	6	1,488E-54	0,01	Rejected
$SYN_8^{\downarrow\uparrow}$	7	9,514E-78	0,008	Rejected
$SYN_{13}^{\downarrow\uparrow}$	8	3,919E-105	0,007	Rejected
$PSC_{0,1}^{\uparrow}$	9	1,033E-136	0,006	Rejected
$PSC_{0,01}^{\uparrow}$	10	1,733E-172	0,006	Rejected
$SYN_{10}^{\downarrow\uparrow}$	11	1,846E-212	0,005	Rejected
$PF_{0,1}^{\uparrow}$	12	1,244E-256	0,005	Rejected
$SYN_6^{\downarrow\uparrow}$	13	0E0	0,004	Rejected
$SYN_1^{\downarrow\uparrow}$	14	0E0	0,004	Rejected
$SYN_4^{\downarrow\uparrow}$	15	0E0	0,004	Rejected
$SYN_{11}^{\downarrow\uparrow}$	16	0E0	0,003	Rejected
$SYN_5^{\downarrow\uparrow}$	17	0E0	0,003	Rejected
$EC_{0,001}^{\downarrow}$	18	0E0	0,003	Rejected
$SYN_2^{\downarrow\uparrow}$	19	0E0	0,003	Rejected
$SYN_3^{\downarrow\uparrow}$	20	0E0	0,003	Rejected
$SYN_{12}^{\downarrow\uparrow}$	21	0E0	0,003	Rejected
$PF_{0,001}^{\uparrow}$	22	0E0	0,002	Rejected
$PSC_{0,001}^{\uparrow}$	23	0E0	0,002	Rejected
$SC_{0,01}^{\downarrow}$	24	0E0	0,002	Rejected
$SC_{0,001}^{\downarrow}$	25	0E0	0,002	Rejected
Canonical	26	0E0	0,002	Rejected
$HF_{0,1}^{\uparrow}$	27	0E0	0,002	Rejected
$HF_{0,01}^{\uparrow}$	28	0E0	0,002	Rejected
$SC_{0,1}^{\downarrow}$	29	0E0	0,002	Rejected
$HF_{0,001}^{\uparrow}$	30	0E0	0,002	Rejected

Table C.101: Average ranking of NSGA-II in HL.

Algorithm	Ranking	p-value	Holm	Hypothesis
$SYN_9^{\downarrow\uparrow}$	1	0E0	0	-
$SYN_8^{\downarrow\uparrow}$	2	1,865E-3	0,05	Rejected
$SYN_7^{\downarrow\uparrow}$	3	4,918E-10	0,025	Rejected
$SYN_6^{\downarrow\uparrow}$	4	1,033E-20	0,017	Rejected
$SYN_{10}^{\downarrow\uparrow}$	5	1,519E-35	0,013	Rejected
$SYN_4^{\downarrow\uparrow}$	6	1,488E-54	0,01	Rejected
$SYN_{14}^{\downarrow\uparrow}$	7	9,514E-78	0,008	Rejected
$SYN_{13}^{\downarrow\uparrow}$	8	3,919E-105	0,007	Rejected
$SYN_{11}^{\downarrow\uparrow}$	9	1,033E-136	0,006	Rejected
$SYN_5^{\downarrow\uparrow}$	10	1,733E-172	0,006	Rejected
$SYN_1^{\downarrow\uparrow}$	11	1,846E-212	0,005	Rejected
$EC_{0,1}^{\downarrow}$	12	1,244E-256	0,005	Rejected
$SYN_2^{\downarrow\uparrow}$	13	0E0	0,004	Rejected
$SYN_3^{\downarrow\uparrow}$	14	0E0	0,004	Rejected
$EC_{0,01}^{\downarrow}$	15	0E0	0,004	Rejected
$SYN_{12}^{\downarrow\uparrow}$	16	0E0	0,003	Rejected
$PSC_{0,1}^{\uparrow}$	17	0E0	0,003	Rejected
$PSC_{0,01}^{\uparrow}$	18	0E0	0,003	Rejected
$PF_{0,1}^{\uparrow}$	19	0E0	0,003	Rejected
$PF_{0,01}^{\uparrow}$	20	0E0	0,003	Rejected
$EC_{0,001}^{\downarrow}$	21	0E0	0,003	Rejected
$PSC_{0,001}^{\uparrow}$	22	0E0	0,002	Rejected
$PF_{0,001}^{\uparrow}$	23	0E0	0,002	Rejected
$HF_{0,001}^{\uparrow}$	24	0E0	0,002	Rejected
$HF_{0,01}^{\uparrow}$	25	0E0	0,002	Rejected
$HF_{0,1}^{\uparrow}$	26	0E0	0,002	Rejected
$SC_{0,01}^{\downarrow}$	27	0E0	0,002	Rejected
$SC_{0,001}^{\downarrow}$	28	0E0	0,002	Rejected
Canonical	29	0E0	0,002	Rejected
$SC_{0,1}^{\downarrow}$	30	0E0	0,002	Rejected

Table C.102: Average ranking of MOCcell in HL.

Algorithm	Ranking	p-value	Holm	Hypothesis
$EC_{0,1}^{\downarrow}$	1	0E0	0	-
$EC_{0,001}^{\downarrow}$	2	1,865E-3	0,05	Rejected
$EC_{0,01}^{\downarrow}$	3	4,918E-10	0,025	Rejected
$PF_{0,1}^{\uparrow}$	4	1,033E-20	0,017	Rejected
$PSC_{0,1}^{\uparrow}$	5	1,519E-35	0,013	Rejected
$PSC_{0,01}^{\uparrow}$	6	1,488E-54	0,01	Rejected
$PF_{0,001}^{\uparrow}$	7	9,514E-78	0,008	Rejected
$PF_{0,01}^{\uparrow}$	8	3,919E-105	0,007	Rejected
$PSC_{0,001}^{\uparrow}$	9	1,033E-136	0,006	Rejected
$SC_{0,01}^{\downarrow}$	10	1,733E-172	0,006	Rejected
$SC_{0,001}^{\downarrow}$	11	1,846E-212	0,005	Rejected
$SYN_{13}^{\downarrow\uparrow}$	12	1,244E-256	0,005	Rejected
$SYN_{10}^{\downarrow\uparrow}$	13	0E0	0,004	Rejected
$SYN_{6}^{\downarrow\uparrow}$	14	0E0	0,004	Rejected
$SYN_{7}^{\downarrow\uparrow}$	15	0E0	0,004	Rejected
$SYN_{14}^{\downarrow\uparrow}$	16	0E0	0,003	Rejected
$SYN_{8}^{\downarrow\uparrow}$	17	0E0	0,003	Rejected
$SYN_{9}^{\downarrow\uparrow}$	18	0E0	0,003	Rejected
$SYN_{11}^{\downarrow\uparrow}$	19	0E0	0,003	Rejected
$SYN_{1}^{\downarrow\uparrow}$	20	0E0	0,003	Rejected
$SYN_{4}^{\downarrow\uparrow}$	21	0E0	0,003	Rejected
$HF_{0,001}^{\uparrow}$	22	0E0	0,002	Rejected
Canonical	23	0E0	0,002	Rejected
$HF_{0,01}^{\uparrow}$	24	0E0	0,002	Rejected
$SC_{0,1}^{\downarrow}$	25	0E0	0,002	Rejected
$SYN_{5}^{\downarrow\uparrow}$	26	0E0	0,002	Rejected
$HF_{0,1}^{\uparrow}$	27	0E0	0,002	Rejected
$SYN_{3}^{\downarrow\uparrow}$	28	0E0	0,002	Rejected
$SYN_{2}^{\downarrow\uparrow}$	29	0E0	0,002	Rejected
$SYN_{12}^{\downarrow\uparrow}$	30	0E0	0,002	Rejected

Table C.103: Average ranking of SMS-EMOA in HL.

Algorithm	Ranking	p-value	Holm	Hypothesis
$SYN_4^{\downarrow\uparrow}$	1	0E0	0	-
$SYN_5^{\downarrow\uparrow}$	2	1,865E-3	0,05	Rejected
$SYN_9^{\downarrow\uparrow}$	3	4,918E-10	0,025	Rejected
$SYN_6^{\downarrow\uparrow}$	4	1,033E-20	0,017	Rejected
$SYN_8^{\downarrow\uparrow}$	5	1,519E-35	0,013	Rejected
$SYN_{10}^{\downarrow\uparrow}$	6	1,488E-54	0,01	Rejected
$EC_{0,1}^{\downarrow}$	7	9,514E-78	0,008	Rejected
$SYN_7^{\downarrow\uparrow}$	8	3,919E-105	0,007	Rejected
$EC_{0,001}^{\downarrow}$	9	1,033E-136	0,006	Rejected
$EC_{0,01}^{\downarrow}$	10	1,733E-172	0,006	Rejected
$SYN_2^{\downarrow\uparrow}$	11	1,846E-212	0,005	Rejected
$SYN_1^{\downarrow\uparrow}$	12	1,244E-256	0,005	Rejected
$SYN_3^{\downarrow\uparrow}$	13	0E0	0,004	Rejected
$SYN_{12}^{\downarrow\uparrow}$	14	0E0	0,004	Rejected
$SYN_{13}^{\downarrow\uparrow}$	15	0E0	0,004	Rejected
$SYN_{14}^{\downarrow\uparrow}$	16	0E0	0,003	Rejected
$PF_{0,001}^{\uparrow}$	17	0E0	0,003	Rejected
$SYN_{11}^{\downarrow\uparrow}$	18	0E0	0,003	Rejected
$PSC_{0,1}^{\uparrow}$	19	0E0	0,003	Rejected
$PSC_{0,001}^{\uparrow}$	20	0E0	0,003	Rejected
$PF_{0,01}^{\uparrow}$	21	0E0	0,003	Rejected
$PF_{0,1}^{\uparrow}$	22	0E0	0,002	Rejected
$PSC_{0,01}^{\uparrow}$	23	0E0	0,002	Rejected
$SC_{0,01}^{\downarrow}$	24	0E0	0,002	Rejected
$HF_{0,001}^{\uparrow}$	25	0E0	0,002	Rejected
Canonical	26	0E0	0,002	Rejected
$HF_{0,1}^{\uparrow}$	27	0E0	0,002	Rejected
$SC_{0,001}^{\downarrow}$	28	0E0	0,002	Rejected
$HF_{0,01}^{\uparrow}$	29	0E0	0,002	Rejected
$SC_{0,1}^{\downarrow}$	30	0E0	0,002	Rejected

Table C.104: Average ranking of SparseEA in HL.

Algorithm	Ranking	p-value	Holm	Hypothesis
$SYN_9^{\downarrow\uparrow}$	1	0E0	0	-
$SYN_{14}^{\downarrow\uparrow}$	2	1,865E-3	0,05	Rejected
$SYN_7^{\downarrow\uparrow}$	3	4,918E-10	0,025	Rejected
$EC_{0,1}^{\downarrow}$	4	1,033E-20	0,017	Rejected
$SYN_6^{\downarrow\uparrow}$	5	1,519E-35	0,013	Rejected
$SYN_{13}^{\downarrow\uparrow}$	6	1,488E-54	0,01	Rejected
$SYN_8^{\downarrow\uparrow}$	7	9,514E-78	0,008	Rejected
$SYN_{11}^{\downarrow\uparrow}$	8	3,919E-105	0,007	Rejected
$SYN_4^{\downarrow\uparrow}$	9	1,033E-136	0,006	Rejected
$SYN_{10}^{\downarrow\uparrow}$	10	1,733E-172	0,006	Rejected
$EC_{0,01}^{\downarrow}$	11	1,846E-212	0,005	Rejected
$SYN_{12}^{\downarrow\uparrow}$	12	1,244E-256	0,005	Rejected
$SYN_5^{\downarrow\uparrow}$	13	0E0	0,004	Rejected
$SYN_1^{\downarrow\uparrow}$	14	0E0	0,004	Rejected
$PSC_{0,01}^{\uparrow}$	15	0E0	0,004	Rejected
$PSC_{0,1}^{\uparrow}$	16	0E0	0,003	Rejected
$SYN_3^{\downarrow\uparrow}$	17	0E0	0,003	Rejected
$SYN_2^{\downarrow\uparrow}$	18	0E0	0,003	Rejected
$PF_{0,1}^{\uparrow}$	19	0E0	0,003	Rejected
$PF_{0,01}^{\uparrow}$	20	0E0	0,003	Rejected
$EC_{0,001}^{\downarrow}$	21	0E0	0,003	Rejected
$PSC_{0,001}^{\uparrow}$	22	0E0	0,002	Rejected
$PF_{0,001}^{\uparrow}$	23	0E0	0,002	Rejected
$SC_{0,01}^{\downarrow}$	24	0E0	0,002	Rejected
$SC_{0,001}^{\downarrow}$	25	0E0	0,002	Rejected
$HF_{0,001}^{\uparrow}$	26	0E0	0,002	Rejected
Canonical	27	0E0	0,002	Rejected
$HF_{0,01}^{\uparrow}$	28	0E0	0,002	Rejected
$HF_{0,1}^{\uparrow}$	29	0E0	0,002	Rejected
$SC_{0,1}^{\downarrow}$	30	0E0	0,002	Rejected

Table C.105: Average ranking of NSGA-II in HM.

Algorithm	Ranking	p-value	Holm	Hypothesis
$SYN_9^{\downarrow\uparrow}$	1	0E0	0	-
$SYN_8^{\downarrow\uparrow}$	2	1,865E-3	0,05	Rejected
$SYN_{10}^{\downarrow\uparrow}$	3	4,918E-10	0,025	Rejected
$SYN_6^{\downarrow\uparrow}$	4	1,033E-20	0,017	Rejected
$SYN_7^{\downarrow\uparrow}$	5	1,519E-35	0,013	Rejected
$SYN_4^{\downarrow\uparrow}$	6	1,488E-54	0,01	Rejected
$SYN_5^{\downarrow\uparrow}$	7	9,514E-78	0,008	Rejected
$SYN_{14}^{\downarrow\uparrow}$	8	3,919E-105	0,007	Rejected
$SYN_{11}^{\downarrow\uparrow}$	9	1,033E-136	0,006	Rejected
$SYN_{13}^{\downarrow\uparrow}$	10	1,733E-172	0,006	Rejected
$SYN_1^{\downarrow\uparrow}$	11	1,846E-212	0,005	Rejected
$EC_{0,1}^{\downarrow}$	12	1,244E-256	0,005	Rejected
$SYN_{12}^{\downarrow\uparrow}$	13	0E0	0,004	Rejected
$SYN_2^{\downarrow\uparrow}$	14	0E0	0,004	Rejected
$SYN_3^{\downarrow\uparrow}$	15	0E0	0,004	Rejected
$EC_{0,01}^{\downarrow}$	16	0E0	0,003	Rejected
$PSC_{0,1}^{\uparrow}$	17	0E0	0,003	Rejected
$PSC_{0,01}^{\uparrow}$	18	0E0	0,003	Rejected
$PF_{0,01}^{\uparrow}$	19	0E0	0,003	Rejected
$PF_{0,1}^{\uparrow}$	20	0E0	0,003	Rejected
$EC_{0,001}^{\downarrow}$	21	0E0	0,003	Rejected
$PF_{0,001}^{\uparrow}$	22	0E0	0,002	Rejected
$PSC_{0,001}^{\uparrow}$	23	0E0	0,002	Rejected
$HF_{0,001}^{\uparrow}$	24	0E0	0,002	Rejected
$HF_{0,01}^{\uparrow}$	25	0E0	0,002	Rejected
$HF_{0,1}^{\uparrow}$	26	0E0	0,002	Rejected
$SC_{0,01}^{\downarrow}$	27	0E0	0,002	Rejected
$SC_{0,001}^{\downarrow}$	28	0E0	0,002	Rejected
$SC_{0,1}^{\downarrow}$	29	0E0	0,002	Rejected
Canonical	30	0E0	0,002	Rejected

Table C.106: Average ranking of MOCcell in HM.

Algorithm	Ranking	p-value	Holm	Hypothesis
$EC_{0,1}^{\downarrow}$	1	0E0	0	-
$EC_{0,001}^{\downarrow}$	2	1,865E-3	0,05	Rejected
$PSC_{0,001}^{\uparrow}$	3	4,918E-10	0,025	Rejected
$EC_{0,01}^{\downarrow}$	4	1,033E-20	0,017	Rejected
$PF_{0,1}^{\uparrow}$	5	1,519E-35	0,013	Rejected
$PF_{0,01}^{\uparrow}$	6	1,488E-54	0,01	Rejected
$PSC_{0,1}^{\uparrow}$	7	9,514E-78	0,008	Rejected
$PSC_{0,01}^{\uparrow}$	8	3,919E-105	0,007	Rejected
$PF_{0,001}^{\uparrow}$	9	1,033E-136	0,006	Rejected
$SYN_{10}^{\downarrow\uparrow}$	10	1,733E-172	0,006	Rejected
$SYN_{14}^{\downarrow\uparrow}$	11	1,846E-212	0,005	Rejected
$SYN_{13}^{\downarrow\uparrow}$	12	1,244E-256	0,005	Rejected
$SYN_{7}^{\downarrow\uparrow}$	13	0E0	0,004	Rejected
$SYN_{11}^{\downarrow\uparrow}$	14	0E0	0,004	Rejected
$SC_{0,01}^{\downarrow}$	15	0E0	0,004	Rejected
$SYN_{6}^{\downarrow\uparrow}$	16	0E0	0,003	Rejected
$SYN_{9}^{\downarrow\uparrow}$	17	0E0	0,003	Rejected
$SC_{0,001}^{\downarrow}$	18	0E0	0,003	Rejected
$SYN_{4}^{\downarrow\uparrow}$	19	0E0	0,003	Rejected
$SYN_{1}^{\downarrow\uparrow}$	20	0E0	0,003	Rejected
$SYN_{8}^{\downarrow\uparrow}$	21	0E0	0,003	Rejected
$SYN_{5}^{\downarrow\uparrow}$	22	0E0	0,002	Rejected
$SYN_{2}^{\downarrow\uparrow}$	23	0E0	0,002	Rejected
$SYN_{3}^{\downarrow\uparrow}$	24	0E0	0,002	Rejected
$SYN_{12}^{\downarrow\uparrow}$	25	0E0	0,002	Rejected
Canonical	26	0E0	0,002	Rejected
$SC_{0,1}^{\downarrow}$	27	0E0	0,002	Rejected
$HF_{0,001}^{\uparrow}$	28	0E0	0,002	Rejected
$HF_{0,01}^{\uparrow}$	29	0E0	0,002	Rejected
$HF_{0,1}^{\uparrow}$	30	0E0	0,002	Rejected

Table C.107: Average ranking of SMS-EMOA in HM.

Algorithm	Ranking	p-value	Holm	Hypothesis
$EC_{0.001}^{\downarrow}$	1	0E0	0	-
$SYN_9^{\downarrow\uparrow}$	2	1,865E-3	0,05	Rejected
$EC_{0.1}^{\downarrow}$	3	4,918E-10	0,025	Rejected
$SYN_5^{\downarrow\uparrow}$	4	1,033E-20	0,017	Rejected
$EC_{0.01}^{\downarrow}$	5	1,519E-35	0,013	Rejected
$SYN_4^{\downarrow\uparrow}$	6	1,488E-54	0,01	Rejected
$SYN_7^{\downarrow\uparrow}$	7	9,514E-78	0,008	Rejected
$SYN_6^{\downarrow\uparrow}$	8	3,919E-105	0,007	Rejected
$SYN_8^{\downarrow\uparrow}$	9	1,033E-136	0,006	Rejected
$SYN_{10}^{\downarrow\uparrow}$	10	1,733E-172	0,006	Rejected
$SYN_{11}^{\downarrow\uparrow}$	11	1,846E-212	0,005	Rejected
$SYN_{14}^{\downarrow\uparrow}$	12	1,244E-256	0,005	Rejected
$SYN_1^{\downarrow\uparrow}$	13	0E0	0,004	Rejected
$SYN_2^{\downarrow\uparrow}$	14	0E0	0,004	Rejected
$SYN_{12}^{\downarrow\uparrow}$	15	0E0	0,004	Rejected
$PSC_{0.001}^{\uparrow}$	16	0E0	0,003	Rejected
$PSC_{0.01}^{\uparrow}$	17	0E0	0,003	Rejected
$SYN_3^{\downarrow\uparrow}$	18	0E0	0,003	Rejected
$SYN_{13}^{\downarrow\uparrow}$	19	0E0	0,003	Rejected
$PSC_{0.1}^{\uparrow}$	20	0E0	0,003	Rejected
$PF_{0.1}^{\uparrow}$	21	0E0	0,003	Rejected
$PF_{0.01}^{\uparrow}$	22	0E0	0,002	Rejected
$PF_{0.001}^{\uparrow}$	23	0E0	0,002	Rejected
$SC_{0.01}^{\downarrow}$	24	0E0	0,002	Rejected
$SC_{0.001}^{\downarrow}$	25	0E0	0,002	Rejected
$SC_{0.1}^{\downarrow}$	26	0E0	0,002	Rejected
$HF_{0.01}^{\uparrow}$	27	0E0	0,002	Rejected
$HF_{0.001}^{\uparrow}$	28	0E0	0,002	Rejected
Canonical	29	0E0	0,002	Rejected
$HF_{0.1}^{\uparrow}$	30	0E0	0,002	Rejected

Table C.108: Average ranking of SparseEA in HM.

Algorithm	Ranking	p-value	Holm	Hypothesis
$EC_{0,1}^{\downarrow}$	1	0E0	0	-
$SYN_{6}^{\downarrow\uparrow}$	2	1,865E-3	0,05	Rejected
$SYN_{8}^{\downarrow\uparrow}$	3	4,918E-10	0,025	Rejected
$SYN_{9}^{\downarrow\uparrow}$	4	1,033E-20	0,017	Rejected
$SYN_{7}^{\downarrow\uparrow}$	5	1,519E-35	0,013	Rejected
$SYN_{1}^{\downarrow\uparrow}$	6	1,488E-54	0,01	Rejected
$SYN_{11}^{\downarrow\uparrow}$	7	9,514E-78	0,008	Rejected
$SYN_{4}^{\downarrow\uparrow}$	8	3,919E-105	0,007	Rejected
$SYN_{13}^{\downarrow\uparrow}$	9	1,033E-136	0,006	Rejected
$SYN_{5}^{\downarrow\uparrow}$	10	1,733E-172	0,006	Rejected
$SYN_{14}^{\downarrow\uparrow}$	11	1,846E-212	0,005	Rejected
$SYN_{2}^{\downarrow\uparrow}$	12	1,244E-256	0,005	Rejected
$SYN_{12}^{\downarrow\uparrow}$	13	0E0	0,004	Rejected
$SYN_{3}^{\downarrow\uparrow}$	14	0E0	0,004	Rejected
$SYN_{10}^{\downarrow\uparrow}$	15	0E0	0,004	Rejected
$EC_{0,01}^{\downarrow}$	16	0E0	0,003	Rejected
$PSC_{0,1}^{\uparrow}$	17	0E0	0,003	Rejected
$PSC_{0,01}^{\uparrow}$	18	0E0	0,003	Rejected
$PF_{0,01}^{\uparrow}$	19	0E0	0,003	Rejected
$PF_{0,1}^{\uparrow}$	20	0E0	0,003	Rejected
$EC_{0,001}^{\downarrow}$	21	0E0	0,003	Rejected
$PSC_{0,001}^{\uparrow}$	22	0E0	0,002	Rejected
$PF_{0,001}^{\uparrow}$	23	0E0	0,002	Rejected
$SC_{0,01}^{\downarrow}$	24	0E0	0,002	Rejected
$SC_{0,001}^{\downarrow}$	25	0E0	0,002	Rejected
Canonical	26	0E0	0,002	Rejected
$SC_{0,1}^{\downarrow}$	27	0E0	0,002	Rejected
$HF_{0,001}^{\uparrow}$	28	0E0	0,002	Rejected
$HF_{0,1}^{\uparrow}$	29	0E0	0,002	Rejected
$HF_{0,01}^{\uparrow}$	30	0E0	0,002	Rejected

Table C.109: Average ranking of NSGA-II in HH.

Algorithm	Ranking	p-value	Holm	Hypothesis
$SYN_8^{\downarrow\uparrow}$	1	0E0	0	-
$SYN_7^{\downarrow\uparrow}$	2	1,865E-3	0,05	Rejected
$SYN_9^{\downarrow\uparrow}$	3	4,918E-10	0,025	Rejected
$SYN_6^{\downarrow\uparrow}$	4	1,033E-20	0,017	Rejected
$SYN_{10}^{\downarrow\uparrow}$	5	1,519E-35	0,013	Rejected
$SYN_4^{\downarrow\uparrow}$	6	1,488E-54	0,01	Rejected
$SYN_{13}^{\downarrow\uparrow}$	7	9,514E-78	0,008	Rejected
$SYN_1^{\downarrow\uparrow}$	8	3,919E-105	0,007	Rejected
$SYN_5^{\downarrow\uparrow}$	9	1,033E-136	0,006	Rejected
$SYN_{14}^{\downarrow\uparrow}$	10	1,733E-172	0,006	Rejected
$SYN_{12}^{\downarrow\uparrow}$	11	1,846E-212	0,005	Rejected
$SYN_{11}^{\downarrow\uparrow}$	12	1,244E-256	0,005	Rejected
$SYN_3^{\downarrow\uparrow}$	13	0E0	0,004	Rejected
$SYN_2^{\downarrow\uparrow}$	14	0E0	0,004	Rejected
$EC_{0.1}^{\downarrow}$	15	0E0	0,004	Rejected
$EC_{0.01}^{\downarrow}$	16	0E0	0,003	Rejected
$PSC_{0.1}^{\uparrow}$	17	0E0	0,003	Rejected
$PSC_{0.01}^{\uparrow}$	18	0E0	0,003	Rejected
$PF_{0.01}^{\uparrow}$	19	0E0	0,003	Rejected
$PF_{0.1}^{\uparrow}$	20	0E0	0,003	Rejected
$EC_{0.001}^{\downarrow}$	21	0E0	0,003	Rejected
$PSC_{0.001}^{\uparrow}$	22	0E0	0,002	Rejected
$PF_{0.001}^{\uparrow}$	23	0E0	0,002	Rejected
$HF_{0.001}^{\uparrow}$	24	0E0	0,002	Rejected
$HF_{0.01}^{\uparrow}$	25	0E0	0,002	Rejected
$HF_{0.1}^{\uparrow}$	26	0E0	0,002	Rejected
$SC_{0.01}^{\downarrow}$	27	0E0	0,002	Rejected
$SC_{0.001}^{\downarrow}$	28	0E0	0,002	Rejected
Canonical	29	0E0	0,002	Rejected
$SC_{0.1}^{\downarrow}$	30	0E0	0,002	Rejected

Table C.110: Average ranking of MOCcell in HH.

Algorithm	Ranking	p-value	Holm	Hypothesis
$EC_{0,1}^{\downarrow}$	1	0E0	0	-
$EC_{0,001}^{\downarrow}$	2	1,865E-3	0,05	Rejected
$EC_{0,01}^{\downarrow}$	3	4,918E-10	0,025	Rejected
$SYN_{13}^{\downarrow\uparrow}$	4	1,033E-20	0,017	Rejected
$PF_{0,001}^{\uparrow}$	5	1,519E-35	0,013	Rejected
$PF_{0,1}^{\uparrow}$	6	1,488E-54	0,01	Rejected
$PF_{0,01}^{\uparrow}$	7	9,514E-78	0,008	Rejected
$PSC_{0,01}^{\uparrow}$	8	3,919E-105	0,007	Rejected
$PSC_{0,1}^{\uparrow}$	9	1,033E-136	0,006	Rejected
$SYN_{11}^{\downarrow\uparrow}$	10	1,733E-172	0,006	Rejected
$SYN_{14}^{\downarrow\uparrow}$	11	1,846E-212	0,005	Rejected
$PSC_{0,001}^{\uparrow}$	12	1,244E-256	0,005	Rejected
$SYN_{10}^{\downarrow\uparrow}$	13	0E0	0,004	Rejected
$SYN_{6}^{\downarrow\uparrow}$	14	0E0	0,004	Rejected
$SYN_{8}^{\downarrow\uparrow}$	15	0E0	0,004	Rejected
$SYN_{1}^{\downarrow\uparrow}$	16	0E0	0,003	Rejected
$SYN_{9}^{\downarrow\uparrow}$	17	0E0	0,003	Rejected
$SYN_{7}^{\downarrow\uparrow}$	18	0E0	0,003	Rejected
$SC_{0,01}^{\downarrow}$	19	0E0	0,003	Rejected
$SYN_{5}^{\downarrow\uparrow}$	20	0E0	0,003	Rejected
$SYN_{4}^{\downarrow\uparrow}$	21	0E0	0,003	Rejected
$SC_{0,001}^{\downarrow}$	22	0E0	0,002	Rejected
$SYN_{12}^{\downarrow\uparrow}$	23	0E0	0,002	Rejected
$SYN_{3}^{\downarrow\uparrow}$	24	0E0	0,002	Rejected
$SYN_{2}^{\downarrow\uparrow}$	25	0E0	0,002	Rejected
Canonical	26	0E0	0,002	Rejected
$SC_{0,1}^{\downarrow}$	27	0E0	0,002	Rejected
$HF_{0,001}^{\uparrow}$	28	0E0	0,002	Rejected
$HF_{0,01}^{\uparrow}$	29	0E0	0,002	Rejected
$HF_{0,1}^{\uparrow}$	30	0E0	0,002	Rejected

Table C.111: Average ranking of SMS-EMOA in HH.

Algorithm	Ranking	p-value	Holm	Hypothesis
$SYN_4^{\downarrow\uparrow}$	1	0E0	0	-
$SYN_5^{\downarrow\uparrow}$	2	1,865E-3	0,05	Rejected
$EC_{0,1}^{\downarrow}$	3	4,918E-10	0,025	Rejected
$EC_{0,001}^{\downarrow}$	4	1,033E-20	0,017	Rejected
$SYN_{10}^{\downarrow\uparrow}$	5	1,519E-35	0,013	Rejected
$SYN_6^{\downarrow\uparrow}$	6	1,488E-54	0,01	Rejected
$SYN_9^{\downarrow\uparrow}$	7	9,514E-78	0,008	Rejected
$EC_{0,01}^{\downarrow}$	8	3,919E-105	0,007	Rejected
$SYN_7^{\downarrow\uparrow}$	9	1,033E-136	0,006	Rejected
$SYN_8^{\downarrow\uparrow}$	10	1,733E-172	0,006	Rejected
$SYN_{11}^{\downarrow\uparrow}$	11	1,846E-212	0,005	Rejected
$SYN_{12}^{\downarrow\uparrow}$	12	1,244E-256	0,005	Rejected
$PF_{0,001}^{\uparrow}$	13	0E0	0,004	Rejected
$SYN_1^{\downarrow\uparrow}$	14	0E0	0,004	Rejected
$PSC_{0,001}^{\uparrow}$	15	0E0	0,004	Rejected
$SYN_3^{\downarrow\uparrow}$	16	0E0	0,003	Rejected
$SYN_{14}^{\downarrow\uparrow}$	17	0E0	0,003	Rejected
$SYN_{13}^{\downarrow\uparrow}$	18	0E0	0,003	Rejected
$PSC_{0,01}^{\uparrow}$	19	0E0	0,003	Rejected
$SYN_2^{\downarrow\uparrow}$	20	0E0	0,003	Rejected
$PF_{0,1}^{\uparrow}$	21	0E0	0,003	Rejected
$PSC_{0,1}^{\uparrow}$	22	0E0	0,002	Rejected
$PF_{0,01}^{\uparrow}$	23	0E0	0,002	Rejected
Canonical	24	0E0	0,002	Rejected
$SC_{0,001}^{\downarrow}$	25	0E0	0,002	Rejected
$SC_{0,01}^{\downarrow}$	26	0E0	0,002	Rejected
$HF_{0,001}^{\uparrow}$	27	0E0	0,002	Rejected
$HF_{0,01}^{\uparrow}$	28	0E0	0,002	Rejected
$SC_{0,1}^{\downarrow}$	29	0E0	0,002	Rejected
$HF_{0,1}^{\uparrow}$	30	0E0	0,002	Rejected

Table C.112: Average ranking of SparseEA in HH.

D

COMCOM SUPPLEMENTARY MATERIAL

This supplementary material for COMCOM (Section 4.1) contains the results of the evaluation metrics.

Contents:

D.1 Evaluation Metrics Results

D.1 Evaluation Metrics Results

The results obtained for the precision, recall, and F1-score of the six LmomRD in Figure 3 are shown below.

	Balanced accuracy	Precision	Recall	F_1 -score
KNN Uniform	0.9994	0.9990	0.9988	0.9989
KNN Distance	0.9995	0.9991	0.9990	0.9990
SVC (Linear)	0.9995	0.9991	0.9990	0.9990
SVC (RBF)	0.9994	0.9990	0.9988	0.9989
SVC (Polynomial)	0.9924	0.9990	0.9988	0.9989

Table D.1: Metrics obtained for scenario (a) defined in Section 4 of the main document.

	Balanced accuracy	Precision	Recall	F_1 -score
KNN Uniform	0.8708	0.9997	0.9997	0.9997
KNN Distance	0.9666	0.9999	0.9999	0.9999
SVC (Linear)	0.9791	0.9999	0.9999	0.9999
SVC (RBF)	0.9791	0.9999	0.9999	0.9999
SVC (Polynomial)	0.9916	0.9999	0.9999	0.9999

Table D.2: Metrics obtained for scenario (b) defined in Section 4 of the main document.

	Balanced accuracy	Precision	Recall	F_1 -score
KNN Uniform	0.9991	0.9985	0.9983	0.9984
KNN Distance	0.9991	0.9985	0.9983	0.9984
SVC (Linear)	0.9991	0.9984	0.9982	0.9982
SVC (RBF)	0.9991	0.998	0.9983	0.9984
SVC (Polynomial)	0.9978	0.9965	0.9957	0.9959

Table D.3: Metrics obtained for scenario (c) defined in Section 4 of the main document.

	Balanced accuracy	Precision	Recall	F_1 -score
KNN Uniform	0.9989	0.9982	0.9979	0.9980
KNN Distance	0.9800	0.9990	0.9989	0.9989
SVC (Linear)	0.8584	0.9901	0.9895	0.9889
SVC (RBF)	0.9795	0.9981	0.9979	0.9979
SVC (Polynomial)	0.9784	0.9966	0.9958	0.9959

Table D.4: Metrics obtained for scenario (d) defined in Section 4 of the main document.

	Balanced accuracy	Precision	Recall	F_1 -score
KNN Uniform	0.6660	0.9970	0.9984	0.9977
KNN Distance	0.7549	0.9982	0.9988	0.9984
SVC (Linear)	0.8438	0.9992	0.9991	0.9990
SVC (RBF)	0.9556	0.9998	0.9998	0.9998
SVC (Polynomial)	0.6660	0.9970	0.9984	0.9977

Table D.5: Metrics obtained for scenario (e) defined in Section 4 of the main document.

	Balanced accuracy	Precision	Recall	F_1 -score
KNN Uniform	0.9370	0.9978	0.9979	0.9979
KNN Distance	0.9545	0.9982	0.9982	0.9982
SVC (Linear)	0.6125	0.9929	0.9928	0.9905
SVC (RBF)	0.9995	0.9991	0.9990	0.9991
SVC (Polynomial)	0.9820	0.9987	0.9986	0.9986

Table D.6: Metrics obtained for scenario (f) defined in Section 4 of the main document.

E

SPRINGER RIGHTS

Springer rights to use the ANTS22 article (Section 3.1) in this dissertation.

SPRINGER NATURE LICENSE
TERMS AND CONDITIONS

Feb 02, 2024

This Agreement between Mr. Jesús Galeano-Brajones ("You") and Springer Nature ("Springer Nature") consists of your license details and the terms and conditions provided by Springer Nature and Copyright Clearance Center.

License Number	5720620959254
License date	Feb 02, 2024
Licensed Content Publisher	Springer Nature
Licensed Content Publication	Springer eBook
Licensed Content Title	Binary Particle Swarm Optimization for Selective Cell Switch-Off in Ultra-Dense 5G Networks
Licensed Content Author	Juan Jesús Espinosa-Martínez, Jesús Galeano-Brajones, Javier Carmona-Murillo et al
Licensed Content Date	Jan 1, 2022
Type of Use	Thesis/Dissertation
Requestor type	academic/university or research institute
Format	print and electronic
Portion	full article/chapter
Will you be translating?	no
Circulation/distribution	1 - 29
Author of this Springer Nature content	yes
Title of new work	Advanced optimization techniques for energy efficiency improvement in ultra-dense 5G-6G networks
Institution name	University of Extremadura
Expected presentation date	Jun 2024
	Mr. Jesús Galeano-Brajones Av. Sta. Teresa de Jornet, 38
Requestor Location	Mérida, 06800 Spain Attn: Mr. Jesús Galeano-Brajones
Billing Type	Invoice Mr. Jesús Galeano-Brajones Av. Sta. Teresa de Jornet, 38
Billing Address	Mérida, Spain 06800 Attn: Mr. Jesús Galeano-Brajones
Total	0.00 EUR

Terms and Conditions

Springer Nature Customer Service Centre GmbH Terms and Conditions

The following terms and conditions ("Terms and Conditions") together with the terms specified in your [RightsLink] constitute the License ("License") between you as Licensee and Springer Nature Customer Service Centre GmbH as Licensor. By clicking 'accept' and completing the

transaction for your use of the material ("Licensed Material"), you confirm your acceptance of and obligation to be bound by these Terms and Conditions.

Grant and Scope of License

The Licensor grants you a personal, non-exclusive, non-transferable, non-sublicensable, revocable, world-wide License to reproduce, distribute, communicate to the public, make available, broadcast, electronically transmit or create derivative works using the Licensed Material for the purpose(s) specified in your RightsLink Licence Details only. Licenses are granted for the specific use requested in the order and for no other use, subject to these Terms and Conditions. You acknowledge and agree that the rights granted to you under this License do not include the right to modify, edit, translate, include in collective works, or create derivative works of the Licensed Material in whole or in part unless expressly stated in your RightsLink Licence Details. You may use the Licensed Material only as permitted under this Agreement and will not reproduce, distribute, display, perform, or otherwise use or exploit any Licensed Material in any way, in whole or in part, except as expressly permitted by this License.

You may only use the Licensed Content in the manner and to the extent permitted by these Terms and Conditions, by your RightsLink Licence Details and by any applicable laws.

A separate license may be required for any additional use of the Licensed Material, e.g. where a license has been purchased for print use only, separate permission must be obtained for electronic re-use. Similarly, a License is only valid in the language selected and does not apply for editions in other languages unless additional translation rights have been granted separately in the License.

Any content within the Licensed Material that is owned by third parties is expressly excluded from the License.

Rights for additional reuses such as custom editions, computer/mobile applications, film or TV reuses and/or any other derivative rights requests require additional permission and may be subject to an additional fee. Please apply to journalpermissions@springernature.com or bookpermissions@springernature.com for these rights.

Reservation of Rights

Licensor reserves all rights not expressly granted to you under this License. You acknowledge and agree that nothing in this License limits or restricts Licensor's rights in or use of the Licensed Material in any way. Neither this License, nor any act, omission, or statement by Licensor or you, conveys any ownership right to you in any Licensed Material, or to any element or portion thereof. As between Licensor and you, Licensor owns and retains all right, title, and interest in and to the Licensed Material subject to the license granted in Section 1.1. Your permission to use the Licensed Material is expressly conditioned on you not impairing Licensor's or the applicable copyright owner's rights in the Licensed Material in any way.

Restrictions on use

Minor editing privileges are allowed for adaptations for stylistic purposes or formatting purposes provided such alterations do not alter the original meaning or intention of the Licensed Material and the new figure(s) are still accurate and representative of the Licensed Material. Any other changes including but not limited to, cropping, adapting, and/or omitting material that affect the meaning, intention or moral rights of the author(s) are strictly prohibited.

You must not use any Licensed Material as part of any design or trademark.

Licensed Material may be used in Open Access Publications (OAP), but any such reuse must include a clear acknowledgment of this permission visible at the same time as the figures/tables/illustration or abstract and which must indicate that the Licensed Material is not part of the governing OA license but has been reproduced with permission. This may be indicated according to any standard referencing system but must include at a minimum 'Book/Journal title, Author, Journal Name (if applicable), Volume (if applicable), Publisher, Year, reproduced with permission from SNCSC'.

STM Permission Guidelines

An alternative scope of license may apply to signatories of the STM Permissions Guidelines ("STM PG") as amended from time to time and made available at <https://www.stm-assoc.org/intellectual-property/permissions/permissions-guidelines/>.

For content reuse requests that qualify for permission under the STM PG, and which may be updated from time to time, the STM PG supersedes the terms and conditions contained in this License.

If a License has been granted under the STM PG, but the STM PG no longer apply at the time of publication, further permission must be sought from the Rightsholder. Contact journalpermissions@springernature.com or bookpermissions@springernature.com for these rights.

Duration of License

Unless otherwise indicated on your License, a License is valid from the date of purchase ("License Date") until the end of the relevant period in the below table:

Reuse in a medical communications project	Reuse up to distribution or time period indicated in License
Reuse in a dissertation/thesis	Lifetime of thesis
Reuse in a journal/magazine	Lifetime of journal/magazine
Reuse in a book/textbook	Lifetime of edition
Reuse on a website	1 year unless otherwise specified in the License
Reuse in a presentation/slide kit/poster	Lifetime of presentation/slide kit/poster. Note: publication whether electronic or in print of presentation/slide kit/poster may require further permission.
Reuse in conference proceedings	Lifetime of conference proceedings
Reuse in an annual report	Lifetime of annual report
Reuse in training/CME materials	Reuse up to distribution or time period indicated in License
Reuse in newsmedia	Lifetime of newsmedia
Reuse in coursepack/classroom materials	Reuse up to distribution and/or time period indicated in license

Acknowledgement

The Licensor's permission must be acknowledged next to the Licensed Material in print. In electronic form, this acknowledgement must be visible at the same time as the figures/tables/illustrations or abstract and must be hyperlinked to the journal/book's homepage.

Acknowledgement may be provided according to any standard referencing system and at a minimum should include "Author, Article/Book Title, Journal name/Book imprint, volume, page number, year, Springer Nature".

Reuse in a dissertation or thesis

Where 'reuse in a dissertation/thesis' has been selected, the following terms apply: Print rights of the Version of Record are provided for; electronic rights for use only on institutional repository as defined by the Sherpa guideline (www.sherpa.ac.uk/romeo/) and only up to what is required by the awarding institution.

For theses published under an ISBN or ISSN, separate permission is required. Please contact journalpermissions@springernature.com or bookpermissions@springernature.com for these rights.

Authors must properly cite the published manuscript in their thesis according to current citation standards and include the following acknowledgement: '*Reproduced with permission from Springer Nature*'.

License Fee

You must pay the fee set forth in the License Agreement (the "License Fees"). All amounts payable by you under this License are exclusive of any sales, use, withholding, value added or similar taxes, government fees or levies or other assessments. Collection and/or remittance of such taxes to the relevant tax authority shall be the responsibility of the party who has the legal obligation to do so.

Warranty

The Licensor warrants that it has, to the best of its knowledge, the rights to license reuse of the Licensed Material. **You are solely responsible for ensuring that the material you wish to license is original to the Licensor and does not carry the copyright of another entity or third party (as credited in the published version).** If the credit line on any part of the Licensed Material indicates that it was reprinted or adapted with permission from another source, then you should seek additional permission from that source to reuse the material.

EXCEPT FOR THE EXPRESS WARRANTY STATED HEREIN AND TO THE EXTENT PERMITTED BY APPLICABLE LAW, LICENSOR PROVIDES THE LICENSED MATERIAL "AS IS" AND MAKES NO OTHER REPRESENTATION OR WARRANTY. LICENSOR EXPRESSLY DISCLAIMS ANY LIABILITY FOR ANY CLAIM ARISING FROM OR OUT OF THE CONTENT, INCLUDING BUT NOT LIMITED TO ANY ERRORS, INACCURACIES, OMISSIONS, OR DEFECTS CONTAINED THEREIN, AND ANY IMPLIED OR EXPRESS WARRANTY AS TO MERCHANTABILITY OR FITNESS FOR A PARTICULAR PURPOSE. IN NO EVENT SHALL LICENSOR BE LIABLE TO YOU OR ANY OTHER PARTY OR ANY OTHER PERSON OR FOR ANY SPECIAL, CONSEQUENTIAL, INCIDENTAL, INDIRECT, PUNITIVE, OR EXEMPLARY DAMAGES, HOWEVER CAUSED, ARISING OUT OF OR IN CONNECTION WITH THE DOWNLOADING, VIEWING OR USE OF THE LICENSED MATERIAL REGARDLESS OF THE FORM OF ACTION, WHETHER FOR BREACH OF CONTRACT, BREACH OF WARRANTY, TORT, NEGLIGENCE, INFRINGEMENT OR OTHERWISE (INCLUDING, WITHOUT LIMITATION, DAMAGES BASED ON LOSS OF PROFITS, DATA, FILES, USE, BUSINESS OPPORTUNITY OR CLAIMS OF THIRD PARTIES), AND WHETHER OR NOT THE PARTY HAS BEEN ADVISED OF THE POSSIBILITY OF SUCH DAMAGES. THIS LIMITATION APPLIES NOTWITHSTANDING ANY FAILURE OF ESSENTIAL PURPOSE OF ANY LIMITED REMEDY PROVIDED HEREIN.

Termination and Cancellation

The License and all rights granted hereunder will continue until the end of the applicable period shown in Clause 5.1 above. Thereafter, this license will be terminated and all rights granted hereunder will cease.

Licensor reserves the right to terminate the License in the event that payment is not received in full or if you breach the terms of this License.

General

The License and the rights and obligations of the parties hereto shall be construed, interpreted and determined in accordance with the laws of the Federal Republic of Germany without reference to the stipulations of the CISG (United Nations Convention on Contracts for the International Sale of Goods) or to Germany's choice-of-law principle.

The parties acknowledge and agree that any controversies and disputes arising out of this License shall be decided exclusively by the courts of or having jurisdiction for Heidelberg, Germany, as far as legally permissible.

This License is solely for Licensor's and Licensee's benefit. It is not for the benefit of any other person or entity.

Questions? For questions on Copyright Clearance Center accounts or website issues please contact springernaturesupport@copyright.com or +1-855-239-3415 (toll free in the US) or +1-978-646-2777. For questions on Springer Nature licensing please visit <https://www.springernature.com/gp/partners/rights-permissions-third-party-distribution>

Other Conditions:

Version 1.4 - Dec 2022

Questions? customercare@copyright.com.
